UNIQUE ARCHITECTURES BUILT ON CHIRAL POLYCARBODIIMIDES

by

Dumindika Aththanayake Siriwardane

APPROVED BY SUPERVISORY COMMITTEE:

Bruce M. Novak, Chair

John P. Ferraris

Mihaela C. Stefan

Ronald A. Smaldone

This effort is dedicated to my father, A.M. Siriwardane, mother, W. Nawarathne, husband, Nikila Rathnayake and brother, Malinda Siriwardane.

UNIQUE ARCHITECTURES BUILT ON CHIRAL POLYCARBODIIMIDES

by

DUMINDIKA ATHTHANAYAKE SIRIWARDANE, BS

DISSERTATION

Presented to the Faculty of

The University of Texas at Dallas

in Partial Fulfillment

of the Requirements

for the Degree of

DOCTOR OF PHILOSOPHY IN

CHEMISTRY

THE UNIVERSITY OF TEXAS AT DALLAS

May 2017

ACKNOWLEDGMENTS

The process of earning a doctorate degree is a long and strenuous journey not carried through alone. First and foremost, I would like to thank my mother and father for allowing me to realize my own potential and all the support and love gifted to me over the years. My very precious thanks goes to my husband, Nikila Rathnayake, I may never have gotten to where I am today without your unconditional love and encouragement. I cannot say enough to show my level of appreciation for your dedication during these past five years. To my ever loving brother, Malinda Siriwardane, thank you so much for being the best brother ever to me. Whenever I need to share my ups and downs, you cared for me even if we were far from each other.

I am so proud to say that I am also a Novakian under the supervision of Dr. Bruce Novak as my advisor. I would like to express my sincere gratitude for his continuous support, guidance, and immense knowledge he has shared with me. This work was not possible without you. I would like to acknowledge the rest of my committee members, Dr. John P. Ferraris, Dr. Mihaela Stefan and Dr. Ronald Smaldone for their insightful comments and guidance to widen my research from various perspectives. Very special thanks goes to Dr. Oleg Kulikov for spending countless hours to correct my manuscripts and doing TEM imaging. You are a wonderful person that I had the privilege of meeting in the Novak lab.

I also need to thank Dr. James Reuther who was my first mentor and former Novakians, Dr. Raymond Campos, Dr. Benjamin Batchelor for their kind support and guidance. I would also like to extend my gratitude to all current members in Novak group, Nimmy Mammoottil, Chamni Jayarathna, and Enosha de Silva for their support and friendship to overcome numerous obstacles during my research work. Finally, I would like to thank all of the UTD staff and friends

in the chemistry department, and all of the Srilankan community for supporting me in various ways.

March 2017

UNIQUE ARCHITECTURES BUILT ON CHIRAL POLYCARBODIIMIDES

Dumindika Aththanayake Siriwardane, PhD
The University of Texas at Dallas, 2017

Supervising Professor: Bruce M. Novak

The helix is a very fascinating and unique macrostructure that can be found in biological systems, as well as, throughout nature. The ability to transfer this basic structure into synthetic architecture will offer many advantages for the development of chiral scaffolds important in novel applications. These discoveries include chiral sensing materials, liquid crystalline materials, and amphiphilic block-copolymers for drug delivery applications, to name a few. Therefore, it is important to enhance the synthesis strategy to improve structural control by accessing greater chemical diversity and versatile functionality for these polycarbodiimide systems.

Chapter one introduces the basic synthetic routes for ureas, carbodiimide monomers, polymers and strategies utilized for screw sense polymerization to achieve control chiral architectures. It also presents a comprehensive review of the most recent developments in post-polymerization modifications, properties of polycarbodiimides and their potential applications in the material sciences and bio-medical field. Chapter two illustrates the synthesis of novel Ni(II) initiators for screw sense polymerization of chiral monomers and it explained Ni(II) mediated “living” polymerization used in the synthesis of multi-arm star polymers. This star and its linear analogs

have been used to conduct kinetic of polymerization and solvent tunable self-assembly behavior studies. Chapter three describes the unusual observation made years ago, that a particular chiral polymer (predominantly *P* or *M* helices) synthesized by using chiral BINOL-Ti(IV) catalysts which show specific racemization behavior when heated. This behavior was unique in more than 150 different carbodiimides we have polymerized to date. We postulated that it was due to stereocomplexation formed *via* racemization between two opposite helical sense. Different characterization techniques and molecular models were employed to investigate this particular observation.

By enhancing helical, polycarbodiimide architectures, chapter four introduces the synthesis of hairy polymers which showed micellization in an aqueous medium. These types of amphiphilic graft co-polymers can be utilized in drug delivery applications. The synthesis and optical switching behavior of UV and thermo responsive polycarbodiimides have been illustrated in chapter five. Properties of the polymer were altered through the isomerization behavior, such as its topology and liquid crystallinity. The synthesis of various chiral designs build upon polycarbodiimide helical frameworks are also included to pursue possible future projects.

TABLE OF CONTENTS

LIST OF FIGURES

LIST OF SCHEMES

LIST OF TABLES

CHAPTER 1

INTRODUCTION TO CARBODIIMIDES

1.1 Abstract

Naturally occurring macromolecules like protein, DNA, and peptides share a helicity as a prime structural motif and provides great inspiration to engineer synthetic scaffolds which assemble with their structure and functions. By transferring this precisely ordered stereo-structures to synthetic macromolecules, it elaborates itself as a powerful tool for various applications such as molecular sensors, biomimetic materials, and drug-delivery vehicles. To date, various kind of helical polymers have been synthesized by polymer chemists and their properties and applications been investigated extensively. This manuscript will discuss unique architectures built on helical polycarbodiimides by emphasizing various orthogonal functionalization on helical backbone and grafting strategies towards versatile architectures in a controllable fashion. These chiral architectures impart intriguing properties as chiroptical switches, nano-carriers to deliver hydrophobic cargos, and self-assembled diverse nano-structures.

1.2 Introduction

Carbodiimides are a unique class of small molecules which possess heterocumulene structure. They are isoelectronic with isocyanates and structurally assemble with heteroallenes which possess cumulated double bonds as R-N=C=N-R' where R and R' are pendant groups attached to the nitrogen atoms.[1] X-ray studies reveal that these cumulative double bonds are not linear and it possess 166˚ and 170˚ bond angles for di-substituted carbodiimides. However, carbodiimides were first synthesized by Hinterberger and Zinin in 1852 and were firstly reported by Weith in

1873.[2] Due to the allene type structure, carbodiimides exist as stereoisomers and the separation of enantiomeric forms remains as a challenge as it possesses a low racemization barrier. However, *N*, *N*'-diferrocenylcarbodiimides, containing two sterically demanding substituents has been partially resolved into its enantiomers by using an acetylated cellulose column and the separation takes place due to a stabilizing interaction between the ferrocenyl groups.[3] These carbodiimides are very useful in many syntheses routes as precursors and are widely used as biomarkers in peptide chemistry.[4]

1.2.1 Synthesis of carbodiimides

Carbodiimides can be synthesized by using dehydration or dehydrosulfonation reactions with ureas and thioureas respectively. In these regards, primary amines can be reacted with a coupling agent such as phosgene, triphosgene or bis-(4-nitrophenyl)carbonate. Through dehydration reaction of 1, 3-disubstituted urea, carbodiimides can be obtained (**Scheme 1.1**).[5]

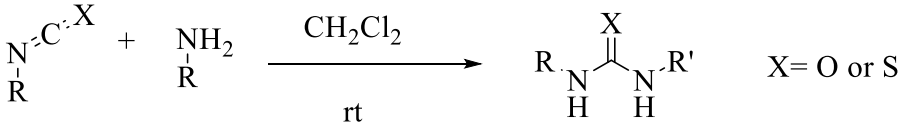

Scheme 1.1 Generalized reaction for urea synthesis.

Both a primary amine and isothiocyanate or isocyanate can be utilized for preparation of thiourea and urea, respectively. During the mechanism, the nucleophilic nitrogen from the primary amine attacks the electrophilic carbon center of the isocyanate and it leads to the formation of 1,3-disubtituted urea (**Figure 1.1**).

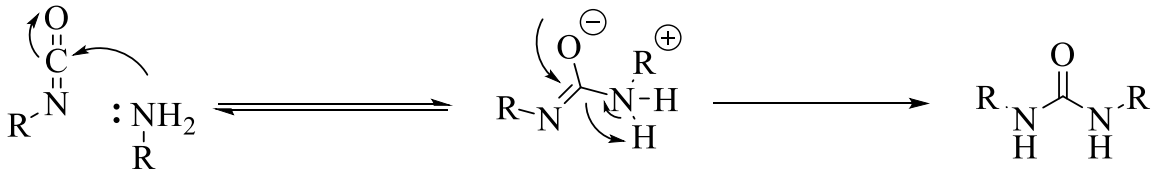

Figure 1.1 Mechanism for urea synthesis.

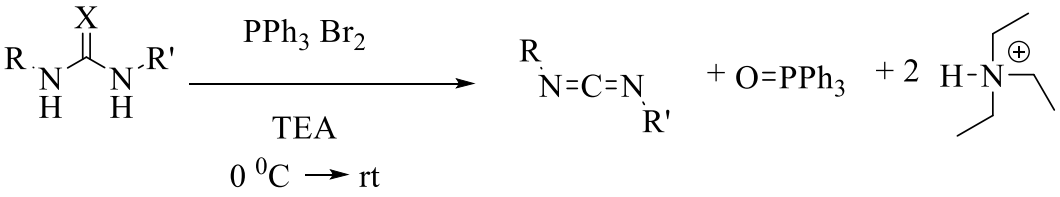

Scheme 1.2 Reaction for dehydration of urea.

Use of PPh_3Br_2 with the acid scavenger of triethylamine are common reagents used for the dehydration reaction to synthesis carbodiimide monomers (**Scheme 1.2**). During the mechanism, triethylaminium bromide salt and triphenylphosphine oxide are formed as by-products and thus purification of carbodiimide monomer involves colum chromatography and reduced pressure distillation for thermally stable forms of carbodiimides (**Figure 1.2**).

Another synthesis route to prepare carbodiimides is through reacting urea or thiourea with phosgene in the presence of a base.[3] The mechanism for this reaction is not well understood yet and it may lead to yield carbodiimides through the formation of a four-membered ring, or formation of choro imide intermediate as shown scheme 1.3. Anderson and co-workers reported the formation of carbodiimides via heterocumulene metathesis by using titanium-imido complex. The formation of the carbodiimide takes place *via* intermediate metallocycles as shown scheme 1.4.

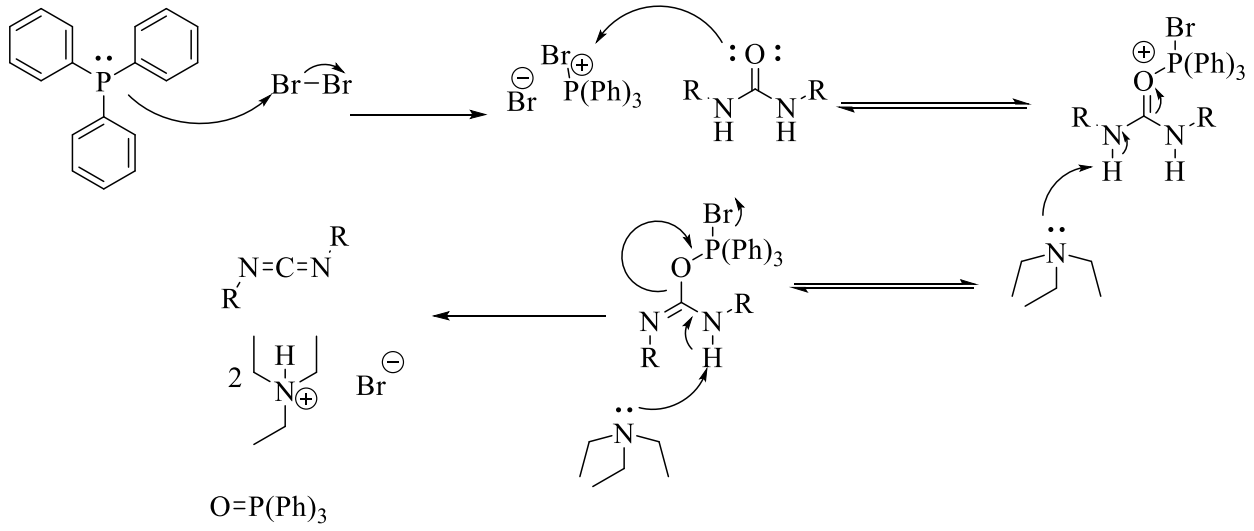

Figure 1.2 Mechanism for the synthesis of carbodiimides.

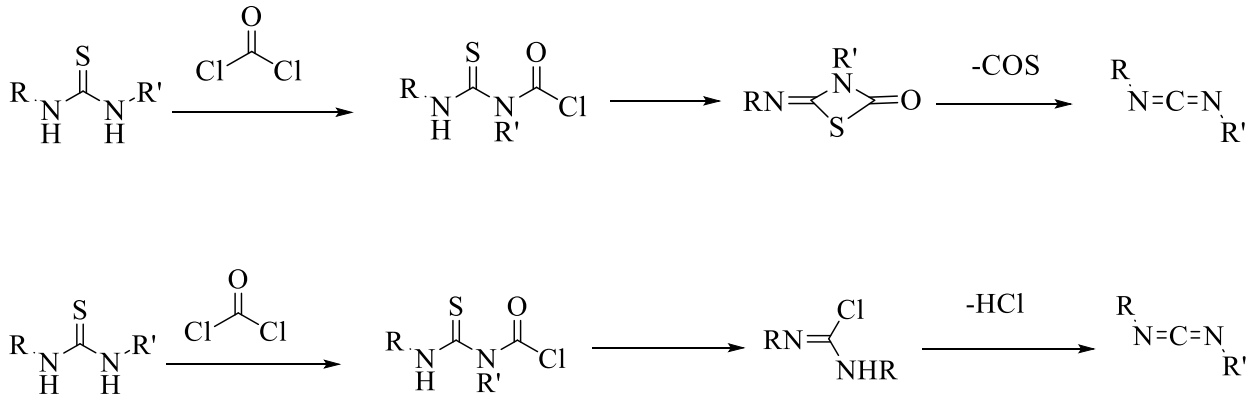

Scheme 1.3 Synthesis of carbodiimide via a chloro-imide intermediate.

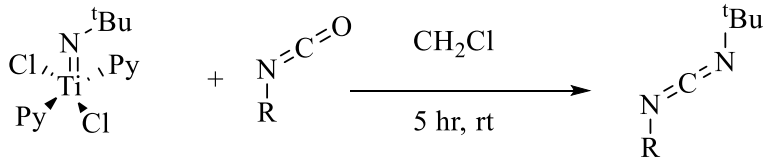

Scheme 1.4 Synthesis of carbodiimide via heterocumulene metathesis.

Hao co-workers reported the synthesis of symmetric and asymmetric functionalized carbodiimides by using I_2/ CHP (Cumene hydroperoxide) mediated cross coupling reaction.[6]

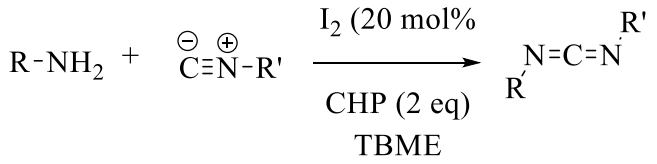

Scheme 1.5 Synthesis of carbodiimide via I_2 mediated cross coupling reaction.

The coupling reaction between isocyanide and primary amines employed the preparation of carbodiimides. The reaction mechanism is initiated upon 1,1-addition of I_2 into isocyanide by forming an intermediate. Through several dehydrohalogenation reactions, it forms carbodiimides in moderate and excellent yield under mild condition (**Scheme 1.5 and Figure 1.3**).

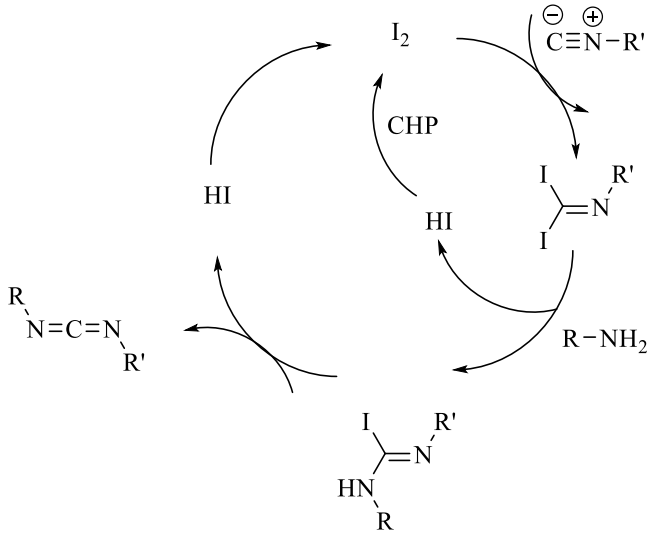

Figure 1.3 Mechanism for the formation of carbodiimide via I_2 mediated cross coupling reaction.

1.2.2 Polymerization of carbodiimides

The first synthetic helical macromolecule was discovered in 1955 when Natta successfully polymerized propylene monomers in a stereoregular fashion to yield highly isotactic polypropylene.[7] Due to the 1,3- steric interactions of adjacent methyl groups, this polymer adopts a helical, semi-crystalline conformation in the solid state as identified by XRD. The helix is an

example of conformational chirality with the two oppositely rotating helices being enantiomers of one another. The *P* or (+) helix rotates clockwise as it proceeds away from the viewer and vice-versa for the *M* or (-) helix. Today, the number of helical polymers has grown tremendously with examples including polyacetylenes,[8,9] polyisocyanate,[10,11] polymethacrylamides[12] and polyisocyanides.[13,14] Polymerization of carbodiimides were discovered by Goodwin and Novak in 1994 with polymerizing carbodiimide monomers with Ti-based initiators.[15] These polymers are composed of nitrogen rich amidine like helical backbone accompanied with two tunable arms per repeat unit. The presence of partial conjugation of the backbone and steric repulsion are induced by pendant groups and these polymers adopt into helical conformations. The 18-mer of the poly(*N*,*N*'-methylcarbodiimide) structure has been optimized by using molecular mechanics and it showed the six monomers involved to make a single helical turn creating a 6/1 helical pitch and corresponding dihedral angle is 60˚ (**Figure 1.4**).[5]

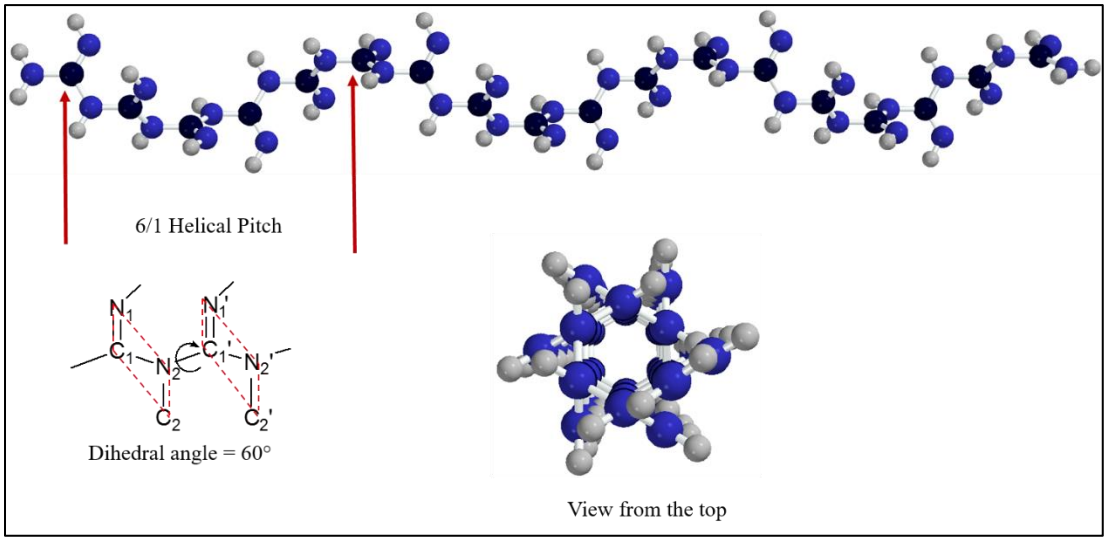

Figure 1.4 Molecular mechanics (at AM1 level) and modeling results of a simple, dimethyl polycarbodiimide backbone reveals a 6/1 helical sense (six repeat units to make one complete helical turn) with a helical pitch of 13.8 Å and a dihedral angle of approximately 60º between repeat units. (Reprinted with permission from reference 5. Copyright 2011 Elsevier).

1.2.3 Initiators

During the past two decades, various types of transition metal mediated catalyst systems including Ti(IV),[16] Cu(I),[17] and Ni(II)[18,19] have been utilized for the successful polymerization of carbodiimides. These initiators have been synthesized by incorporating chiral or achiral ligands. All these initiators have been designed for helix-sense selective polymerization and to make this strategy viable, either chiral monomer with achiral initiators or chiral initiators with achiral monomers can be utilized during the polymerization. Various kinds of ligands can be incorporated into the metal center depending on the chirality or size (steric) and contributors, such as chirality and inductive effect, that would influence the polymerization. More often, either (*R*) or (*S*) BINOL-Ti(IV) are utilized during the polymerization and these Ti(IV) based initiators are sensitive to air and moisture, thus use of an inert environment is essential for handling them. The 1,1'-binaphth-2,2'-ol (BINOL) ligand can be incorporated to the metal center and these ligands possess axial chirality due to the presence of aryl-aryl bridging bonds (**Figure 1.5**). Thus, they exist as two isomeric forms, (*R*) and (*S*). Due to steric reasons, isomerization of this ligand is not possible and this assures the helix-sense selective polymerization of both symmetric and asymmetric achiral carbodiimide monomers successfully.[20-22] Ni(II) initiators are substantially air and moisture stable, assuring synthesis of such catalysts are easier. Almost all Ni based initiators that have been synthesized are achiral, thus, chiral monomers were utilized for polymerization to achieve a helical backbone (**Figure 1.6**).[23] Cu based initiators can also be utilized to polymerization of carbodiimide monomers (**Figure 1.7**). The absence of chiral ligand and the low solubility of the copper salt complexes are some of the drawbacks associate with these initiators.

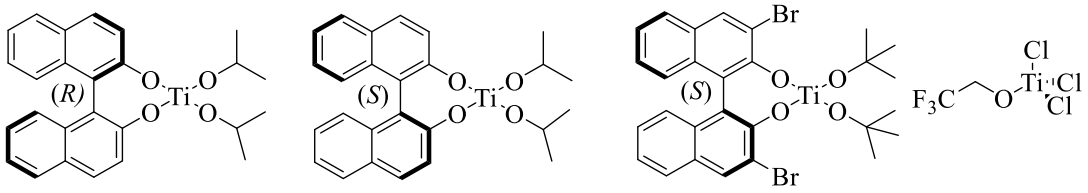

Figure 1.5 Ti(IV) based initiators: **Cat-1**, **Cat-2**, and **Cat-3**, the chiral BINOL ligand has been utilized whereas, in **Cat-4**, alkoxy ligand has been used.

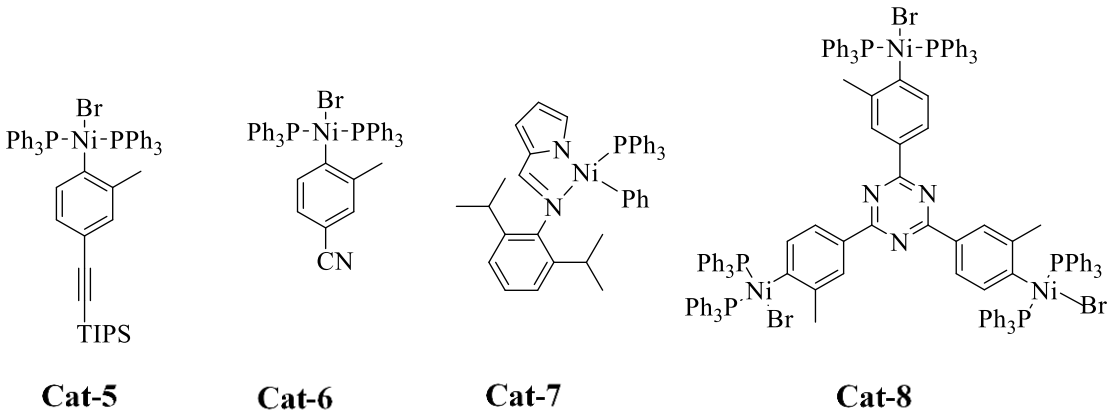

Figure 1.6 Ni(II) based initiators: **Cat-5.6,7** possess single initiator site and **Cat-8** has multiple initiating sites.

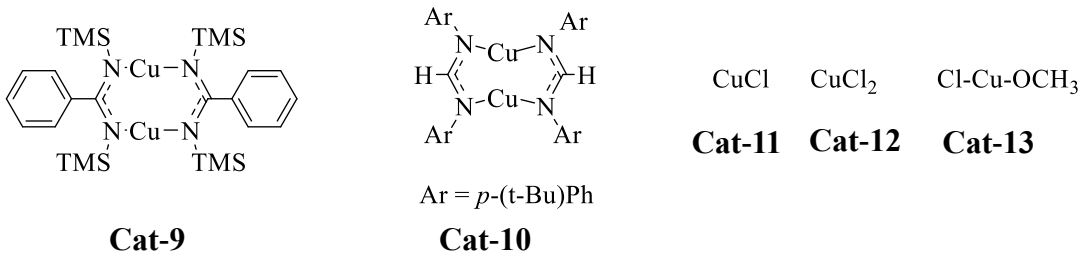

Figure 1.7 Copper based viable initiators for polymerization of carbodiimides.

1.2.4 Monomers

Carbodiimide monomers are synthesized through the dehydration of urea as discussed in section 1.1. The stability of the carbodiimides depends on the side groups attached, while the presence of short alkyl chains and less steric enhance the rate of polymerization (**Figure 1.8**). For instance, with the presence of the methyl group as one of the pendants in a carbodiimide monomer (**Mono-10**), the polymerization takes place in the span of a few minutes, whereas the presence of hexyl chains (**Mono-5**) would increase the polymerization time up to 1-2 days under the same conditions. The presence of aryl pendants would yield the polycarbodiimides with more static helices (**Figures 1.9** and **1.10**)

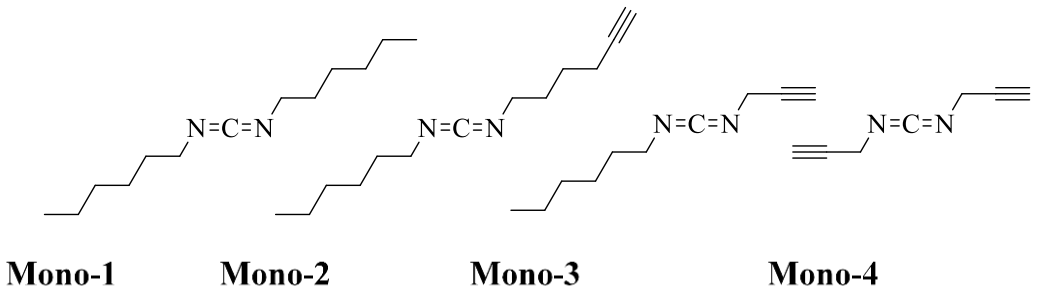

Figure 1.8 Carbodiimide monomers with alkyl chains.

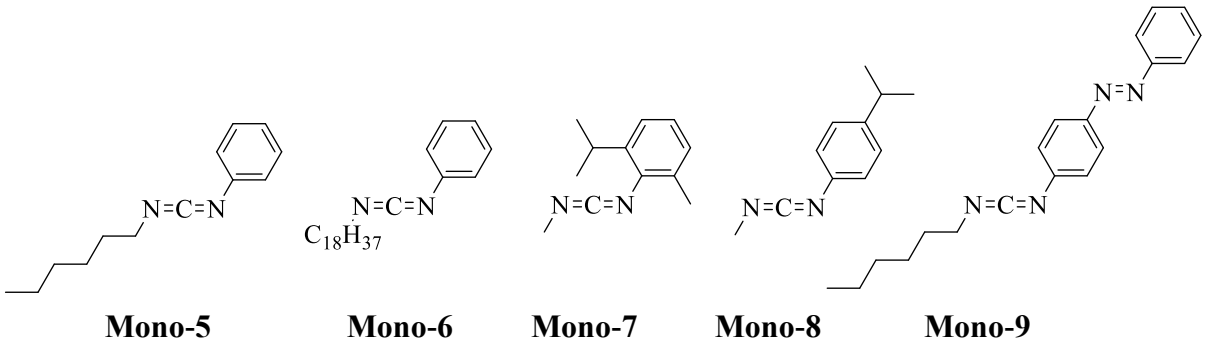

Figure 1.9 Carbodiimide monomers with aryl pendant groups.

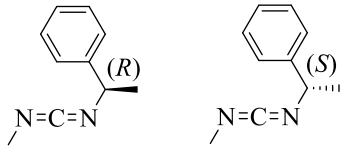

Mono-10 (*R*) **Mono-10 (*S*)**

Figure 1.10 Chiral carbodiimides monomers.

1.2.5 Polymers

To date, Ti(IV) and Ni(II) based transition metal mediated polymerization methods have proven to be more viable in terms of yield and controllability.[19,23] We utilize these initiator systems for screw sense polymerization and it takes place *via* reversible-coordination insertion mechanism (**Figure 1.11**). The polymerization is first initiated upon transfer of ligand into more electrophilic carbon center of carbodiimide by forming a metal-amidinate complex. Sequential insertion of monomer into this metal-N bond will propagate the polymer chain in a living fashion.[5,19] Formation of regioisomers are possible when asymmetric carbodiimide monomers are employed and base on ^{15}N labeling studies, it is conclusive that the polymers are 100% regioregular.[24,25] The relative steric of pendant group determine which position they occupy in and thus the pendant with more steric occupy imine position whereas the least steric group goes to amine position in the helical backbone (**Figures 1.12** and **1.13**). It is important to achieve screw sense polymers for different applications and these applications include synthesis of liquid crystalline materials, formation of self-aggregation assemblies for chiral molecule encapsulation and chiroptical switches. This screw sense can be induced by using chiral initiators with achiral monomers or *vice-versa* during the polymerization. Use of chiral monomers for screw sense polymerization is limited due to viable number of monomers and the cost (**Figure 1.14**).

Therefore, use of achiral monomers with chiral initiators is the feasible way to achive screw sense in polycarbodiimides systems.

1.2.6 Polymerization mechanism

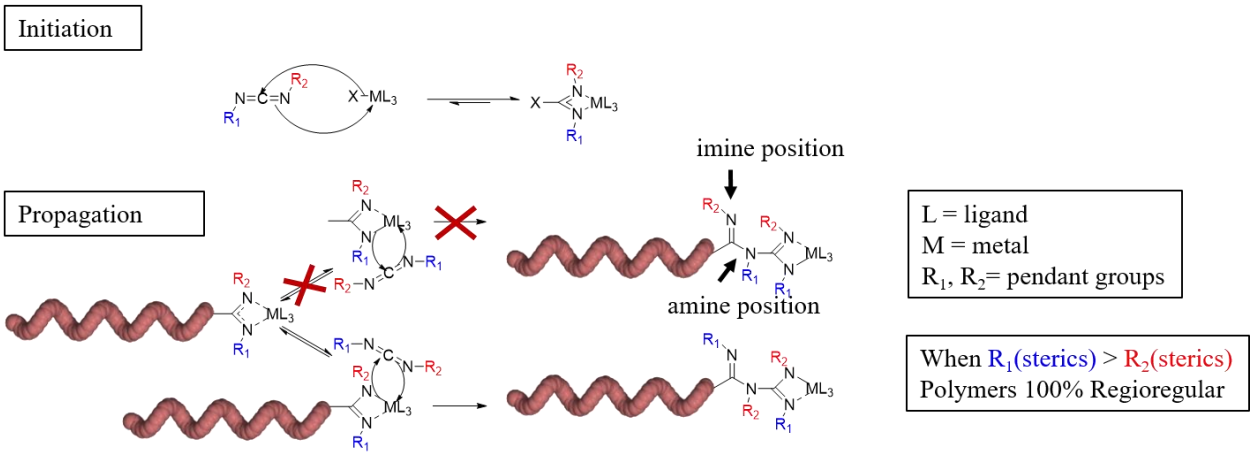

Figure 1.11 Cartoon representing initiation and propagation steps in carbodiimide polymerization.

Most of the initiators employed in carbodiimide polymerization are moisture sensitive, thus, the polymerizations carryout in an inert environment such as inside the glove box.

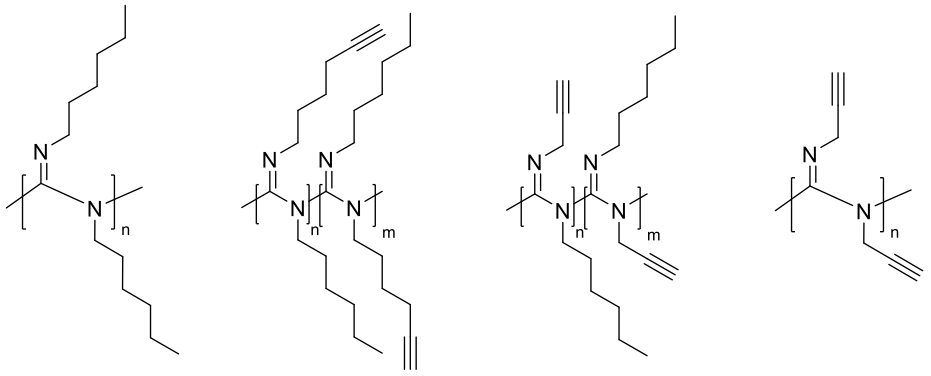

Poly-1 **Poly-2** **Poly-3** **Poly-4**

Figure 1.12 Structure representing polymers with alkyl pendant groups: regioregularity is not significant when less bulky groups (like alkyl chains) are present.

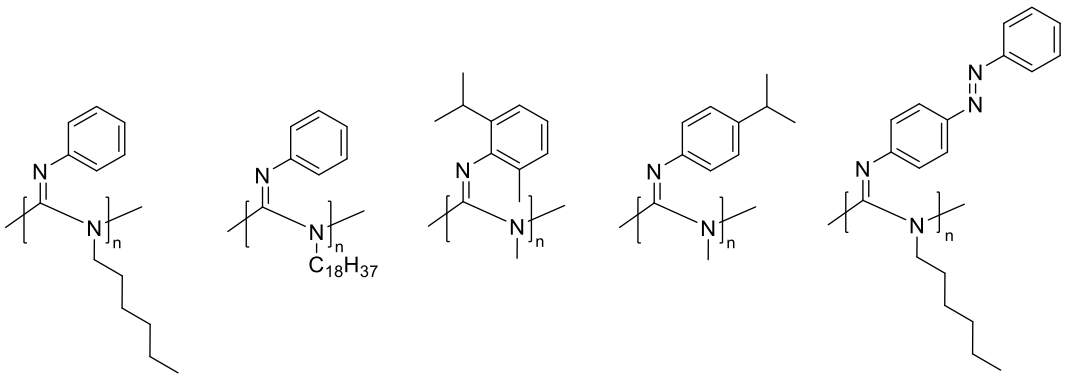

Poly-5 **Poly-6** **Poly-7** **Poly-8** **Poly-9**

Figure 1.13 Regioregular polycarbodiimides; Presence of bulky aryl substituent enhance the regioregularity.

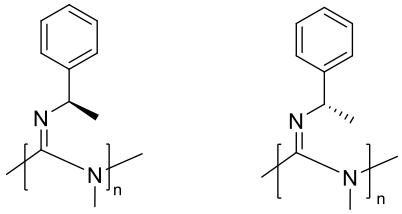

Poly-10 (*R*) **Poly-10 (*S*)**

Figure 1.14 Polycarbodiimides from chiral monomers.

1.3 Helicity of polymers

Helical polymers can be synthesized via helix-sense selective polymerization accompanied by chiral or pro-chiral monomers and/or chiral initiators or chiral monomers along with achiral initiators. Use of achiral monomers with chiral initiators is the most preferred way due to the number of viable monomers and the cost. During the polymerization, the helicity is solely biased by chiral molecule/stimulant and thus the preferred excess helical sense can be obtained which is termed as helical-sense selective polymerization. These right-handed or left-handed complementary helices are mirror images of each other and behave as enantiomers. These chiral

entities are existing as (*M*) or (*P*) helices and they rotate polarized light in opposite directions. Right-handed helices are designated as (*P*) helices (travels away in a clock-wise direction), whereas the left-handed helices are termed as (*M*) helices (travels away in anti-clock-wise direction, **Figure 1.15**).

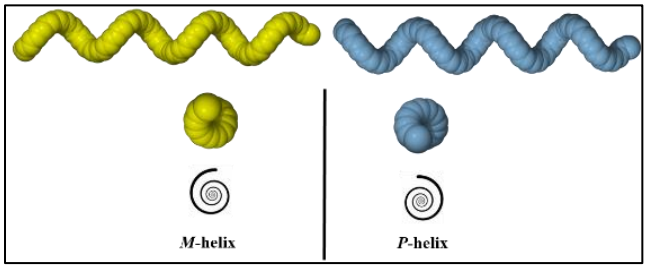

Figure 1.15 Cartoon showing left and right handed screw sense.

Racemic mixtures are composed of 1:1 ratio of both (*P*) and (*M*) helices. The preferred screw sense can be achieved in many ways namely, by using chiral catalyst,[16] chiral stimulant, molecular chaperones and through sergeants-and-soldier effect.[26-29] Helical polymers can be divided into two sub-groups, such as dynamic helices and static helices. The important measure for this classification is based on the helical inversion barrier. The helical inversion barrier energy (E_i) involves the energy required to switch one helical sense into another (**Figure 1.16**). Helical polymers with higher E_i are categorized as static helices, thus possess a large helical sense and higher optical activity (**Figure 1,17**). Polyisocyanides, polymethacrylates, polymethacrylamides, poly(quinoxaline-2-3-diyl)s belong to dynamic helical polymers (**Figure 1.18**). The dynamic helices possess lower E_i and includes polymers such as polysilanes, polyacetylenes, and polyisocyanates. The helical backbone of these polymers is composed of kinked or mobile chains and higher population of helical reversals cause polymers to change particular conformations and contain short persistence length. Particularly in polyisocyanates, the

energy of helical reversal state is around 19 kcal/mol which has been calculated from statistical method.[30]

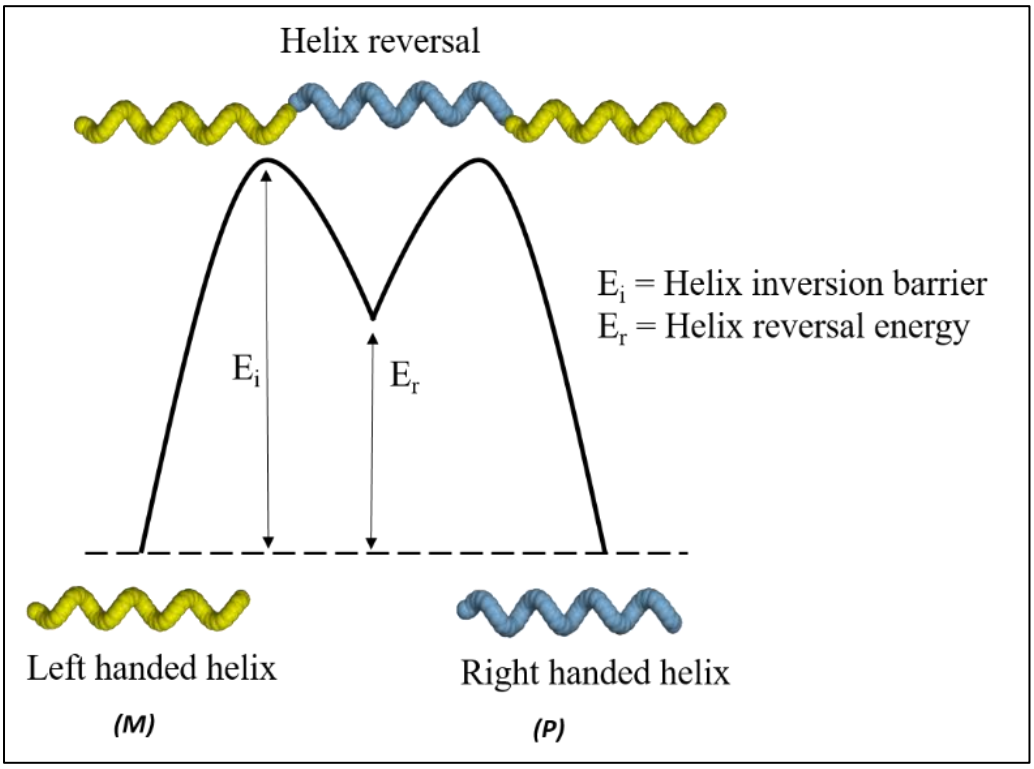

Figure 1.16 Energy diagram for helical polymers; Both (*M*) and (*P*) helices are equal in energy.

1.3.1 Static helical polymers

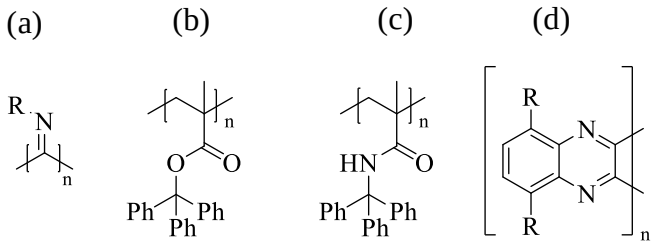

Figure 1.17 Examples for static helical polymers; (a) polyisocyanaides (b) polymethacrylates, (c) polymethacrylamides, (d) poly(quinoxaline-2-3-diyl)s.

1.3.2 Dynamic helical polymers

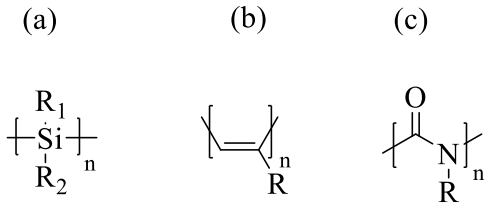

Figure 1.18 Examples for static helical polymers; (a) polysilanes (b) polyacetylenes (c) polyisocyanates.

1.3.3 Helicity induction

The helical backbone of dynamic polymers is composed of helical reversals and their reversals are peculiarities (or defects) present throughout the backbone. These defects move throughout the backbone thus, the presence of chiral stimulants allows the polymer backbone to be biased toward a helical sense. Synthesis strategies which involve chiral amplification were first applied for polyisocyanates with 1% of chiral isocyanate monomers by Green and co-workers.[31,32] The presence of minute chiral 'sergeant' bias the screw sense by receiving high cooperativity from an achiral 'soldier'. The helicity of the macromolecules can be successfully controlled by using the monomers with a chiral center during the polymerization. The polymer retains its preferred handedness even though the ratio of chiral:achiral monomer was lowered from 100:0 to 15:85. Interestingly when the chiral stimulant is present as low as 0.5 %, the chiral induction also takes place (**Figure 1.19-right**). Another way to achieve this excess helical sense by using a slight enantiomeric excess of chiral monomers, commonly referred to as the majority effect (**Figure 1.19-left**). This synthesis methodology is viable when the enantiomeric excess of one monomer over its enantiomer is around 12%.[33]

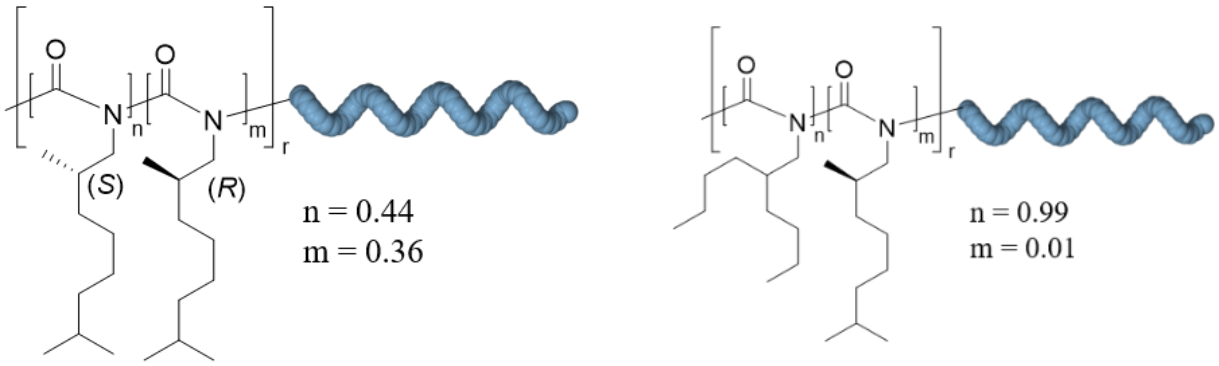

Figure 1.19 Left - Sergeant and soldier effect; chiral amplification occurs with less than 1% of chiral stimulant, right - majority rule; slight excess of enantiomeric stimulant induces the screw sense.

Another interesting way to amplify chirality is by using chiral guest molecules through non-covalent or ionic interactions (**Figure 1.20**). Due to the dynamic nature of polyphenylacetylenes, the preferred helicity can be induced *via* adding 'molecular chaperones' such as chiral amines or chiral acids.[34] These small chiral entities can bind on monomers or on the helical backbone to perturbate helicity.

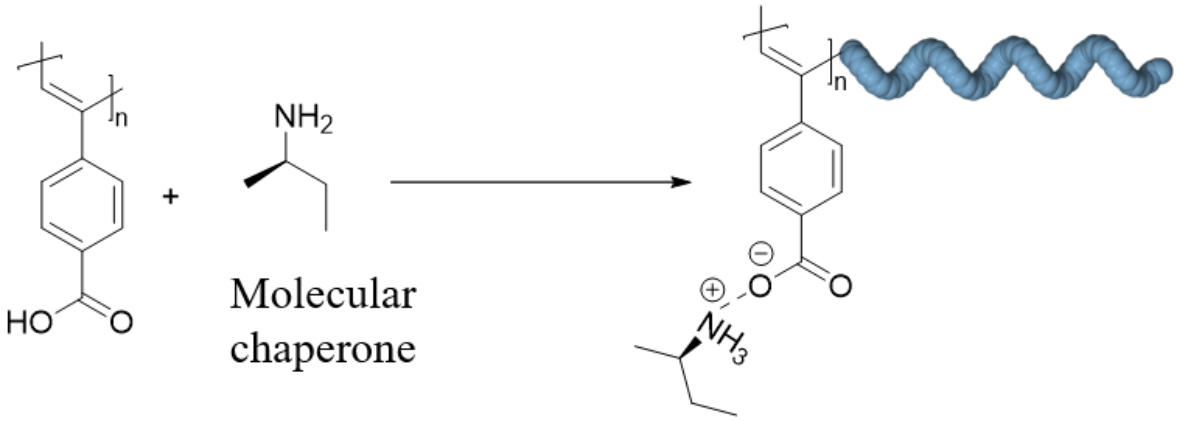

Figure 1.20 Helicity induction by a small chiral guest amine.

1.4 Synthesis of different chiral polymeric architectures

1.4.1 Ligation of small molecules into helical backbone

To date, various kinds of helical polycarbodiimide homo-polymers have been synthesized bearing aliphatic or aromatic pendant scaffolds appending around helical-rigid backbone. The presence of a rigid-helical amidine backbone along with two tunable pendant groups for each monomer, these polymers offer a more robust nature for diverse post-polymerization modifications with end-functionalities or pendant scaffolds and chemistries involved with 'click' (CuAAC) reaction, Huisgen 1,3-dipolar cycloaddition reaction, Sonogashira coupling reaction, to name few. This offers the accessibility of fine tuning the polymer backbone's hydrophobicity, the degree of backbone stiffness and assure the synthesis of polymer-peptide/drug conjugates. Novak and co-workers have successfully synthesized various functional polycarbodiimides through the ligation of small molecules (**Scheme 1.6**). The synthesis strategy they have utilized here is click chemistry[35-37] and Sonogashira cross coupling reactions.[38] By incorporating alkyne functionalized aliphatic and aromatic scaffolds into the helical backbone, it provides a more robust nature for clickable azide functionalized small molecules of benzyl azides, acid azides and small peptides. [39]

Further, they have developed a synthesis strategy by incorporating propargyl chains into the helical backbone and this provides two clickable hands per repeat unit by enhancing the functionality (**Scheme 1.7**). This grafting strategy is a powerful tool in the synthesis of new polymer-peptide or polymer-drug conjugates as well as new coupling sites for peptides with carboxylic acid functionalities for various biomedical applications.

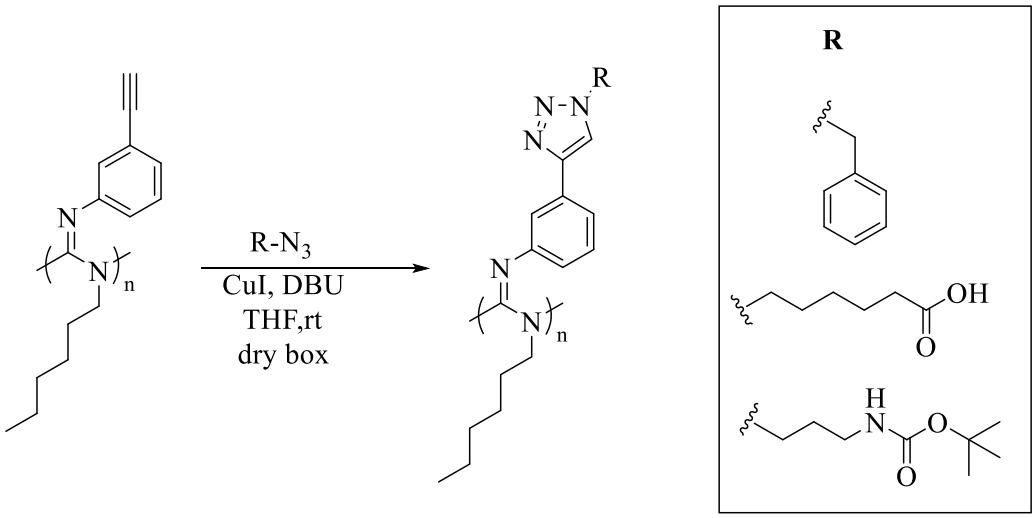

Scheme 1.6 Ligation of small azide functionalized molecules into helical polycarbodiimide backbone by using click reaction.

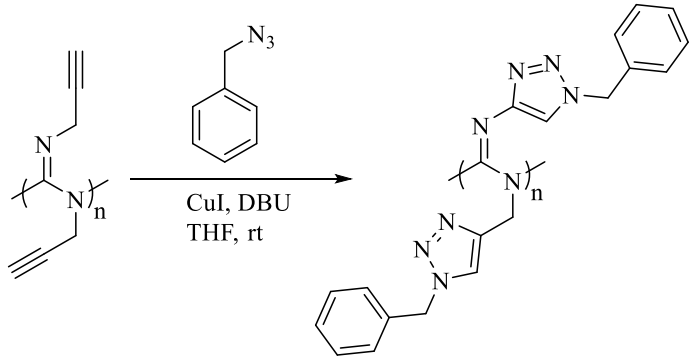

Scheme 1.7 Ligation of azide functionalized small molecules into both alkyne functionalized end of pendant groups in the helical backbone.

1.4.2 Synthesis of end functionalized carbodiimides and synthesis of block co-polymers

Polymerization of carbodiimides is taking place through the reversible coordination-insertion mechanism. Upon transfer of specific/modifiable ligand from initiator to electrophilic carbon center of carbodiimides initiate the polymerization by forming an amidinate complex. Though the propagation of the polymer chain, this modifiable ligand will be the end functionality of the

polymer chain. This synthesis strategy provides many opportunities for block co-polymer synthesis. In this regard, Reuther, Novak and co-workers have developed Ni(II) based initiators for polymerization of carbodiimides.[18] These Ni(II) based initiators are substantially air and moisture stable and involved in living polymerization controllable fashion by providing specific end functionality into the homopolymer. This approach would provide more facile incorporation of random-coil block into rigid-rod helical block by opening new polymer architecture which imparts new intriguing properties, such as liquid crystallinity, self-assembly into divers amphiphilic, microstructures.[40]

1.4.3 Synthesis of Ni(II) Initiators

In the presence of specific aryl bromide (the ligand), bis(1,5-cyclooctadiene) nickel (0) undergoes oxidative addition onto the aryl ligand by forming a square complex and it bears the active site for the polymerization of carbodiimide monomers (**Scheme 1.8**). For many applications, it is important to bias the helicity of polymers and it has been achieved successfully by using these achiral initiators with chiral *N*-phenethyl-*N*'-methyl carbodiimides monomer. The polymerization takes place *via* a reversible coordination-insertion mechanism in a controllable living fashion as evident by kinetics studies.[19,40] Interestingly, these studies also proved that the polymerization leads to the formation of specific helical sense. Because these enantiomeric monomers of *N*-phenethyl-*N*'-methylcarbodiimide (PEMC) have been polymerized with this **Cat-5,6,7**, the specific optical rotation for resulting polymers was in oppositely signed. This implies that the chirality of the polymer is governed by the helicity of the backbone instead of the chirality biasing from the chiral center of appended pendant group.

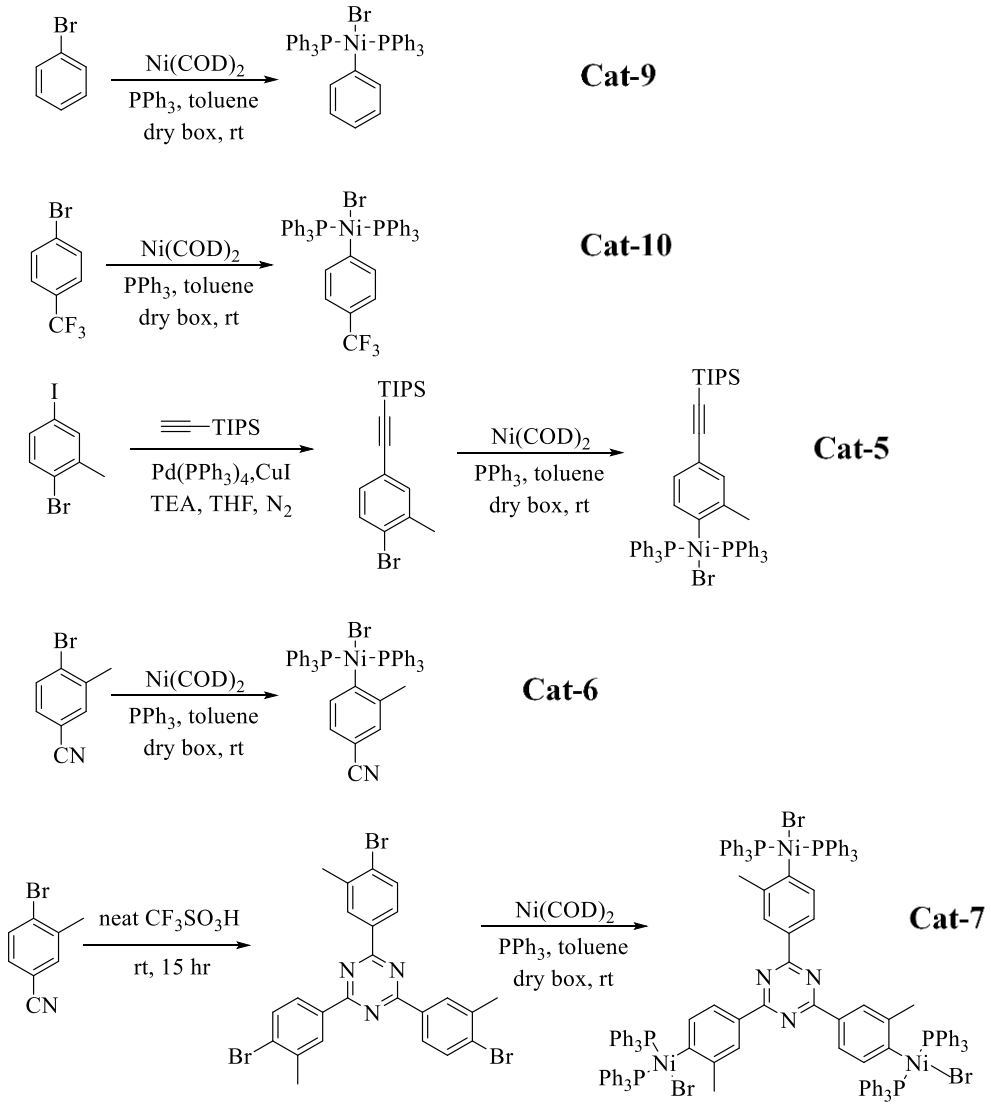

Scheme 1.8 Ni(II) based functional initiators for polymerization of carbodiimides.

1.4.4 Block co-polymer Synthesis

Newly developed synthesis strategies can be utilized to incorporate random-coil polymer segments into helical scaffolds through post-polymerization modifications. By incorporating second chemically diverse segments, these macromolecular architectures show novel properties like liquid crystallinity, self-assembly behavior *via* microphase separation. During the past five

years, we developed controlled, chiral polymer architectures for rigid helical rod-random coil block polymer as they show self-assembly phenomena in a different solvent. Implications of this technique extend towards using rigid-helical polycarbodiimides scaffolds as potential nanocarriers in many applications such as drug delivery and catalysis. Taking advantages of end-functionalization, enantiomeric *N*-phenethyl-*N*'-methylcarbodiimide monomers have been polymerized with TIPS-protected alkyne end functional Ni(II) initiator (**cat**-**5**). Through post-polymerization modification, azide functionalized polystyrene and polyethylene glycol have been clicked on to yield a triazole ring to form a rigid helical rod random-coil block co-polymer (**Scheme 1.9**). Further, tri-block co-polymers have been synthesized by using di-azide functionalized PEG polymers using the same synthesis strategy.[41] These amphiphilic block co-polymers self-assembled into diverse nano-structures including micelles, vesicles, maggot-like structures simply upon altering the solvent.[40]

1.4.5 Graft co-polymers

These offer new opportunities for post-polymerization modifications for the synthesis of graft co-polymers using 'graft from' strategy. Kulikov et al. reported the synthesis of graft co-polymers from (*R*) and (*S*) families of polycarbodiimides.[42] In this strategy, they utilized click chemistry as the post-polymerization modification. First, the *meta*-alkyne functionalized phenyl ring was incorporated into the helical backbone through random co-polymerization of *N*-ethynylphenyl-*N*'-hexylcarbodiimide and *N*-phenyl-*N'*-hexylcarbodiimide. Next, the azide functionalized tertiary alkyl bromide initiator was clicked into the alkyne functionality to create an initiating site for atom transfer radical polymerization of (ATRP) of styrene (**Scheme 1.10**).

This creates graft co-polymers by extending random coil polystyrene chains away from polycarbodiimide helical backbone.

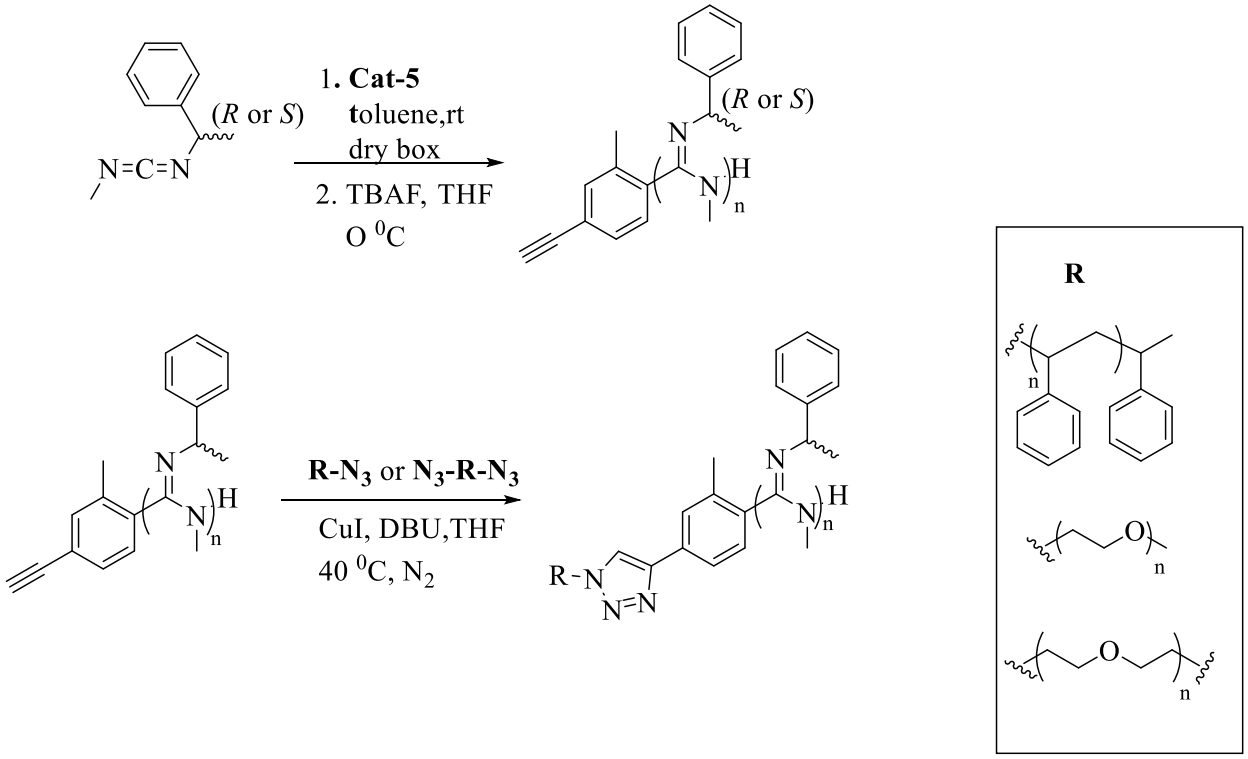

Scheme 1.9 Synthesis of alkyne end-functionalized polycarbodiimides and synthesis of block co-polymers via click reaction.

As reported in Reuther et al, graft co-polymers have been synthesized which composed of rigid-random backbone of bromo-polystyrene. Multiple initiating sites have been created *in situ* along the polymer chain and each initiating site will initiate to grow a polycarbodiimide chain. In this graft co-polymer architecture, helical arms are growing from the poly bromostyrene backbone.[18] Self-assembly behavior has been studied for these polymers by using AFM imaging technique (**Scheme 1.11**).

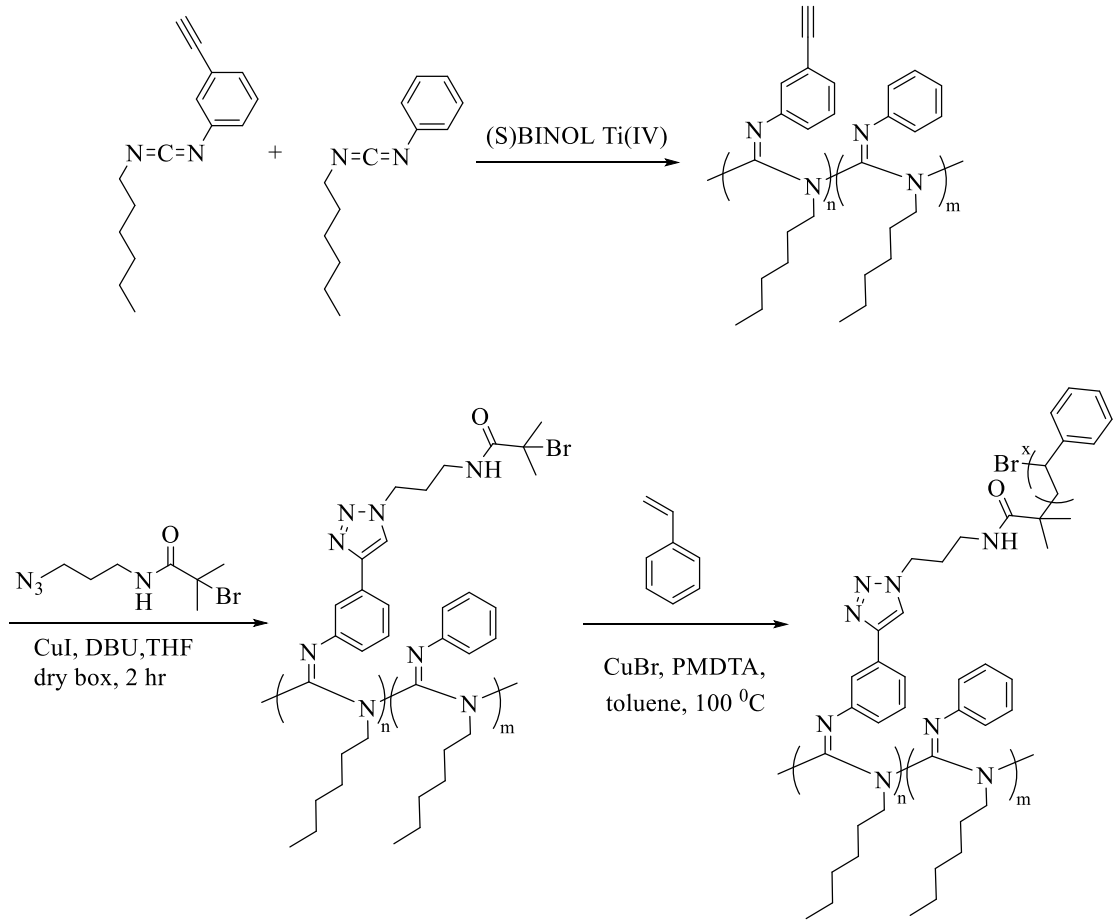

Scheme 1.10 Synthesis of random co-polymers and synthesis of graft co-polymers.

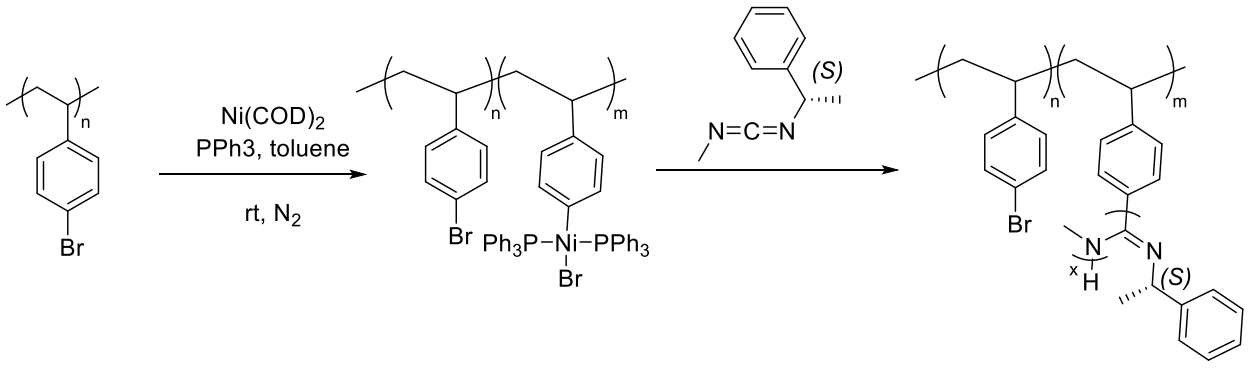

Scheme 1.11 Synthesis of macro initiator and synthesis of graft co-polymer; graft from synthesis strategy.

1.4.6 Multi-arm star polymers

Star polymer architecture attract attention among polymer chemists due to its facile synthesis, a high degree of functionality and unique self-assembly behavior. To achieve multi-arm star polymers, both core first strategy or arm first method can be employed. In this regard, we attempted the arm first method by synthesizing nitrile end-functionalized poly *N*-phenethyl-*N*'-methylcarbodiimide by using **Cat-6**. Trimerization reaction of nitrile group was utilized in the presence of neat CF_3SO_3H acid and the reaction was not successful due to the repulsion of protonated amidine backbone in this polymer system Then in our growth in strategy, the core-first method was employed and the initiator was specifically designed by incorporating multiple initiating sites. Using chiral PEMC monomer, radial, helical, rigid rod-arms were growing from the core in a living fashion by yielding a multi-arm star polymer (**Scheme 1.12**).[19]

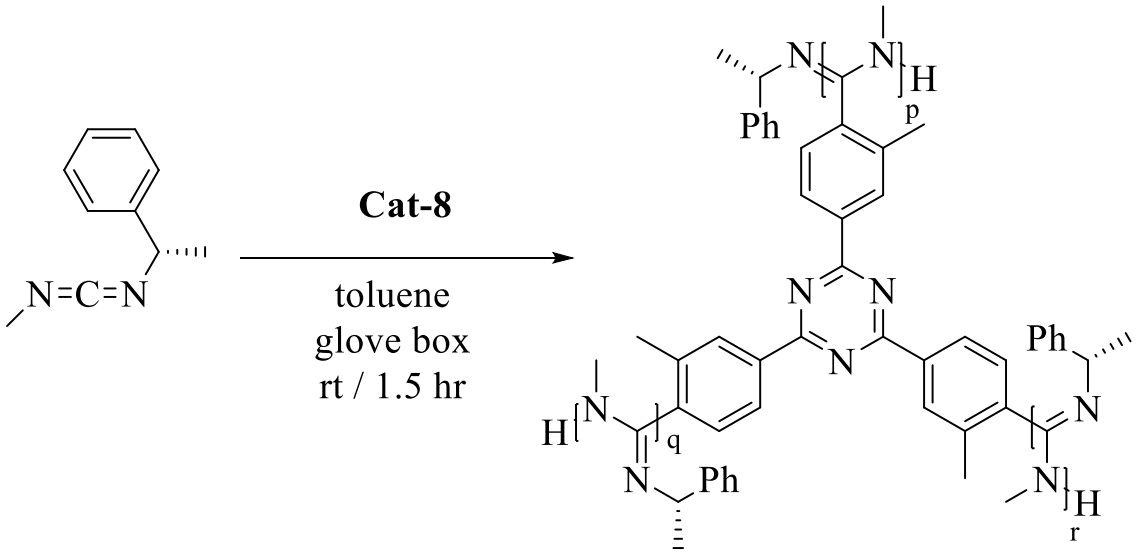

Scheme 1.12 Synthesis of the three-arm star polymer.

1.5 Properties of polycarbodiimides

1.5.1 Chiroptical switching behavior

The effect of aromatic systems attached to carbodiimide backbone represents a unique behavior derived from aromatic π-based interactions and it plays a vital role in many applications. These systems may be involved in structural stability and switching phenomena. By utilizing this chemistry, different types of polyarene pendant groups have been introduced on polycarbodiimide helical backbone and several investigations have been performed towards chiroptical switching behavior. Very interestingly, temperature and solvent tunable reversible chiroptical switching behavior have been observed for some polymers.[43,44] It was explored that the specific optical rotation was dramatically changed in terms of magnitude and sign upon changes in solvent polarity and temperature, for instance, poly(*N*-anthracene-*N*'-octadecyl)carbodiimide, which has been obtained from helix-sense selective polymerization of chiral dibromo-BINOL-Ti(IV)-di-*tert*-butoxide catalyst with *N*-anthracene-*N'*-octadecyl)carbodiimide monomer. The optical rotation changed by approximately 500˚ with a sign upon thermal annealing, between 30 ˚C - 45 ˚C in toluene. This process was observed to be reversible and it was hypothesized that it was taking place via conformational changes. In the presence of aromatic pendants, this polymer should possess the high energy of inversion. Upon dissolving this polymer in chloroform and THF, the high negative value of SOR and strong ECD cotton effects were observed but switching behavior was not exhibited as a function of temperature. VCD analysis concluded that the backbone inversion was not possible as the imine stretch around 1641 cm^{-1} did not show any changes. Later, it was figured out that the two distinct orientation of anthracene groups takes place which is different in energy as evident by computer

modeling data. These two distinct orientations induce the changes in conformation that evolved from dipole moment. In polar solvents, like $CHCl_3$ and THF, the conformation with the higher dipole moment will be stabilized without switching phenomena (**Figure 1.21**).

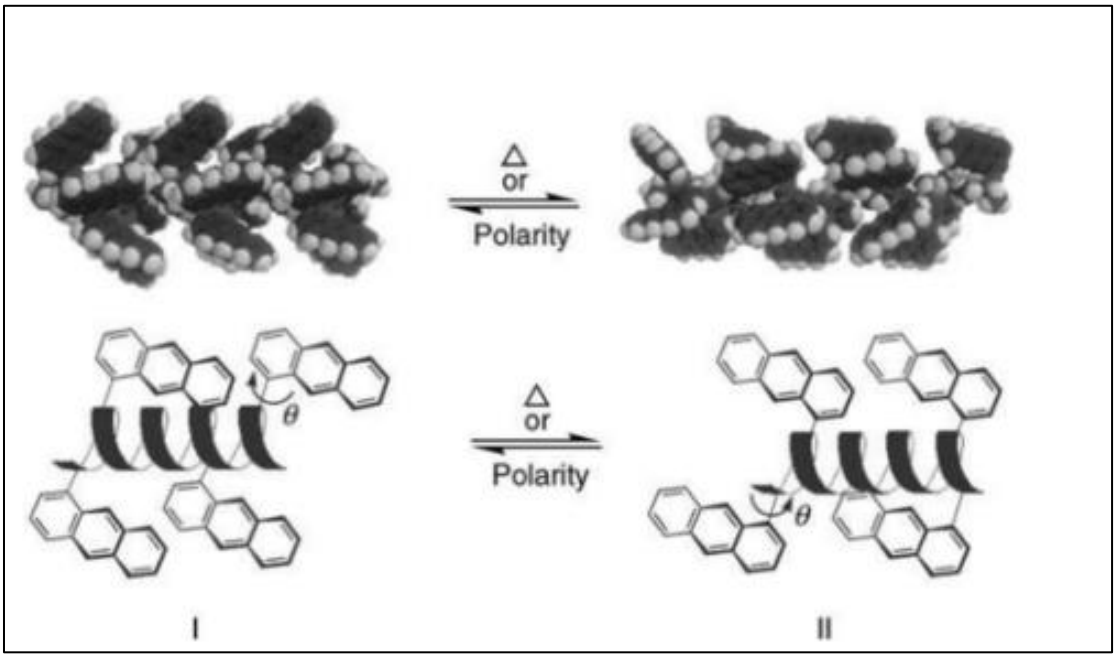

Figure 1.21 Two distinct molecular states showed by poly(*N*-anthracene-*N*'-octadecyl)carbodiimide; shutter-like motion displayed by anthracene pendant groups. (Reprinted with permission from reference. 20. Copyright 2005 John Wiley & Sons Inc.).

Another chiroptical switching behavior is shown by poly(*N*-naphthyl-*N*'-octadecyl)carbodiimide and the switching behavior observed dependent upon temperature and solvent. The reversible changes in SOR from positive to negative values have occurred upon changing the temperature and solvent. Changes in the two distinct imine stretch at 1621 cm^{-1} and 1640 cm^{-1} were seen by performing IR and VCD experiments. VCD spectroscopy and DFT calculations suggested that this particular polymer undergoes the helical switching process by yielding two conformations through the expansion (5/1) and contraction (7/2) of the helical pitch, which is shown below

(**Figure 1.22**).[45] The discovery of the chiroptical switching behavior possesses great potential in the advancement of chiral sensors, optics, and storage technologies.

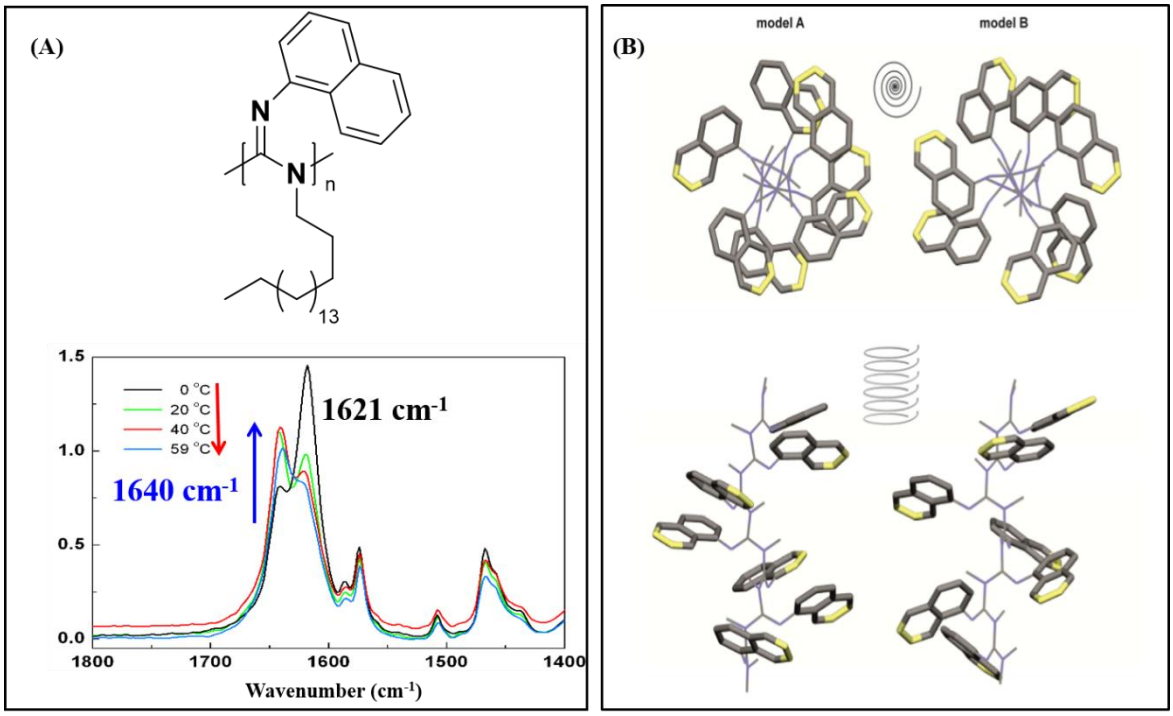

Figure 1.22 (A) PNOC showing two distinct imine stretches in VCD; (B) 7- mer model for (*R*)-PNOC showing right handed helicity and oppositely oriented naphthyl pendant groups. (Reprinted with permission from reference 43. Copyright 2014 Royal Society of Chemistry).

1.5.2 Liquid crystalline behavior

Due to the presence of helicity and rigid-rod like nature, polycarbodiimides can adopt into specific phases in the lyotropic state, termed as liquid crystallinity.[46,13] Liquid crystallinity emerges as a powerful tool for many applications which involves optics, electronics, and sensors, etc. It is a mesophase character which exists in between solid and isotropic liquid. As polycarbodiimides adopt into its helical arrangement, these motifs naturally rearranged into a

specific long range order induced by different solvents. These orientational orders include cholesteric, nematic and smectic phases. When these crystallites possess both positional and directional order, it is called smectic mesophase. Depending on the arrangement of adjacent layers of crystallites, these can be further categorized into smectic A, smectic B, and smectic C. In nematic phase, the polymer is aligned in a particular direction without positional order. As reported by Kim and co-workers, poly(*N*,*N*'-dihexylcarbodiimides) adopt into an ordered smectic mesophase with the positional order as evident by small angle-XRD analysis.[47] By substituting hexyl chains with dodecyl aliphatic chains (*i.e.*, poly(*N*,*N*'-didodecylcarbodiimides)), it showed more ordered smectic phase both in solution and melt (**Figure 1.23**). By using SA-XRD (Small Angle X-Ray Diffraction) and POM (Polarized Optical Microscope) studies, liquid crystalline behavior has been investigated in **poly-1, 10, 11,** and **12,** implying that they adopt into more ordered smectic mesophase. When the polymer is composed of chiral pendant group of phenethyl-methyl (**Poly-10 (*R*/*S*)**), it forms a chiral nematic mesophase, whereas the racemic polymer shows a nematic mesophase when racemic pendant groups are present. Depending on the temperature some macromolecules show crystalline phases and it is called thermotropic behavior. Thermotropic mesophase is not a common phenomenon in polycarbodiimides as the polymer degrades around 150˚C. The presence of long aliphatic scaffolds contributes to an increase in the degradation temperature of polycarbodiimides and it induces these polymers to exhibit thermotropic behavior. **Poly-12** shows thermotropic behavior and it forms a smectic mesophase around 130 ˚C as evident by X-ray diffraction analysis. By altering pendant groups which can interdigitate with adjacent polymer domains would lead for ordered packing thus, such polymer systems possess potential as novel crystalline materials.

Poly-11 **Poly-12**

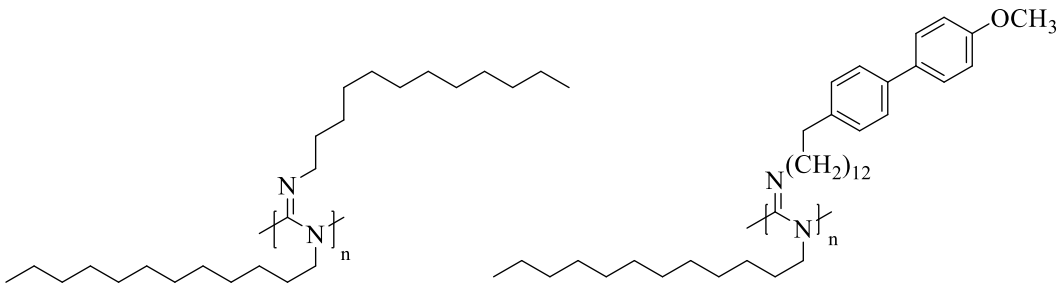

Figure 1.23 Examples of polymers for lyotropic behavior.

1.5.3 Self-assembly behavior

Nano-scale morphologies, derived from different rigid-rod, random-coil polycarbodiimide assemblies, have been investigated by using DLS, TM-AFM, SEM, and TEM techniques. The immiscibility of these two chemically distinct segments induce self-aggregation into nano-scale morphologies upon changing the solvent and the sample concentrations. Kulikov et al. Reported that the synthesis of graft co-polymers, composed of polystyrene random coil segments, forms nano-rings, 'craters', and spherical particles, investigated by changing the solvents and concentration. In these assemblies, polycarbodiimides form globular domains due to the influence of hydrophobic interactions caused by polystyrene side chains.[42] Reuther, Novak and co-workers have synthesized graft co-polymers by using PC and bromo-styrene and examined thin film morphology exhibiting nanofiber domains.[41] The average diameter of this type of assembly was around 171 nm and these are typical for conjugated co-polymers and oligomers. Further, they have inspected different families of (*R*) and (*S*) grafted polycarbodiimides, showing that these polymer families have self-aggregated into densely packed curly, fiber architectures. Upon thermal annealing at 76 ˚C, they form long fibular, randomly looped, or worm-like and ribbon nano assemblies. It is hypothesized that thermal annealing facilitates reaching thermal

equilibrium. These self-aggregation behaviors associate with interdigitation of n-hexyl side chains and aliphatic side chains influence on hydrophobic interactions. This controls the self-aggregation behavior.

Reuther, Novak and co-workers have studied self-aggregation behavior of di- and tri-block amphiphilic co-polymers of PC.[40] These studies are mainly performed in binary solvent systems and nano-worm and nano-maggot assemblies have been observed in THF-MeOH solvent combo. By making polymer blends with high molecular weight PC of *N*-phenethyl-*N*'-methylcarbodiimides with these amphiphilic block co-polymers, long interconnected nano-fibers have been observed. By switching solvent combo from THF-MeOH to THF-25% in EtOH, formation of defined super-helical structures has been observed with *R*-*R* and *S*-*S* homopolymer-copolymer blends.

Siriwardane et al. has reported self-assembly behavior of three arm-star polymer with respect to linear analogues of the star polymer by using AFM and DLS techniques. In solvent systems, such as chloroform, THF and toluene, adopted into fiber morphology, regardless the architecture. In solvent combinations like THF: 25% EtOH, super helical structure formation has been observed. Based on DLS studies, it was revealed that star architecture adopts into more compact architecture than its linear analogs in solution state.[19]

1.5.4 Miscellaneous applications in bio-medical field

Nitrogen-rich, rigid-rod nature of polycarbodiimide polymers emerge interesting ways to modify *via* post-polymerization modifications and orthogonal functionalization.[48,49] This provides more opportunities to conjugate biologically important motifs like guanidines, amino acids, carboxylic acids and hydrophilic polymers to create different therapeutics which have potentials in the

biomedical field. Different architectures of these polymer systems adopt in to diverse self-assemblies including super-helical structures, spherical aggregates, maggot-like assemblies and micellar domains. These nanocarriers show potential to encapsulate hydrophobic drugs like Doxorubicin and such nano-domains can be utilized in various applications as drug delivery agents, as well as, miniature entrapment agents for various applications.

1.6 References

(1) Vincent, A. T.; Wheatley, P. J. Crystal Structure of Bis-P-Nitrophenylcarbodi-Imide, O2N.C6H4.N:C:N.C6H4.NO2. *J. Chem. Soc. Perkin Trans. 2* **1972**, No. 11, 1567–1571 DOI: 10.1039/P29720001567.

(2) Ulrich, H.; Richter, R.; Tucker, B. [2 + 2] Cycloaddition Reactions of Unsymmetrically Substituted Carbodiimides. *J. Heterocycl. Chem.* **1987**, *24* (4), 1121–1123 DOI: 10.1002/jhet.5570240438.

(3) Williams, A.; Ibrahim, I. T. Carbodiimide Chemistry: Recent Advances. *Chem. Rev.* **1981**, *81* (6), 589–636 DOI: 10.1021/cr00046a004.

(4) Merrifield, R. B. Solid Phase Synthesis (Nobel Lecture). *Angew. Chemie Int. Ed. English* **1985**, *24* (10), 799–810 DOI: 10.1002/anie.198507993.

(5) Kennemur, J. G.; Novak, B. M. Advances in Polycarbodiimide Chemistry. *Polymer (Guildf).* **2011**, *52* (8), 1693–1710 DOI: 10.1016/j.polymer.2011.02.040.

(6) Zhu, T.-H.; Wang, S.-Y.; Tao, Y.-Q.; Ji, S.-J. Synthesis of Carbodiimides by I2/CHP-Mediated Cross-Coupling Reaction of Isocyanides with Amines under Metal-Free Conditions. *Org. Lett.* **2015**, *17* (8), 1974–1977 DOI: 10.1021/acs.orglett.5b00722.

(7) Natta, G.; Pino, P.; Corradini, P.; Danusso, F.; Mantica, E.; Mazzanti, G.; Moraglio, G. CRYSTALLINE HIGH POLYMERS OF α-OLEFINS. *J. Am. Chem. Soc.* **1955**, *77* (6), 1708–1710 DOI: 10.1021/ja01611a109.

(8) Maeda, K.; Wakasone, S.; Shimomura, K.; Ikai, T.; Kanoh, S. Chiral Amplification in Polymer Brushes Consisting of Dynamic Helical Polymer Chains through the Long-Range Communication of Stereochemical Information. *Macromolecules* **2014**, *47* (19), 6540–6546 DOI: 10.1021/ma501612e.

(9) Ohsawa, S.; Sakurai, S.; Nagai, K.; Banno, M.; Maeda, K.; Kumaki, J.; Yashima, E. Hierarchical Amplification of Macromolecular Helicity of Dynamic Helical Poly(phenylacetylene)s Composed of Chiral and Achiral Phenylacetylenes in Dilute Solution, Liquid Crystal, and Two-Dimensional Crystal. *J. Am. Chem. Soc.* **2011**, *133* (1), 108–114 DOI: 10.1021/ja1087453.

(10) Lifson, S.; Green, M. M.; Andreola, C.; Peterson, N. C. Macromolecular Stereochemistry: Helical Sense Preference in Optically Active Polyisocyanates. Amplification of a Conformational Equilibrium Deuterium Isotope Effect. *J. Am. Chem. Soc.* **1989**, *111* (24), 8850–8858 DOI: 10.1021/ja00206a013.

(11) Green, M. M.; Khatri, C. A.; Reidy, M. P.; Levon, K. Dilute-Solution Chiral Optical Changes Signal the Thermally Reversible Gelation of Poly(n-Hexyl Isocyanate) in Hydrocarbon Solvents. *Macromolecules* **1993**, *26* (17), 4723–4725 DOI: 10.1021/ma00069a050.

(12) Titkova, L. V; Prokopová, E.; Sedláček, B.; Petrus, V.; Dušek, K.; Bohdanecký, M. Solution Properties of Poly(methacrylamide). *Eur. Polym. J.* **1978**, *14* (2), 145–149 DOI: http://dx.doi.org/10.1016/0014-3057(78)90079-4.

(13) Kajitani, T.; Onouchi, H.; Sakurai, S.; Nagai, K.; Okoshi, K.; Onitsuka, K.; Yashima, E. Latticelike Smectic Liquid Crystal Phase in a Rigid-Rod Helical Polyisocyanide with Mesogenic Pendants. *J. Am. Chem. Soc.* **2011**, *133* (24), 9156–9159 DOI: 10.1021/ja201133d.

(14) Jiang, Z.-Q.; Xue, Y.-X.; Chen, J.-L.; Yu, Z.-P.; Liu, N.; Yin, J.; Zhu, Y.-Y.; Wu, Z.-Q. One-Pot Synthesis of Brush Copolymers Bearing Stereoregular Helical Polyisocyanides as Side Chains through Tandem Catalysis. *Macromolecules* **2015**, *48* (1), 81–89 DOI: 10.1021/ma502283f.

(15) Goodwin, A.; Novak, B. M. Synthesis of New Rigid Rod Helical Polymers through the Living Polymerization of Carbodiimides Using Titanium(IV) Complexes. *Macromolecules* **1994**, *27* (19), 5520–5522 DOI: 10.1021/ma00097a037.

(16) Tian, G.; Lu, Y.; Novak, B. M. Helix-Sense Selective Polymerization of Carbodiimides: Building Permanently Optically Active Polymers from Achiral Monomers. *J. Am. Chem. Soc.* **2004**, *126* (13), 4082–4083 DOI: 10.1021/ja049548m.

(17) Shibayama, K.; Seidel, S. W.; Novak, B. M. Living Polymerization of Carbodiimides Initiated by Copper(I) and Copper(II) Amidinate Complexes. *Macromolecules* **1997**, *30* (11), 3159–3163 DOI: 10.1021/ma961750p.

(18) Reuther, J. F.; Bhatt, M. P.; Tian, G.; Batchelor, B. L.; Campos, R.; Novak, B. M. Controlled Living Polymerization of Carbodiimides Using Versatile, Air-Stable nickel(II) Initiators: Facile Incorporation of Helical, Rod-like Materials. *Macromolecules* **2014**, *47* (14), 4587–4595 DOI: 10.1021/ma5009429.

(19) Siriwardane, D. A.; Kulikov, O.; Reuther, J. F.; Novak, B. M. Rigid, Helical Arm Stars through Living Nickel Polymerization of Carbodiimides. *Macromolecules* **2017** DOI: 10.1021/acs.macromol.6b02456.

(20) Tang, H.-Z.; Boyle, P. D.; Novak, B. M. Chiroptical Switching Polyguanidine Synthesized by Helix-Sense-Selective Polymerization Using [(R)-3,3‘-Dibromo-2,2‘-Binaphthoxy](di-Tert-butoxy)titanium(IV) Catalyst. *J. Am. Chem. Soc.* **2005**, *127* (7), 2136–2142 DOI: 10.1021/ja0453533.

(21) Tang, H.-Z.; Garland, E. R.; Novak, B. M.; He, J.; Polavarapu, P. L.; Sun, F. C.; Sheiko, S. S. Helical Polyguanidines Prepared by Helix-Sense-Selective Polymerizations of Achiral Carbodiimides Using Enantiopure Binaphthol-Based Titanium Catalysts. *Macromolecules* **2007**, *40* (10), 3575–3580 DOI: 10.1021/ma0618777.

(22) Kennemur, J. G.; Clark, J. B.; Tian, G.; Novak, B. M. A New, More Versatile, Optical Switching Helical Polycarbodiimide Capable of Thermally Tuning Polarizations ±359°. *Macromolecules* **2010**, *43* (4), 1867–1873 DOI: 10.1021/ma902657d.

(23) Reuther, J. F.; Bhatt, M. P.; Tian, G.; Batchelor, B. L.; Campos, R.; Novak, B. M. Controlled Living Polymerization of Carbodiimides Using Versatile, Air-Stable Nickel(II) Initiators: Facile Incorporation of Helical, Rod-like Materials. *Macromolecules* **2014**, *47* (14), 4587–4595 DOI: 10.1021/ma5009429.

(24) Reuther, J. F.; DeSousa, J. D.; Novak, B. M. Direct Probing of Regioregularity for Polycarbodiimide Systems via 15N NMR Analysis. *Macromolecules* **2012**, *45* (19), 7719–7728 DOI: 10.1021/ma301448b.

(25) Reuther, J. F.; Novak, B. M. Evidence of Entropy-Driven Bistability through 15N NMR Analysis of a Temperature- and Solvent-Induced, Chiroptical Switching Polycarbodiimide. *J. Am. Chem. Soc.* **2013**, *135* (51), 19292–19303 DOI: 10.1021/ja4098803.

(26) Deng, J.; Luo, X.; Zhao, W.; Yang, W. A Novel Type of Optically Active Helical Polymers: Synthesis and Characterization of poly(N-Propargylureas). *J. Polym. Sci. Part A Polym. Chem.* **2008**, *46* (12), 4112–4121 DOI: 10.1002/pola.22755.

(27) Nomura, R.; Fukushima, Y.; Nakako, H.; Masuda, T. Conformational Study of Helical Poly(propiolic Esters) in Solution. *J. Am. Chem. Soc.* **2000**, *122* (37), 8830–8836 DOI: 10.1021/ja000877y.

(28) Gao, G.; Sanda, F.; Masuda, T. Copolymerization of Chiral Amino Acid-Based Acetylenes and Helical Conformation of the Copolymers. *Macromolecules* **2003**, *36* (11), 3938–3943 DOI: 10.1021/ma021432s.

(29) Yashima, E.; Matsushima, T.; Okamoto, Y. Chirality Assignment of Amines and Amino Alcohols Based on Circular Dichroism Induced by Helix Formation of a Stereoregular Poly((4-

Carboxyphenyl)acetylene) through Acid−Base Complexation. *J. Am. Chem. Soc.* **1997**, *119* (27), 6345–6359 DOI: 10.1021/ja964470y.

(30) Ute, K.; Fukunishi, Y.; Jha, S. K.; Cheon, K.-S.; Muñoz, B.; Hatada, K.; Green, M. M. Dynamic NMR Determination of the Barrier for Interconversion of the Left- and Right-Handed Helical Conformations in a Polyisocyanate. *Macromolecules* **1999**, *32* (4), 1304–1307 DOI: 10.1021/ma981427h.

(31) Green, M. M.; Reidy, M. P.; Johnson, R. D.; Darling, G.; O'Leary, D. J.; Willson, G. Macromolecular Stereochemistry: The out-of-Proportion Influence of Optically Active Comonomers on the Conformational Characteristics of Polyisocyanates. The Sergeants and Soldiers Experiment. *J. Am. Chem. Soc.* **1989**, *111* (16), 6452–6454 DOI: 10.1021/ja00198a084.

(32) Jha, S. K.; Cheon, K.-S.; Green, M. M.; Selinger, J. V. Chiral Optical Properties of a Helical Polymer Synthesized from Nearly Racemic Chiral Monomers Highly Diluted with Achiral Monomers. *J. Am. Chem. Soc.* **1999**, *121* (8), 1665–1673 DOI: 10.1021/ja983202s.

(33) Green, M. M.; Garetz, B. A.; Munoz, B.; Chang, H.; Hoke, S.; Cooks, R. G. Majority Rules in the Copolymerization of Mirror Image Isomers. *J. Am. Chem. Soc.* **1995**, *117* (14), 4181–4182 DOI: 10.1021/ja00119a039.

(34) Yashima, E.; Matsushima, T.; Okamoto, Y. Poly((4-Carboxyphenyl)acetylene) as a Probe for Chirality Assignment of Amines by Circular Dichroism. *J. Am. Chem. Soc.* **1995**, *117* (46), 11596–11597 DOI: 10.1021/ja00151a032.

(35) Huisgen, R. 1,3-Dipolar Cycloadditions. Past and Future. *Angew. Chemie Int. Ed. English* **1963**, *2* (10), 565–598 DOI: 10.1002/anie.196305651.

(36) Kolb, H. C.; Finn, M. G.; Sharpless, K. B. Click Chemistry: Diverse Chemical Function from a Few Good Reactions. *Angew. Chemie Int. Ed.* **2001**, *40* (11), 2004–2021 DOI: 10.1002/1521-3773(20010601)40:11<2004::AID-ANIE2004>3.0.CO;2-5.

(37) Fournier, D.; Du Prez, F. "Click" Chemistry as a Promising Tool for Side-Chain Functionalization of Polyurethanes. *Macromolecules* **2008**, *41* (13), 4622–4630 DOI: 10.1021/ma800189z.

(38) Funhoff, A. M.; van Nostrum, C. F.; Lok, M. C.; Fretz, M. M.; Crommelin, D. J. A.; Hennink, W. E. Poly(3-Guanidinopropyl Methacrylate): A Novel Cationic Polymer for Gene Delivery. *Bioconjug. Chem.* **2004**, *15* (6), 1212–1220 DOI: 10.1021/bc049864q.

(39) Budhathoki-Uprety, J.; Novak, B. M. Synthesis of Alkyne-Functionalized Helical Polycarbodiimides and Their Ligation to Small Molecules Using "Click" and Sonogashira Reactions. *Macromolecules* **2011**, *44* (15), 5947–5954 DOI: 10.1021/ma200960e.

(40) Reuther, J. F.; Siriwardane, D. A.; Campos, R.; Novak, B. M. Solvent Tunable Self-Assembly of Amphiphilic Rod-Coil Block Copolymers with Chiral, Helical Polycarbodiimide Segments: Polymeric Nanostructures with Variable Shapes and Sizes. *Macromolecules* **2015**, *48* (19), 6890–6899 DOI: 10.1021/acs.macromol.5b01564.

(41) Reuther, J. F.; Siriwardane, D. A.; Kulikov, O. V; Batchelor, B. L.; Campos, R.; Novak, B. M. Facile Synthesis of Rod–Coil Block Copolymers with Chiral, Helical Polycarbodiimide Segments via Postpolymerization CuAAC "Click" Coupling of Functional End Groups. *Macromolecules* **2015**, *48* (10), 3207–3216 DOI: 10.1021/acs.macromol.5b00453.

(42) Kulikov, O. V.; Siriwardane, D. A.; Reuther, J. F.; McCandless, G. T.; Sun, H. J.; Li, Y.; Mahmood, S. F.; Sheiko, S. S.; Percec, V.; Novak, B. M. Characterization of Fibrous Aggregated Morphologies and Other Complex Architectures Self-Assembled from Helical Alkyne and Triazole Polycarbodiimides (R)- and (S)-Families in the Bulk and Thin Film. *Macromolecules* **2015**, *48* (12), 4088–4103 DOI: 10.1021/acs.macromol.5b00407.

(43) Merten, C.; Reuther, J. F.; DeSousa, J. D.; Novak, B. M. Identification of the Specific, Shutter-like Conformational Reorientation in a Chiroptical Switching Polycarbodiimide by VCD Spectroscopy. *Phys Chem Chem Phys* **2014**, *16* (23), 11456–11460 DOI: 10.1039/c4cp01226g.

(44) Kennemur, J. G.; Kilgore, C. A.; Novak, B. M. Adjusting Conformational Switching Behavior of Helical Polycarbodiimides through Substituent Induced Polarity Effects. *J. Polym. Sci. Part A Polym. Chem.* **2011**, *49* (3), 719–728 DOI: 10.1002/pola.24484.

(45) Reuther, J. F.; Novak, B. M. Evidence of Entropy-Driven Bistability through 15N NMR Analysis of a Temperature- and Solvent-Induced, Chiroptical Switching Polycarbodiimide. *J. Am. Chem. Soc.* **2013**, *135* (51), 19292–19303 DOI: 10.1021/ja4098803.

(46) Inomata, K.; Iguchi, Y.; Mizutani, K.; Sugimoto, H.; Nakanishi, E. Anisotropic Swelling Behavior Induced by Helix–Coil Transition in Liquid Crystalline Polypeptide Gels. *ACS Macro Lett.* **2012**, *1* (7), 807–810 DOI: 10.1021/mz300132s.

(47) Kim, J.; Novak, B. M.; Waddon, A. J. Liquid Crystalline Properties of Polyguanidines. *Macromolecules* **2004**, *37* (22), 8286–8292 DOI: 10.1021/ma0493527.

(48) Budhathoki-Uprety, J.; Peng, L.; Melander, C.; Novak, B. M. Synthesis of Guanidinium Functionalized Polycarbodiimides and Their Antibacterial Activities. *ACS Macro Lett.* **2012**, *1* (3), 370–374 DOI: 10.1021/mz200116k.

(49) Mammoottil, N. R.; Reuther, J. F.; Siriwardane, D. A.; Kulikov, O. V; Novak, B. M. Developments in Synthesis, Characterization, and Self-Assembly of Polycarbodiimide Systems. *J. Polym. Sci. Part A Polym. Chem.* **2017**, n/a-n/a DOI: 10.1002/pola.28583.

CHAPTER 2

RIGID, HELICAL ARM STARS THROUGH LIVING NICKEL POLYMERIZATION OF CARBODIIMIDES

Authors - Siriwardane, D.A.; Kulikov, O.V.; Reuther, J.F.; Novak, B. M.

Department of Chemistry and Biochemistry, BE 26

The University of Texas at Dallas

800 West Campbell Road

Richardson, TX 75080-3021

Reprinted with permission from Siriwardane, D. A.; Kulikov, O.V.; Reuther, J. F.; Novak, B.M, Rigid, Helical Arm Stars through Living Nickel Polymerization of Carbodiimides. *Macromolecules* **2017** DOI: 10.1021/acs.macromol.6b02456, Copyright 2017 American Chemical Society.

2.1 Abstract

Using the core-first growth strategy, we have synthesized a *tris*-Ni(II) initiator which bears three initiating sites for the ensuing polymerization of *N*-1-phenethyl-*N*'-methylcarbodiimide. The arms of these star polymers bearing chiral side chains adopt single-handed helical rod-like conformations. The polymerization occurs in a controlled, living fashion and this multi-arm architecture imparts a new set of intriguing properties including their self-assembly into diverse nanostructures when casting from different solvents. These assemblies, characterized by AFM, TEM, and DLS, include the formation of nanofiber networks and twisted super-helical nanostructures. Interestingly, by processing these polymers via electro-spraying method, hollow and uniform platelet-like particles were obtained. These solvent-dependent morphologies of micro particles were observed by using SEM. The kinetic studies of polymerizations, inspection of self-aggregation behaviors, and electrosprayed architectures will open up possibilities for a variety of potential biomedical applications.

2.2 Introduction to multi-arm star polymers

Polycarbodiimides are an interesting class of helical polymers that are synthesized using controlled living polymerizations of carbodiimides mediated by transition-metal catalysts.[1-3] These helical polymers show many intriguing properties such as liquid crystallinity,[4-5] chiroptical switching,[6-11] and self-assembly behavior both in solution and the solid state.[12-14] The synthetic strategies have expanded recently to achieve well-defined, chemically versatile nanoscale architectures for this unique class of polymers.[15,16] Recently the development of star polymers composed of rigid-rod, helical arms has become an interest among researchers due to their

unique properties that are not present in their linear analogues.[17] Particularly, these nanoscale functional materials possess many important applications such as chiral recognition[18-19] and enantioselective catalysis.[20] Synthesis strategies to achieve multi-arm star polymers include either core-first method or arm-first method. In the arm-first approach, functional linear polymer counterparts are first synthesized and then linked into a multifunctional core as a single unit.[19] The synthesis strategy for core-first method emphasizes making multifunctional core and growing linear polymeric arms radially from each active site.[21] Even though star polymers show diverse properties based on synthesis route,[22] composition,[23] and functionality,[24] the controlled synthesis of chiral, helical variants, however, remains limited among synthetic chemists.

Several reports detailed the synthesis of rod-like, helical multi-arm peptides which includes the formation of three arm poly(ε-benzyl-L-glutamate) (PBLG) from *N*-carboxyanhydride monomer of ε-benzyl-L-glutamate through ring-opening polymerization (ROP).[25] Zhao and coworkers have synthesized multi-arm and mikto arm star polymers using a branched core *via* arm-first method.[26] Hoff and Novak developed a methodology to synthesize well-defined star polymers with rod-like, helical poly(*n*-hexylisocyanate) (PHIC) via core-first method in the presence of trifunctional Ti (IV) initiator.[27] In that study, they utilized a trihydroxyl functional core that was allowed to react with $CpTiCl_3$ to synthesize the *tris*-Ti(IV) alkoxide initiator. Each titanium alkoxide group provides an initiation site for polymerization, forming a three armed polyisocyanate star in a controlled chain-growth manner. Further, Yashima and co-workers reported the synthesis of optically-active, single-handed helical star polymers composed of helical polyisocyanides by employing arm-first method.[19] Their approach is based on living polymerization of an enantiopure phenyl isocyanide monomer possessing dodecyl functionalized

L-alanine pendant groups. The polymerization active chain-end was then further reacted with diisocyanide cross-linkers forming multi-arm, core-cross-linked star polymers.

In this report, we polymerized carbodiimide monomers in a highly controlled fashion in the presence of Ni(II) initiator with multiple active initiating sites via living reversible coordination-insertion mechanism.[3] The η^1-aryl ligand plays the vital role in this polymerization by transferring itself to the electrophilic carbon of the monomer forming a nickel-amidinate complex and initiating the polymerization. Using chiral monomers, such as (*R*) or (*S*)-*N*-1-phenethyl-*N'*-methylcarbodiimide (PMC), we can form polymeric arms with an exclusive single-handed screw sense. We utilized the trimerization reaction of nitrile groups to form the trifunctional core with the aryl bromide (for initiator formation) appended to the 4-position of each of the three coupled rings. Using this triazine core, three initiating sites for polymerization were created through the oxidative addition into $Ni(COD)_2$ complex. Through the helix-sense selective polymerization of the chiral (*S*)-PMC monomer, three helical, rigid arms grew radially from the core in controlled living fashion as evidenced by kinetic data analysis.

2.3 Result and discussion

2.3.1 Synthesis of Initiators for multi-arm star polymers

Helix-sense selective polymerization of carbodiimides can be achieved in two ways: the use of chiral initiators with achiral carbodiimides or chiral monomers with achiral initiators.[29] One route previously employed to modify the end terminus of polycarbodiimides is incorporating the relevant η^1-aryl ligands onto Ni(II) initiators which bear specific, reactive functionalities. Previously, we have reported the synthesis and utilization of a Ni(II) initiator with protected

alkyne functionality appended to the 4-position of the aryl transfer ligand.[3] To synthesize three-arm star helical polymer, both arm-first method and core-first method were attempted.

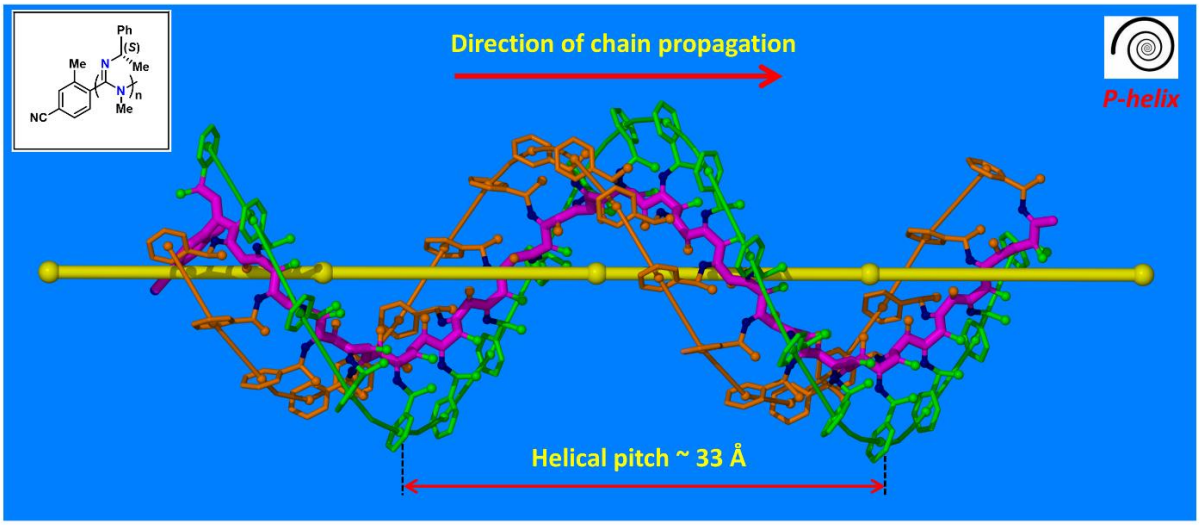

Figure 2.1 This model represents the linear **Poly-10**. It is composed of amidine backbone (magenta) spinning around the yellow axis which shows the direction of main chain propagation. Brown and green lines are shown to connect aromatic ring centroids to emphasize the secondary helical motif.

For the arm-first approach, nitrile end-functionalized homopolymer (**Poly-10**) was synthesized (**Figure 2.1**) using **Cat-6** and then trimerization of the nitrile in the presence of CF_3SO_3H was attempted (**Figure 2.2**). This method was not successful and we believe that in the presence of acid, the basic, helical backbone is heavily protonated causing ionic repulsion of positively charged chains. We then turned to the core-first method by using an aryl bromide-functionalized triazine core synthesized via trimerization of nitrile functional groups in the neat acid.[28, 30] The formation of the triazine ring was confirmed by ^{13}C NMR as the nitrile chemical shift at 125 ppm disappears resulting in the new triazine ^{13}C-chemical shift at 171 ppm.

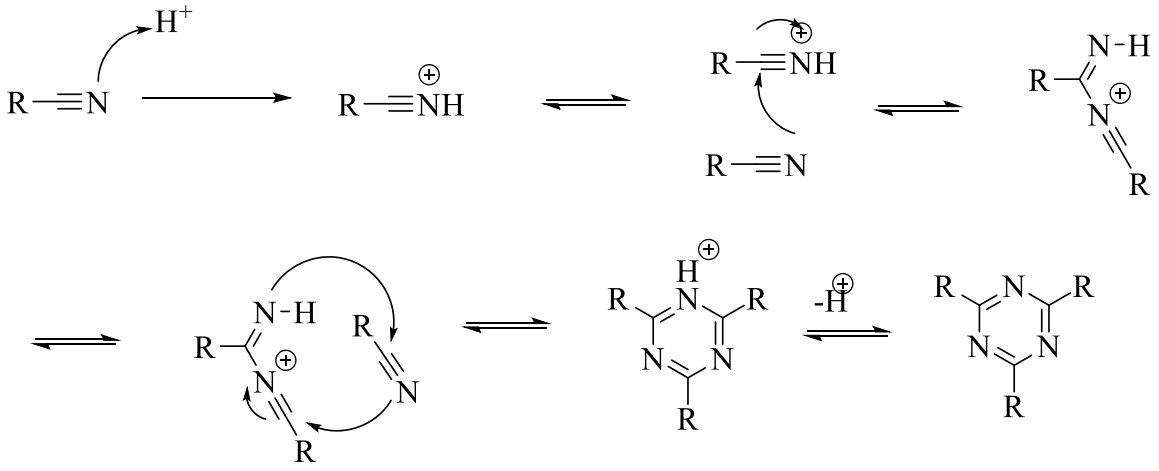

Figure 2.2 Mechanism showing the trimerization reaction of nitrile functionality.

In the presence of PPh_3 and this aryl bromide, the Ni(0) center of $Ni(COD)_2$ undergoes oxidative addition forming *tris*-Ni(II) complex (**Cat-6** and **-8**; **Scheme 2.1**). This molecule contains three initiation sites for the controlled synthesis of three-armed polycarbodiimide star polymers. The formation of square planar Ni(II) complex in **Cat-6** and **8** was confirmed by ^{31}P NMR with a single chemical shift at 21.55 (**Cat-6**) and 22.26 ppm (**Cat-8**) associated with the symmetric triphenylphosphine ligands, respectively. We synthesized both monometallic initiator **(Cat-6)** and trimetallic initiator **(Cat-6)** to yield single chain and three-arm polymers, respectively, for polymerization kinetics and self-assembly behavior in solution. The polymerization of (*S*)-PMC monomer with **Cat-6** and **8** is shown in **Scheme 2.2**.

The resulting three-arm star polymer is composed of triazine core and rigid helical arms extending radially from the core. This polymer possesses amidine helical backbone with chiral pendant groups spiraling around the helical backbone. Molecular model of **Poly-11** featuring its non-planar geometry is shown below (**Figure 2.3**).

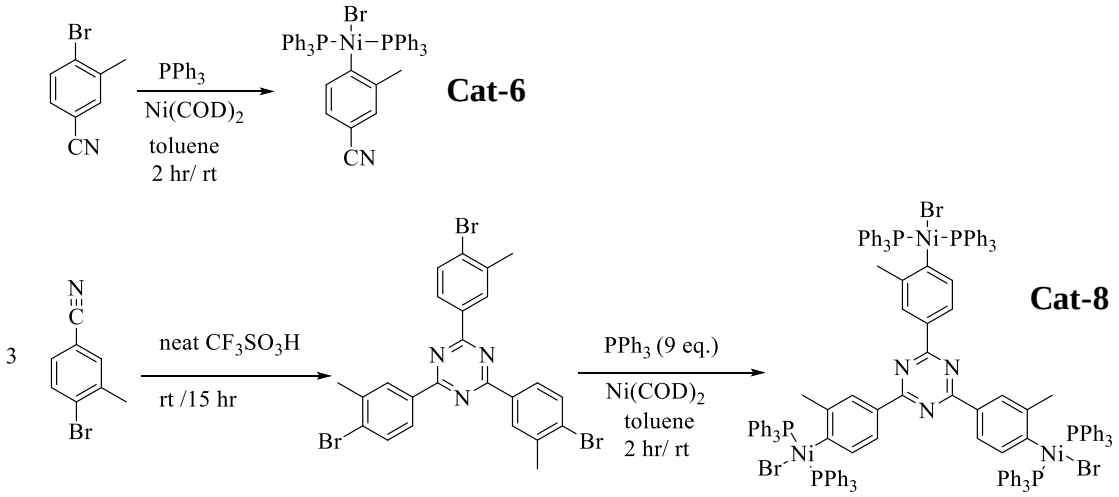

Scheme 2.1 Synthesis of mono- and tri-functional Ni(II) initiators

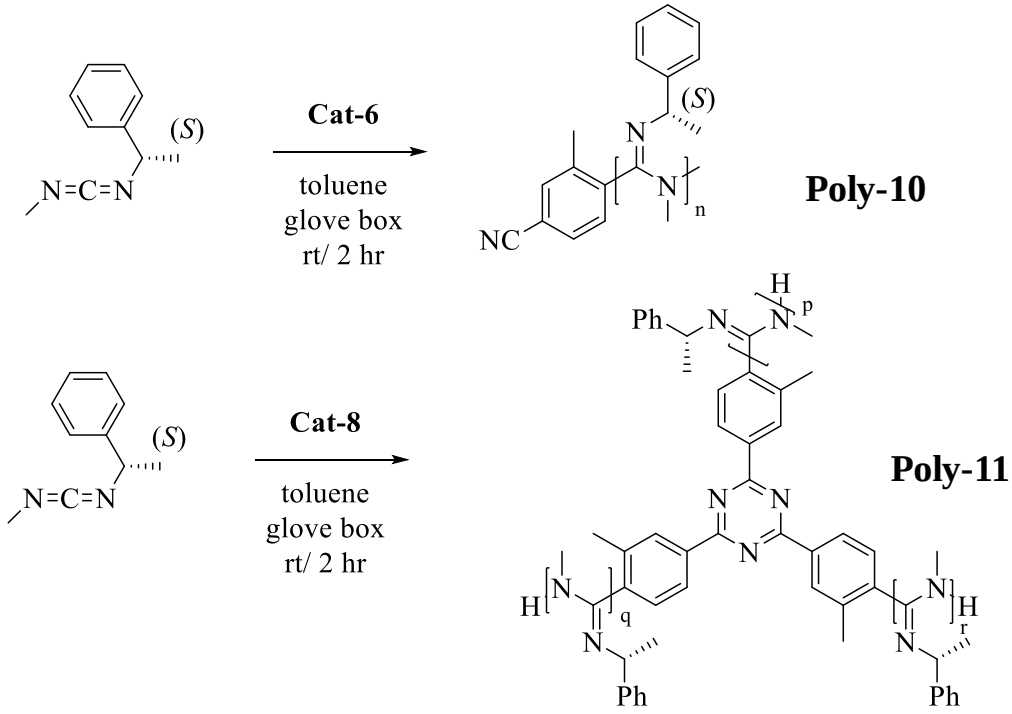

Scheme 2.2 Synthesis of linear (**Poly-10**) and star (**Poly-11**) polycarbodiimides.

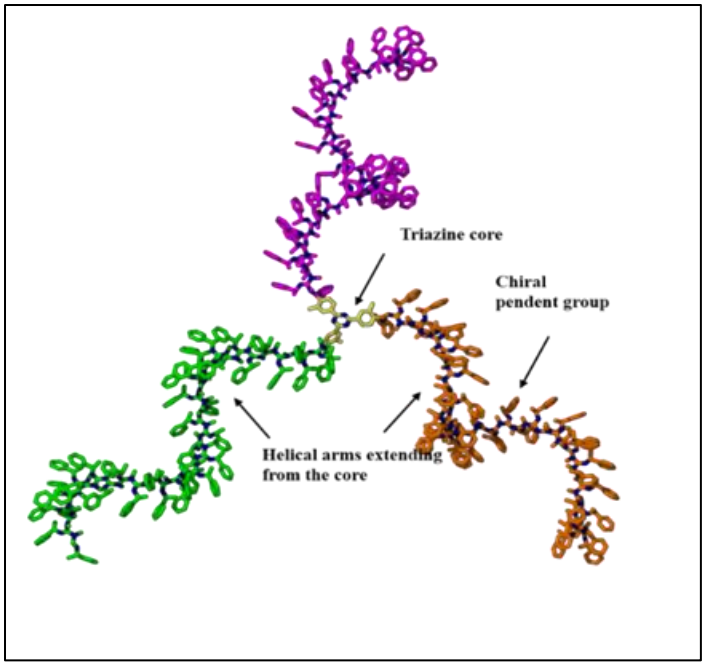

Figure 2.3 Cartoon representation of three-arm star polymer (**Poly-11**).

2.3.2 Kinetic Studies of Polymerization

To determine whether this polymerization occurs in a controlled fashion with minimal termination, the kinetics of the reaction with **Cat-6** and **8** were investigated using real-time FTIR spectroscopy. The monomer:initiator ratio used in these studies was 250:1 and all polymerizations were carried out under N_2 at room temperature. Both the bulk polymerizations (a typical condition for carbodiimide polymerizations) of PMC with **Cat-6** and **8** were found to proceed very rapidly with complete monomer consumption in less than 30 min. Therefore, the polymerization was performed at lower concentrations in toluene at 125 mg/mL monomer. At a 500:1 of monomer to initiator ratio (which corresponds to three initiating sites per one tris-initiator), the polymerization of (*S*)-PMC with **Cat-8** is faster than that of **Cat-6** (which corresponds to one initiating site per one initiator molecule) with each conversion reaching ~90% after 1 and 6 hours, respectively. To confirm this polymerization takes place without

terminations, the graph of ln([M_0/M]) / [M] vs. time was plotted by acquiring IR data simultaneously during the reaction using a fiber-optic IR spectroscopy probe inserted directly into the polymerization medium. Here, we monitored the disappearance of the diagnostic carbodiimide N=C=N stretching mode at 2134 cm^{-1} and the appearance of the C=N imine stretching mode of the synthesized polymer at 1630 cm^{-1} -1667 cm^{-1}**(Figure 2.4-C)**. As the polymerization proceeded, the peak intensity of 2134 cm^{-1} decreased and the peak intensities at 1630 cm^{-1}- 1667 cm^{-1} region increased, indicating that polymer was being formed (**Figures 2.5** and **2.6**). The relative rate constant for each polymerization with **Cat-6** and **Cat-8** was calculated as 2.87 x 10^{-3} min^{-1} and 2.08 x 10^{-2} min^{-1}, respectively. A rate enhancement of seven times was observed for **Cat-8** compared to **Cat-6**. The main reason for this observation is that **Cat-6** needs more time to get dissolved than **Cat-8**.

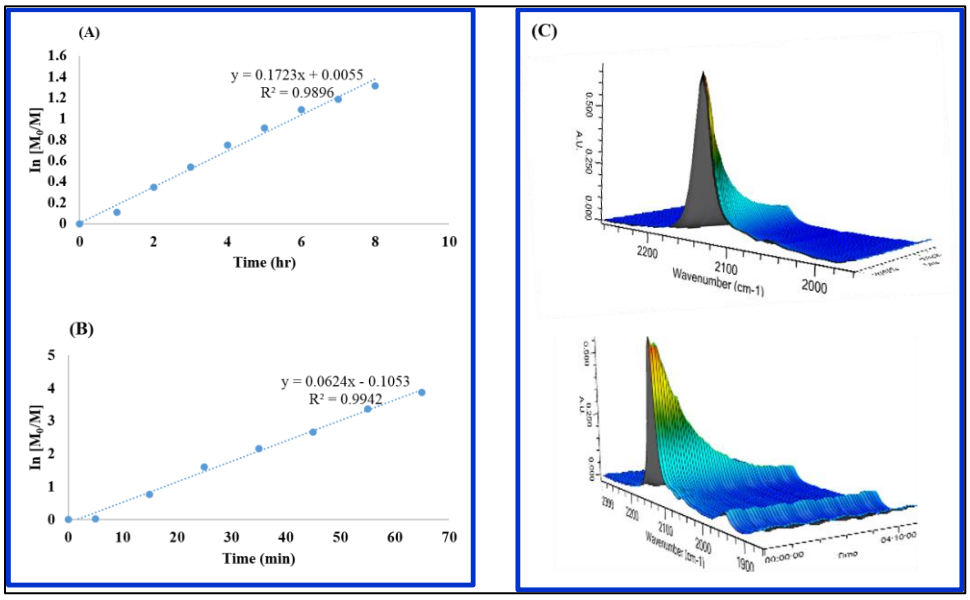

Figure 2.4 Polymerization kinetics for PMC with **Cat-6** and **8** in two plots: ln M_0/M *vs* time for **Poly-10** (A) and **Poly-11** (B) and graphs showing a change of monomer concentration over time (C): **Poly-10** (top), **Poly-11** (bottom).

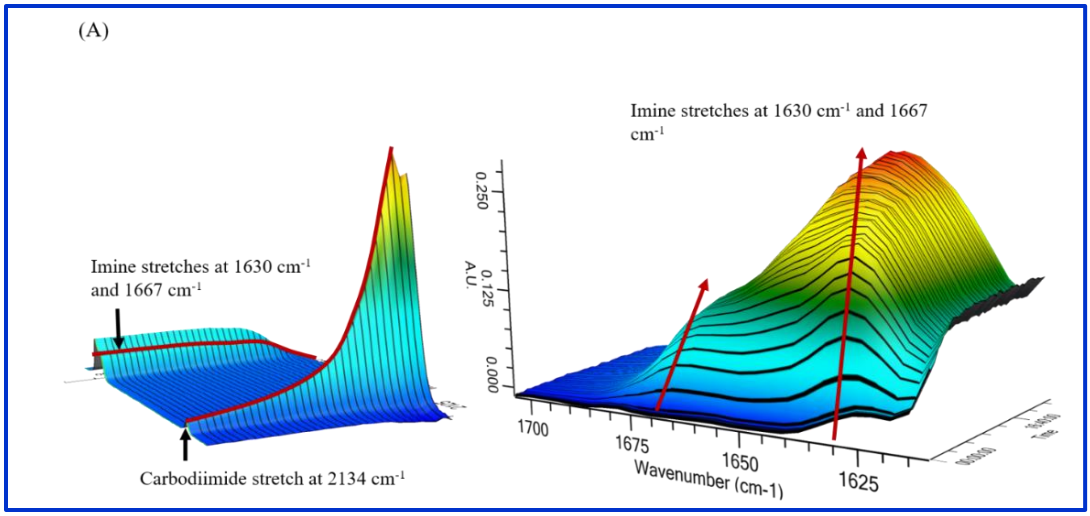

Figure 2.5 Changes in intensities observed for carbodiimide stretch (N=C=N) and imine stretches (N=C) during the polymerization for **Poly-10**.

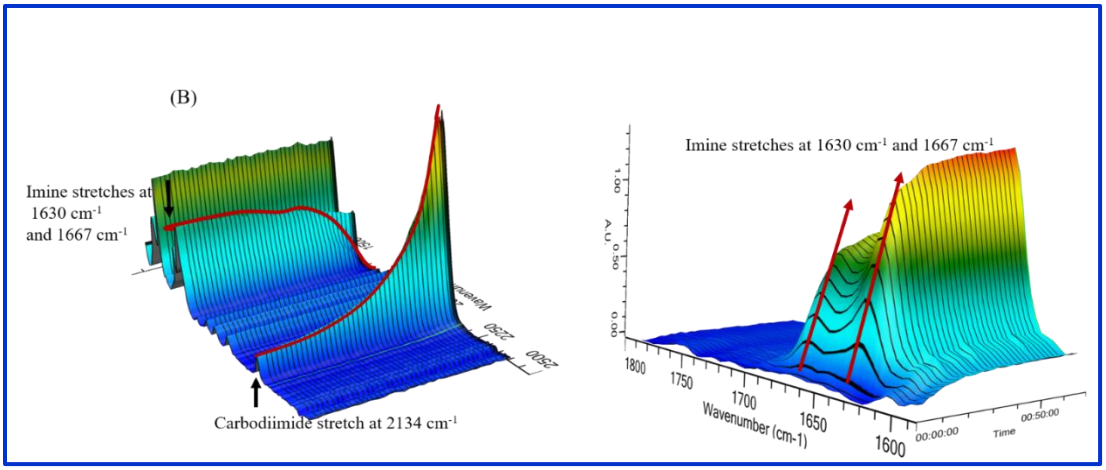

Figure 2.6 Changes in intensities observed for carbodiimide stretch (N=C=N) and imine stretches (N=C) during the polymerization for **Poly-11**.

^{1}H NMR of the synthesized star polymer allows end-group analysis with the chemical shift of the *ortho*-methyl group attached to aryl core at 1.60 ppm (**Figure 2.6**). This chemical shift can be integrated with respect to the pendant methine proton in the 1-phenethyl side group to provide an accurate quantification of the degree of polymerization which is then converted into M_n. In the

same way, the molecular mass was determined for linear analogs (**Figure 2.7**). ^{1}H NMR spectroscopy was used due to difficulties of molecular mass determination for polycarbodiimides by SEC.[3] Additionally, the topology of the three-arm star polycarbodiimide also proved to complicate the SEC even further and ^{1}HNMR was utilized to calculate M_n (**Figure 2.8**). Therefore, SEC was not used to characterize the level of control in plots of M_n vs percentage of conversion and ^{1}HNMR studies were performed to determine M_n of all polymers (**Figure 2.9**).

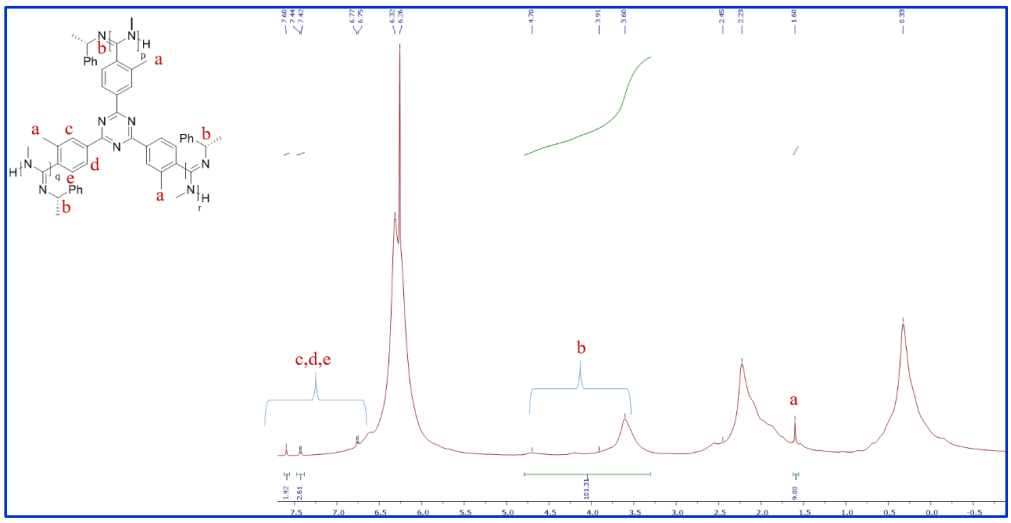

Figure 2.7 ^{1}HNMR spectrum showing end functional integration for **Poly-11**.

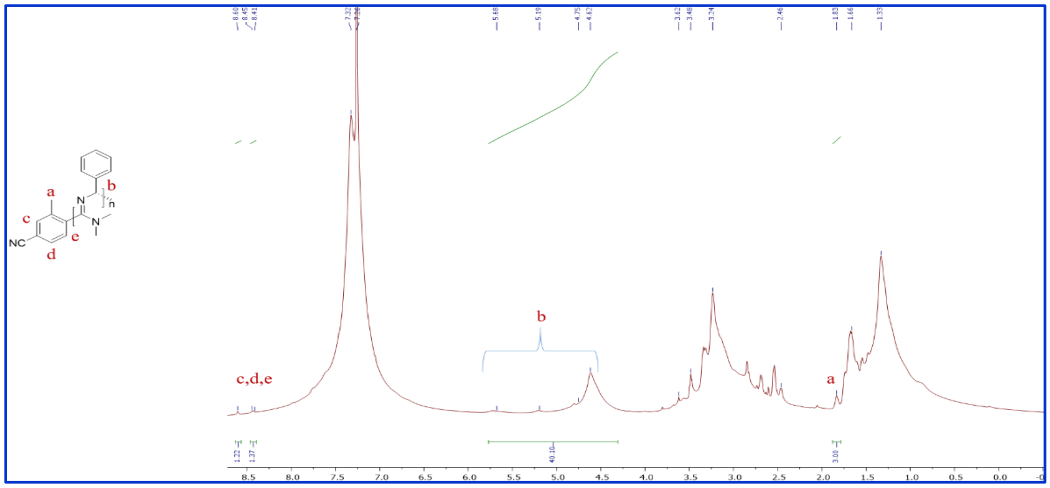

Figure 2.8 ^{1}HNMR spectrum showing end functional integration for **Poly-10**.

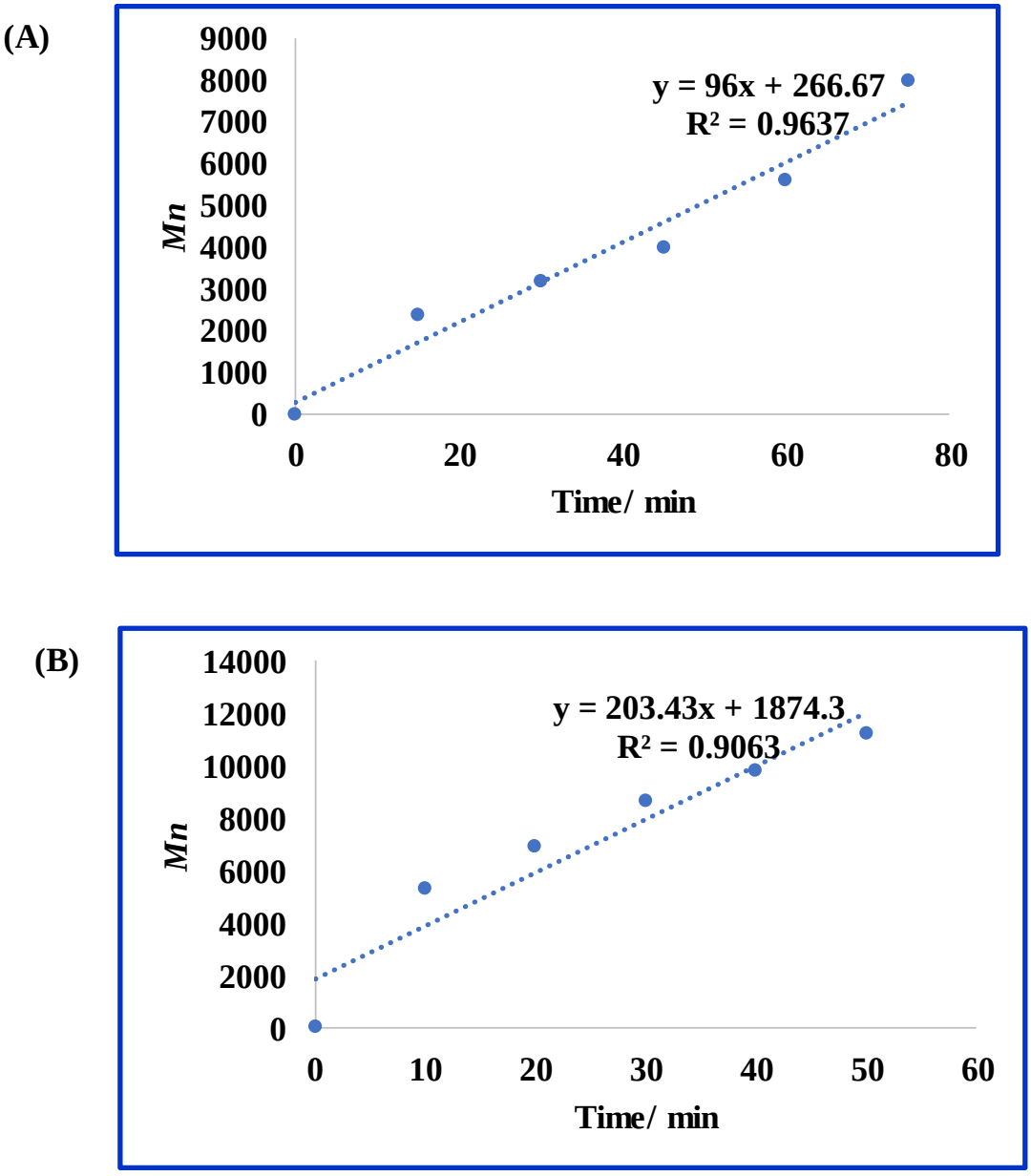

Figure 2.9 Graphs showing a change of molecular weight with time as the polymerization progress (**A**) **Poly-10** and (**B**) **Poly-11**.

As the polymerization progress, the intensity of carbodiimide stretch of monomer (2134 cm^{-1}) is getting decreased while the intensities of two bands corresponding to imine bond (at 1630 cm^{-1} and 1667 cm^{-1}, respectively) are increased. To further confirm the extent of living character in the formation of **Poly-11,** we performed chain extension experiments by using sequential

monomer addition method. The same *in situ* real-time IR spectrophotometry method was used. For this, we have introduced the first aliquot of PMC monomer and the monomer consumption was monitored (All kinetics data are given in 2.5.2 section, **Tables 2.2, 2.3** and **2.4**). At 91% consumption of the first portion of PMC monomer, the propagation was resumed with the addition of a second portion of PMC monomer **(Figure 2.10)**. This shows that three-arm star polymers preserve their living chain termini and this feature enables us to prepare of block copolymers using sequential monomer addition method.[31,32] The existence of the macroinitiators and consumption of the second monomer provided indirect evidence for extension of polymer chains.

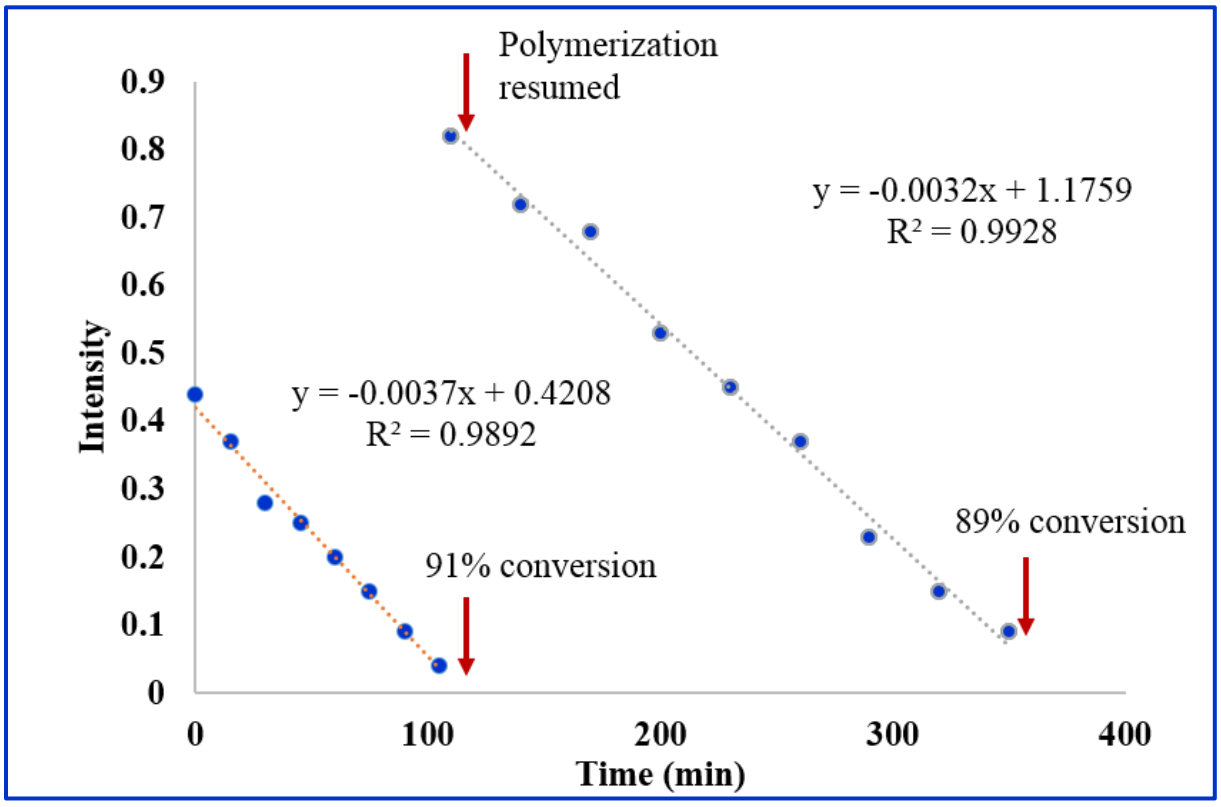

Figure 2.10 Sequential monomer addition kinetics for the polymerization of PMC with **Cat-8**.

2.3.3 Chirality Analysis of Polymers

To bias the helicity of the radial arms, the pure (*S*)-PMC and (*R*)-PMC monomers were separately used. The specific optical rotation (SOR) of resulting polymers were +40.2 and -47.2 for ***(S)*** and ***(R)*****-Poly-10**, respectively, and +39.7 and -48.5 for **Poly-11**. For enantiomeric monomers utilized for the polymerization, SOR of resulting polymers is opposite in sign. This implies that chirality of resulting polymer is predetermined by helical backbone rather than chiral pendant groups. Thus, helix sense selective polymerization is taking place. The SOR data is also indicative of the formation of opposite handed helices.

Vibrational circular dichroism (VCD) was used to determine exact handedness of the resulting star polymers and linear analogs and this is one of the powerful tool to determine the absolute configuration of chiral analytes. VCD has been coupled with IR spectroscopy with circular dichroism and it measures the preferential absorption of right and left handed circularly polarized IR light through vibrational motion. Both **Poly-10** and **11** polymerized with (*R*)-PMC and (*S*)-PMC show mirror image spectra again confirming the formation of oppositely handed helices upon polymerization of monomer enantiomers. The most intense, diagnostic stretching mode in the VCD spectra for all polymers is the C=N imine stretching mode at 1640 cm^{-1}. For **(*R*)-Poly-10** and **-11**, this bisignate mode is phased -/+ which can be correlated to previously calculated DFT models of polycarbodiimides to suggest *P*-helix formation. Moreover, the +/- bisignate C=N stretching mode for **(*S*)-Poly-10** and **-2** also matches with previously reported VCD spectra of polycarbodiimides with *M*-helically rotating backbones (**Figure 2.11**).[3]

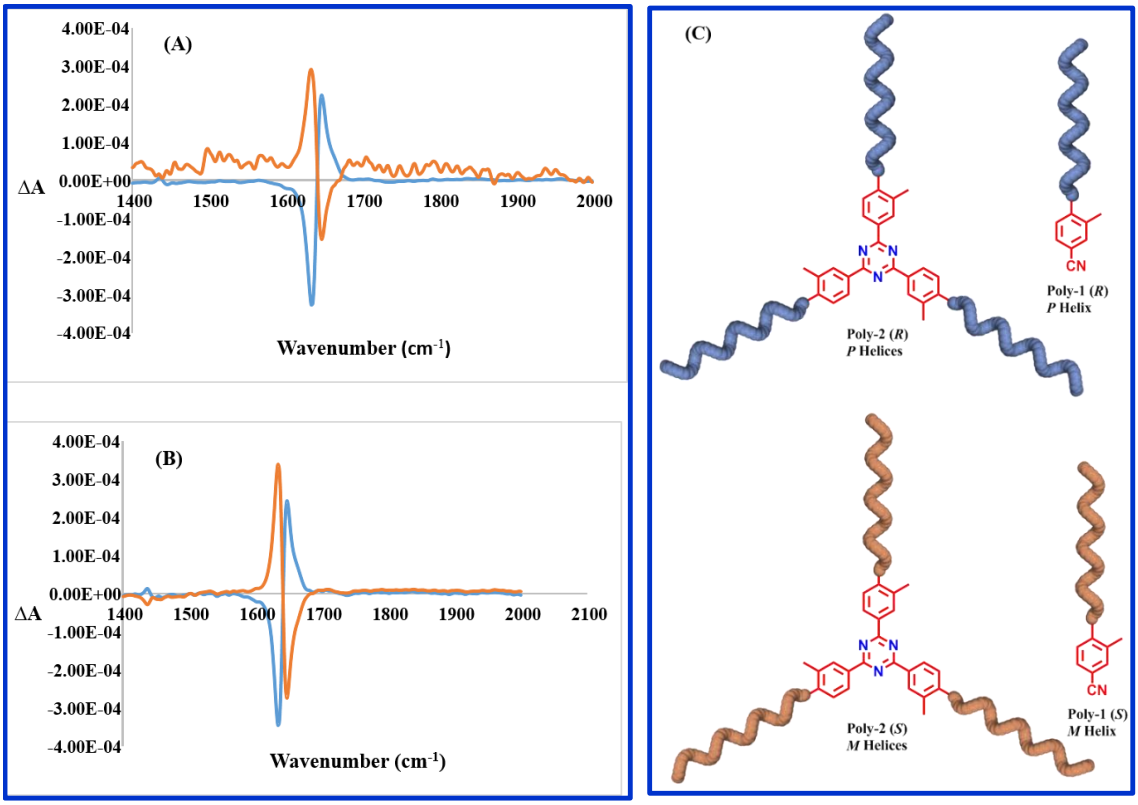

Figure 2.11 VCD spectra of (A) **Poly-10** and (B) **Poly-11**: orange (*S*) and blue (*R*) plots showing opposite handedness (C = 25 mg/mL in $CDCl_3$), (C) Cartoons showing helicity of **Poly-10** (*R* and *S*) and **Poly-11** (*R* and *S*).

2.3.4 Thin film morphologies of Poly-10 and Poly-11

The thin film morphologies of each polymer were studied using tapping-mode atomic force microscopy (AFM). We have recently published that the use of low concentration sample solution and specific substrates are critical in the acquisition of high resolution images for AFM analysis.[12] Therefore, we used a silicon wafer as the substrate and the concentration range used for these studies was 0.1 - 0.5 mg/mL to image individual nanofibers. To investigate the self-assembly behavior of both **Poly-10** and **-11**, we spun-cast polymer films from THF, $CHCl_3$, and toluene solutions. Based on AFM studies, the self-assembly behavior of both **Poly-10** and **-11** is solvent dependent **(Figure 2.12-Top panel** and **Figure 2.12-Bottom panel** respectively**)**. Cast

from THF, for both **Poly-10** and **-11,** show worm-like aggregates. The **Poly-11** aggregates seem to be larger with average diameter around 70 (±10) nm than those found for **Poly-10** (45±8) nm. The polymer samples cast from chloroform were visualized as looped nanofiber aggregates. The observed porous domains are believed to be associated with the crystallizing of individual fibers but also may be due to surface dewetting phenomena similar to our previous reports.[33] In toluene, densely packed, thin nanofiber morphologies were observed for both the linear **Poly-10** and star **Poly-11**.

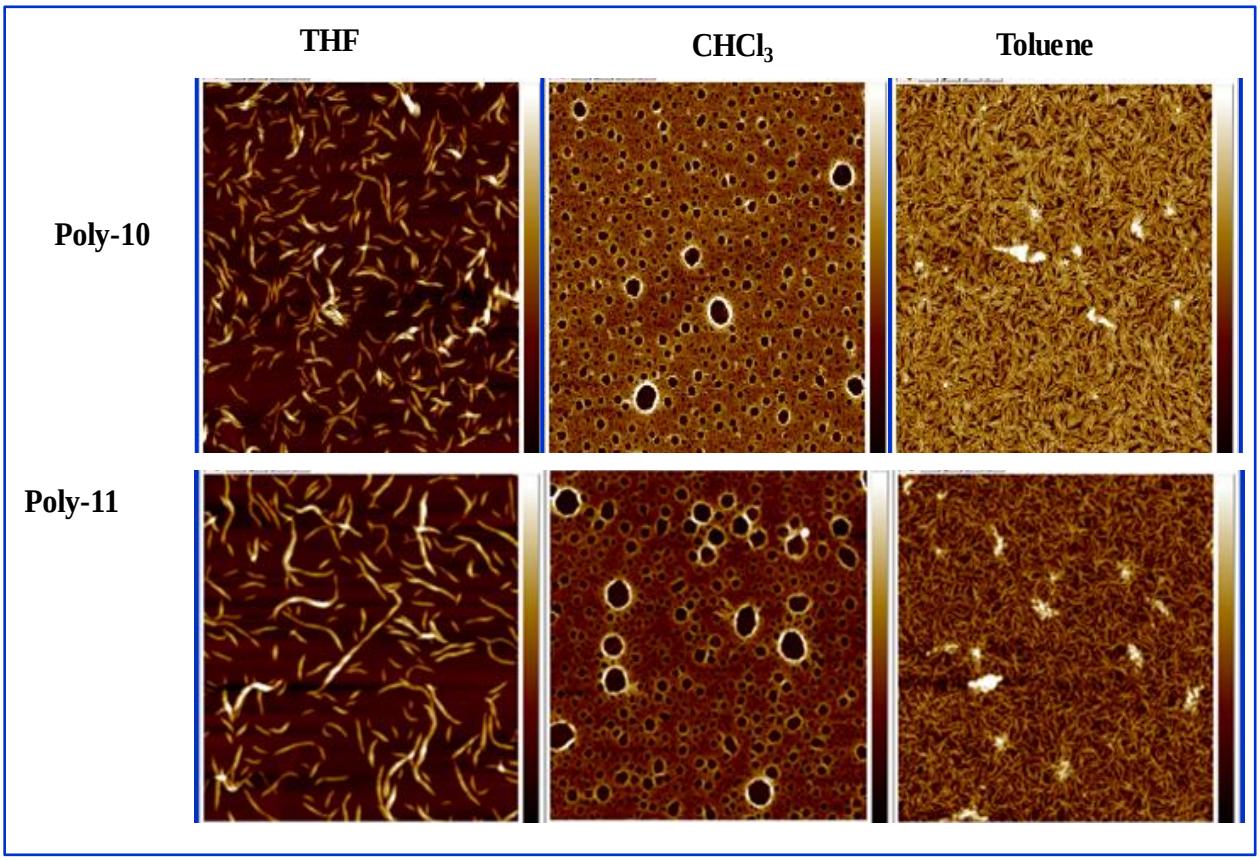

Figure 2.12 Height AFM micrographs of **Poly–10** spin-cast from different solvents on silicon wafers: C = 0.1 mg/ mL, 5 μm scan size.

2.3.5 Study of polymer morphology in binary solvent systems

Next, we switched the solvent systems for spin-coating solutions to binary mixtures to further investigate the solvent effect on morphology. Due to the inherent chirality, we have shown that polycarbodiimide homopolymers and copolymers self-assemble to form super-helical nanostructures when spin-cast from mixed solvents such as THF/ 25 vol% EtOH.[14, 34] Therefore, we have investigated both **Poly-10** and **-11** spin-coated from this solvent combination to see if these morphologies persist for the star polymer analogs. For helical scaffolds, by twisting into the super-coil structure, the system can minimize unfavorable polymer-solvent interactions.[35] By switching the solvent to the binary system, the three-arm star polycarbodiimde forms super-helical nanostructure as evidenced by AFM images **(Figures 2.13, 2.14)**. This formation of well-defined super-helical nanofiber is easily taking place in **Poly-11** whereas **Poly-10** forms regular nanofibers.

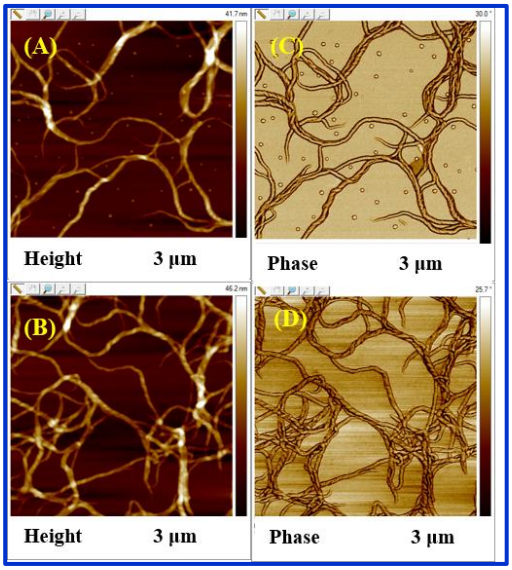

Figure 2.13 Height and Phase AFM micrographs of **(A)**, **(C) Poly–10** and **(B)**, **(D) Poly–11** spin-cast from THF/ 25 vol% EtOH solvents mixture onto silicon wafers (C = 0.5 mg/mL, scan size = 3 x 3 µm).

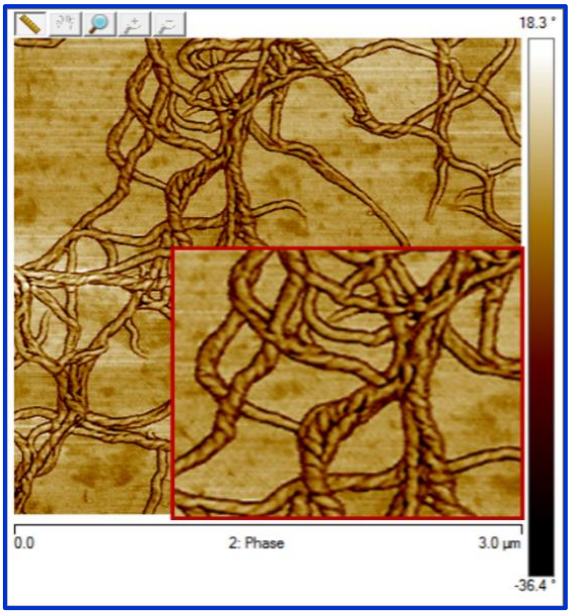

Figure 2.14 AFM phase image of (*S*)-**Poly-11** showing super-helix formation (C = 0.5 mg/mL, scan size = 3 x 3 µm).

These PPMC arms are hydrophobic in nature and when it disperses in EtOH: THF, the polymer adopts energetically favorable twisted nanofiber architecture. This super-helical formation is not significant when spin-cast from THF/ 5 vol% EtOH or THF/ 15 vol% EtOH. **(Figure 2.15)**. It can be speculated that when the polymer solution in THF has introduced into EtOH: THF mixture, the formation of super-helical structures is induced and becomes visible at specific concentrations of EtOH (25%).

In a binary solvent system, such as 25% EtOH:THF, **Poly-10** toroidal aggregates were also observed **(Figure 2.15)**. We hypothesize that these types of structures are possible as the helical chains grow in molecular mass allowing for more flexibility in the polymer backbone.[34] For comparable molecular masses, **Poly-10** demonstrates a greater persistence length, whereas **Poly-11** represents more compact structure. Therefore, in AFM images we have seen short polymeric bundles for **Poly-11**. We have investigated self-assembly behavior of these samples using TEM

and toroids and short fiber formation was observed for **Poly-10** whereas fiber network was observed for **Poly-11 (Figure 2.16** and **2.17** respectively).

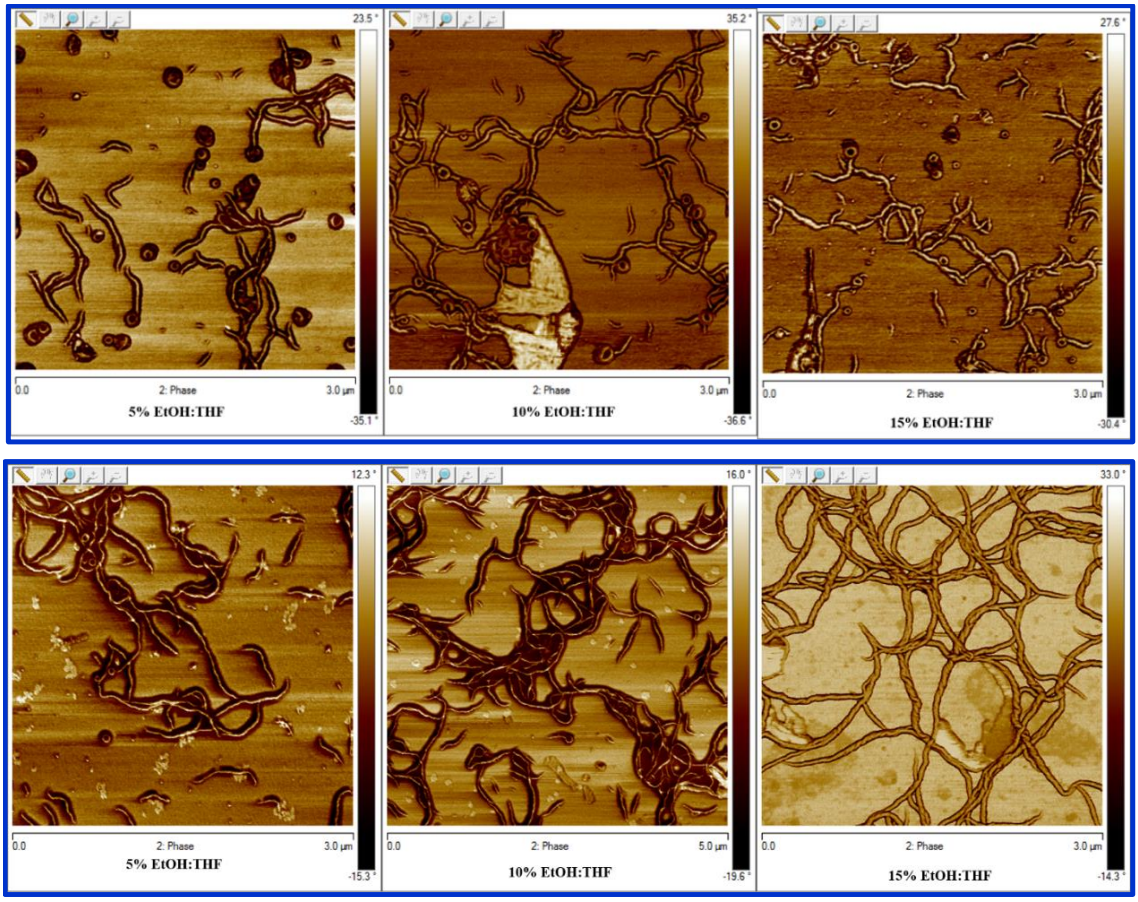

Figure 2.15 AFM micrographs of **Poly - 10** (top) and **Poly - 11** (bottom) spin-cast from THF/25 vol%EtOH solvents mixture onto silicon wafers (C = 0.5 mg/mL), 3x3 μm scan size images.

2.3.6 Study of polymer morphology by using TEM

To confirm fiber morphology and toroidal aggregations, the samples were inspected using TEM. Toroids and small fibers are observed for **Poly-10**, whereas fiber network was observed for **Poly-11**. The formation of toroid structures may be due to long polymer chains.

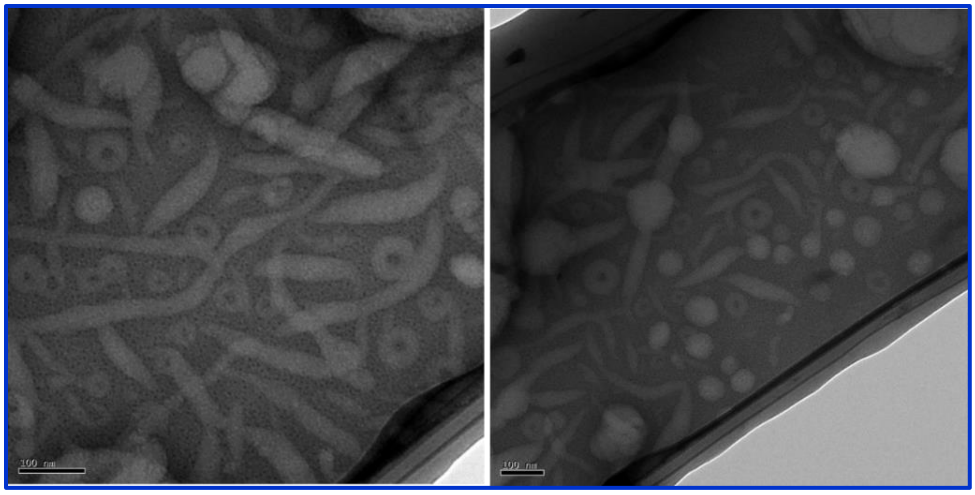

Figure 2.16 TEM micrographs of **Poly–10** in 25% EtOH: THF solvents mixture on carbon-coated copper grid stained with 2.0% uranyl acetate; aggregation of toroid-like structures.

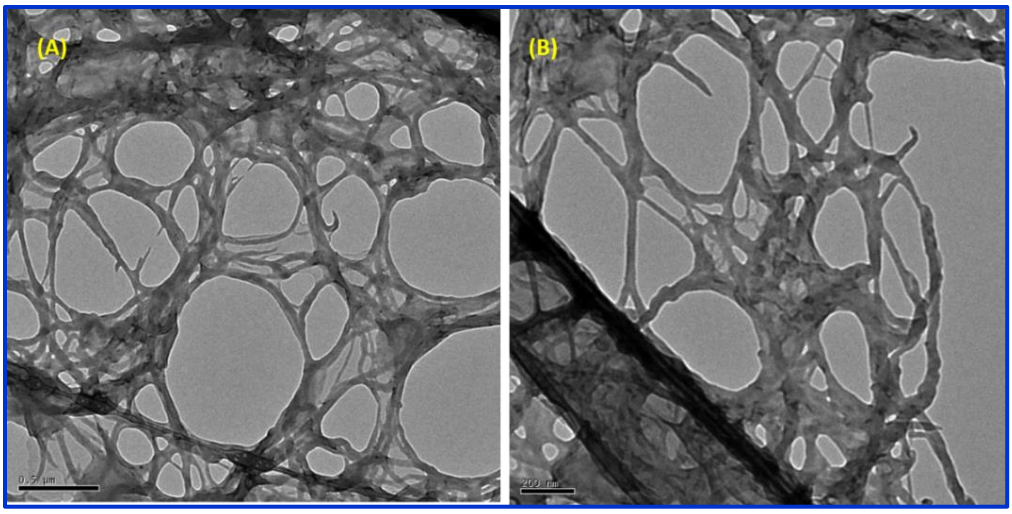

Figure 2.17 TEM images of **Poly-11** in 25% EtOH:THF solvents mixture on copper grid stained with uranyl acetate; aggregation of toroid-like structures.

Further, concentration series of 0.1 - 0.5 mg/mL solution of **Poly-10** and **Poly-11** were prepared and the samples were inspected using AFM. The solvent mixture we used here is 25% EtOH:THF. Interestingly, for **Poly-11**, we observed unique nanofiber bundles with diameters varying from 160 - 260 nm. This behavior was not found in **Poly-10** which is a linear analog of

the three-arm star polymer. For **Poly-10**, elongated nanofiber assemblies were identified by AFM **(Figure 2.18**). The average diameters of these aggregates were measured to be 80 nm-100 nm. For both **Poly-10** and **Poly-11**, as the concentration increases, it forms a densely packed network structure (**Figure 2.19**). Further for **Poly-11**, toroidal structures are formed and we believed this can take place due to the presence of long fibers (*i.e.*, when termini of bent fibers may fuse together and eventually form looped assemblies). The appearance of that type of assemblies is significant at low concentration.

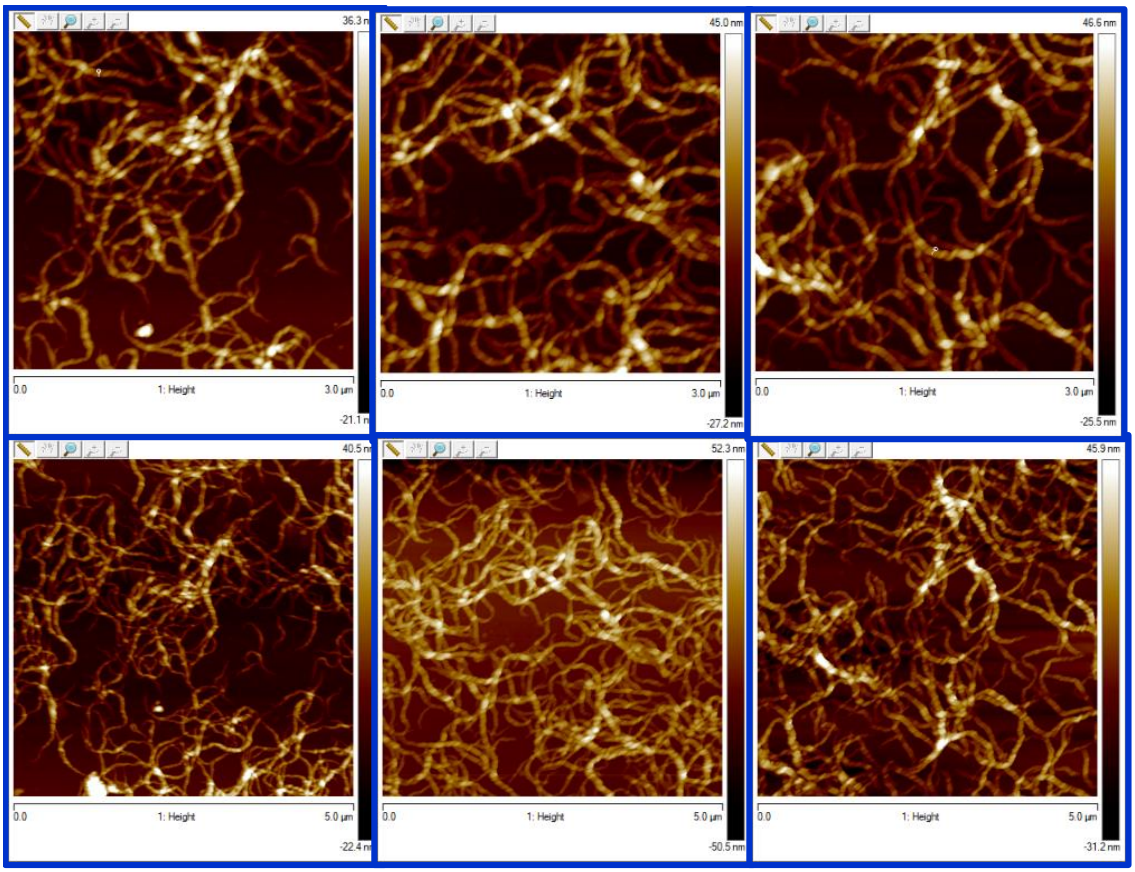

Figure 2.18 AFM micrographs of **Poly – 10** spin-cast from THF/ 25 vol% EtOH solvents mixture onto silicon wafers: (top row, C = 0.3 mg/ mL, bottom row, C = 0.5 mg/mL), 5 µm scan size images.

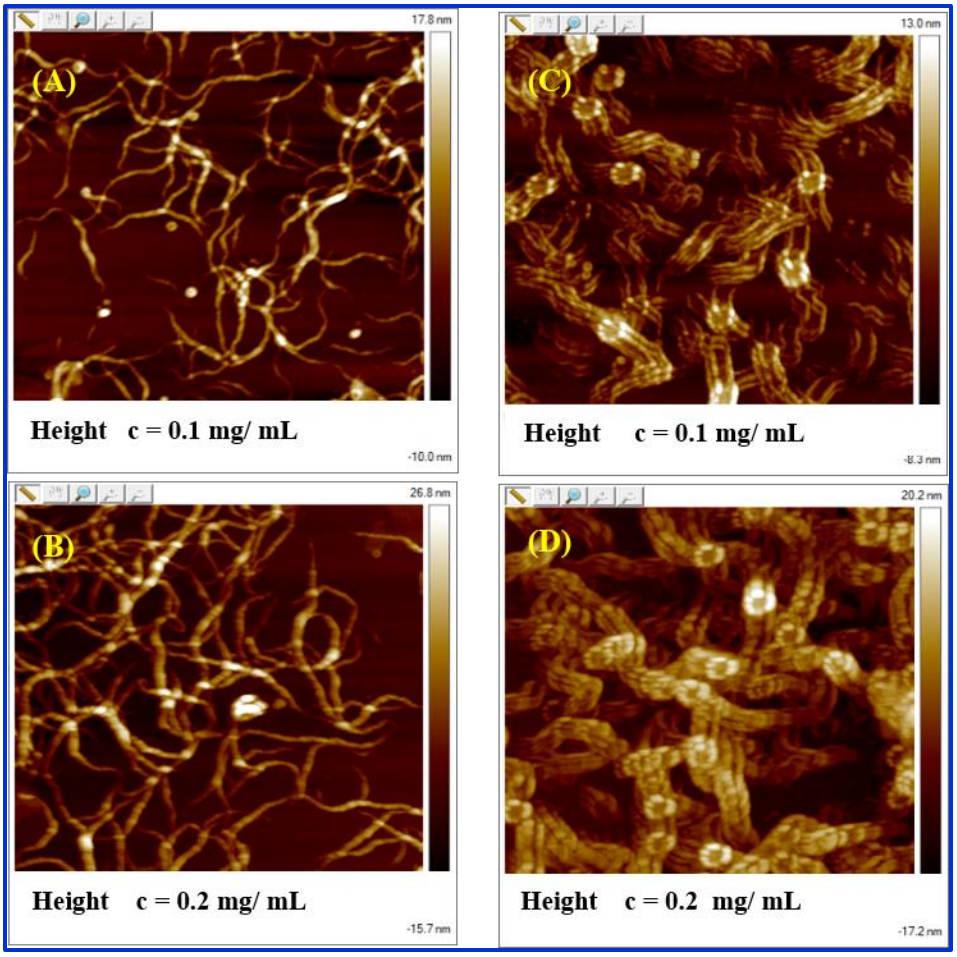

Figure 2.19 AFM micrographs of **Poly-10** (**A, B**) and **Poly-11** (**C, D**) spin-cast from 25 vol% EtOH: THF solvents mixture onto silicon wafers (3 x 3 μm scan size).

2.3.7 Electro-sprayed morphology

Electrospinning/electrospraying is a widely used method to obtain well-defined fibers/spheres. The morphology would depend on the viscosity of the sample, surface tension and the potential applied.[36] We used this technique to create well-defined morphologies for polycarbodiimide polymers. During the electrospinning process, the viscoelastic force and coulombic forces are acting against each other by causing the sample jet to stretch to fibers along the electric field.[37] For dilute polymer solutions, the low viscoelastic forces are not strong enough to act against the

electric force and as a result, spheres are formed. These spherical droplets are formed due to surface tension and in low concentrations, hollow spheres are formed.[38] Our solvents of choice for this electrospraying work are toluene and 1,1,2,2-tetracholoroethane due to their relatively high boiling points that prevent fast evaporation. The morphology obtained through this process is solvent dependent. We have used both 14.4% (w/w) of **Poly-10** and **Poly-11** samples in toluene and hollow spheres formation was observed. These hollow spheres are large and in the range of 10-30 µm scale **(Figure 2.20).** Platelet-like aggregates were obtained from 1,1,2,2-tetracholoroethane for both 19% (w/w) of **Poly-10** and 12% (w/w) of **Poly-11**. These platelet-like spherical morphologies are small in size ranging from 1-4 µm **(Figure 2.21** and **2.22)** and their morphology was further confirmed with bright field microscope **(Figure 2.23** and **2.24)**. We believe that right tuning of the electrospraying conditions would yield desired nano/micro particulate materials for diverse applications such as solid dispersion for water insoluble drugs[39,40] and self-assembled particulates matters.[41,42]

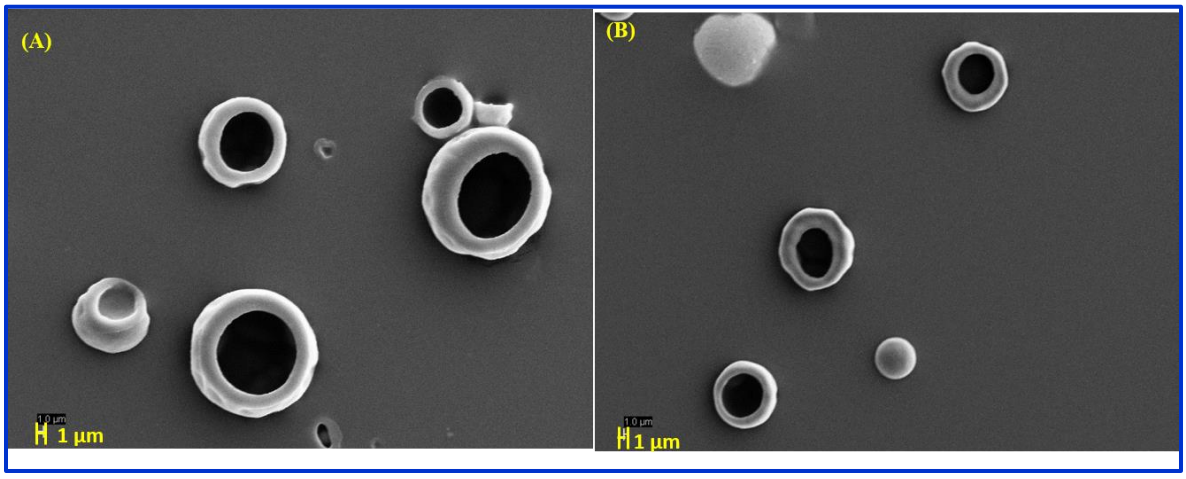

Figure 2.20 SEM images of the electro-sprayed morphology of **Poly – 10** (**A**) and **Poly – 11** (**B**) in toluene.

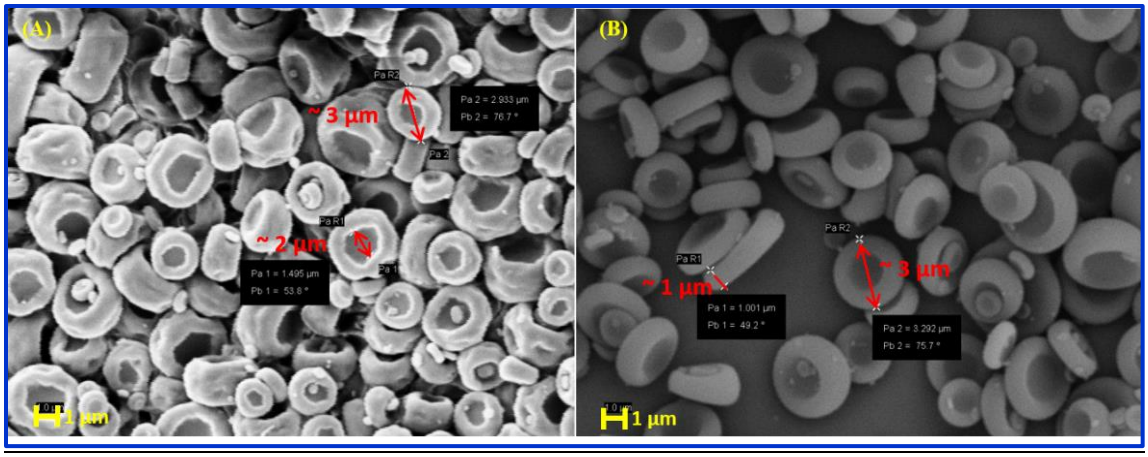

Figure 2.21 SEM images of electro-sprayed morphology of **Poly – 10** (**A**) and **Poly – 11** (**B**) in 1,1,2,2-tetrachloroethane.

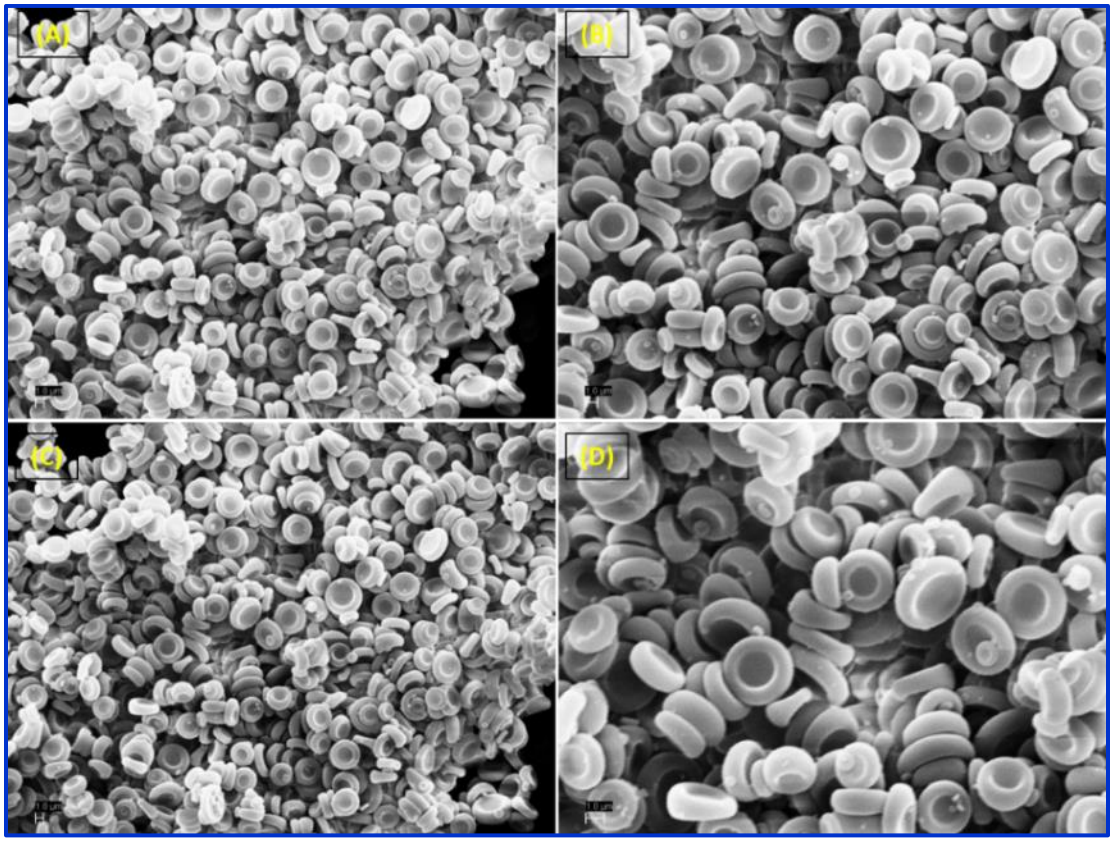

Figure 2.22 SEM images of the electrosprayed morphology of **Poly – 11** in 1,1,2,2-tertachloroethane: Showing platelet-like aggregates.

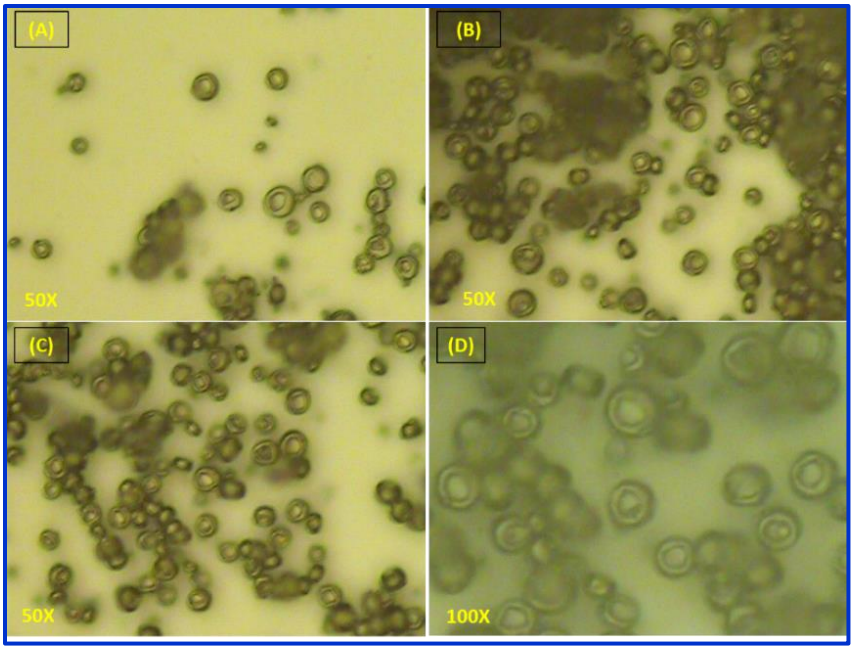

Figure 2.23 Optical microscope images of electro-sprayed morphology of **Poly – 10** in 1,1,2,2-tertachloroethane.

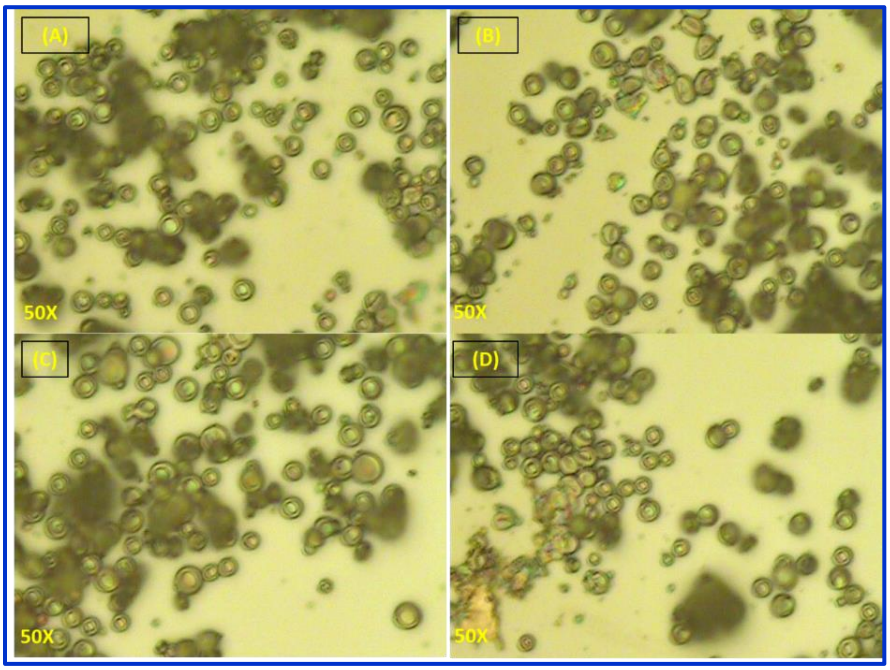

Figure 2.24 Optical microscope images of electro-sprayed morphology of **Poly – 11** in 1,1,2,2-tertachloroethane.

2.3.8 DLS (Dynamic Light Scattering)

DLS studies were performed to investigate the hydrodynamic radius and self-assembly behavior in solution. For polymers with the same molecular mass, the hydrodynamic radius which is the radius of the sphere defined by molecules in solution will be different for star-like polymers when compared to their linear analogs. For DLS studies we have investigated for different sample concentrations similar to those used in AFM studies in toluene (C = 0.1 mg/mL to 0.5 mg/mL). To obtain the polymer samples for this study, the polymerization was conducted by taking 250:1 ratio of monomer to initiator using the same polymerization time.

The values we have obtained from the experiment reveal that **Poly-11** has a less hydrodynamic diameter (Z) than that of **Poly-10**. For sample concentration of 0.1 mg/mL, Z was calculated to be 39 nm and 119 nm for **Poly-11** and **Poly-10**, respectively. This observation is consistent with the three-arm star polymer is confined into a smaller volume due to shorter arms (**Table 2.1**). In **Poly-10**, due to its inherent rigid-rod nature of polycarbodiimide scaffold and a longer polymer chain, it occupies larger volume in solution, thus it possesses a higher Z value. For all samples at all concentrations, they show an intense peak with tailing/shoulder portion as the concentration increases **(Figures 2.25** and **2.26).** This tailing should account for self-aggregation of macromolecules and this aggregation behavior is also observed in AFM imaging as discussed in 2.3.5 section. According to AFM imaging, these polymers tend to form super helical aggregates and formation of such structures are energetically favorable to minimize the interactions with solvent. Overall, the presence of long polymer chains in **Poly-10** would induce them to aggregate into large spheres when compared with **Poly-11** (**Figure 2.27**).

Table 2.1 Z average diameter of Poly-**10** and **Poly-11** in different concentrations

	Poly- 10		**Poly -11**	
Concentration (mg/ mL)	Z average diameter (nm)	PDI	Z average diameter (nm)	PDI
0.1	119.1 (10.81)	0.09	38.22 (3.87)	0.101
0.2	55.50 (4.32)	0.174	31.76 (9.03)	0.253
0.3	45.8 (3.21)	0.39	7.46 (0.10)	0.370
0.4	7.11 (8.26)	0.24	25.74 (0.48)	0.387
0.5	29.80 (1.15)	0.26	25.07 (0.28)	0.351

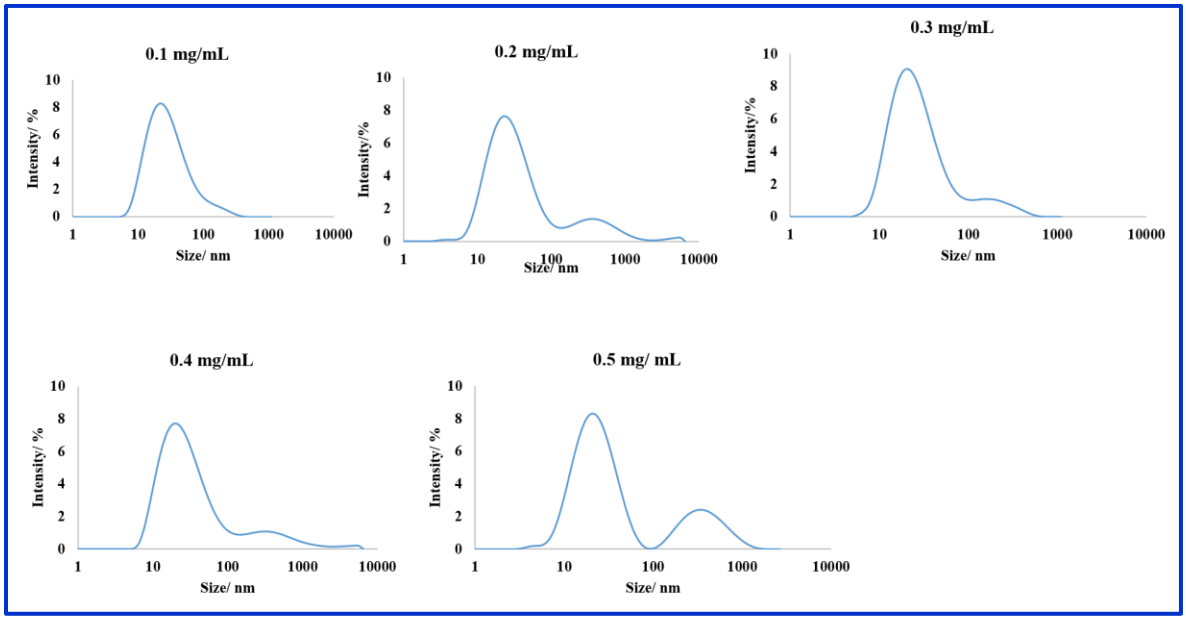

Figure 2.25 DLS profiles of **Poly-10** in different concentrations in toluene.

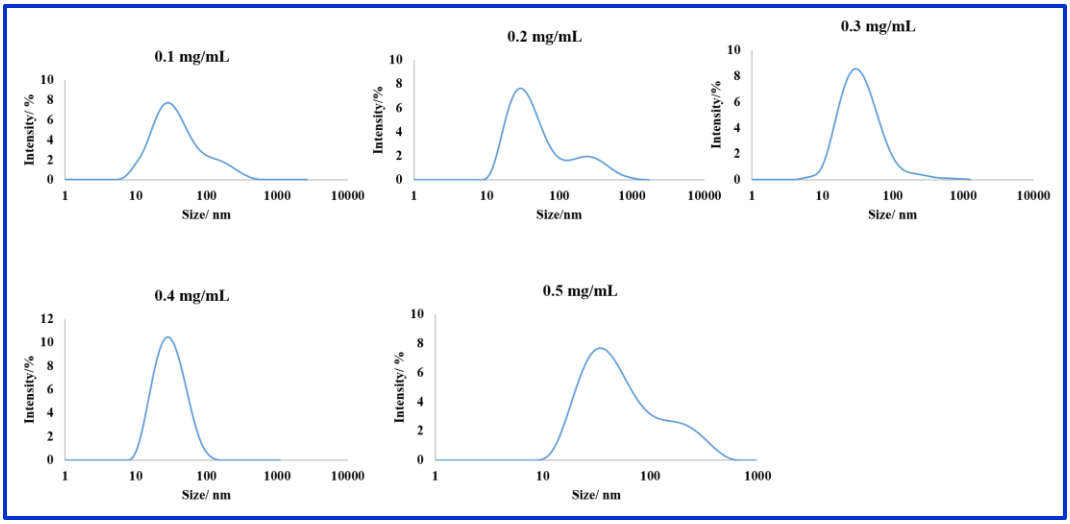

Figure 2.26 DLS profiles of **Poly-11** in different concentrations in toluene.

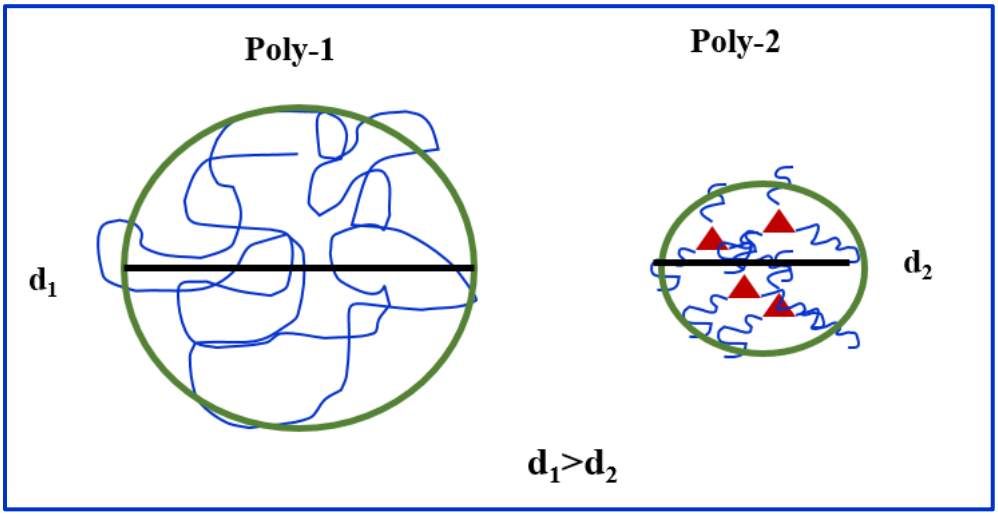

Figure 2.27 Cartoon showing behaviour of **Poly-10** and **Poly-11** in solution; polymer stars possesses compact structure while linear analogus adopt into more free volumn.

2.3.9 *p*-XRD (Powder X-ray Diffraction)

We have investigated both **Poly-10** and **Poly-11** by *p*-XRD to reveal the details of crystal packing. For that, we have deposited solid materials on Si-wafer. Using AFM imaging, it was found that width of fiber is around 70-200 nm and this implies that the formation of super-helical

associations/bundling. Therefore, for **Poly-10** and **Poly-11**, the corresponding *d*-spacing values are 11.04 Å and 10.88 Å (for **a** and **a'**, respectively) indicative of inter-helical distance and the broad peaks at 6.059 Å and 6.023 Å may arise due to lateral spacing of bulky pendant groups of *N*- phenethyl scaffold (**Figure 2.28**). Based on the first order reflection peaks for both **Poly-10** and **Poly-11**, it can be speculated that this resulted from self-assembly behavior in the solid state. **Poly-11** shows more intense first order peak at 10.88 Å whereas 11.04 Å for **Poly-10** implying that **Poly-11** possesses higher crystallinity (more ordered structure) than **Poly-10**.

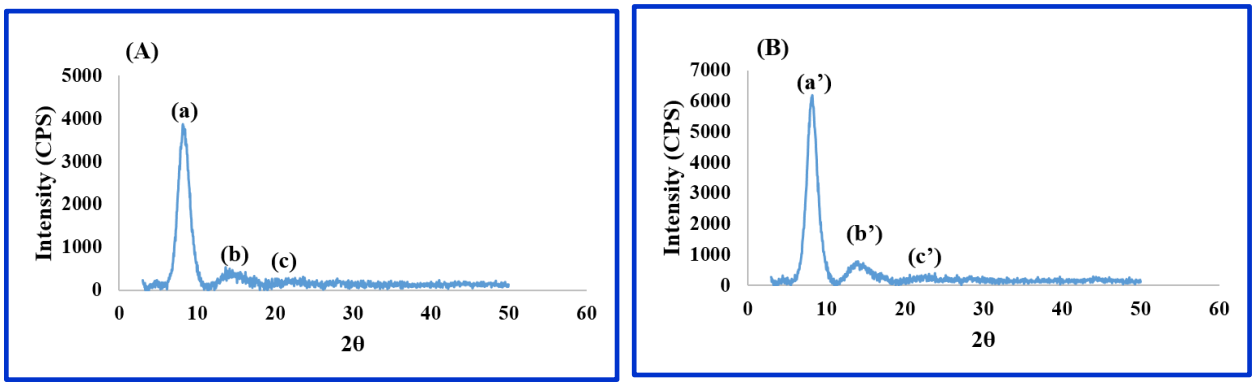

Figure 2.28 Powder X-ray diffraction pattern for **Poly-10 (A)** and **Poly-11 (B).**

We hypothesize that individual helices of the polymer can self-aggregate to form intertwining structures with interhelical distance around 11 Å that correlates nicely with *d*-spacing values (*i.e.*, *p*-XRD profiles of both **Poly-10** and **Poly-11** showed an intense peak around 11.04 Å and 10.88 Å). Another broad peak arising around 6 Å can be attributed to the distance between centroids of adjacent phenyl groups (**Figure 2.29**, alternatively, this could be a distance between adjacent chiral centers of phenethylmethyl pendant groups).

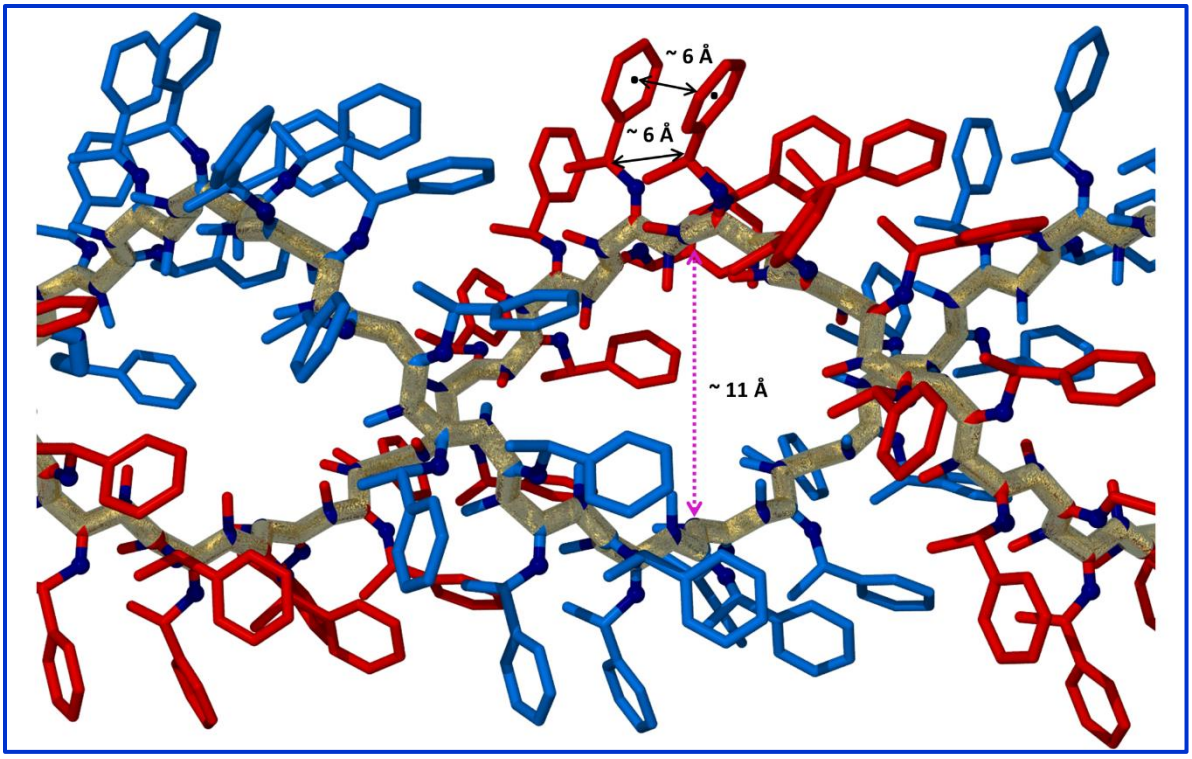

Figure 2.29 Two intertwined right-handed helices (red & blue) forming dimeric bundle: amidine scaffold depicted as gold spiral, hydrogen atoms are omitted for clarity.

2.4 Conclusions

In summary, nitrile functionalized Ni(II) initiator and trimetallic Ni(II) initiator bearing multiple initiating sites were synthesized to achieve the controlled polymerization of chiral carbodiimides. Using these initiators, excess single-handed screw sense linear homopolymers and three-arm star helical polymers were obtained, respectively. Both VCD and SOR studies confirmed the single handed helical structure of **Poly-10** and **Poly11**. Their self-assembly behavior was shown to be solvent-dependent by AFM and TEM data indicating the formation of nanofiber aggregation behaviors along with super-helical formations. This includes wormlike aggregation cast from THF, densely-packed network morphology from chloroform, and nanofiber morphology from toluene. In binary solvent systems, these polymers self-assemble into super-helical structure

which is pronounced when casting from 25% EtOH:THF solvent combination. These types of assemblies are hypothesized to be due to inter-helical communication among adjacent polymer chains and may result from their interpenetration. Another important finding is that both linear and multi-arm star polymer can be processed by electrospraying technique to obtain uniform assemblies, such as platelet-like particles and hollow spheres. The morphology obtained is also solvent-dependent which is evident by SEM studies. We presume that these spheres can be used to create different blends/composites with drug molecules and lipid droplets which may be utilized in medical applications including drug delivery.

2.5 Experimental Section

General Data

The chemicals were purchased from Sigma-Aldrich (Milwaukee, WI) and used as received unless stated otherwise. The polymerization solvents, *i.e.*, toluene and chloroform were distilled prior to use. The solvents used for self-assembly studies, *i.e.*, MeOH, EtOH, THF, toluene, and $CHCl_3$ were used as received. For electro-spaying work, toluene and 1,1,2,2-tetrachloroethane were used as received.

Instrumentation

^{1}H NMR, ^{13}C NMR, and ^{31}P NMR were recorded on Bruker Advance III^{TM} 500 MHz NMR spectrometer at room temperature. Powder X-ray Diffraction (*p*-XRD) data profiles were obtained on the Rigaku Ultima III X-Ray diffractometer. Tapping-mode atomic force microscopy (AFM) was performed using a Nanoscope IV Multimode Veeco instrument, equipped with an E-type vertical engage scanner. The all images were acquired at room temperature by using silicon cantilevers with nominal spring constant of 42 N/m and 320 kHz

OTESPA tips purchased from Bruker. For all AFM analysis, the samples were spin-coated on silicon wafers (Wafer world, diameter, d = 2.5 cm) spun at 1000 rpm for 30 s. Specific optical rotation were recorded on a JASCO P-1010 polarimeter (C = 2.0 mg/mL, l = 10.0 cm, and λ = 435 nm) and solution-state vibrational circular dichroism (VCD) spectra were obtained using BioTools ChiralIR-2X VCD spectrometer in deuterated chloroform (C = 25 mg/mL and l = 50 μm). For kinetic studies, Mettler Toledo icIR –ReactIR–15 and ic IR4.3 software package was used to monitor the loss of the carbodiimide N=C=N stretching mode as the polymerization progressed. All FTIR spectra were collected by using Thermo Scientific Nicolet380 TR-FTIR spectrometer. For dynamic light scattering (DLS) measurement, Malvern Zetasizer particle sizer Nano ZS model equipped with He-Ne laser source at 633 nm, Max 4 Mw was used. Transmission electron microscope (TEM) images were recorded on a Tecnai Spirit electron microscope operating at 200 kV (UT Southwestern Medical School). The carbon coated copper grid was used as a support and negative staining with 2% aqueous uranyl acetate was applied to the specimens. Electrospraying of **Poly-10** and **Poly-11** was done by using a custom built electrospinner, 12 kV voltage was applied using a power supply (Gamma High Voltage Research) to the needle tip and the sprayed polymer was collected at the ground collector. The flow rate was adjusted to 0.5 mL/hr with a syringe pump. The distance between the needle tip and the collector was 15 cm and it was kept constant throughout the process. Scanning electron microscopy (SEM) imaging was done by using Zeiss Supra 40 instrument at UTD nano characterization facility. The samples were mounted on silicon wafers and it was coated with conductive Pd/Au film. Leica INM100 optical microscopy was used to observe the electro-sprayed material under bright field. All cartoons have been generated by using Gaussian software

package. Semi-empirical calculations were carried out by using AM1 force field, as integrated in Gaussian 09W. To produce output graphics, PyMOL software package has been used (PyMOL 1.7 rol build).

2.5.1 Synthesis

Synthesis of 2,4,6-*tri*(4-bromo-3-methyl)-1,3,5-triazine (**Compound - 1**)

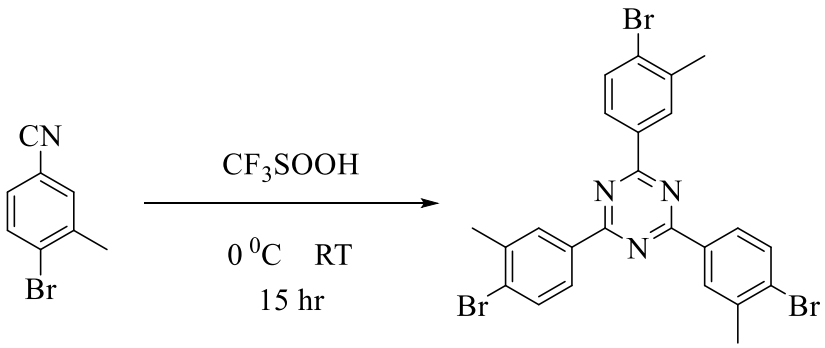

Triflic acid (CF_3SO_3H) (10.0 g, 66.6 mmol) was placed in a 50 mL round bottom flask and it was cooled at 0 °C by using an ice bath. The 4-bromo-3-methylbenzonitrile (3.570 g, 18.2 mmol) was added dropwise and it was stirred for 30 min at 0 °C. The mixture was further stirred at room temperature for 15 hours. Subsequently, 100 mL of deionized water was added and it was suspended with 1.0 M NaOH for 30 min. The resulting white precipitate was filtered and dissolved in chloroform:acetone (1:1) mixture. Then the organic phase was extracted with DCM and evaporated using rotary evaporator. The resulting white precipitate was dried under vacuum for overnight.

Yield = 10. 170 g (17.3 mmol, 95%).

Elemental analysis: Br = 40.36%, C = 40.03%, H = 2.96%, N = 6.89%).

^{1}H NMR (500 MHz, $CDCl_3$, δ ppm): 8.53 (s, 1H, Ar-H), 8.39, 8.37, (d, 1H, Ar-H) 7.72 and 7.71 (d, 1H, Ar-H), 2.57 (s, 3H, CH_3).

^{13}C NMR (125 MHz, $CDCl_3$, δ ppm): 171.12 (triazine core, C=N), 138.40, 135.06, 132.79, 130.89, 130.20, 127.76 (C-Ar), 23.17 (CH_3).

Synthesis of *tris*-Ni (II) initiator (**Cat-8**)

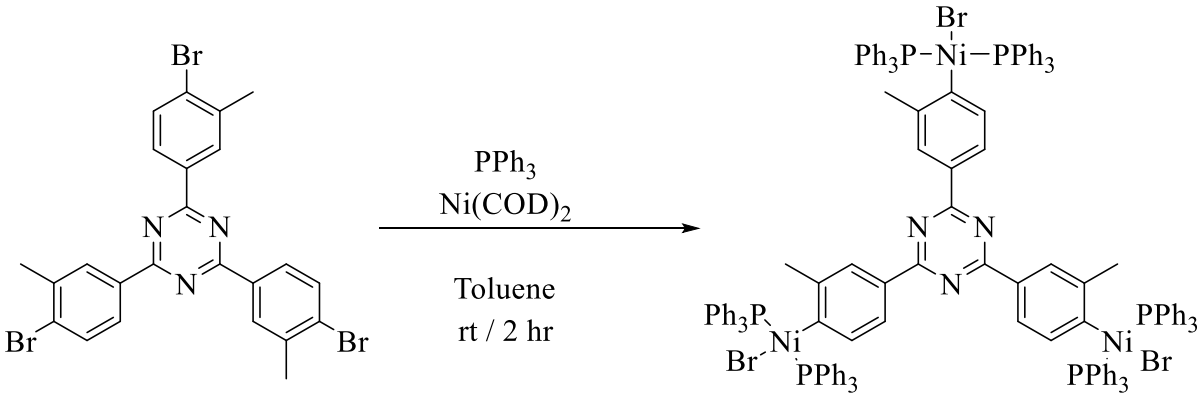

Inside the glove box 0.500 g (1eq., 85.0 mmol) of 2,4,6-*tri*(4-bromo-3-methyl)-1,3,5-triazine and 2.006 g (9 eq., 7.7 mmol) of *tri*phenylphosphine (PPh_3) were placed in an oven-dried vial and were dissolved in 4.0 mL of dried toluene. It was then stirred for 10 min until all starting materials dissolved completely. 0.700 g (3 eq., 2.6 mmol) of $Ni(COD)_2$ (bis(1,5-cyclooctadiene) nickel(0)) was added along with another 0.5 mL of dried toluene.The resulting red color solution was allowed to stir for 2 hr. The reaction vial then was removed from the glove box and 40 ml of dried hexane was added and it was allowed to stir for 15 min. The resulting orange color precipitate was filtered and subsequently washed with hexane and methanol. The product was isolated and dried under vacuum.

Yield = 1.540 g (66.3 mmol, 78%).

^{1}H NMR (500 MHz, $CDCl_3$, δ ppm): 7.56, 7.54, 7.37, 7.36, 7.34, 7.27, 7.26, 7.25, PPh_3 (Overlapped, 5 H, Ar-H,), 7.22, 7.20 (d, core. 1H, Ar-H), 6.44, 6.42, (d, core. 1H, Ar-H), 6.10 (s, core. 1H, Ar-H), 2.29 (s. 3H, CH_3).

^{31}P NMR (202 MHz, toluene, δ ppm): 22.26.

Synthesis of nitrile functionalized initiator **(Cat-6)**

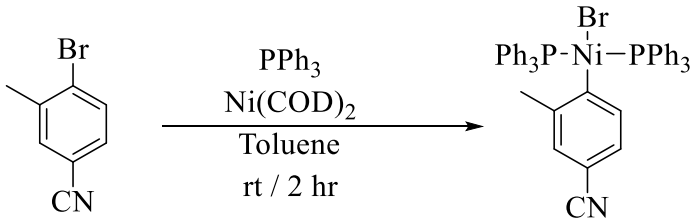

Similar procedure as **Cat-8** was followed to synthesized **Cat-6** by using 0.500 g (1 eq., 2.6 mmol) of 4-bromo-3-methylbenzonitrile, 0.702 g (1 eq., 2.6 mmol) of $Ni(COD)_2$, and 2.007 g (3 eq., 7.7 mmol) of PPh_3.

Yield = 1.620 g (2.1 mmol, 82%).

^{1}H NMR (500 MHz, $CDCl_3$, δ ppm): 7.55, 7.37, 7.36, 7.34, 7.27, 7.25 PPh_3 (overlapped, 5H, Ar-H), 7.22, 7.20 (d, 1H, Ar-H), 6.44, 6.42 (d, 1H, Ar-H), 6.10 (s, 1H, Ar-H), 2.29 (s, 3H, CH_3).

^{13}C NMR (126 MHz, $CDCl_3$, δ ppm): 143.98 (Ni-Ar-C), 137.46, 135.58, 133.88, 131.52, 130.96 (Ar-C), 128.95(CN), 125.43, 117.62, 111.47 (Ar-C), 23.59 (CH_3).

Synthesis of *N*-1-phenylethyl-*N*'-methylurea (**Compound 2**)

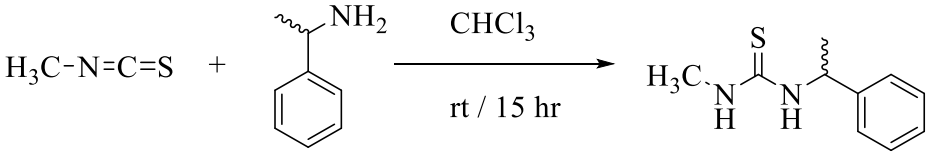

6.034 g (1 eq. 82.5 mmol) of methylisothiocyanate was dissolved in 40 mL anhydrous $CHCl_3$ in a 250 ml round bottom flask. Then 10.000 g (82.5 mmol) of (*S*-(+)-(α)-methylbenzylamine was

added dropwise. It was then allowed to stir for overnight. The reaction mixture was concentrated using rotary evaporator and 100 mL of hexane was added. It was allowed to stir for 3 hours and a white color precipitate of urea was isolated and recrystallized with hot ethanol. The product was dried under vacuum.

Yeild = 14.43 g (74.24 mmol, 90 %).

^{1}H NMR (500 MHz, $CDCl_3$, δ ppm): 7.30-7.39 (overlapped, 5 aromatic H), 6.18 (broad, N-H), 5.51 (broad, N-H), 4.87 (broad, methine-H), 2.96 (N-CH_3), 1.52 (d, benzyl CH_3).

^{13}C NMR (125 MHz, $CDCl_3$ δ ppm): 182.18 (C=S), 142.00, 129.34, 128.19, 125.9 (Ar-C), 54.01 (N-CH_3), 31.76 (methyne-C), 23.72 (benzyl CH_3).

Synthesis of *N*-phenylethyl-*N*'-metylcarbodiimide monomer (**Compound 3**)

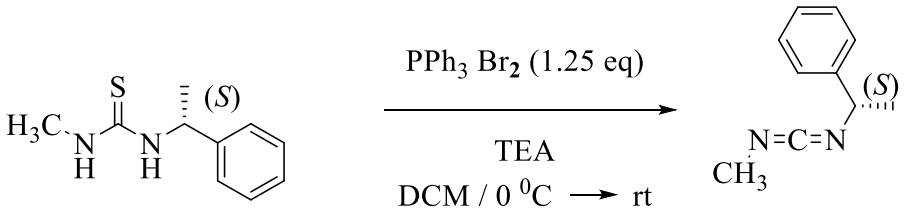

27.200 g (1.25 eq. 61.9 mmol) of dibromotriphenyl phosphorane was suspended in 50 mL of anhydrous DCM under nitrogen. Then the reaction mixture was cooled to 0 ^{o}C and 18 mL (2.5 eq. 128.4 mmol) of triethylamine (TEA) was added very slowly. Then 10.000 g (51.5 mmol) of *N*-phenylethyl-*N'*-methylurea was added and the reaction mixture was allowed to warm to room temperature. Dehydration of thiourea into carbodiimide monomer can be monitored by appearance of N=C=N stretch at ≈ 2140 cm^{-1} in infrared spectroscopy.

Yield = 5.760 g (36.1 mmol, 70%).

^{1}H NMR (500 MHz, $CDCl_3$, δ ppm): 7.24 -7.36 (aromatic H, overlapped), 4.58 - 4.62 (q, methine H), 2.93 (t, N-CH_3), 1.53 (d, benzyl-CH_3, 3H).

^{13}C NMR (125 MHz, $CDCl_3$, δ ppm): 140 (N=C=N), 144.08, 128.65, 127.43, 125.94 (Ar -C=C), 56.67 (benzylic-C), 32.89 (N-CH_3), 25.14 (benzyl-CH_3).

Synthesis of 3-arm star polymer (**Poly-11**)

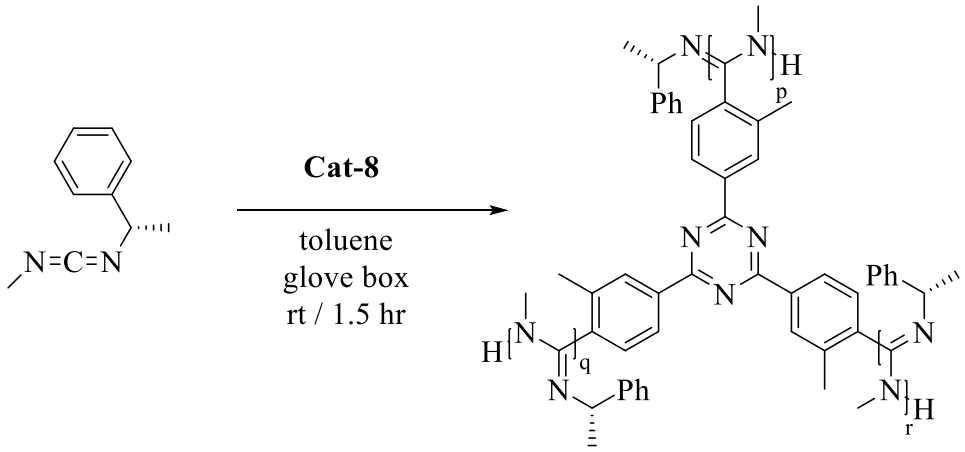

Monomer: initiator ratio = 500:1 was used for polymerization.

Inside the glove box, 1.000 g (500 eq. 249.6 mmol) of monomer was mixed with 0.5 mL of dried toluene and 29.2 mg (eq. 6.2 mmol) of **cat-8** was added. The reaction mixture was allowed to stir for 2 hours inside the glove box. The resulting gel-like mixture was taken out from the glove box and dissolved in chloroform and reprecipitated in methanol for 3 times along with 2 drops of DBU. The polymer was collected and finally dried under vacuum overnight. Yield = 0.850 g (85%).

^{1}H NMR (500 MHz, $CDCl_3$, δ ppm): 7.60-7.26 (broad, aromatic H), 5.70, 5.20, 4.61 (broad, pendent methine H), 3.54-2.87 (broad, N-CH_3), 2.13 (CH_3 groups of the core, 9 H), 1.32 (benzylic CH_3).

^{13}C NMR (125 MHz, $CDCl_3$, δ ppm): 171.24 (triazine core C=N), 148.50, 138.47, 135.14, 132.85, 130.96,130.24 128.08, (overlapped, pendant phenyl C=C), 127.83,126.25 (overlapped,

three phenyl groups in periphery of triazine ring, C=C), 56.84 (benzylic pendant group C), 34.41 (N-CH_3), 26.26 (three CH_3 groups in periphery aromatic groups), 23.19 (benzylic CH_3).

Synthesis of linear polymer **(Poly-10)**

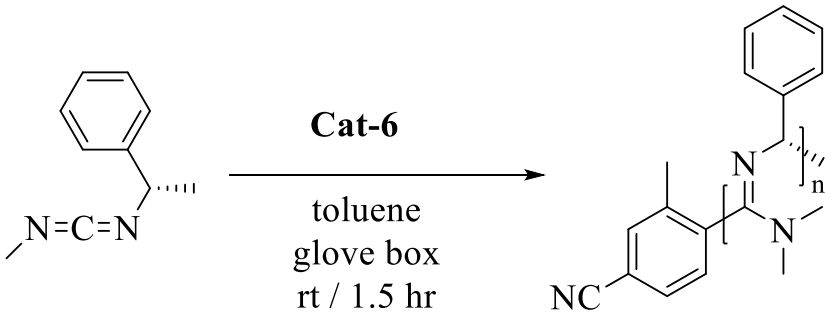

Similar procedure as **Poly-11** was followed to synthesize **Poly-10** by using 1.0 g of *N*-1-phenylethyl-*N'*-metylcarbodiimide monomer and 9.7 mg (124.7 mmol) of **Cat-6**.

Yield = 0.950 g (90%).

^{1}H NMR (500 MHz, $CDCl_3$, δ ppm): 7.60-7.23 (broad, aromatic H), 5.68, 5.21, 4.6 (broad, pendant methine H), 3.21-2.87 (broad, N-CH_3), 2.13 (CH_3 end group, 3H), 1.38 (benzylic CH_3).

2.5.2 Polymer kinetics data

Table 2.2 Kinetic data for **Poly-11**

Time / min	Peak height (A.U.I) = $[M]_t$	$In[M]_0/[M]_t$	% Conversion
0	0.723	0	
5	0.709	0.019	14.01
15	0.338	0.760	53.25

25	0.146	1.599	79.81
35	0.083	2.1645	88.52
45	0.050	2.671	93.08
55	0.025	3.364	96.54
65	0.015	3.875	97.93

Table 2.3 Kinetics data for **Poly-10**

Time / hours	Peak height (A.U.I) = $[M]_t$	$In[M]_0/[M]_t$	% Conversion
0	0.725	0	0
1	0.650	0.109	10.32
2	0.512	0.348	29.36
3	0.422	0.542	41.86
4	0.342	0.751	52.79
5	0.291	0.913	59.86
6	0.244	1.090	66.39
7	0.222	1.184	69.41
8	0.195	1.314	73.12
9	0.186	1.362	74.39
10	0.178	1.405	75.47

Sequential monomer addition kinetics

Under nitrogen, in a 100 mL three neck flask 0.5 g (500 eq. 3.1 mmol) of monomer (PMC) was placed and 4.0 mL of dried toluene was added. Then a fiber-optic IR probe was inserted into the flask. Then 14.7 mg (1 eq. 124.8 mmol) of **Cat-8** was added into monomer solution and the change of intensity of N=C=N peak was monitored simultaneously. At the 90% consumption of monomer, the second portion of 1.250 g (7.802 mmol) of PMC monomer was added and the polymerization was resumed. Again the change of intensity of N=C=N peak was monitored simultaneously with fiber-optic IR probe.

Table 2.4 Kinetics data for sequential monomer addition experiment

Time (min)	**Intensity**	**% conversion**
0	0.44	0
15	0.37	16
30	0.28	36
45	0.25	43
60	0.20	54
75	0.15	66
90	0.09	80
105	0.04	91
110	0.82	0
140	0.72	12
170	0.68	17

200	0.53	35
230	0.45	45
260	0.37	55
290	0.23	72
320	0.15	82
350	0.09	89

2.6 References

(1) Shibayama, K.; Seidel, S. W.; Novak, B. M., Living Polymerization of Carbodiimides Initiated by Copper(I) and Copper(II) Amidinate Complexes. *Macromolecules* **1997,** *30* (11), 3159-3163.

(2) Goodwin, A.; Novak, B. M., Synthesis of New Rigid Rod Helical Polymers through the Living Polymerization of Carbodiimides Using Titanium(IV) Complexes. *Macromolecules* **1994,** *27* (19), 5520-5522.

(3) Reuther, J. F.; Bhatt, M. P.; Tian, G.; Batchelor, B. L.; Campos, R.; Novak, B. M., Controlled Living Polymerization of Carbodiimides Using Versatile, Air-Stable Nickel(II) Initiators: Facile Incorporation of Helical, Rod-like Materials. *Macromolecules* **2014,** *47* (14), 4587-4595.

(4). Kim, J.; Novak, B. M.; Waddon, A. J., Liquid Crystalline Properties of Polyguanidines. *Macromolecules* **2004,** *37* (22), 8286-8292.

(5). Kim, J.; Novak, B. M.; Waddon, A. J., Lyotropic Liquid Crystalline Properties of Poly(N,N‘-di-n-hexylguanidine). *Macromolecules* **2004,** *37* (4), 1660-1662.

(6). Reuther, J. F.; Novak, B. M., Evidence of Entropy-Driven Bistability through 15N NMR Analysis of a Temperature- and Solvent-Induced, Chiroptical Switching Polycarbodiimide. *Journal of the American Chemical Society* **2013,** *135* (51), 19292-19303.

(7). Tang, H.-Z.; Lu, Y.; Tian, G.; Capracotta, M. D.; Novak, B. M., Stable Helical Polyguanidines: Poly{N-(1-anthryl)-N‘-[(R)- and/or (S)-3,7-dimethyloctyl]guanidines}. *Journal of the American Chemical Society* **2004,** *126* (12), 3722-3723.

(8). Qi, S.; Iida, H.; Liu, L.; Irle, S.; Hu, W.; Yashima, E., Electrical Switching Behavior of a [60]Fullerene-Based Molecular Wire Encapsulated in a Syndiotactic Poly(methyl methacrylate) Helical Cavity. *Angewandte Chemie International Edition* **2013,** *52* (3), 1049-1053.

(9). Kennemur, J. G.; Clark, J. B.; Tian, G.; Novak, B. M., A New, More Versatile, Optical Switching Helical Polycarbodiimide Capable of Thermally Tuning Polarizations ±359°. *Macromolecules* **2010,** *43* (4), 1867-1873.

(10). Tang, H.-Z.; Boyle, P. D.; Novak, B. M., Chiroptical Switching Polyguanidine Synthesized by Helix-Sense-Selective Polymerization Using [(R)-3,3‘-Dibromo-2,2‘-binaphthoxy](di-tert-butoxy)titanium(IV) Catalyst. *Journal of the American Chemical Society* **2005,** *127* (7), 2136-2142.

(11). Kennemur, J. G.; Kilgore, C. A.; Novak, B. M., Adjusting conformational switching behavior of helical polycarbodiimides through substituent induced polarity effects. *Journal of Polymer Science Part A: Polymer Chemistry* **2011,** *49* (3), 719-728.

(12). Kulikov, O. V.; Siriwardane, D. A.; Reuther, J. F.; McCandless, G. T.; Sun, H.-J.; Li, Y.; Mahmood, S. F.; Sheiko, S. S.; Percec, V.; Novak, B. M., Characterization of Fibrous Aggregated Morphologies and Other Complex Architectures Self-Assembled from Helical Alkyne and Triazole Polycarbodiimides (R)- and (S)-Families in the Bulk and Thin Film. *Macromolecules* **2015,** *48* (12), 4088-4103.

(13). Zhang, J.; Chen, X.-F.; Wei, H.-B.; Wan, X.-H., Tunable assembly of amphiphilic rod-coil block copolymers in solution. *Chemical Society Reviews* **2013,** *42* (23), 9127-9154.

(14). Reuther, J. F.; Siriwardane, D. A.; Campos, R.; Novak, B. M., Solvent Tunable Self-Assembly of Amphiphilic Rod–Coil Block Copolymers with Chiral, Helical Polycarbodiimide Segments: Polymeric Nanostructures with Variable Shapes and Sizes. *Macromolecules* **2015,** *48* (19), 6890-6899.

(15). Tew, G. N.; Pralle, M. U.; Stupp, S. I., Supramolecular Materials from Triblock Rodcoil Molecules Containing Phenylene Vinylene. *Journal of the American Chemical Society* **1999,** *121* (42), 9852-9866.

(16). Yashima, E., Synthesis and structure determination of helical polymers. *Polym J* **2010,** *42* (1), 3-16.

(17). Lapienis, G., Star-shaped polymers having PEO arms. *Progress in Polymer Science* **2009,** *34* (9), 852-892.

(18). Mueller, M.; Zentel, R., Photochemical Amplification of Chiral Induction in Polyisocyanates. *Macromolecules* **1994,** *27* (15), 4404-4406.

(19). Miyabe, T.; Iida, H.; Banno, M.; Yamaguchi, T.; Yashima, E., Synthesis and Visualization of a Core Cross-Linked Star Polymer Carrying Optically Active Rigid-Rod Helical Polyisocyanide Arms and Its Chiral Recognition Ability. *Macromolecules* **2011,** *44* (21), 8687-8692.

(20). Yashima, E.; Maeda, K., Chirality-Responsive Helical Polymers. *Macromolecules* **2008,** *41* (1), 3-12.

(21). Gao, H.; Matyjaszewski, K., Synthesis of Star Polymers by a Combination of ATRP and the "Click" Coupling Method. *Macromolecules* **2006,** *39* (15), 4960-4965.

(22). Iha, R. K.; Wooley, K. L.; Nyström, A. M.; Burke, D. J.; Kade, M. J.; Hawker, C. J., Applications of Orthogonal "Click" Chemistries in the Synthesis of Functional Soft Materials. *Chemical Reviews* **2009,** *109* (11), 5620-5686.

(23). Connal, L. A.; Li, Q.; Quinn, J. F.; Tjipto, E.; Caruso, F.; Qiao, G. G., pH-Responsive Poly(acrylic acid) Core Cross-Linked Star Polymers: Morphology Transitions in Solution and Multilayer Thin Films. *Macromolecules* **2008,** *41* (7), 2620-2626.

(24). Giguère, G.; Zhu, X. X., Functional Star Polymers with a Cholic Acid Core and their Thermosensitive Properties. *Biomacromolecules* **2010,** *11* (1), 201-206.

(25). Oka, M.; Nakajima, A., Synthesis and characterization of three-branched star-like poly(γ-benzyl-l-glutamate). *Polymer Bulletin* **1984,** *11* (5), 447-451.

(26). Zhang, M.; Liu, H.; Shao, W.; Ye, C.; Zhao, Y., Versatile Synthesis of Multiarm and Miktoarm Star Polymers with a Branched Core by Combination of Menschutkin Reaction and Controlled Polymerization. *Macromolecules* **2012,** *45* (23), 9312-9325.

(27). Goodson, S. H.; Novak, B. M., Synthesis and Characterization of Wormlike Three-Arm Poly(n-hexyl isocyanate) Star Polymers. *Macromolecules* **2001,** *34* (12), 3849-3855.

(28). Tanaka, H.; Shizu, K.; Nakanotani, H.; Adachi, C., Twisted Intramolecular Charge Transfer State for Long-Wavelength Thermally Activated Delayed Fluorescence. *Chemistry of Materials* **2013,** *25* (18), 3766-3771.

(29). Kennemur, J. G.; Novak, B. M., Advances in polycarbodiimide chemistry. *Polymer* **2011,** *52* (8), 1693-1710.

(30). Pin, J.-M.; Sbirrazzuoli, N.; Sacarescu, L.; Mija, A., Star-epoxy mesogen with 1,3,5-triazine core: a model of A4B3 fractal polymerization in a liquid crystalline thermoset media. *Polymer Chemistry* **2016,** *7* (6), 1221-1225.

(31). Robinson, K. L.; Khan, M. A.; de Paz Báñez, M. V.; Wang, X. S.; Armes, S. P., Controlled Polymerization of 2-Hydroxyethyl Methacrylate by ATRP at Ambient Temperature. *Macromolecules* **2001,** *34* (10), 3155-3158.

(32). Lee, H.-i.; Matyjaszewski, K.; Yu-Su, S.; Sheiko, S. S., Hetero-Grafted Block Brushes with PCL and PBA Side Chains. *Macromolecules* **2008,** *41* (16), 6073-6080.

(33). Kulikov, O. V.; Siriwardane, D. A.; McCandless, G. T.; Barnes, C.; Sevryugina, Y. V.; DeSousa, J. D.; Wu, J.; Sommer, R.; Novak, B. M., Self-Assembly of n-Alkyl- and Aryl-Side Chain Ureas and Their Derivatives as Evidenced by SEM and X-ray Analysis. *European Journal of Organic Chemistry* **2015,** *2015* (34), 7511-7518.

(34). Cai, C.; Lin, J.; Chen, T.; Wang, X.-S.; Lin, S., Super-helices self-assembled from a binary system of amphiphilic polypeptide block copolymers and polypeptide homopolymers. *Chemical Communications* **2009,** (19), 2709-2711.

(35). Snir, Y.; Kamien, R. D., Entropically Driven Helix Formation. *Science* **2005,** *307* (5712), 1067.

(36). Luo, C. J.; Stride, E.; Edirisinghe, M., Mapping the Influence of Solubility and Dielectric Constant on Electrospinning Polycaprolactone Solutions. *Macromolecules* **2012,** *45* (11), 4669-4680.

(37). Haghighi Poudeh, L.; Saner Okan, B.; Seyyed Monfared Zanjani, J.; Yildiz, M.; Menceloglu, Y., Design and fabrication of hollow and filled graphene-based polymeric spheres via core-shell electrospraying. *RSC Advances* **2015,** *5* (111), 91147-91157.

(38). Liu, J.; Rasheed, A.; Dong, H.; Carr, W. W.; Dadmun, M. D.; Kumar, S., Electrospun Micro- and Nanostructured Polymer Particles. *Macromolecular Chemistry and Physics* **2008,** *209* (23), 2390-2398.

(39). Mustapha, O.; Din, F. u.; Kim, D. W.; Park, J. H.; Woo, K. B.; Lim, S.-J.; Youn, Y. S.; Cho, K. H.; Rashid, R.; Yousaf, A. M.; Kim, J. O.; Yong, C. S.; Choi, H.-G., Novel piroxicam-loaded nanospheres generated by the electrospraying technique: physicochemical characterisation and oral bioavailability evaluation. *Journal of Microencapsulation* **2016,** *33* (4), 323-330.

(40). Nguyen, D. N.; Clasen, C.; Van den Mooter, G., Pharmaceutical Applications of Electrospraying. *Journal of Pharmaceutical Sciences* **2016,** *105* (9), 2601-2620.

(41). Yu, D.-G.; Williams, G. R.; Yang, J.-H.; Wang, X.; Yang, J.-M.; Li, X.-Y., Solid lipid nanoparticles self-assembled from electrosprayed polymer-based microparticles. *Journal of Materials Chemistry* **2011,** *21* (40), 15957-15961.

(42). Yuan, W.; Lu, Z.; Li, C. M., Controllably layer-by-layer self-assembled polyelectrolytes/nanoparticle blend hollow capsules and their unique properties. *Journal of Materials Chemistry* **2011,** *21* (13), 5148-5155.

CHAPTER 3

HELIX SENSE SELECTIVE POLYMERIZATION OF ACHIRAL CARBODIIMIDE MONOMERS BEARING ISOPROPYL SCAFFOLDS AND EFFECT OF REGIOREGULARITY ON STEREOCOMPLEXATION

Authors – Siriwardane, D. A.; Kulikov, O.; Novak, B. M.

Department of Chemistry and Biochemistry, BE 26

The University of Texas at Dallas

800 West Campbell Road

Richardson, TX 75080-3021

Manuscript is in preparation for publishing in the Journal of the American Chemical Society.

3.1 Abstract

Here we report the formation of stereocomplex from poly(*N*-methyl-*N*'-(2-isopropyl-6-methylphenyl)carbodiimide. Predominantly *P* and *M* helices have been synthesized through helix sense selective polymerization by using chiral BINOL-Ti(IV) diisopropoxide initiator with achiral (*N*-methyl-*N*'-(2-isopropyl-6-methylphenyl) carbodiimide monomer. Interestingly, upon thermal annealing, specific optical rotation (SOR) of the single handed polymer is getting decreased but never goes to zero. SOR would plateau out at a large value (-286 for *M* helices or + 283 for *P* helices) and shortly thereafter, it forms a precipitate. We describe this process in terms of stereocomplexation between two complementary strands *via* racemization. Inspired by analogy with classical leucine zippers isopropyl scaffolds (interlocking motifs), we designed unique polycarbodiimide scaffold bearing isopropyl pendant groups that play a vital role in aggregation process with calculated energy barrier of around 19 kcal/mol. To investigate the effect of regioregularity of isopropyl groups, similar structural isomers of polymers bearing isopropyl segments at *ortho*, *meta*, and *para* position have been synthesized and self-assembly behavior has been studied by using AFM, SEM, XRD and TEM. By taking advantage of zipping of isopropyl scaffold, block co-polymer of poly(*N*-methyl-*N*'-(2-isopropyl-6-methylphenyl)carbodiimide)-*b*-poly(*N*-phenyl-*N*'-octadecylcarbodiimide) (**P-2**) has been synthesized and it affords interesting spherical aggregations. This type of stereocomplex formation studies may be advantages in improving polymer properties as well as lead for new assemblies such as nanocarriers for drug delivery applications and encapsulation of chiral guest molecules.

3.2 Introduction

The helix is an interesting macrostructure that is utilized as a building motif in various macromolecules, such as DNA, polypeptides, and proteins.[1,2] Inspired by helical nature, these structural scaffolds regulate essential and specific functions in various biological systems. Synthetically, diverse helical polymer architectures were developed and their miscellaneous applications include molecular recognitions,[3] enantioseparation,[4] optoelectronic properties,[5] external stimuli responsive behavior[6] and formation of various tunable self-assemblies.[7,8]

Screw sense nature of polycarbodiimides offers a fascinating way to self-assemble into supramolecular constructs that can be used as drug carriers, catalysts, and for chiral separations. The presence of 'ridges-in-groves' or 'knobs-in-to-holes' model of the propagating chains in these macromolecules enhances the formation of the heterochiral associations which are energetically more favorable than respective homochiral spices.[9-11] The assemblies formed between two complementary strands are termed as stereocomplexes.[12-15] This kind of complexes gives rise to various intriguing properties which are not shown by parent, enantiomerically pure strands.[16,17,5]

Stereocomplexation offers some remarkable biological, chemical, and physical properties which can be important in various applications such as catalysis, drug delivery, improving thermal and mechanical properties.[18-21] For example, Coates and co-workers have been synthesized poly(propylene succinate) based stereocomplexes which possess improved thermal stability and semi-crystalline properties.[22] The synthetic route has been reported by Qiao and co-workers to prepare syndiotactic and isotactic PPMA (Polymethylmethacrylate) based triple helix-stereocomplexes is important for the creation of new functional nanomaterials.[23] Notably, Nanda

and co-workers have reported triple-helix stereocomplex which is based on L and D proline composed collagen peptides.[10] The complexation behavior has been characterized by using various techniques, such as X-ray scattering, SAXS profiles, AFM, and TEM techniques.

Here we report the formation of stereocomplex between complementary strands of poly(*N*-methyl-*N*'-(2-isopropyl-6-methylphenyl) **(P-1)** under thermal annealing conditions. The first observation was made by Novak and co-workers in 2004.[24] Predominantly, *P* and *M* helices have been synthesized by using achiral (*N*-methyl-*N*'-(2-isopropyl-6-methylphenyl)carbodiimide (**M-1**) monomer through helix-sense-selective polymerization along with chiral (*R*)/(*S*) BINOL-Ti(IV) diisopropoxide initiator. Loss of specific optical rotation (SOR) without reaching zero value (plateau out around +286˚ for *P* helices) has been observed upon thermal annealing and interestingly, shortly thereafter, the precipitate was formed. This unique behavior we have observed among 150 different polycarbodiimides reported so far. Accompanied with different techniques including polarimetry, vibrational circular dichroism, AFM, TEM, SEM, *p*-XRD and SAXS, parent single hand helices undergo with partial racemization to form stereocomplex upon thermal annealing. In this complexation, isopropyl scaffold plays a pivotal role in self-organizing molecules as evident by VCD and SAXS, and *p*-XRD data.

By taking advantage of this complexation, formation of spherical aggregates observed through the synthesis of block co-polymer (**P-1,2**). Aggregated morphologies caused by stereocomplex formation have been studied by using different imaging techniques, such as *p*-XRD, AFM, TEM, and SEM.

3.3 Result and Discussion

3.3.1 Helix-sense-selective polymerization of achiral monomers

Use of chiral initiators with achiral monomer is one of the interesting ways to obtain single handed polymers. During the course of the polymerization reaction, the initial chiral stimulant (*i.e.*, either chiral end group or continuous chiral influence from chiral monomers) solely biases the formation of specific handedness, which is called helix sense selective polymerization.[24,25] Through this polymerization either *P* (right handed) helix or *M* (left handed) helix can be formed and the interconversion between two helical senses is also possible, but it does not readily take place. However, the transformation of kinetically controlled excess helical sense into energetically favored thermodynamically stable conformation takes place via helical inversion barrier and the energy associated with this process is called helical inversion energy (or activation energy, E_a). By introducing substituted, bulky functional groups into two tunable pendant groups of carbodiimide monomer, static helices which possess high helical inversion energy polymers can be obtained. Bearing in mind that 2,6-disubstitution pattern may be used to introduce permanent asymmetry to the monomer, we have synthesized *N*-methyl-*N*'-(2-isopropyl-6-methylphenyl)carbodiimide monomer (**M-1**). Helix-sense selective polymerization was employed by using both chiral (*R*) and (*S*)-BINOL Ti(IV) diispropoxide initiators with achiral **M-1 (Scheme 3.1)**. Being 100% regioregular polymer, the 2,6-disubstituted aryl group is appended to sp^2 nitrogen (at imine position), thus providing polycarbodiimide with permanent asymmetry. Our postulate is based on the formation of stereocomplex due to isopropyl groups in aryl pendant groups and they undergo different aggregation process.

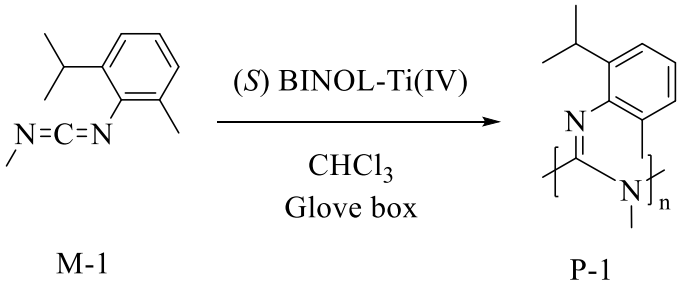

M-1 P-1

Scheme 3.1 Synthesis of **P-1:** poly(*N*-methyl-*N*'-(2-isopropyl-6-methylphenyl)carbodiimide).

3.3.2 Racemization behavior of P-1

This polymer shows very unusual behavior upon thermal annealing as reported previously by our group.[24] Before thermal annealing, this polymer exhibited high specific optical rotation (SOR) that tends to decrease without hitting zero. Shortly after plateauing around 286 (for (***R***) **P-1**), the polymer solution forms a precipitate when heated for several hours. Our hypothesis behind this phenomenon is the formation of stereocomplex *via* racemization process between the parent helical sense and '*in-situ*' generated opposite helical sense.

The formation of enantiomeric helices is entropically and thermodynamically favorable process that involves various kinds of non-covalent interactions, such as hydrophobic and electrostatic interactions. This process can be represented by following energy diagram (**Figure 3.1**).

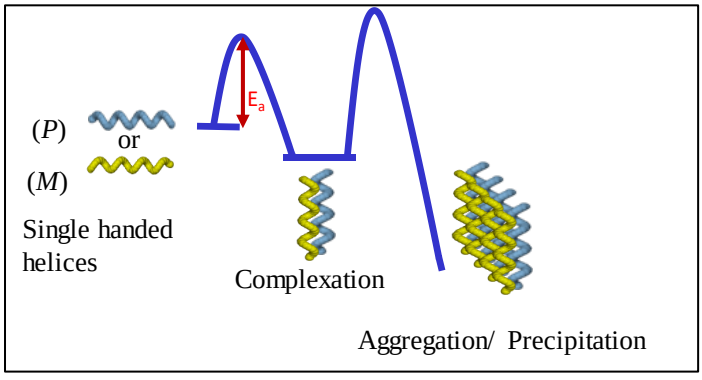

Figure 3.1 Energy diagram representing the formation of 'stereocomplex'.

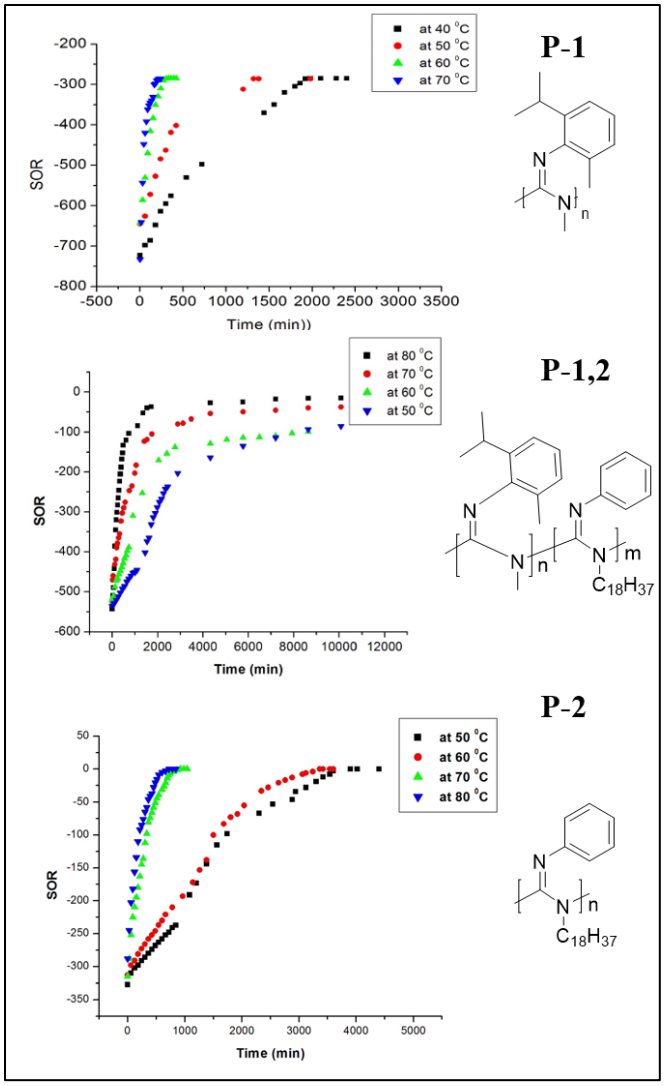

Figure 3.2 Charts showing a change of SOR upon thermal annealing for **P-1**, **P-2**, and block co-polymer of **P-1,2**.

The racemization process is confirmed by a decrease of SOR using polarized optical microscopy studies (**Figure 3.2**). Even though SOR begins to change with time, it comes to the plateau value at -286˚ for (***S***) **P-1**, implying that the polymer complex retains persistence of chirality. For this particular polymer, there are potentially two types of chirality and one of them is due to the helical backbone, whereas another contributor is assigned to the specific arrangement of asymmetric, aryl groups appended around the helical backbone. For a complete racemization, all

isopropyl and methyl groups should be aligned in the same registry to allow helical inversion. The presence of residual chirality (as evident by VCD data) implies that the racemization is not fully complete. Indeed, there are three molecular motions were hypothesized to be the cause of this interesting behavior of **P-1**. The proposed mechanism involves helical racemization (φ), imine inversion (ω), and N-aryl bond rotation (θ) (**Figure 3.3**). Helical racemization takes place *via* the rotation of the helical backbone and it required the highest energy. Imine inversion is the second molecular motion which can cause the change of the chirality of the polymer. The least energy involved process is the N-aryl bond rotation and this can be facilitated by bulky, asymmetric substituent at imine position of the polymer. N-aryl bond rotation contributes to different positioning of isopropyl scaffold and this bias is to change of helicity of the backbone. Thus, isopropyl scaffolds interact with same groups in adjacent polymer chain by zipping them together to (**Figure 3.4**) form a complex and this aggregation causes the polymer to precipitate by losing its chirality, that refers to stereocomplexation phenomenon. Making parallels into well known for biological macromolecules leucine zipper arrangement, we assume that the presence of isopropyl groups appended to polycarbodiimide scaffolds is essential to form a stereocomplex.[26,27] This interdigitation phenomenon is very common in regulatory proteins which have leucine residue at every 7^{th} position (**Figure 3.5**). These macromolecules adopt α-helical conformation. The presence of isopropyl segment in leucine residue will facilitate interdigitation with adjacent isopropyl segment, thus it forms dimeric units due to 'knobs-into-holes' packing'. We postulate that, in the same way, by interdigitating with isopropyl scaffold with adjacent polymer chains, this type of stereocomplex can be formed (**Figure 3.4**). Change of

chirality upon thermal annealing was further investigated by using vibrational circular dichroism (VCD).

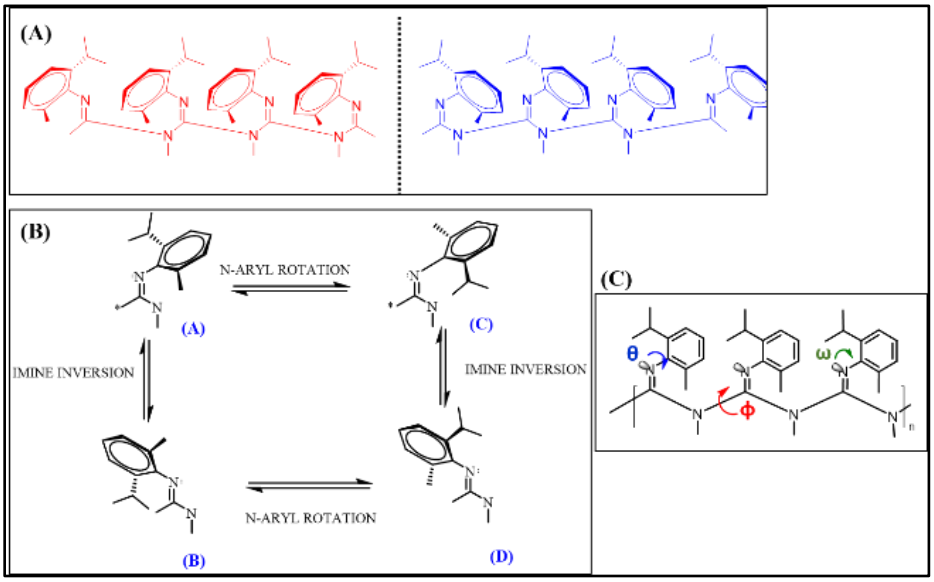

Figure 3.3 Schemes for racemization pathways and different molecular motions.

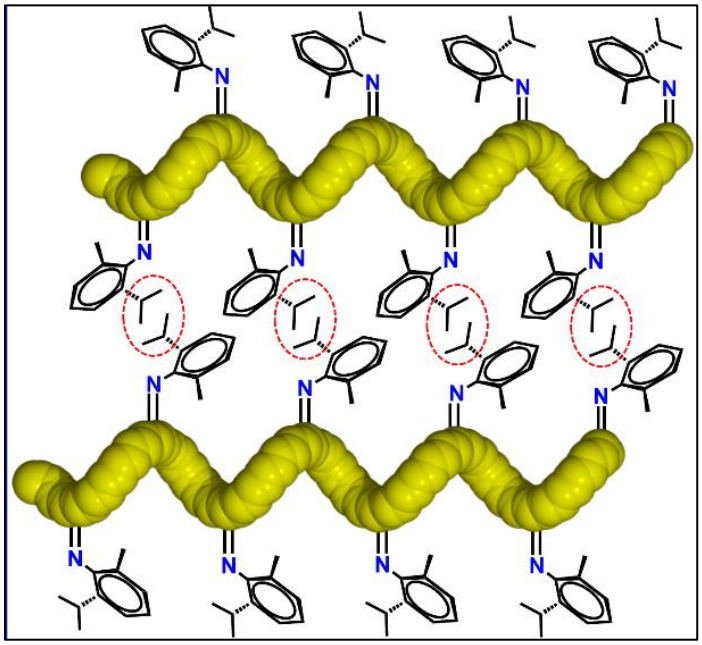

Figure 3.4 Cartoon showing the zipping of isopropyl scaffolds in adjacent polymer chains.

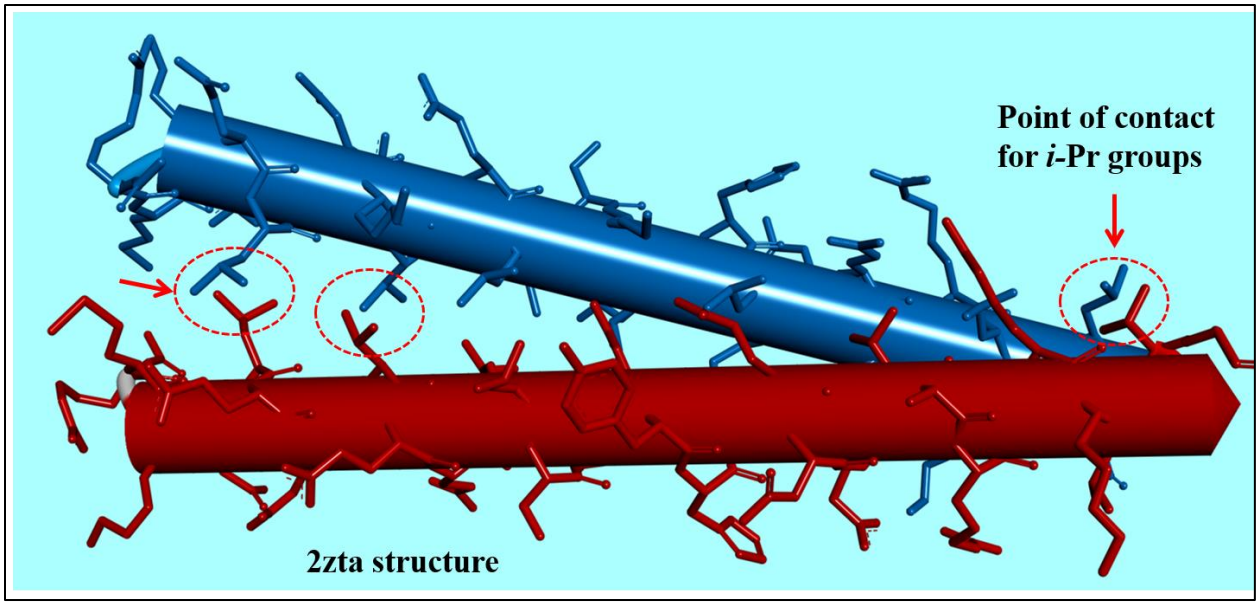

Figure 3.5 Classical leucine zippers; This shows how nature zips peptidic molecules via non-covalent interactions (data obtained from PDB).[27]

3.3.3 Determination of the helicity of the polymer

VCD is one of the most powerful tools for determining the absolute configuration of the chiral analyte. It has been coupled with IR spectroscopy and vibration dichroism and it shows bi-signate peak due to sample chirality. For the initial (*S*) polymer, it shows +/- bi-signate peak at 1640 cm^{-1} which associate with imine stretch. Upon thermal annealing, the bi-signate couplet is diminished when the polymer solution became turbid. After disappearing bi-signate couplets, new peaks arose at 1606 cm^{-1}, 1494 cm^{-1}, 1462 cm^{-1}. Those peaks at 1606 cm^{-1} (aromatic C=C) and 1494 cm^{-1} (asymmetric C-H bending or scissoring) can be assigned to chirality changes in aromatic C=C stretches, whereas the band at 1462 cm^{-1} (C-H bending or scissoring) may be attributed to zipping of adjacent isopropyl scaffolds in polymer strands projected towards each other (**Figure 3.6**). Interestingly, these all three peaks observed at room temperature in (***RAC*)-P-**

1 which is obtained from (***RAC***)-BINOL-Ti(IV) diisopropoxide initiator that further confirms the racemization process.

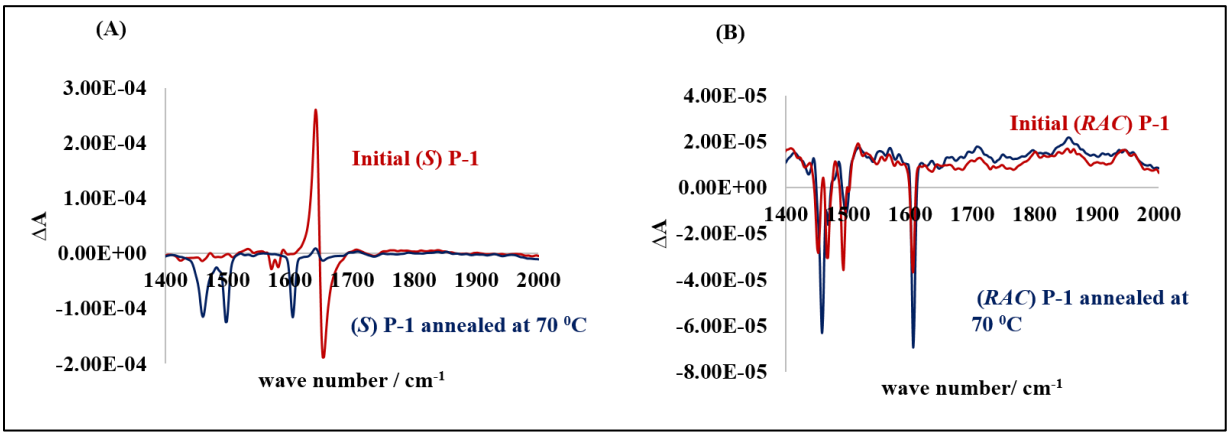

Figure 3.6 VCD spectra of **P-1** polymers before and after thermal annealing.

3.3.4 Powder X-ray profile analysis

We have analyzed *p*-XRD profiles of all polymers before (initial) and after thermal annealing. In all polymer samples, the sharp, intense peak is observed at ≈11 Å. This peak may appear due to intertwined super helices formation is shown in the model (**Figure 3.7**). Peaks at 7.12 Å and 4.47 Å peaks appeared could be assigned to periodic arrangement of helical turn. Interestingly, after thermal annealing of **P-1** at 70 °C, the new peak appeared at around 4 Å (**Figure 3.8**) and we believe that this peak that is not shown in the initial (*R*) and (*S*) **P-1**, may be associated with complexation of complementary strands (**Figure 3.9**). Hamilton and coworkers reported the range of 3.8 Å- 4.50 Å for hydrophobic side chain interactions of terminal isopropyl groups in dimeric amide foldamers (as determined by single crystal X-ray analysis).[28] Again, the appearance of 4 Å peak should be indicative of interactions of isopropyl groups in this complexation. These data are consistent with SAXS experiment results (**Figure 3.8-C**). Notably,

all peak intensities have been increased that is conclusive of crystallinity changes as a result of macromolecules reorganization/reordering when thermally annealed.

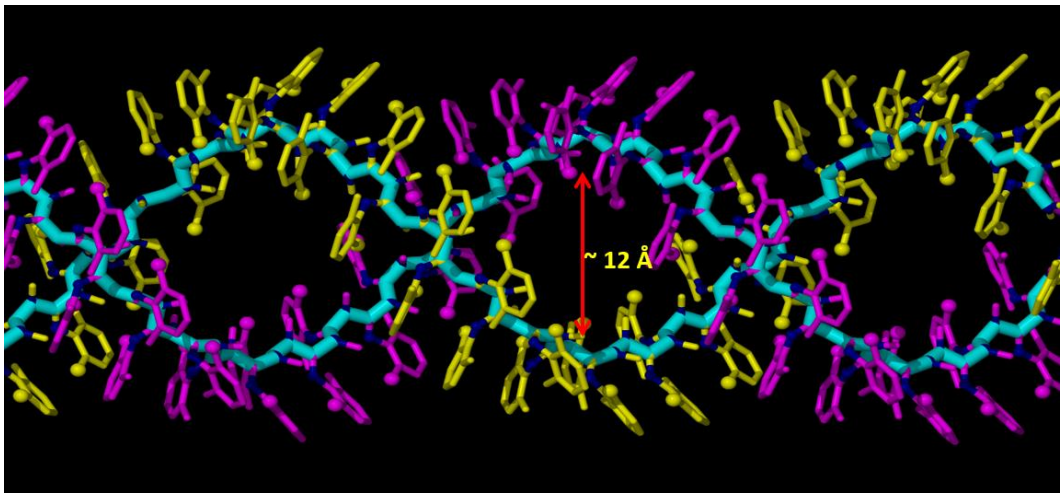

Figure 3.7 Cartoon representing two intertwined right-handed helices forming a supramolecular dimeric bundle of **P-1**; the distance between the adjacent helices was shown to be ≈12 Å which is in a good agreement with *p*-XRD data.

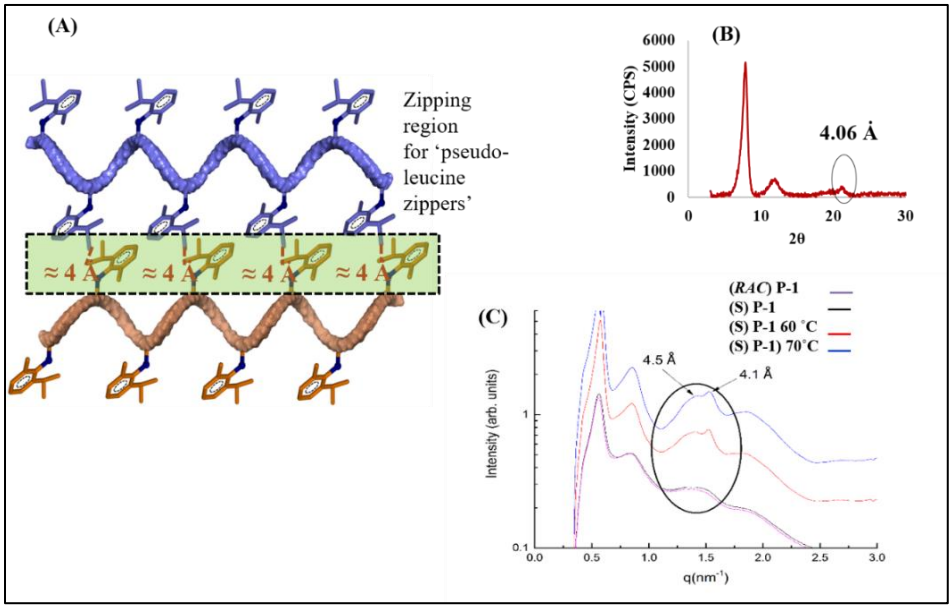

Figure 3.8 (A) Cartoon showing the formation of stereocomplex, (B) *p*-XRD profile for annealed **P-1** (C) SAXS profiles for **P-1** polymers.

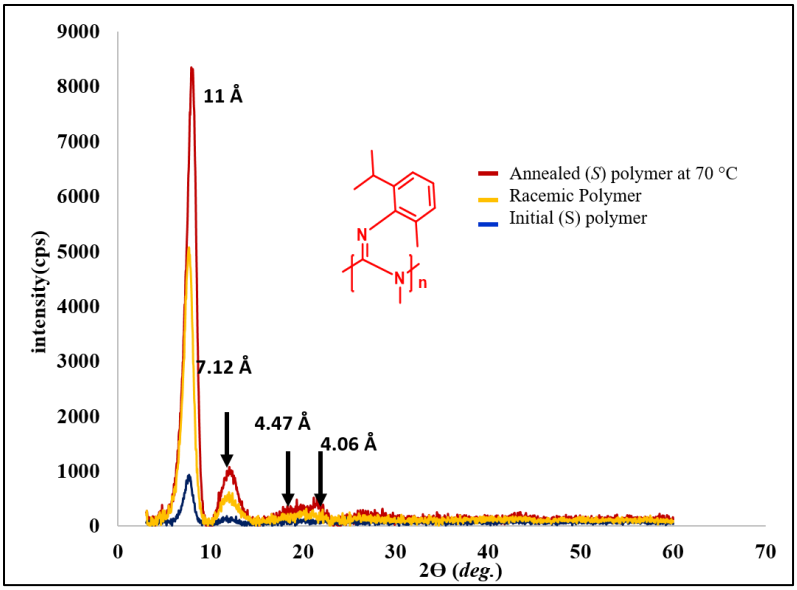

Figure 3.9 *p*-XRD profiles for **P-1** polymers before and after annealing.

3.3.5 Determination of activation energy for complexation

The energy associated with this process can be determined inclusively by observing loss of optical activity. When the two helical senses are in reverse equilibrium, the first order rate equation can be used and all concentration terms should be replaced with SOR terms since the concentration of excess helical sense cannot measure directly. Therefore, the first order kinetic equation can be rearranged as shown in Eq. 01. The plots of ln (α_0/α) vs time were constructed to find the observed rate constant k_{obs} at different temperatures by using first order kinetics equation (**Figure 3.10**). Then, using Arrhenius equation, the energy of activation (E_a) can be calculated (**Figure 3.11**). From this method, for **P-1** E_a was calculated as 19 kcal/mol. For the **P-1,2** and **P-2**, it was found 20 kcal/mol and 22 kcal/mol, respectively. According to our previous studies, the energy of activation was found to be 22.8 kcal/mol and 25.6 kcal/mol for poly(*N*, *N*'-dihexylpolycarbodiimide) and poly(*N*-phenyl-*N*'-hexylcarbodiimide), correspondingly. Based on these results, we inferred that the presence of aryl pendant group yields more static helices which

possess higher helix inversion energy.[24] In **P-1**, the presence of 2,6-disubstituted aryl group at imine position contribute to the stability of helical sense, but, the presence of small methyl group at amine position would lower the activation barrier for this polymer to racemize.

$$\ln \left(\frac{([M]_0 - [M]_{eq})}{([M] - [M]_{eq}} \right) = K_{obs}\, t$$

All M terms can be replaced by α terms,

$$\ln \left(\frac{([\alpha]_0 - [\alpha]_{eq})}{([\alpha] - [\alpha]_{eq}} \right) = K_{obs}\, t$$

At the equilibrium, $\alpha_{0} = 0$,
Thus,

$$\ln \left(\frac{[\alpha]_0}{[\alpha]} \right) = K_{obs}\, t \quad \ldots\ldots\ldots\ldots\ldots\ldots\ldots\ldots \text{Eq. 01}$$

$$Y = m\ x$$

Then, by using Arrhenius equation (Eq. 02), the energy associated with racemization can be determined.

$$\ln K_{obs} = \frac{E_r}{R} * \frac{1}{T} + \ln A \quad \ldots\ldots\ldots\ldots\ldots\ldots\ldots\ldots \text{Eq. 02}$$

$$Y = m\ x + c$$

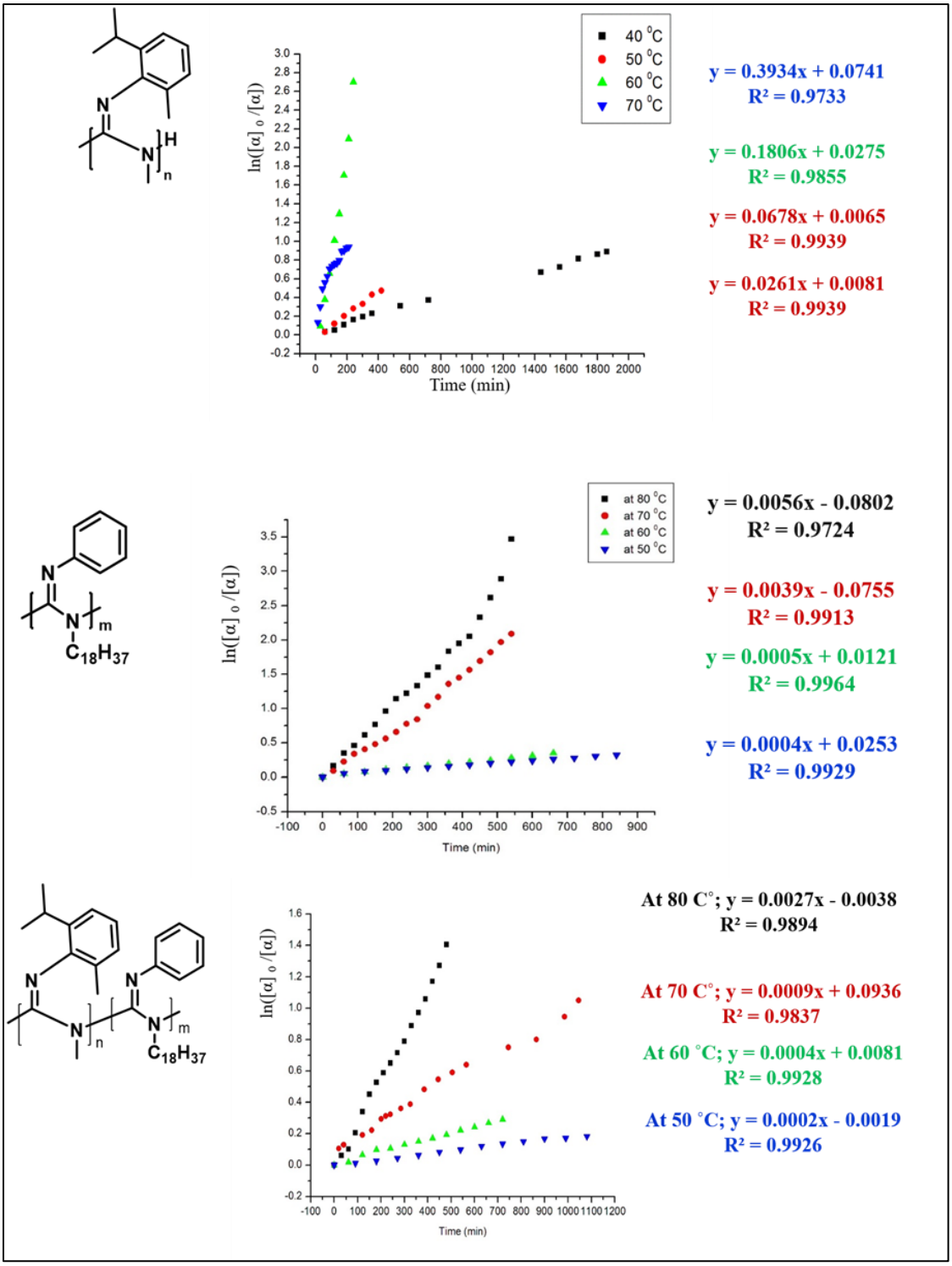

Figure 3.10. Kinetic plots for polymers **P-1**, **P-2**, and **P-1,2,** correspondingly.

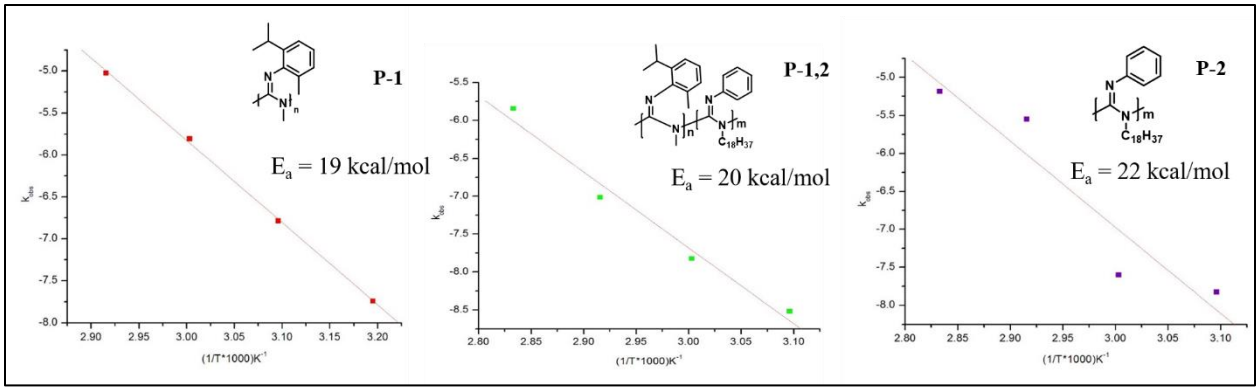

Figure 3.11 Graphs for activation energy barriers for **P-1**, **P-2**, and **P-1,2**.

3.3.6 Towards the block co-polymer (P-1,2)

All together SOR, VCD, *p*-XRD, and SAXS data provided unambiguous evidence to prove changes in an excess helical sense into racemization *via* different molecular motions which led to the formation of stereocomplex. Zipping or the interactions among isopropyl groups play a vital role in this process as evident by VCD data. To take advantage of this complexation, block co-polymer of **P-1,2** (composed of a short block of **P-1** and a long block of **P-2**) was synthesized **(Scheme 3.2** and **Figure 3.12)**. The presence of octadecyl chains in a long segment of **P-2,** the solubility of a block polymer of **P-1,2** has been enhanced. Based on our hypothesis, if isopropyl scaffold of **P-1** is zipped to form an aggregate, this block co-polymer should be able to form spherical aggregates in such a way that the core composed of the **P-1** of zipped units while the corona consists of phenyloctadecyl scaffolds of **P-2**. We performed the thermal annealing experiment for this block co-polymer **P-1,2**, which also demonstrated significant decrease SOR with time at elevated temperature and ultimately came to zero after an extended period of hours. This behavior was confirmed with VCD studies (**Figure 3.13**). We describe this phenomenon as

the racemization upon thermal annealing and it never forms a precipitate since the presence of the octadecyl chain that enhances the solubility in toluene.

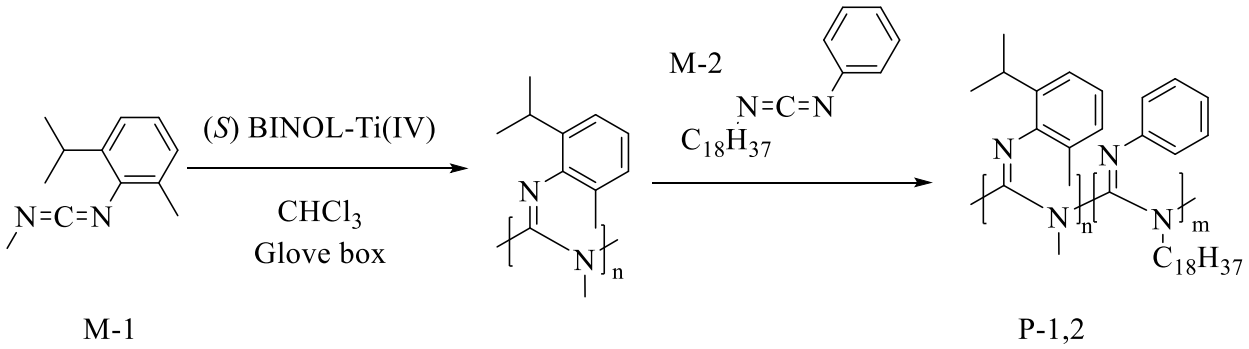

Scheme 3.2 Synthesis of block co-polymer, **P-1,2**.

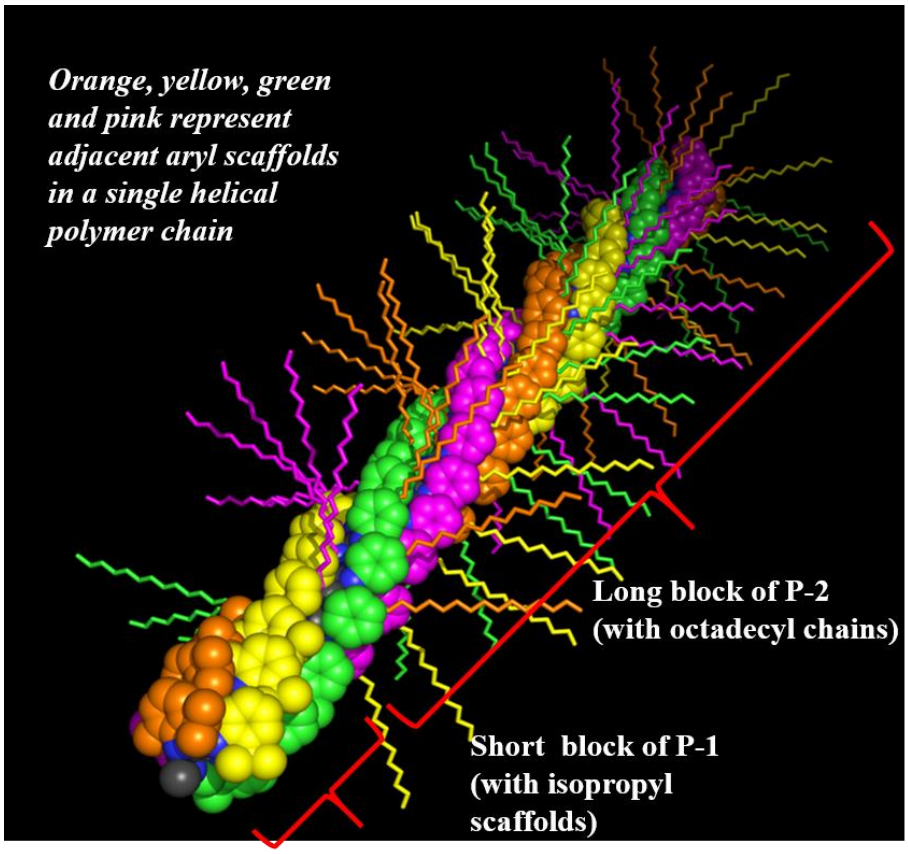

Figure 3.12. Cartoon showing a block co-polymer (**P-1,2**) composed of a short block of **P-1**with isopropyl substituent and a long block of **P-2** with octadecyl chains.

We inspected the block co-polymer, **P-1,2** by using VCD before and after thermal annealing and the result reveals that the disappearance of imine bi-signate peak as well as appearing new peak around 1400 cm^{-1} were taking place implying that racemization and changes of the chiral environment around the isopropyl pendant groups correspondingly. In IR spectrum, the peaks correspond to imine region also have been changes. We believe that these changes occur due to zipping phenomena of isopropyl pendants, thus induces the formation of polymeric assemblies.

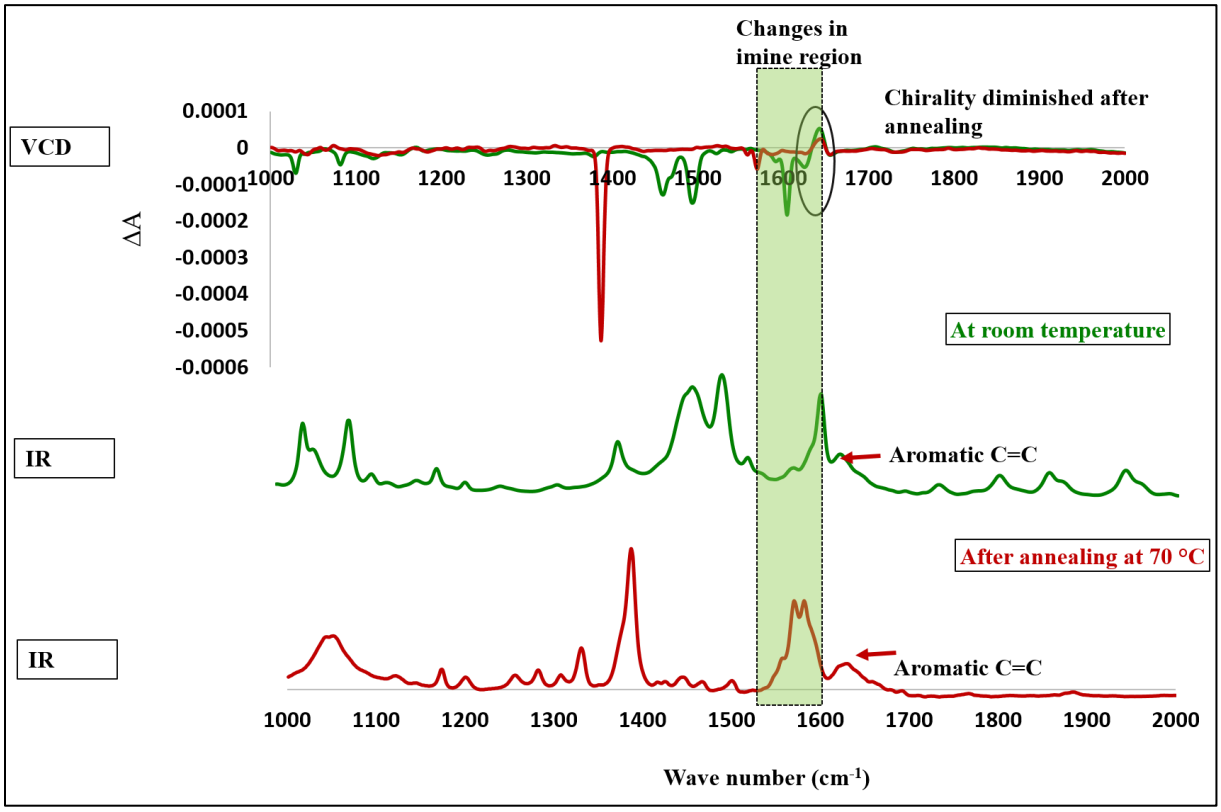

Figure 3.13 VCD and IR spectra for **P-1,2** polymer before and after thermal annealing; the peak changes around 1400 cm^{-1} and 1587 cm^{-1} reveal that changes in different vibrations of alkane C-H and C=N imine bond.

By employing DLS, TEM and SEM techniques, sphere formation has been investigated. DLS studies were performed to measure the particle size (**Figure 3.14**). At room temperature, hydrodynamic radius (D_h) was found to be 1778 nm implying that block co-polymer occupies a random volume when the main chain is fully extended. After 4 hr, D_h became 342 nm suggested of sphere formation and further annealing at 70 °C causes the polymer to form a larger aggregate with D_h around 3380 nm. It seems likely that driving force behind this sphere formation is interlocking of isopropyl scaffolds at the core of the assembly. We have conducted the same DLS experiment for homopolymer **P-1** having (*S*) helical sense. It also shows the formation of spheres when thermally annealed for 4 hr and further heating caused the appearance of largely defined aggregates successfully observed by TEM and SEM techniques (**Figure 3.15**).

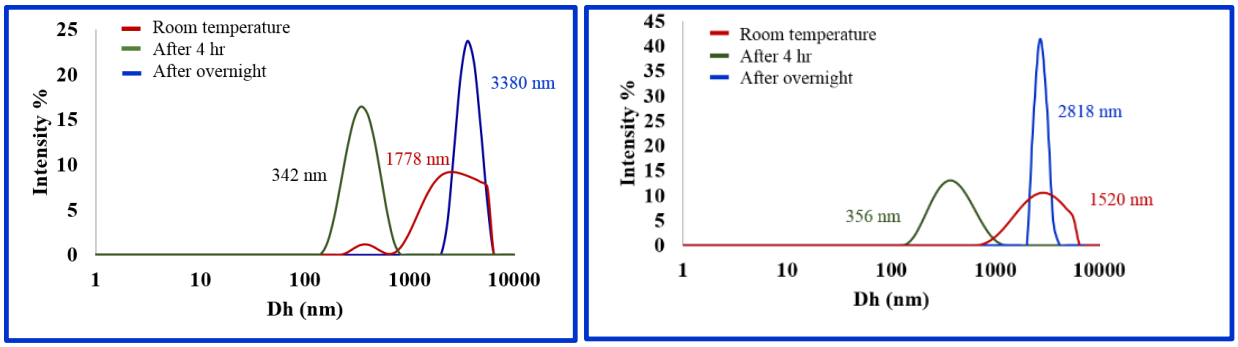

Figure 3.14 DLS profiles for **P-1** and **P-1,2**.

Again, we were excited to inspect to block co-polymer poly(*N*-methyl-*N*'-(2-isopropyl-6-methylphenyl)carbodiimide)-*b*-poly(*N*-methyl-*N*'-octadecyl)carbodiimide), **P-1,2**. According to the ^{1}H NMR data, this polymer incorporates 10% of poly(*N*-methyl-*N*'-(2-isopropyl-6-methylphenyl)carbodiimide.

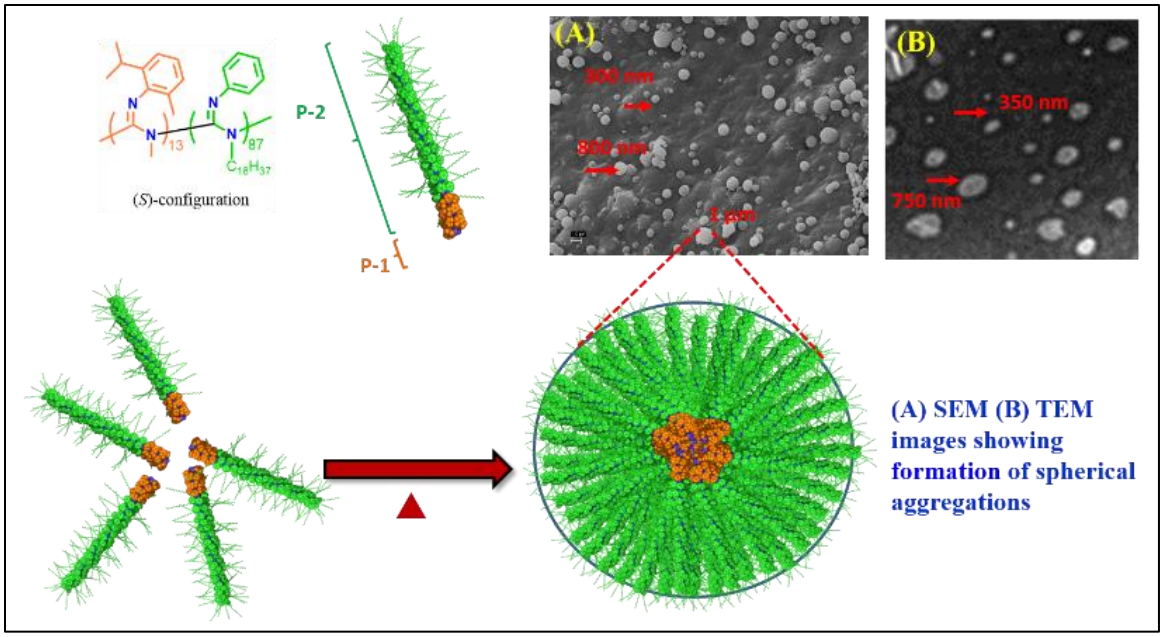

Figure 3.15 Formation of spherical aggregates from **P-1,2** upon thermal annealing; both SEM and TEM prove that the formation of spheres.

Based on the *p*-XRD profile of **P-1,2**, it mainly shows the spectrum for poly(*N*-methyl-*N*'-octadecyl)carbodiimide segments due to overlapping peaks from the short block of the poly(*N*-methyl-*N*'-(2-isopropyl-6-methylphenyl)carbodiimide) (**Figure 3.16**). According to the ^{1}H NMR analysis, this block co-polymer is composed of around 13% of **P-1** and thus, *p*-XRD profile exhibits mainly the profile for **P-2**. However, we have observed a sharp peak at ≈ 26 Å in all *p*-XRD profiles which is indicative of presence poly(*N*-phenyl-*N*'-octadecyl)carbodiimide. According to the cartoon showed here, this peak may arise due to the specific packing of individual helices. We hypothesized that in the presence of long interdigitating octadecyl chains may facilitate this packing of macromolecules and the most of the octadecyl side chains are bent or twisted to avoid direct contact with the average aromatic or aliphatic C-C distance of around 3.9 Å (**Figure 3.17**).

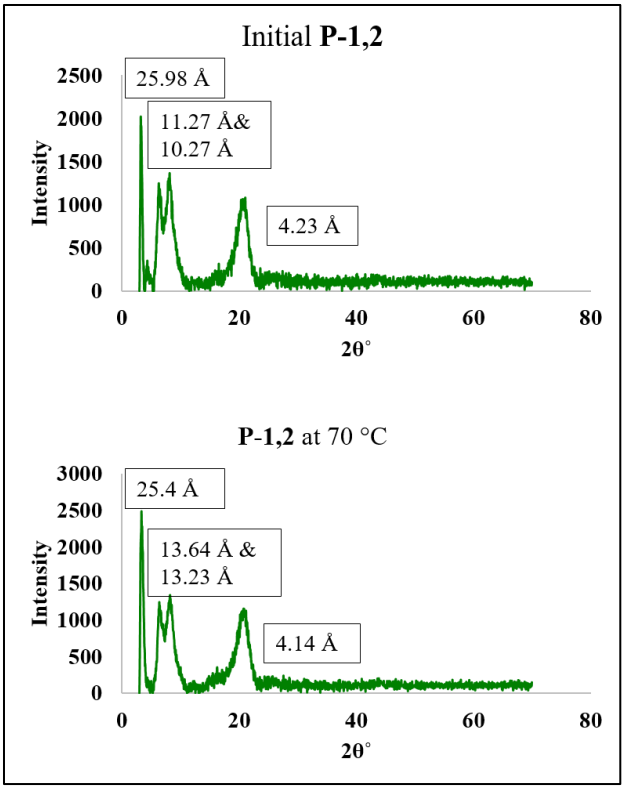

Figure 3.16 *p*-XRD profiles for block co-polymer of **P-1,2** before annealing (initial) and after annealing (at 70 ˚C).

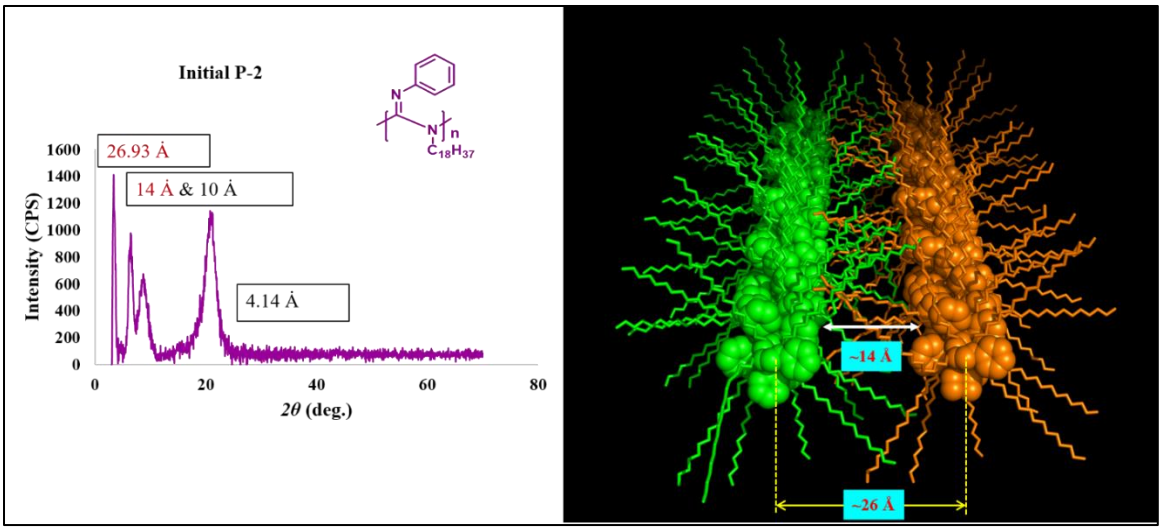

Figure 3.17 *p*-XRD profiles for **P-2** and cartoon showing interdigitation of octadecyl chains in **P-2** with polycarbodiimide scaffolds separations of 14 Å and 26 Å, respectively.

3.3.7 Transmittance experiment to prove racemization/stereocomplexation

It appears that **P-1** polymer solution turned turbid as the complexation progressed over time upon thermal annealing. Therefore, to validate the proposed mechanism, we have measured the change of transmittance while annealing the sample at 70 ˚C. For this experiment, we have used (*S*), (*R*), (*RAC*) types of **P-1** and **P-1,2** (block co-polymer) to compare the transmittance change rate as expressed by equations outlined for each graph (**Figure 3.18**). Based on the results for (*R*) and (*S*) configurations, polymers undergo around 100 min induction period before dropping down the transmittance while analysis of (*RAC*) **P-1** implied instant changes upon annealing. We believed that racemization caused their formation of helices of opposite handednesses. The behavior of racemic polymer *vs* excess helical sense polymer is interesting according to this transmittance experiment. As the racemic polymer (*RAC*) is composed of a mixed array of 50:50 complementary strands, the induction period is absent whereas the single-handed polymer requires these periods of time to the *in-situ* formation of the polymer with opposite handedness. Once the opposite handedness is achieved, it tends to undergo 'knobs-in-to-holes' packing which is energetically favorable (**Figure 3.19**). However, transmittance change rate is nearly the same for all **P-1** type polymers. The block co-polymer of **P-1,2**, for instance, which has short block composed of isopropyl scaffold and a long block of phenyl-octadecyl chains around the polycarbodiimide backbone, transmittance changes very slowly and it does not drop down significantly over time. Also, we believe that the presence of octadecyl chain on the periphery of the polymer backbone enhances the solubility. Interestingly, the change of transmittance occurs after the SOR reach to the plateau value.

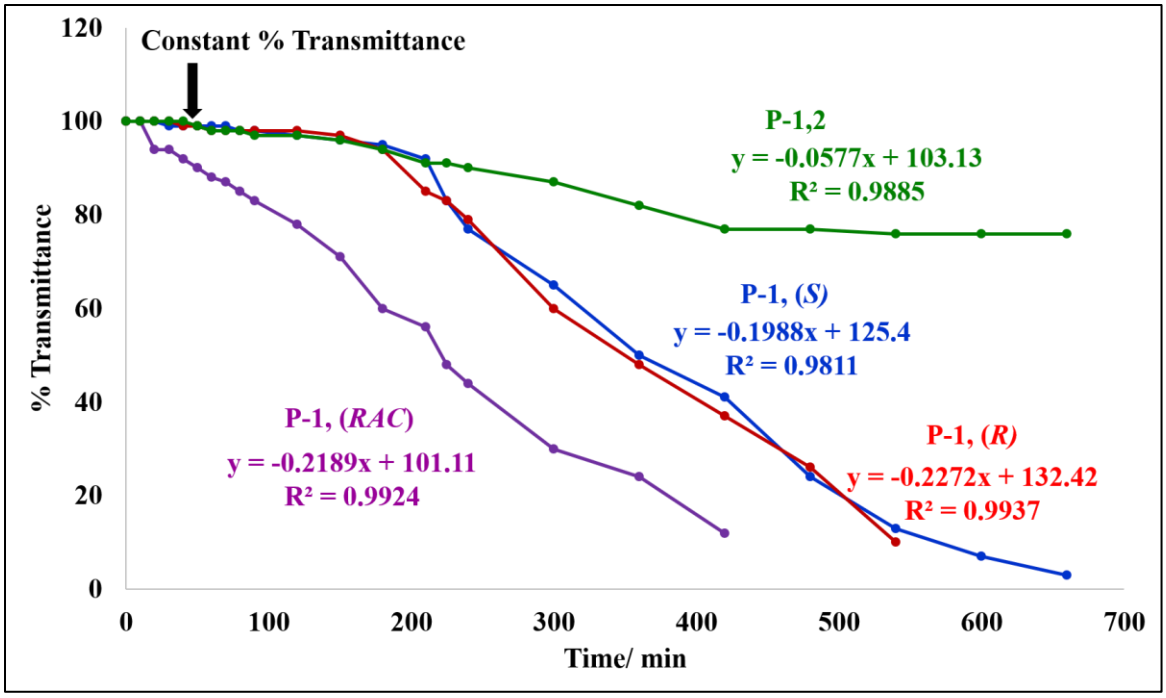

Figure 3.18 Chart showing change transmittance percentage for **P-1** type polymers and **P-1,2** upon thermal annealing.

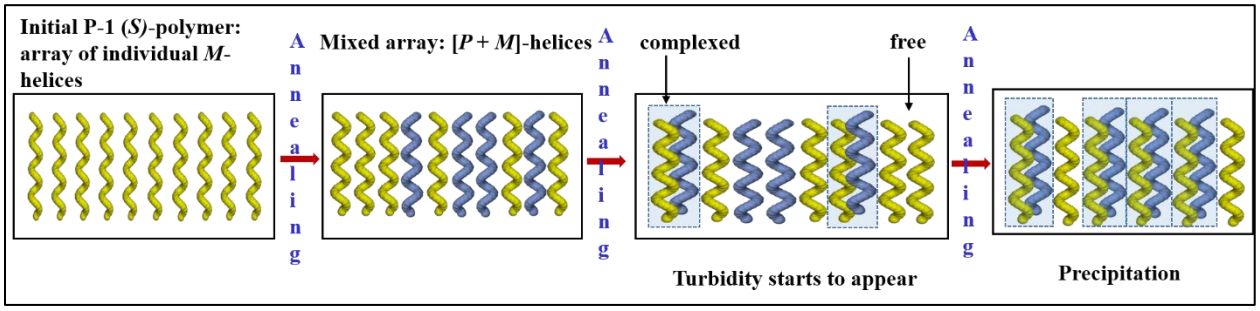

Figure 3.19 Cartoon representation for stereocomplexation upon thermal annealing.

3.3.8 Investigation of complexation behavior of different polymer derivatives

We have synthesized different polymer derivatives (*i.e.*, **P-3**, **P-4**, **P-5**) having pendant isopropyl group at the *ortho*, *meta*, and *para* position respectively, to investigate the complexation behavior. Unfortunately, both *ortho* and *meta* derivatives formed insoluble, gelled polymer

material during the polymerization suggestive of aggregation. Formation of insoluble material during the polymerization proves that they already aggregated. Even though the *para* derivative forms a soluble polymer, it does not retain excess helical sense as evident by VCD and SOR data. To clarify the mechanism of aggregation, we have performed *p*-XRD and morphological studies of these polymers.

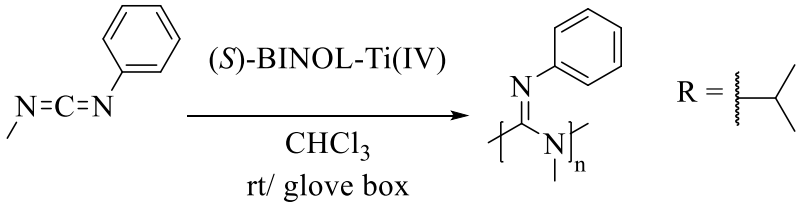

R	Monomer	Polymer
ortho	**M-3**	**P-3**
meta	**M-4**	**P-4**
para	**M-5**	**P-5**

Scheme 3.3 Synthesis of different derivatives of the polymer.

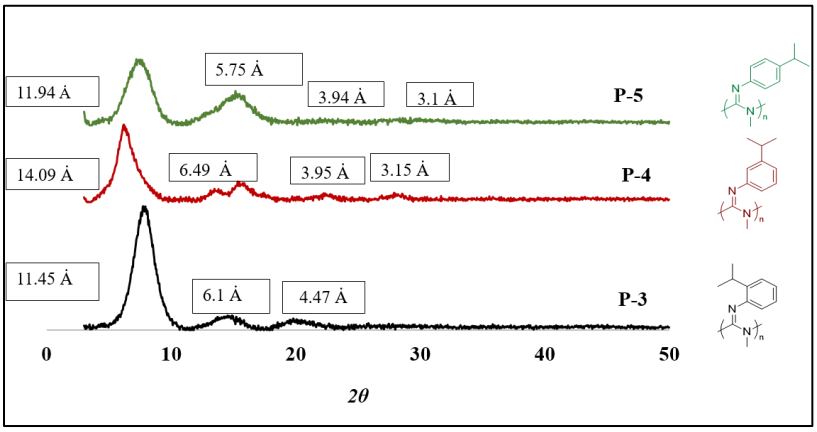

Figure 3.20 *p*-XRD profiles for **P-3**, **P-5**, **P-5**.

3.3.9 Morphological studies of helical homopolymers and block co-polymers for self-aggregation behavior

For morphological studies of newly synthesized polymers, AFM, SEM, and TEM determinations have been used before and after thermal annealing. We have found that morphology is greatly

dependent on sample preparation. Therefore, it was of interest to study electro spun samples along with thin film morphologies and bulk material of the same polymers.

AFM imaging of **P-1**, **P-2**, and **P-1,2**

The initial polymers of **P-1** types were inspected by using AFM. These polymers adopt into nano fibers with average diameter around 15-30 nm. When annealed, **P-1** formed both irregular aggregates nearly spherical which are in the range of 180 nm -200 nm and, also, very small 20-50 nm motifs (**Figure 3.21**). In addition to that we inspected (*RAC*) of the **P-1** polymer without annealing and, in this case, the 'maggot-like' crystalline domains were observed **(Figure 3.22**). Upon thermal annealing, very large aggregations were formed. Conversely, the block co-polymer of **P-1,2** were observed as elongated helical domains and after annealing, it forms large aggregates stacking together (**Figure 3.21, C** and **D**). Also, inspected polymer samples of **P-2** and there was not a significant change in morphology before and after annealing process (**Figure 3.23**). This revealed that presence of isopropyl pendants through polymer chains facilitates the formation of aggregates.

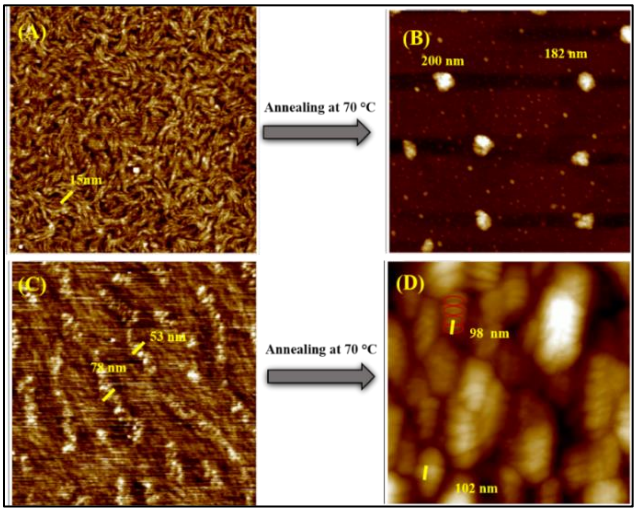

Figure 3.21 AFM images for (*S*) **P-1** (A) and (B), and **P-1,2** (C, (D), scan size 3x3 µm.

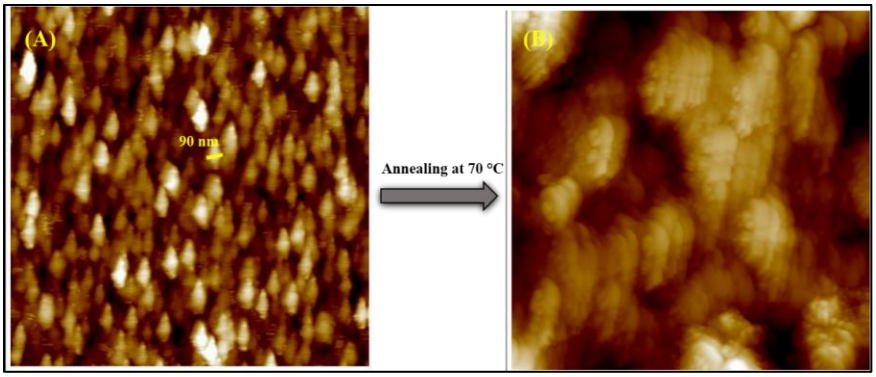

Figure 3.22 AFM images for (*RAC*) **P-1** (A) and (B), and **P-1,2** (C, (D), scan size 3x3 µm.

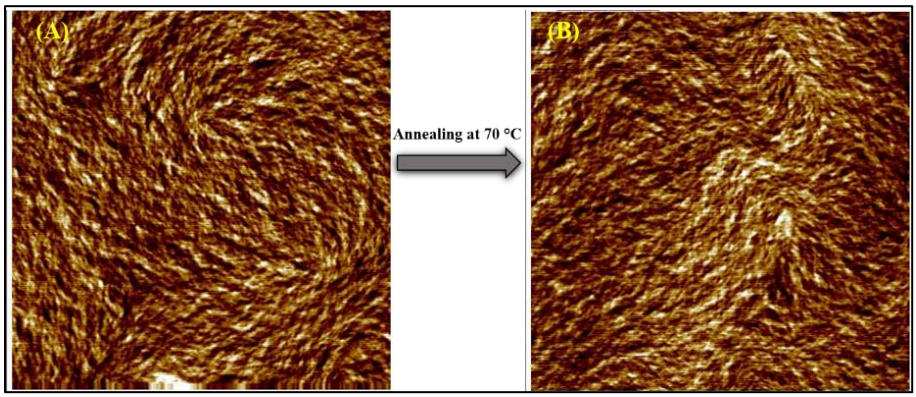

Figure 3.23 AFM images showing **P-2** before and after thermal annealing, scan size 3x3 µm.

Scanning electron microscopy imaging of bulk and electro-sprayed morphologies

The initial polymer of **P-1** (prior to thermal annealing), fiber-like morphology was observed while 'macroporous' interior structure was obtained upon thermal annealing at 70 ˚C (**Figure 3.24A**). Interestingly, we have observed both fiber-like and 'macroporous' morphologies in the initial (*RAC*) **P-1(Figures 3.25** and **3.26)**. We believe that its porous nature is due to knobs-in-to-holes' like packing due to the presence of enantiomeric helices. For the block co-polymer of **P-1,2**, we observed the mixed morphology of fiber-like morphology accompanied by few spherical aggregates in the initial state (before annealing). After thermal annealing at 70 °C, this polymer

adopts into well-defined spheres (**Figures 3.24 (E, F)**) with fiber width is around 2µm and the diameter of the spheres around 4-6 µm. For the homopolymer **P-2** which is poly(*N*-phenyl-*N*'-octadecyl)carbodiimide, fiber-like morphology was shown as a predominant motif in bulk. Even though and of poly(*N*-methyl-*N*'-(2-isopropylphenyl)carbodiimide **(P-3)**, and poly(*N*-methyl-*N*'-(3-isopropylphenyl)carbodiimide polymer (**P-4)** are not soluble, they confined into unique, homogeneous morphology at room temperature. When the isopropyl group at *ortho* position (**P-3**), the polymer samples adopt into clusters of irregular-shaped, fused grainy-like morphology (**Figure 3.27)**. In contrast, the corresponding meta isomer tends to form very crystalline, hard materials (**P-4**) (**Figure 3.28**). The *para* substituted **P-5** also forms crystalline material upon thermally annealing (**Figure 2.29**).

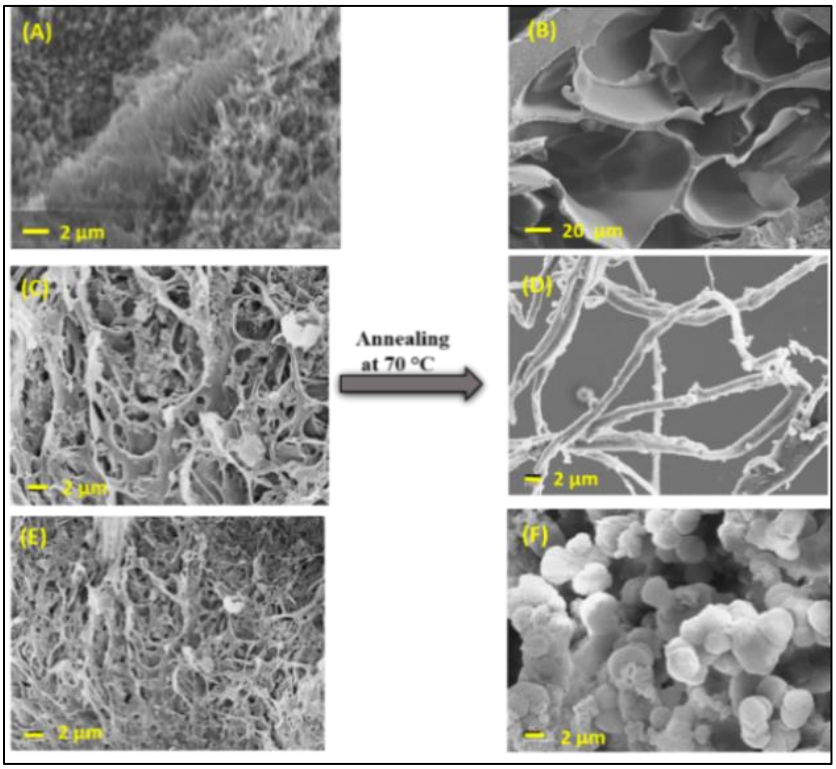

Figure 3.24 SEM images for **P-1** (A, B), **P-2** (C, D), and **P-1,2** (E, F) before and after thermal annealing.

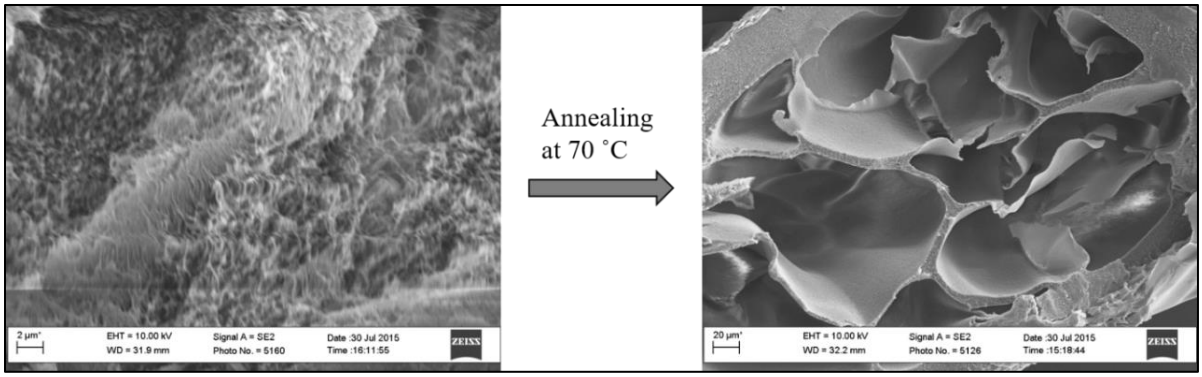

Figure 3.25 SEM images of **P-1** before and after thermal annealing: it forms large compartments upon annealing.

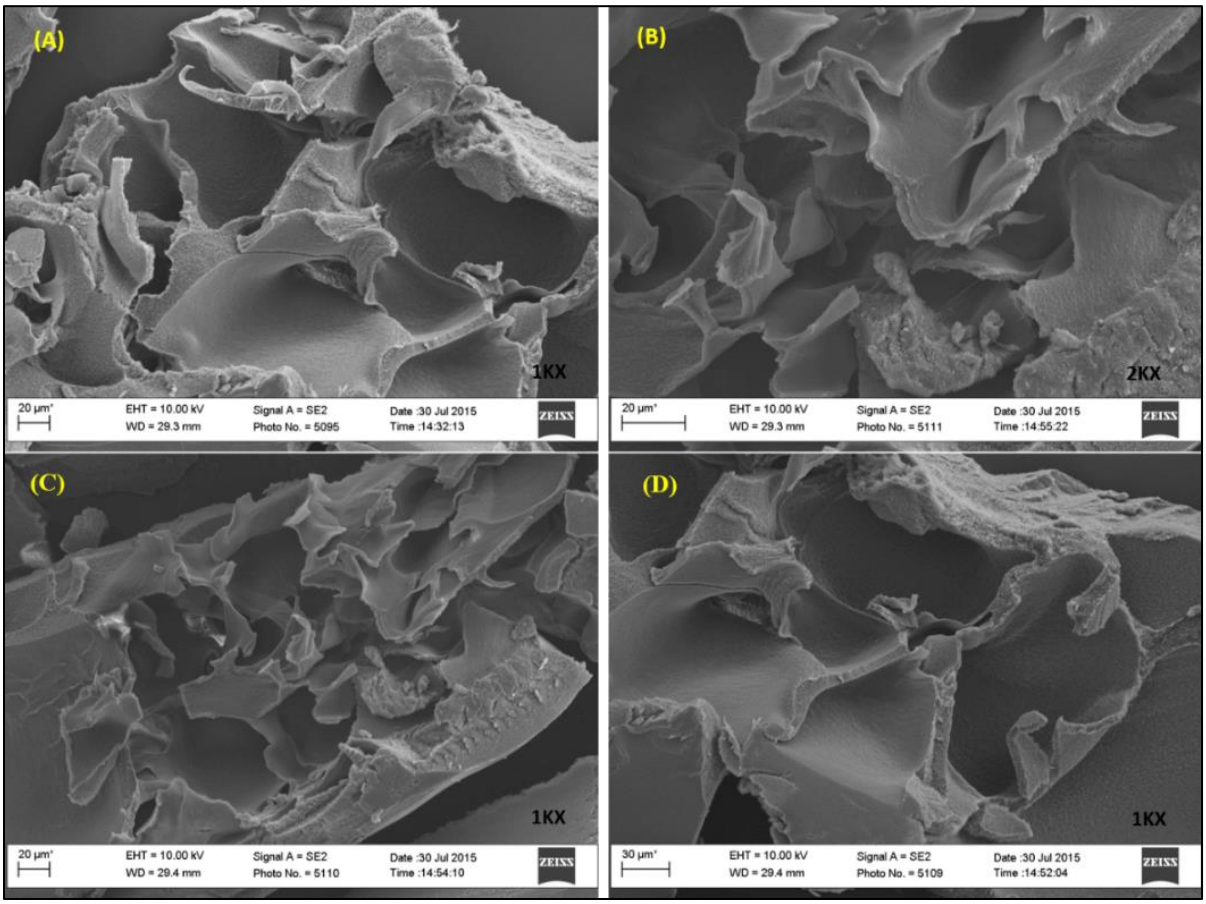

Figure 3.26 SEM images of (***RAC***)-**P-1:** a well-developed inner structure comprising of multiple compartments and the large cavities.

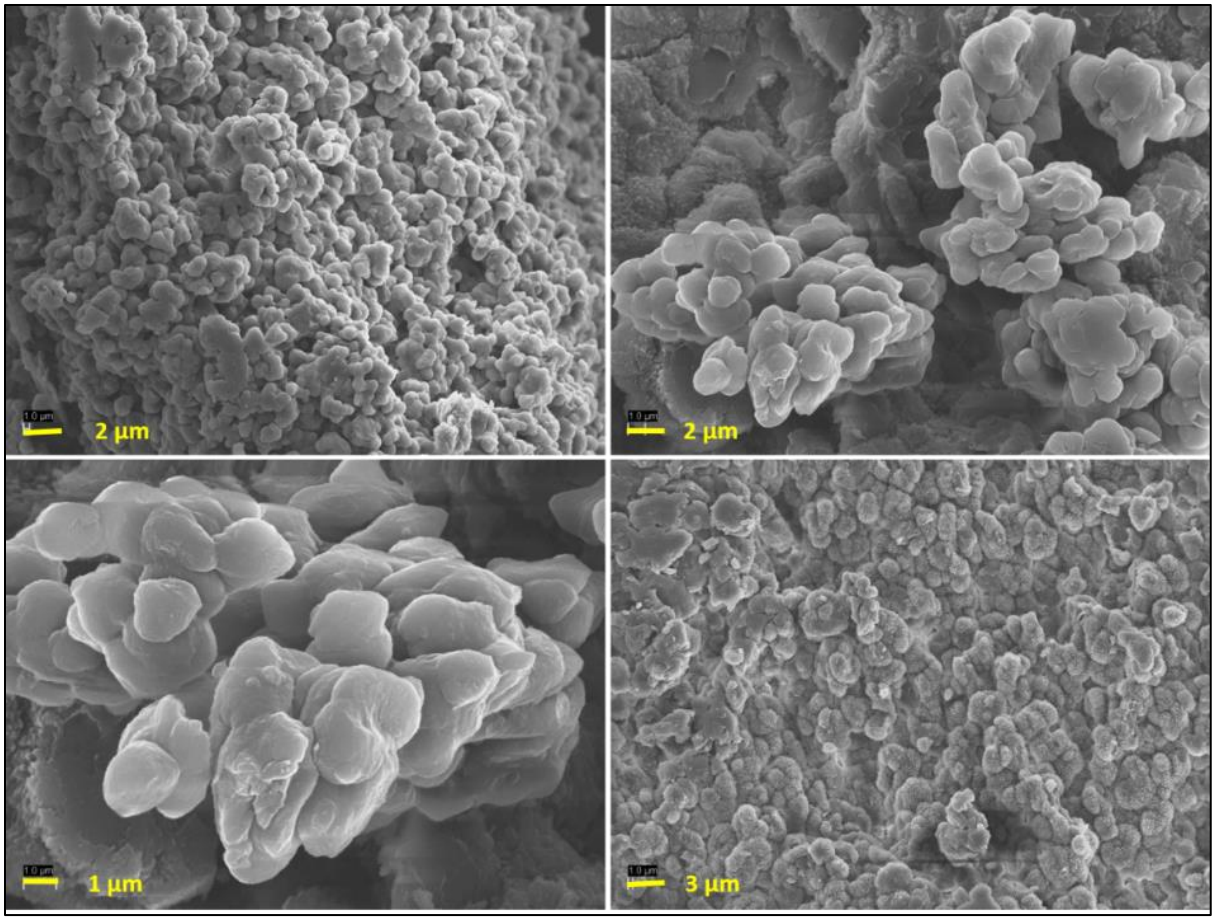

Figure 3.27 SEM images of poly(*N*-methyl-*N*'-(2-isopropylphenyl)carbodiimide), **P-3:** clusters of irregularly shaped particles or 'fused grains'.

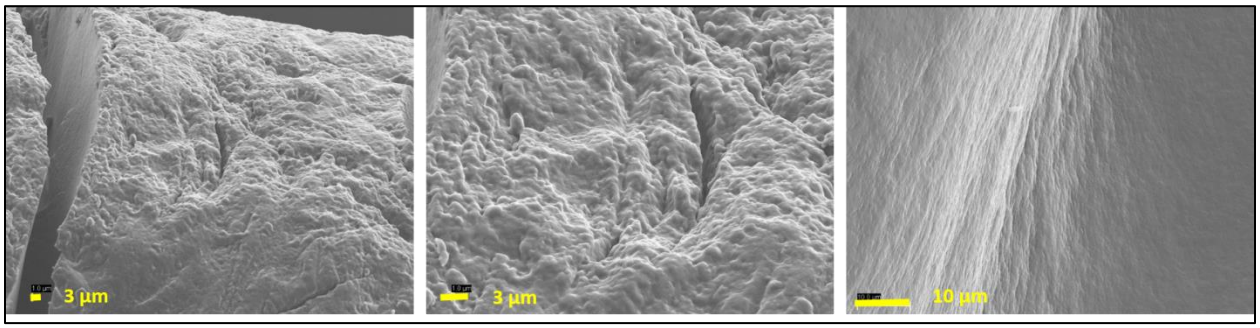

Figure 3.28 SEM images of poly(*N*-methyl-*N*'-(3-isopropylphenyl)carbodiimide), **P-4** as solid, monolithic material.

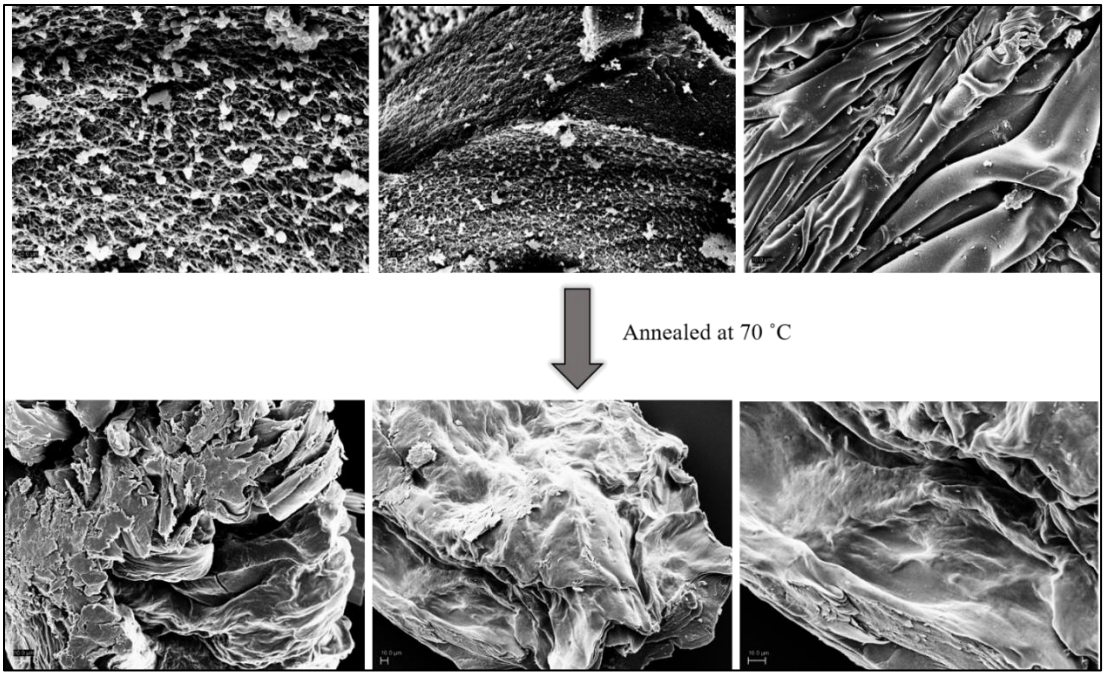

Figure 3.29 SEM images of poly(*N*-methyl-*N*'-(4-isopropylphenyl)carbodiimide), **P-5** initial polymer showing 'porous', rough surface. Upon thermal annealing, it forms a crystalline, solid material.

So far, we have noted that morphologies may look different depending on the way the sample were prepared. Then we thought to process these **P-1** and **P-1,2** *via* the electro-sprayed method. Our solvent of interest was toluene and 0.43 (w/w%) sample concentration was used. The morphologies we obtained are quite interesting and homogeneous. For initial **P-1**, before annealing large, hollow, hemispheres were obtained whereas the annealed sample did form few microspheres and the closed-up image of the surface of the spheres seems to be 'porous' in nature. It also formed the irregular chip-like morphology that arises due to the formation of precipitate/turbid solution upon thermal annealing (**Figures 3.30, 3.31,** and **3.32**). For the block co-polymer **P-1,2,** plate-like morphologies in 10-17 μm in range with dimpled surfaces were obtained. Noteworthy, some fibers were obtained upon annealed **P-1,2** polymer sample with electro-spun (**Figures 3.33, and 3.34**). With thermal annealing, this polymer did not form any

turbid solution due to the presence of octadecyl scaffold as it enhances the solubility. We believe that the presence of this octadecyl scaffold also contributes to increasing of polymer viscosity to an optimum value, thus, to form fibers.

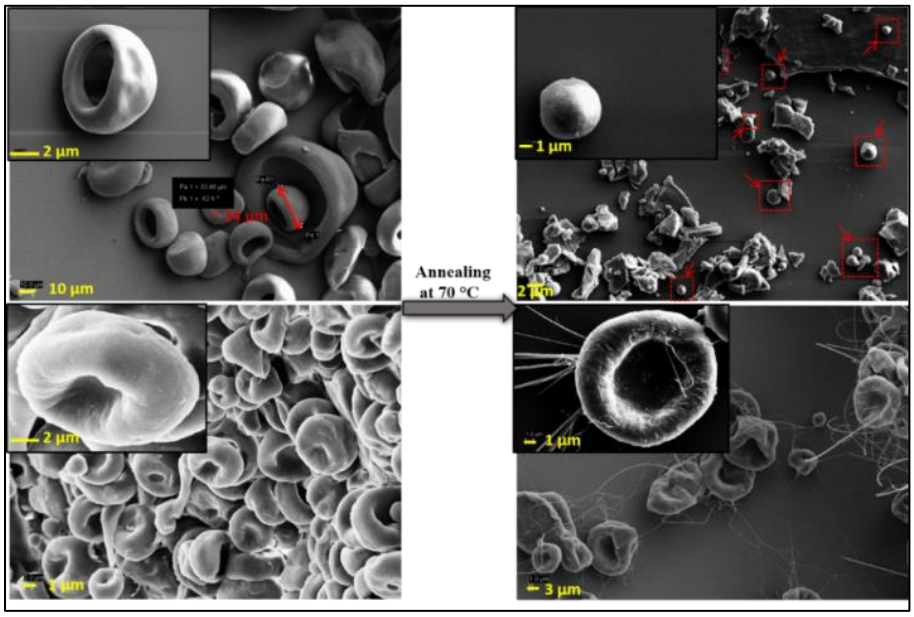

Figure 3.30 SEM images detailing observed morphologies for electro-sprayed **P-1**(top panel), and **P-1,2** (bottom panel) before and after thermal annealing.

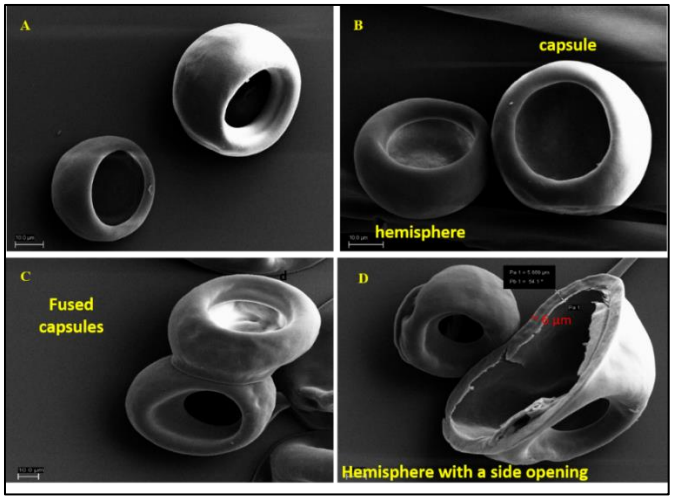

Figure 3.31 SEM images of electro-sprayed **P-1**featuring formation of caps and capsules.

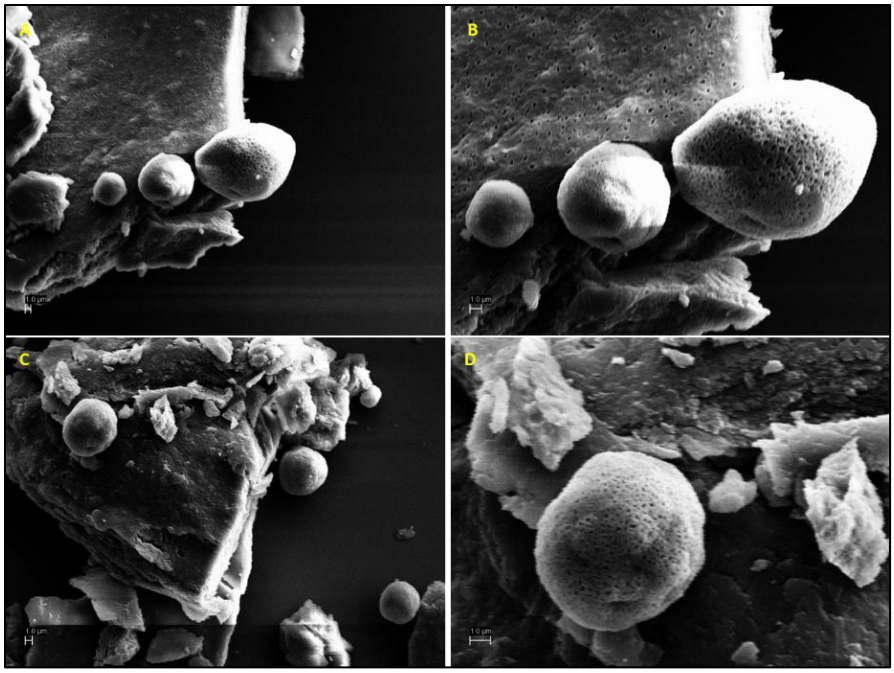

Figure 3.32 SEM images of electro-sprayed **P-1** after thermal annealing: solution is turbid thus it forms chips along with randomly disperses irregularly shaped spheres**.**

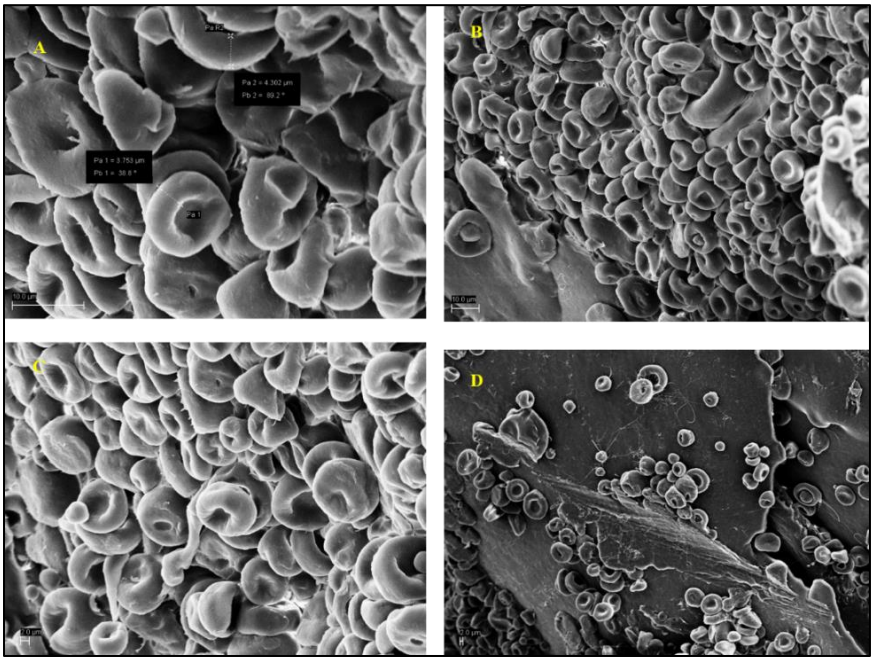

Figure 3.33. SEM images of electro-sprayed block co-polymer **P-1,2** before thermal annealing.

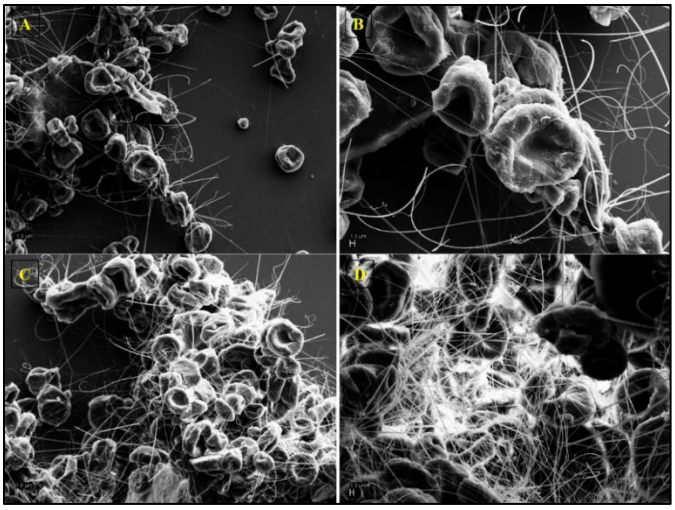

Figure 3.34 SEM images of electro-sprayed block co-polymer **P-1,2** after thermal annealing: formation of fibers and hollow hemispheres.

TEM imaging of **P-1** and **P-1,2**

By doing TEM studies, it was confirmed the aggregate formation upon thermal annealing of the **P-1** polymer. Nano fibrillar morphology observed for **P-1 and P-1,2** by AFM technique, thus providing ambiguous evidence for the presence of elongated motifs (**Figures 3.35** and **3.36**) and upon thermal annealing, it forms large aggregates as a result of macromolecule supramolecular bundling.

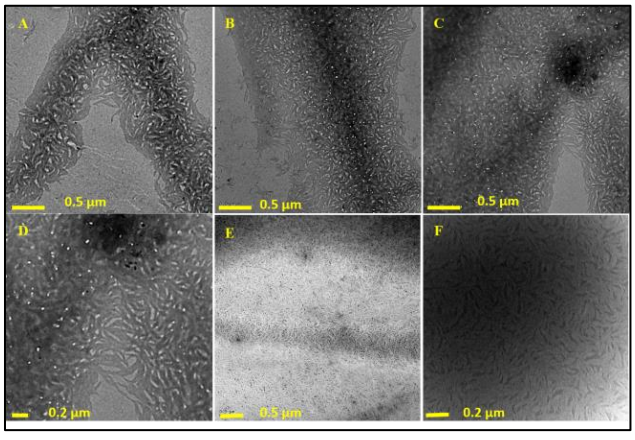

Figure 3.35 TEM imaging of initial polymer **P-1**: fibrillar morphology.

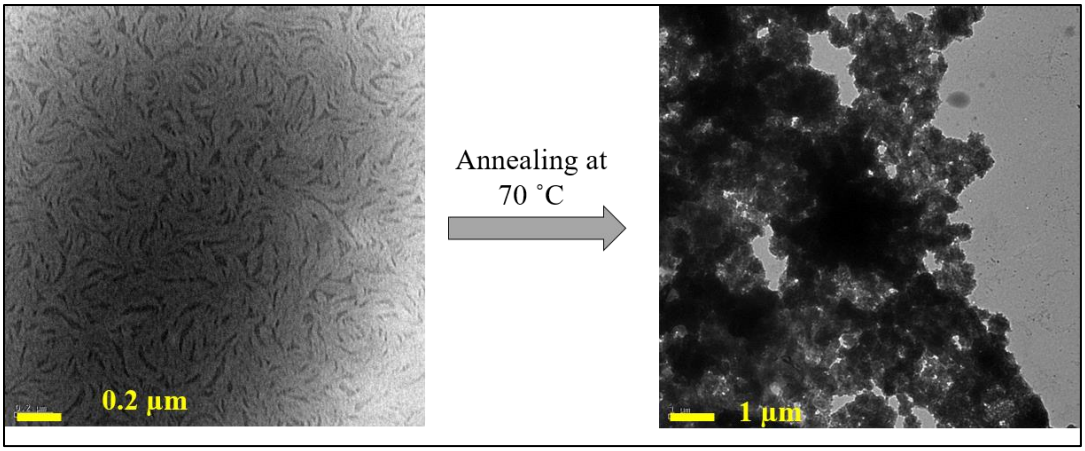

Figure 3.36 TEM imaging polymer **P-1** before and after thermal annealing at 70 ˚C: formation of clusters of aggregates upon thermal annealing.

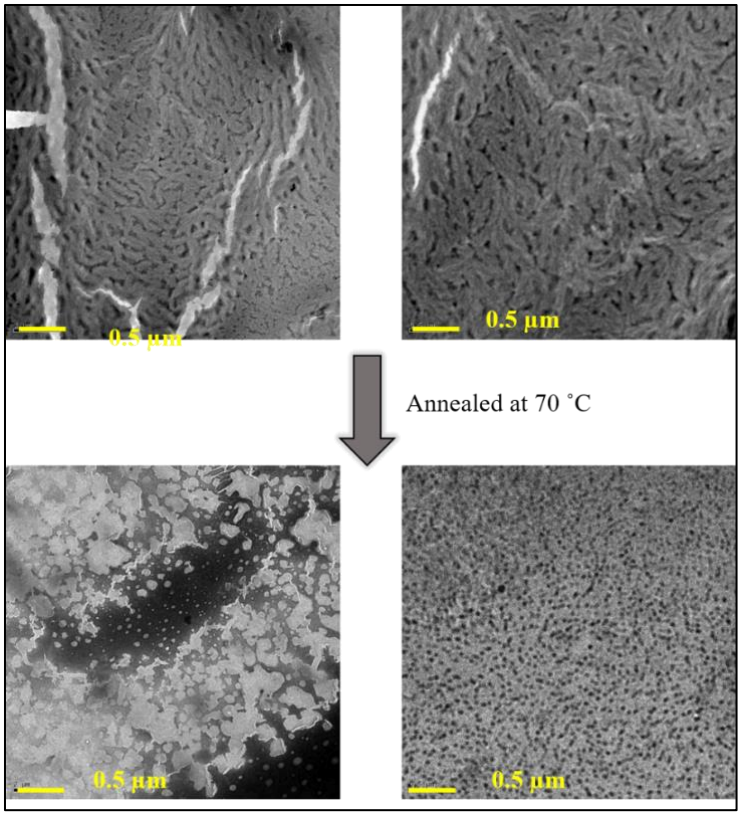

Figure 3.37 TEM imaging block co-polymer **P-1,2** before and after thermal annealing at 70 ˚C: formation of spheres upon thermal annealing.

3.4 Conclusions

The helix sense selective polymerization of achiral *N*-methyl-*N*'-(2-isopropyl-6-methylphenyl)carbodiimide monomer was achieved by using chiral BINOL-Ti (IV) initiator. A persistent level of asymmetry was built into the polymer system as a result of bulky disubstituted aryl pendant group, thus an unusual behavior upon thermal annealing was observed. Prolonger heating causes the racemization of screw sense polymer into equal proportions of complementary screws. After racemization process, the unique aggregation process takes place between parent helices and opposite screw sense which is formed *in situ* and as the result the stereocomplexes are formed as evidenced from VCD and SOR data. We postulated that different molecular motions which are operating within the polymer system as well as zipping of adjacent isopropyl groups contribute for this fascinating aggregation phenomena. Due to formation of stereocomplexes, the overall chirality is decrease to zero. Stereocomplex aggregated morphologies were studied by AFM, SEM, TEM to review the formation of fibers, spheres, and maggot-like architectures. To take advantage of macromolecular zipping, a block co-polymer with two chemically distinct segments were synthesized displaying spherical aggregates as evident by SEM, TEM, DLS and AFM techniques. These results strongly suggested that short block segments may crystallize together to form the core of the round-shape particles. Aforementioned aggregations are important to improve polymer thermal and physical properties, such as glass transition temperature, melting temperature, and crystallinity of material which are responsible for various applications. Overall, understanding their mechanism of complex formation, based on stereo regularity changes may advance the area of molecular or drug separation and chiral catalysis.

3.5 Materials and methods

3.5.1 Instrumentation

^{1}H NMR, and ^{13}C NMR were recorded by using Bruker Advance III^{TM} 500 MHz NMR spectrometer at room temperature. Specific optical rotation data were recorded on JASCO P-1010 polarimeter at λ=435 nm and at sample concentration was 2.0 mg/mL by using 100 mm path length cell. Solution state vibrational circular dichroism spectra were obtained by using Bio Tool Chiral-2X VCD spectrometer by dissolving samples in deuterated toluene (C = 25 mg/mL and l = 50 μm). Malven Zetasizer particle sizer Nano ZC model equipped with He-Ne laser source at 633 nm (Max 4 Mw) was used for dynamic light scattering (DLS) measurement. Transmittance measurements were done by using UV-Visible spectrometer (UV-1601PC SHIMADSU) at 600 nm wavelength. Raguku Ultima III X-Ray diffractometer was used to record all *p*-XRD profiles on powder samples. Tapping mode atomic force microscopy (TM-AFM) was done by using Nanoscope IV Multimode Veeco instrument on silicon wafers (diameter, d =2.5 cm, Wafer World). All imaging was performed at room temperature with silicon cantilever with a nominal constant of 42 N/m and 320 kHz OTESPA tip. Scanning electron microscopy imaging was done by using Zeiss Supra 40 instrument at UTD nano-characterization facility. The samples were mounted on silicon wafers and it was coated with conductive Pd/Au film. The potential applied to the inspection sample was 10 kV. Transmission electron microscope (TEM) was acquired on Tecnai Spirit electron microscope under 200 kV at UT Southwestern Medical School. The samples were mounted on the carbon coated copper grid and negative staining with 2% aqueous uranyl acetate was applied to the specimens. Small-angle X-ray scattering (SAXS) was performed in vacuum with a pinhole-collimated instrument

(Rigaku SMAX3000) using Cu Kα radiation (λ = 1.542 Å). The beam has a 1 mm diameter at the sample plane and the accessible range of scattering vectors is 0.02 to 0.22 $Å^{-1}$. SAXS data was calibrated with a silver behenate standard.

3.5.2 Synthesis of ureas, and carbodiimide monomers and polycarbodiimides

Synthesis of *N*-methyl-*N*'-(5-methyl-2-isopropylphenyl)thiourea

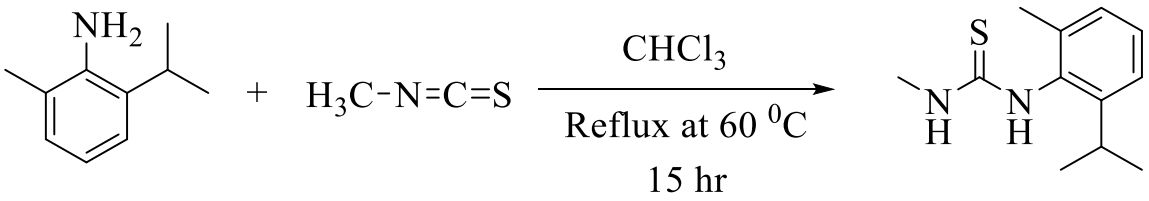

5.000 g (1 eq., 33.5 mmol) of 5-methyl-3-isopropylphenylaniline and 2.450 g (1 eq., 33.5 mmol) of methyl isothiocyanate were dissolved in 150 mL of $CHCl_3$ and refluxed overnight. At the end of the reaction time, the solvent was evaporated and the solid was isolated by filtration. After drying, the urea was recrystallized from EtOH and the crystals were isolated by filtration after cooling. The crystals were dried under vacuum. Yield = 6.330 g (85%), white, shiny, flake-like crystals.

^{1}H NMR (500 MHz, $CDCl_3$, δ ppm): 8.80 (s, 1H, N-H), 7.10 - 6.99 (m, 3H, overlapped Ar-H), 5.30 (s, 1H, N-H), 3.04 (s, 1H, methyn H), 2.84 (s, 3H, N-CH_3), 2.13 (s, 3H, Ar-CH_3), 1.06 (d, 6H, isopropyl H).

^{13}C NMR (126 MHz, $CDCl_3$, δ ppm): 180.89 (C=S), 147.18, 136.71, 131.23, 128.66, 128.18, 123.99 (Ar-C=C), 31.18 (N-CH_3), 27.80 (Ar-CH_3), 23.78 - 22.79, (methyn CH), 17.72 (isopropyl CH_3).

Synthesis of *N*-methyl-*N*'-(2-isopropylphenyl)thiourea

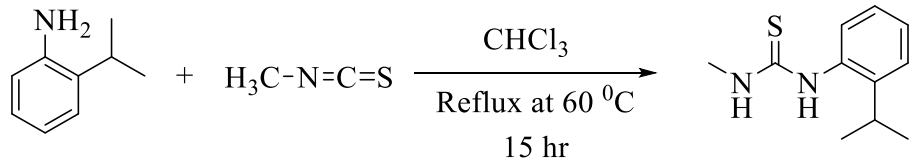

5.000 g (1 eq., 37.0 mmol) of 2-isopropylphenylaniline and 2.710 g (1 eq., 37.0 mmol) of methyl isothiocyanate were dissolved in 150 mL of $CHCl_3$ and refluxed overnight. The urea was recrystallized from EtOH and the crystals were isolated after cooling. The final product was dried under vacuum for 1 day. Yield = 7.230 g (94%), light pinkish, needle-like crystals.

^{1}H NMR (500 MHz, $CDCl_3$, δ ppm): 8.26 (br, 1H, N-H), 7.33-7.09 (m, overlapped, 4H, Ar-H), 5.60 (br, 1H, N-H), 3.15, 3.13, 3.12, 3.11, 3.09, 3.08, 3.01, 3.00, (septet, 1H, C-H), 2.97 (s, 3H, CH_3), 1.13, 1.11 (d, 6H, $2CH_3$).

^{13}C NMR (126 MHz, $CDCl_3$, δ ppm): 181.89 (C=S), 146.56, 132.83, 128.93, 128.16, 127.07 (Ar-C=C), 31.74 (N-CH_3), 27.93 (Ar-CH_3), 23.39 (2 CH_3).

Synthesis of *N*-methyl-*N*'-(3-isopropylphenyl)thiourea

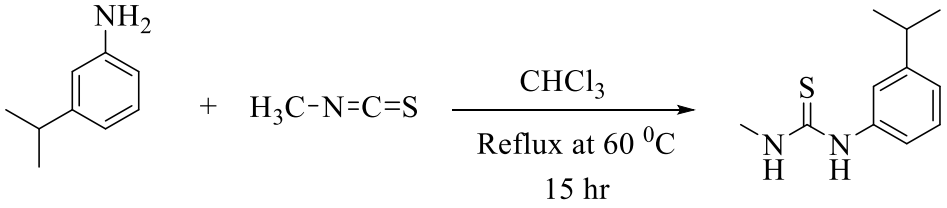

5.000 g (1 eq., 37.0 mmol) of 3-isopropylphenylaniline and 2.710 g (1 eq., 37.0 mmol) of methyl isothiocyanate were dissolved in 200 mL of $CHCl_3$ and refluxed overnight. The urea was recrystallized from EtOH and the crystals was isolated by filtration after cooling. It was dried under vacuum overnight. Yield = 6.853 g (89%), light pinkish, needle-like crystals.

^{1}H NMR of (500 MHz, $CDCl_3$, δ ppm): 8.63 (br, 1H, N-H), 7.24 (s, 1H, Ar-H), 7.22-6.96 (m, overlapped, 3H, Ar-H), 6.17 (b, 1H, N-H), 2.99 (s, 3H, N-CH_3), 2.84, 2.82, 2.81, 2.79, 2.78, 2.77 (septet, 1H, C-H), 1.15, 1.14 (d, 6H, 2 CH_3).

^{13}C NMR (126 MHz, $CDCl_3$, δ ppm): 180.95 (C=S), 150.92, 136.19, 129.59, 124.94, 123.09, 122.29 (Ar-C=C), 33.68 (N-CH_3), 31.70 (Ar-CH_3), 23.61(2 CH_3).

Synthesis of *N*-methyl-*N*'-(4-isopropylphenyl)thiourea

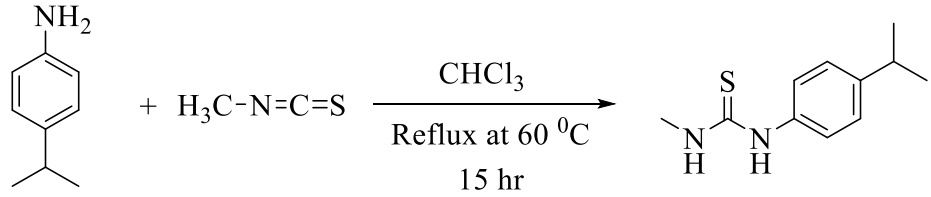

5.000 g (1 eq., 37.0 mmol) of 3-isopropylphenylaniline and 2.701 g (1 eq., 37.0 mmol) of methyl isothiocyanate were dissolved in 250 mL of $CHCl_3$ and refluxed overnight. The urea was recrystallized from EtOH and the crystals were isolated by filtration after cooling. It was dried under vacuum overnight. Yield = 7. 470 g (97%), pinkish, needle-like crystals.

^{1}H NMR (500 MHz, $CDCl_3$, δ ppm): 8.83 (br, 1H, N-H), 7.08 - 6.15 (d, 4H, Ar-H), 2.89 (s, 3H, N-CH_3), 2.75 - 2.69 (m, 1H, C-H), 1.08, 1.06 (d, 6H, 2CH_3).

^{13}C NMR (126 MHz, $CDCl_3$, δ ppm): 180.53 (C=S), 147.06, 133.73, 127.30, 124.72 (Ar C=C), 33.15 (N-CH_3), 31.29 (C-H), 23.43 (2 CH_3).

Synthesis of Monomers

Synthesis of *N*-methyl-*N*'-(5-methyl-2-isopropylphenyl)carbodiimide, **M-1**

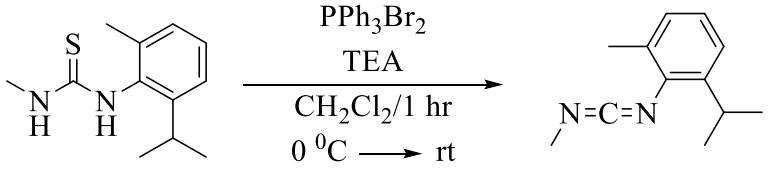

Dehydrosulfonation of thiourea was carried out by using 5.000 g (1 eq., 22.5 mmol) of thiourea, 11.870 g (1,25 eq., 28.1 mmol) of PPh_3Br_2, 5.620 g (2.5 eq., 56.2 mmol) of TEA in CH_2Cl_2 medium. After 1 hr, an excess of hexanes was added and the precipitate formed was filtered out. The filtrate was evaporated under reduced pressure (rotavap) to isolate the monomer. The monomer was purified using vacuum distillation at 60 ˚C. Yield = 3.302 g (78%), colorless liquid.

^{1}H NMR (500 MHz, $CDCl_3$, δ ppm): 7.14 - 7.04 (m overlapped, 3H, Ar-H), 3.43 - 3.38 (m, 1H, C-H), 2.40 (s, 3H, N-CH_3), 1.28, 1.27 (d, 6H, 2CH_3).

^{13}C NMR (126 MHz, $CDCl_3$, δ ppm): 142.10 (N=C=N), 135.64, 134.48, 132.29, 127.93, 124.48, 123.45 (Ar-C=C), 32.67 (C=N), 28.86 (N-CH_3), 23.01 (C-H), 23.09 (Ar-CH_3), 19.22 (2 CH_3).

Synthesis of *N*-phenyl-*N*'-octadecylcarbodiimide, **M-2**

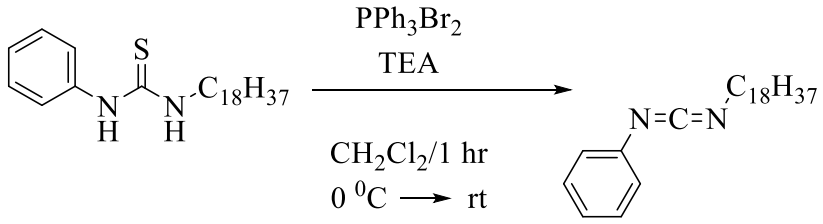

Dehydrosulfonation of thiourea was carried out by using 5.000 g (1 eq., 4.6 mmol) of thiourea, 7.708 g (1.25 eq.,18.3 mmol) of PPh_3Br_2, 3.692 g (2.5 eq., 18.3 mmol) of TEA in CH_2Cl_2 medium. After 1 hr, excess hexanes were added and the precipitate was filtered out. The filtrate was evaporated under reduced pressure (rotavap) to isolate the monomer. The monomer was purified by silica gel chromatography using 10% EtOAc: 90% hexanes mixture as an eluent. Yield = 3.712 g (82%), colorless clear liquid.

^{1}H NMR (500 MHz, $CDCl_3$, δ ppm): 7.35 - 7.12 (m overlapped, 5H, Ar-H) 3.43, 3.42, 3.40 (t, 2 H, N-CH_2), 1.71- 1.30 (m, overlapped, 31 H, alkyl chain CH_2) 0.93, 0.92, 0.90 (t, 3H, terminal CH_3).

^{13}C NMR (126 MHz, $CDCl_3$, δ ppm): 140.90 (N=C=N), 136.06, 129.37, 124.56, 123.55 (Ar-C=C), 46.91 (N-CH_2), 32.06, 31.50, 29.84, 29.50, 29.23, 26.90, 22.82 (CH_2 in alkyl chain), 14.23 (terminal CH_3).

Synthesis of *N*-methyl-*N*'-(2-isopropylphenyl)carbodiimide, **M-3**

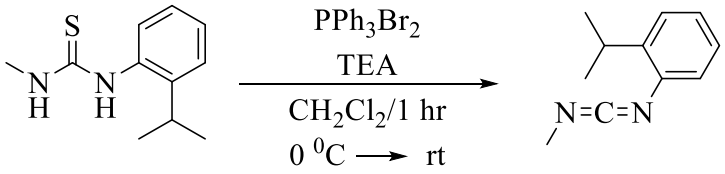

5.000 g (1 eq., 24.0 mmol) thiourea, 12.679 g (1.25 eq, 30.0 mmol) of PPh_3Br_2, 6.066 g (2.25 eq., 60.1 mmol) of TEA were dissolved in CH_2Cl_2 medium. Monomer extraction and purification wERE done as stated in previous. Yield = 3.510 g (84%), clear colorless liquid.

^{1}H NMR (500 MHz, $CDCl_3$, δ ppm): 7.28 - 7.12 (m, overlapped, 4-H, Ar-H), 3.46 - 3.38, (m, 1H, C-H), 3.41 (s, 3H, N-CH_3), 1.28, 1.26 (d, 6H, 2CH_3).

^{13}C NMR (126 MHz, $CDCl_3$, δ ppm): 142.50 (N=C=N), 137.92, 136.65, 128.87, 126.74, 126.38, 125.24, 124.53 (Ar-C=C), 32.94 (N-CH_3), 28.69 (Ph-C-H), 23.29 (2CH_3).

Synthesis of *N*-methyl-*N*'-(3-isopropylphenyl)carbodiimide, **M-4**

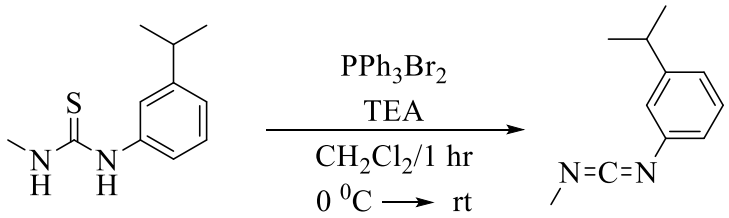

5.000 g (1 eq., 24.0 mmol) thiourea, 12.679 g (1.25 eq, 30.0 mmol) of PPh_3Br_2, 6.067 g (2.25 eq., 60.1 mmol) of TEA were dissolved in CH_2Cl_2 medium. Monomer extraction and purification were done as stated previously. Yield = 2.59 g (62 %), clear colorless liquid.

^{1}H NMR (500 MHz, $CDCl_3$, δ ppm): 7.26 - 6.94 (m, overlapped, 4H, Ar-H), 3.19 (s, 3H, N-CH_3), 2.95 - 2.87 (m, overlapped, 1 H, methyn C-H), 1.28, 1.27 (d, 6H, $2CH_3$).

^{13}C NMR (126 MHz, $CDCl_3$, δ ppm): 150.73 (N=C=N), 140.54, 136.95, 129.52, 123.27, 122.00, 121.31 (Ar-C=C), 34.33 (N-CH_3), 32.93 (Ph-C-H), 24.21 ($2CH_3$).

Synthesis of *N*-methyl-*N*'-(4-isopropylphenyl)carbodiimide, **M-5**

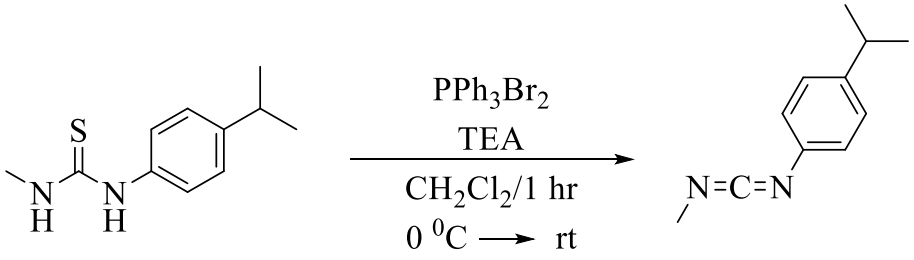

5.000 g (1 eq., 24.0 mmol) thiourea, 12.689 g (1.25 eq., 30.0 mmol) of PPh_3Br_2, 6.067 g (2.25 eq., 60.1 mmol) of TEA were dissolved in CH_2Cl_2 medium. Monomer extraction and purification were done as stated previously.

Yield = 3.720 g (89 %), clear colorless liquid.

^{1}H NMR (500 MHz, $CDCl_3$, δ ppm): 7.26 - 7.05 (m, overlapped, 4H, Ar-H), 3.15 (s, 3H, N-CH_3), 2.95 - 2.87 (m, overlapped, 1H, C-H methyn H), 1.28, 1.26 (d, 6H, $2CH_3$).

^{13}C NMR (126 MHz, $CDCl_3$, δ ppm): 145.45 (N=C=N), 137.85, 136.98, 132.21, 128.45, 127.28, 123.44 (Ar-C=C), 33.63 (N-CH_3), 32.54 (C-H methyn carbon), 24.04 ($2CH_3$).

Synthesis of poly(*N*-methyl-*N*'-(5-methyl-2-isopropylphenyl)carbodiimide), **P-1**

The monomer:initiator ratio used here is 250:1 and (*R*), (*S*), and achiral (*RAC*) polymers were synthesized by using (*R*)-, (*S*)-, and (*RAC*)-BINOL-Ti(IV) diisopropoxide initiators, respectively. All polymerizations have been carried out inside the glove box.

First, 2.000 g (250 eq., 10.6 mmol) of (*N*-methyl-*N*'-(5-methyl-3-isopropylphenyl)carbodiimide monomer was placed in an oven dried sample vial along with a stirring bar. Then, 19.1 mg (1 eq., 42.5 µmol) of (*R*)-BINOL-Ti (IV) isopropoxide initiator was added into the vial along with 0.2 mL of anhydrous chloroform. It was stirred overnight until very viscous sample of polymer was obtained. The same procedures and the same amounts were used to obtain (*S*)-polymer and (*RAC*)- polymers respectively. After 15 hours, the polymers were dissolved in toluene and precipitated into methanol. This step was repeated three time to obtain pure fiber-like, off white polymers. Then all polymers were dried under vacuum for 2 days.

(*R*)-**P-1**, Yield = 1.88 g (94 %).

^{1}HNMR (500 MHz, Tol, δ ppm): 6.90,6-6.82 (b, Ar-H), 3.43-3.23 (b,N-CH_3), 2.71, 2.62, 2.32 (N-CH_3), 1.47 (b, methyn H), 1.35 (b, Ar-CH_3),1.07, 0.81, 0.62 (b, isopropyl CH_3); ^{13}C NMR (500 MHz, Tol, δ ppm): 146.20 (C=N, imine carbon), 142.88, 141.97, 124.56, 123.20, 122.49 (Ar C=C), 34.14 (amine N-CH_3), 27.89 (Ar- CH_3), 21.33 (methyn secondary C), 18.81 (isopropyl CH_3);

$^{25\ ^{\circ}C}[\alpha]_{435\ nm}$ =+688 (toluene), C= 2 mg/mL.

(***S***)-**P-1**, Yield = 1.78 g (90 %).

^{1}H NMR (500 MHz, Tol, δ ppm): 6.97-6.74 (b, Ar-H), 3.44 - 3.22 (b, N-CH_3), 2.69, 2.63 (b, N-CH_3), 1.47 - 1.33 (Ar-CH_3), 1.12, 1.06 (b, methyn H), 0.81(b, isopropyl CH_3);^{13}C NMR (500

MHz, Tol, δ ppm): 148.08-143.05 (C=N, imine carbon and Ar C=C overlapped), 127.17-123.48 (Ar C=C), 57.03 (b, N-CH_3) 34.58 (Ar-CH_3), 28.24-22.08 (b, methyn secondary C), 19.05 (isopropyl CH_3); $^{25\ ^{\circ}C}[\alpha]_{435\ nm}$ = - 714 (toluene), C = 2 mg/mL

(*RAC*)-**P-1**, Yield = 1.73 g (87 %).

^{1}HNMR (500 MHz, Tol, δ ppm): 6.89, 6.81 (b, Ar-H), 3.43, 3.32, 3.22 (b, N-CH_3), 1.34 (Ar-CH_3), 1.16 (C-H, methyn H), 1.08, 0.81(isopropyl CH_3); ^{13}C NMR solid state, δ ppm: 143.15 (b, C=N), 126.45 - 123.24 (b, Ar-C=C), 55.63 (b, N-CH_3) 34.24 (b, Ar-CH_3), 28.25- 22.85 (b, methyn C), 18.99 (b, isopropyl CH_3).

Synthesis of poly(*N*-methyl-*N*'-(2-isopropyl-6-methylphenyl)carbodiimides)-*b*-poly(*N*-methyl-*N*'-octadecylcarbodiimide), **P-1,2**

Inside the glove box, 0.250 g (40 eq., 1.3 mmol) of *N*-methyl-*N*'-(5-methyl-3-isopropylphenyl) carbodiimide and 14.9 mg of (*S*)-BINOL-Ti(IV) diisopropoxide initiator were placed along with 3.0 mL of chloroform and it was allowed to stir for 2 hours. While stirring, every 30 min aliquot of 20 µL was taken and mixed with 4.0 mL of ether. Then it was injected to GC-MS to determine the percentage of monomer consumption. After two hours (90% of monomer consumed), the second monomer of 2.000 g (162 eq., 5.4 mmol) *N*-phenyl-*N*'-octadecylcarbodiimide (**M-2**) was added. And the mixture was allowed to stir overnight until gel-like product formed. The following day, the polymer was dissolved in chloroform and precipitated from methanol two times. The polymer was dried under vacuum for 2 days.

Yield = 1.93 g (86%); ^{1}H NMR (500 MHz, $CDCl_3$, δ ppm): 7.13 -7.01 (b, Ar-H), 3.48 (N-CH_2 from octadecyl chain), 3.13, 2.89 (b, N-CH_3), 1.28 - 0.90 (overlapped peakd from octadecyl chain, Ar-CH_3, methyn H, and isopropyl groups); ^{13}C NMR (126 MHz, $CDCl_3$, δ ppm): 148.69,

148.32 (C=N of both **P-1** and **P-2** blocks), 144.26, 143.17, 141.28, 132.66, 132.58, 130.29, 128.90, 128.24, 124.70, 123.85, 122.93 (Ar-C=C), 54.10 (Ar-CH_3), 34.24 (N-CH_3 from **P-1**), 32.31 (N-CH_2 octadecyl chain), 30.13, 30.06, 29.75, 28.48, 28.30, 27.32, 25.13, 24.18, 23.35, 23.06, 21.71, 19.38, 18.96, 18.81, 18.40, 14.47 (CH_2, isopropyl CH_3 and terminal CH_3 from octadecyl chain); $^{25\ ^{\circ}C}[\alpha]_{435\ nm}$ = - 498 (toluene), C = 2 mg/mL.

Synthesis of poly(*N*-methyl-*N*'-(2-isopropylphenyl)carbodiimide), **P-3**

Inside the glove box, 1.000 g (250 eq., 5.7 mmol) of *N*-methyl-*N*'-(2-isopropylphenyl) carbodiimide and 10.4 mg (1 eq., 22.9 µmol) of (*S*)-BINOL-Ti(IV) diisopropoxide initiator was placed along with 1.0 mL of toluene and it was allowed to stir overnight. The end of the reaction time hard gel-like polymer (insoluble) was obtained and washed with in toluene three times. Then, it was dried under vacuum for 48 hours.

Synthesis of poly (*N*-methyl-*N*'-(3-isopropylphenyl)carbodiimide), **P-4**

Inside the glove box, 1.300 g (250 eq., 7.5 mmol) of *N*-methyl-*N*'-(3-isopropylphenyl) carbodiimide and 13.4 mg (1 eq., 29.8 µmol) of (*S*)-BINOL-Ti(IV) diisopropoxide initiator was placed along with 1.0 mL of toluene and it was allowed to stir overnight. Then the polymer was an insoluble gel and it was washed with toluene to remove trace of initiator three times. Then it was dried under vacuum for 48 hours.

Synthesis of poly*(N*-methyl-*N*'-(4-isopropylphenyl)carbodiimide), **P-5**

Inside the glove box, 2.200 g (250 eq., 12.6 mmol) of (*N*-methyl-*N'*-(4-isopropylphenyl) carbodiimide and 22.7 mg (1 eq., 50.5 µmol) of (*S*)-BINOL-Ti(IV) diisopropoxide initiator was placed along with 1.0 mL of toluene and it was allowed to stir overnight. The polymer was dissolved in toluene and precipitated from methanol. It was vacuum dried for 48 hours.

Yield = 1.730 g (79 %); ^{1}H NMR (500 MHz, $CDCl_3$, δ ppm): 7.26 - 6.42 (b, Ar-H), 2.86 (b, N-CH_3), 2.24 (b, methyn H), 1.22 (b, isopropyl CH_3); ^{13}C NMR (126 MHz, $CDCl_3$) δ: 147.57, 147.11(C=N), 143.15, 126.28, 122.08 (Ar-C=C), 33.91(N-CH_3), 24.74, 24.55 (methyn C-H and isopropyl CH_3).

$^{25\ ^{\circ}C}[\alpha]_{435\ nm}$ = - 498 (toluene), C= 2 mg/mL.

3.5.3 Determination of the activation energy

2 mg/mL of **Poly-1** of (*R*), (*S*) and **Poly-1,2** were dissolved in toluene separately. These polymer solutions were incubated at 40 ˚C, 50 ˚C, 60 ˚C, 70˚ and the specific optical rotation was measured independently. Then the graphs of SOR vs time, ln [α/α_0] vs time and Arrhenius plot was drawn.

3.5.4 Determination of chirality

VCD spectra of above-mentioned samples were recorded upon thermal annealing. For those experiments, 1.0 mL of sample was taken before and after the thermal annealing process.

3.5.5 Dynamic Light Scattering Experiment

Hydrodynamic radius of polymer samples was measured before and after the thermal annealing process.

3.5.6 Transmittance Measurements of Polymer Solutions

2 mg/mL solutions of (*R*), (*S*), (*RAC*) of **Poly-1** and the **Poly-1,2** were prepared and transmittance of each polymer solutions was measured at λ = 600 nm upon thermal annealing at 70 ˚C. Then the transmittance % was plotted against time.

3.5.7 *p*-XRD

The powder sample of each polymer was placed on quartz holder and the *p*-XRD profile was recorded.

3.5.8 Morphological Studies

Tapping-Mode Atomic Force microscopy (TP-AFM)

2 mg/mL polymer solutions were prepared and thermal annealing was done until the SOR reached to plateau value. 1.0 mL of the polymer solution was spun cast on silicon wafers for AFM imaging. Samples were prepared before and after thermal annealing.

Scanning Electron Microscopy (SEM)

For thin film preparations, the solid polymer samples were used before and after thermal annealing. SEM imaging was performed by using bulk materials and electro-sprayed samples. For this, the concentration of 0.43 (w/w%) samples were used in toluene and electro-spraying was carried out by applying 12 kV between the needle tip and grounded collector drum.

Transmission Electron Microscopy (TEM)

For TEM imaging, the samples of all polymers were inspected before and after thermal annealing.

3.6 References

(1) Yashima, E.; Maeda, K.; Iida, H.; Furusho, Y.; Nagai, K. Helical Polymers : Synthesis, Structures , and Functions. **2009**, 6102–6211.

(2) Nakano, T.; Okamoto, Y. Synthetic Helical Polymers: Conformation and Function. *Chem. Rev.* **2001**, *101* (12), 4013–4038 DOI: 10.1021/cr0000978.

(3) Haino, T. Molecular-Recognition-Directed Formation of Supramolecular Polymers. *Polym. J.* **2012**, *45* (March), 1–21 DOI: 10.1038/pj.2012.144.

(4) Shimomura, K.; Ikai, T.; Kanoh, S.; Yashima, E.; Maeda, K. Switchable Enantioseparation Based on Macromolecular Memory of a Helical Polyacetylene in the Solid State. *Nat. Chem.* **2014**, *6* (5), 429–434 DOI: 10.1038/nchem.1916.

(5) Sahu, H.; Gupta, S.; Gaur, P.; Panda, A. N. Structure and Optoelectronic Properties of Helical Pyridine–furan, Pyridine–pyrrole and Pyridine–thiophene Oligomers. *Phys. Chem. Chem. Phys.* **2015**, *17*, 20647–20657 DOI: 10.1039/C5CP02872H.

(6) Liu, L.; Ousaka, N.; Horie, M.; Mamiya, F.; Yashima, E. Helix–helix Inversion of an Optically-Inactive π-Conjugated Foldamer Triggered by Concentration Changes of a Single Enantiomeric Guest Leading to a Change in the Helical Stability. *Chem. Commun.* **2016**, *1* (i), 1–4 DOI: 10.1039/C6CC05753E.

(7) Reuther, J. F.; Siriwardane, D. A.; Campos, R.; Novak, B. M. Solvent Tunable Self-Assembly of Amphiphilic Rod-Coil Block Copolymers with Chiral, Helical Polycarbodiimide Segments: Polymeric Nanostructures with Variable Shapes and Sizes. *Macromolecules* **2015**, *48* (19), 6890–6899 DOI: 10.1021/acs.macromol.5b01564.

(8) Kulikov, O. V.; Siriwardane, D. A.; Reuther, J. F.; McCandless, G. T.; Sun, H. J.; Li, Y.; Mahmood, S. F.; Sheiko, S. S.; Percec, V.; Novak, B. M. Characterization of Fibrous Aggregated Morphologies and Other Complex Architectures Self-Assembled from Helical Alkyne and Triazole Polycarbodiimides (R)- and (S)-Families in the Bulk and Thin Film. *Macromolecules* **2015**, *48* (12), 4088–4103 DOI: 10.1021/acs.macromol.5b00407.

(9) Nanda, V.; DeGrado, W. F. Computational Design of Heterochiral Peptides against a Helical Target. *J. Am. Chem. Soc.* **2006**, *128* (3), 809–816 DOI: 10.1021/ja054452t.

(10) Xu, F.; Khan, I. J.; McGuinness, K.; Parmar, A. S.; Silva, T.; Murthy, N. S.; Nanda, V. Self-Assembly of Left- and Right-Handed Molecular Screws. *J. Am. Chem. Soc.* **2013**, *135* (50), 18762–18765 DOI: 10.1021/ja4106545.

(11) Crick, F. H. C. The Packing of α-Helices: Simple Coiled-Coils. *Acta Crystallogr.* **1953**, *6* (8), 689–697 DOI: 10.1107/S0365110X53001964.

(12) Brochu, S.; Prud'homme, R. E.; Barakat, I.; Jérome, R. Stereocomplexation and Morphology of Polylactides. *Macromolecules* **1995**, *28*, 5230–5239 DOI: 10.1021/ma00119a010.

(13) Sveinbjörnsson, B. R.; Miyake, G. M.; El-Batta, A.; Grubbs, R. H. Stereocomplex Formation of Densely Grafted Brush Polymers. *ACS Macro Lett.* **2014**, *3* (1), 26–29 DOI: 10.1021/mz400568j.

(14) Bertin, A. Emergence of Polymer Stereocomplexes for Biomedical Applications. *Macromol. Chem. Phys.* **2012**, *213* (22), 2329–2352 DOI: 10.1002/macp.201200143.

(15) Slager, J.; Domb, A. J. Biopolymer Stereocomplexes. *Adv. Drug Deliv. Rev.* **2003**, *55* (4), 549–583 DOI: 10.1016/S0169-409X(03)00042-5.

(16) Tsuji, H. Poly(lactide) Stereocomplexes: Formation, Structure, Properties, Degradation, and Applications. *Macromol. Biosci.* **2005**, *5* (7), 569–597 DOI: 10.1002/mabi.200500062.

(17) Uehara, H.; Karaki, Y.; Wada, S.; Yamanobe, T. Stereo-Complex Crystallization of Poly(lactic Acid)s in Block-Copolymer Phase Separation. *ACS Appl. Mater. Interfaces* **2010**, *2* (10), 2707–2710 DOI: 10.1021/am1005755.

(18) Kim, S. H.; Tan, J. P. K.; Nederberg, F.; Fukushima, K.; Yang, Y. Y.; Waymouth, R. M.; Hedrick, J. L. Mixed Micelle Formation through Stereocomplexation between Enantiomeric Poly(lactide) Block Copolymers. *Macromolecules* **2009**, *42* (1), 25–29 DOI: 10.1021/ma801739x.

(19) Chang, R.; Shan, G.; Bao, Y.; Pan, P. Enhancement of Crystallizability and Control of Mechanical and Shape-Memory Properties for Amorphous Enantiopure Supramolecular Copolymers via Stereocomplexation. *Macromolecules* **2015**, *48* (21), 7872–7881 DOI: 10.1021/acs.macromol.5b01986.

(20) Kim, S. H.; Nederberg, F.; Zhang, L.; Wade, C. G.; Waymouth, R. M.; Hedrick, J. L. Hierarchical Assembly of Nanostructured Organosilicate Networks via Stereocomplexation of Block Copolymers. *Nano Lett.* **2008**, *8* (1), 294–301 DOI: 10.1021/nl0726813.

(21) Furuhashi, Y.; Kimura, Y.; Yoshie, N. Self-Assembly of Stereocomplex-Type Poly(lactic Acid). *Polym. J.* **2006**, *38* (10), 1061–1067 DOI: 10.1295/polymj.PJ2005214.

(22) Longo, J. M.; Diciccio, A. M.; Coates, G. W. Poly(propylene Succinate): A New Polymer Stereocomplex. *J. Am. Chem. Soc.* **2014**, *136* (45), 15897–15900 DOI: 10.1021/ja509440g.

(23) Ren, J. M.; Ishitake, K.; Satoh, K.; Blencowe, A.; Fu, Q.; Wong, E. H. H.; Kamigaito, M.; Qiao, G. G. Stereoregular High-Density Bottlebrush Polymer and Its Organic Nanocrystal Stereocomplex through Triple-Helix Formation. *Macromolecules* **2016**, *49* (3), 788–795 DOI: 10.1021/acs.macromol.5b02295.

(24) Tian, G.; Lu, Y.; Novak, B. M. Helix-Sense Selective Polymerization of Carbodiimides: Building Permanently Optically Active Polymers from Achiral Monomers. *J. Am. Chem. Soc.* **2004**, *126* (13), 4082–4083 DOI: 10.1021/ja049548m.

(25) Reuther, J. F.; Bhatt, M. P.; Tian, G.; Batchelor, B. L.; Campos, R.; Novak, B. M. Controlled Living Polymerization of Carbodiimides Using Versatile, Air-Stable nickel(II)

Initiators: Facile Incorporation of Helical, Rod-like Materials. *Macromolecules* **2014**, *47* (14), 4587–4595 DOI: 10.1021/ma5009429.

(26) Hakoshima, T. Leucine Zippers. *Encycl. Life Sci.* **2000**, 1–5 DOI: 10.1002/9780470015902.a0022548.

(27) Krylov, D.; Vinson, C. R. Leucine Zipper. *Encycl. Life Sci.* **2001**, 1–7 DOI: 10.1038/npg.els.0003001.

(28) Kulikov, O. V.; Incarvito, C.; Hamilton, A. D. Hydrophobic Side-Chain Interactions in a Family of Dimeric Amide Foldamers-Potential Alpha-Helix Mimetics. *Tetrahedron Lett.* **2011**, *52* (29), 3705–3709 DOI: 10.1016/j.tetlet.2011.05.004.

CHAPTER 4

PNIPAM AND PEG GRAFTED HAIRY POLYCARBODIIMIDES AS NANO-CARRIERS FOR HYDROPHOBIC DRUGS

Authors – Siriwardane, D. A.; Kulikov, O.V; Novak, B.M.

Department of Chemistry and Biochemistry, BE 26

The University of Texas at Dallas

800 West Campbell Road

Richardson, TX 75080-3021

Manuscript is in preparation for publishing in Macromolecules journal.

4.1 Abstract

A continuous array of alkyne functionalized polycarbodiimides allows access to the synthesis of brush co-polymers *via* post-polymerization modifications. Combining the advantage of side chain functionalization and copper-catalyzed Huisgen 1,3-dipolar cycloaddition reaction, poly(*N*-isopropylacrylamide) (PNIPAM) and poly(ethyleneglycol) (PEG) were grafted on the polycarbodiimide helical backbone. Taking into account that rigid helical guanidine-like backbone structure of these polymers, their self-assembly into micellar domains would likely represent a significant interest in an aqueous medium. This synthetic strategy and self-aggregation properties provide an access to the successful encapsulate of a hydrophobic drug molecule, such as Doxorubicin (DOX), thus revealing a great potential of polycatrbodiimides bearing hydrophobic side chains as nanocarriers for drug delivery applications.

4.2 Introduction

The development of a synthetic strategy for amphiphilic graft co-polymers involves improving control architectures and exploring potential applications.[1,2] The diversity of graft co-polymers can be altered through the modifications of the main chain or by performing different post-polymerization modifications in side arms. These methodologies offer versatile polymer architectures which lead to different nano-assemblies[3] with potential applications as reported for drug delivery applications,[4,5] molecular rotors for controlled delivery of catalysts,[6] stimuli responsive assemblies,[7-9] and cancer cell targeting and imaging[10] to name a few. With regard to polycarbodiimide polymers, they provide the opportunity to fine tuning of the polymer architecture as it composed of two modifiable appending along the rigid guanidine-like

backbone. Correct tuning of functionalities or altering pendant groups of these polymer systems expands applicability for chiroptical switching,[11,12] liquid crystallinity,[13] solvent, and temperature tunable assemblies.[14] For instance, by taking advantage of tunability of these pendant groups, Novak coworkers have designed the guanidinium functionalized water-soluble polycarbodiimides which showed antibacterial activity against a broad spectrum of bacteria.[15] Fortunately, these polymers possess rigid nitrogen-rich backbone having pendant arms that are viable for specific functionalization and that brings more opportunities to create different polymer architectures.[16] Here we report the synthesis of brush co-polymers obtained by using alkyne appended polycarbodiimide scaffolds and azide functionalized PNIPAM and PEG *via* CuAAc reaction through postpolymerization modifications, *i.e*., these random-coil hydrophilic, PNIPAM and PEGylated polymers have been grafted on the helical backbone to yield brush co-polymers.[17,18] This hairy architecture imparts new intriguing properties to polycarbodiimides polymers making them promising for using in biomedical field as drug delivery nano-carriers.[19,20] Very importantly, these polymers can be tailored for easy solubilization and functionalization in many ways, thus showing different aggregation domains up to several hundred nanometers. The PNIPAM and PEGylated polymers we have synthesized show self-aggregation into nano-carriers which can encapsulate hydrophobic drugs. This study has been focused on determination of critical micelle concentration, drug loading capacity (DLC) and encapsulation efficiency (EE) to evaluate their potential of novel polymer architecture in drug delivery applications.

4.3 Discussion

4.3.1 Synthesis of graft co-polymer

Polycarbodiimides are rigid-rod helical polymers that have been synthesized from various transition metal catalysts mediated polymerization *via* the reversible coordination-insertion mechanism.[21,22] These polymers are composed of two tunable pendant groups which are appended around the nitrogen rich backbone. The presence of modifiable pendant groups offers immense interest towards different functionalization, exploring potential applications in the bio-medical field. In this regard, a new set of PNIPAM and PEGylated brush co-polymers were synthesized by using Copper-catalyzed, azide-alkyne cycloaddition (CuAAc) reaction. Our intention was to incorporate hydrophilic random-coil scaffolds onto hydrophobic rigid-rod polycarbodiimide backbone *via* 'grafting to' strategy. Due to the presence of crowded side chains on the helical backbone, solvent tunable microphase separation takes place due to immiscibility of these chemically distinct segments. We have observed that micellar domains are formed through a self-aggregation process as evident by both TEM and AFM studies. Our investigation for this micellar assembly was carried out for two PNIPAM grafted polymers (**P-1** and **P-2**) and two PEGylated polymers (**P-3** and **P-4**) by varying their hydrophilic composition. To synthesize the alkyne appended monomer, propargyl amine was used with hexyl isocyanate because hexyl group enhances the solubility of polymers in different organic solvents. We used chiral, (*S*)-BINOL Ti(IV) isopropoxide catalyst for polymerization and the resulting homo-polymer of poly(*N*-propargyl-*N*'-hexyl)carbodiimide is not 100 % regioregular due to the presence of alkyl chains both in the imine and amine position.

To synthesize PNIPAM grafted polymers, CuAAc reaction was used with azide end-functionalized PNIPAM polymer. Different proportion of 20% (**P-1**) and 50 % (**P-2**) of PNIPAM was grafted to PC backbone (**Scheme 4.1**).

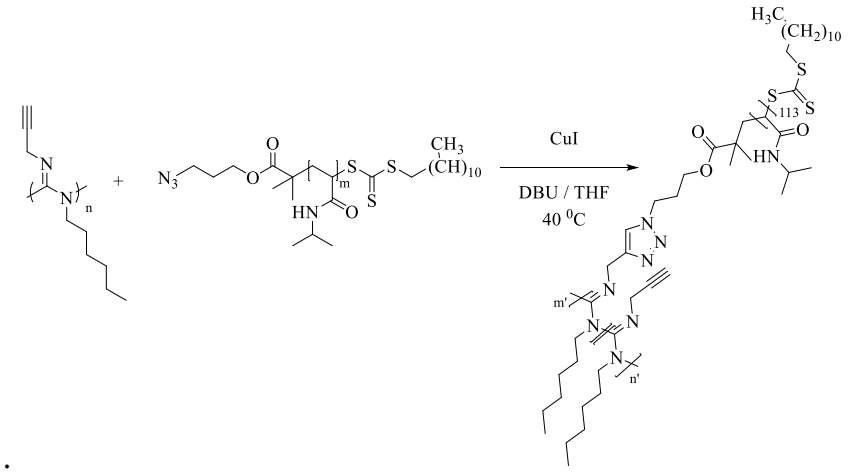

.

Scheme 4.1 Synthesis of PNIPAM grafted polycarbodiimides through 'Click' reaction; synthesis strategy for **P-1** and **P-2**.

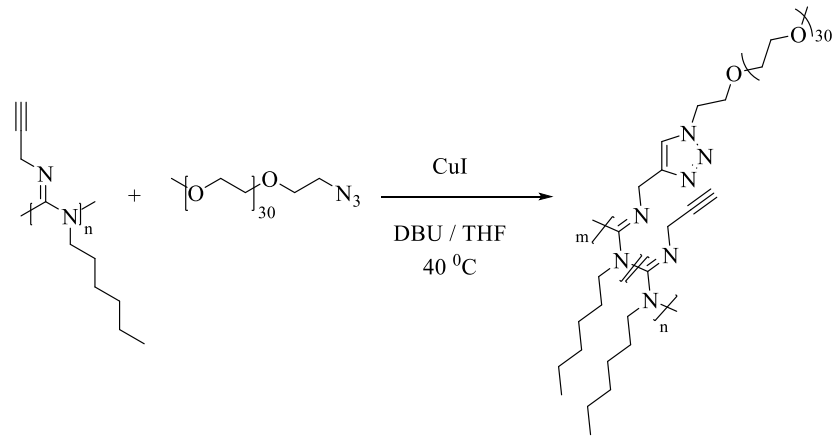

Scheme 4.2 Synthesis of PEG grafted polycarbodiimides through 'Click' reaction; synthesis strategy for **P-3** and **P-4**.

By using the same synthetic strategy, PEGylated brush co-polymers were synthesized by using azide functionalized 2000 Da PEG polymers (**Scheme 4.2**). We attempted to graft high molar

mass polymer into the amidine backbone and the resulting polymers were not soluble in organic solvents, thus we used 2000 Da PEG segments in 50% (**P-3**) and 70% (**P-4**) proportions. The click chemistry utilized here facilitates the link to hydrophilic polymer segments on the polycarbodiimide scaffold, thus their self-aggregation behavior could be observed upon dispersing in an aqueous medium.

4.3.2 Self-assembly behavior of graft co-polymers

We have investigated self-aggregation behaviors of various diblock polycarbodiimides in different organic solvent systems and have been extensively studied their self-assembly behaviour.[14] As reported in Reuther et.al, for diblock and triblock amphiphilic polymers self-assemble into various shapes and sizes simply upon altering the solvents. These shapes include spheres, maggot-like assemblies, and vesicles and these various nano structures are formed due to microphase immiscibility of chemically distinct segments. By grafting hydrophilic PEG and PNIPAM scaffolds onto helical polycarbodiimides, amphiphilic graft co-polymers have been synthesized. Expanding applicability of different polymer architectures of polycarbodiimide systems for potential applications, self-assembly behavior of these polymers has been investigated in an aqueous medium. Upon dispersion of the polymer solution in an aqueous medium, the stable slight turbid solution was observed as a preliminary indication of the micellization process. The formed nano-sized domain was investigated by using TEM (**Figures 4.1-4.4**) and AFM imaging techniques and hydrodynamic radius was calculated by using dynamic light scattering method.

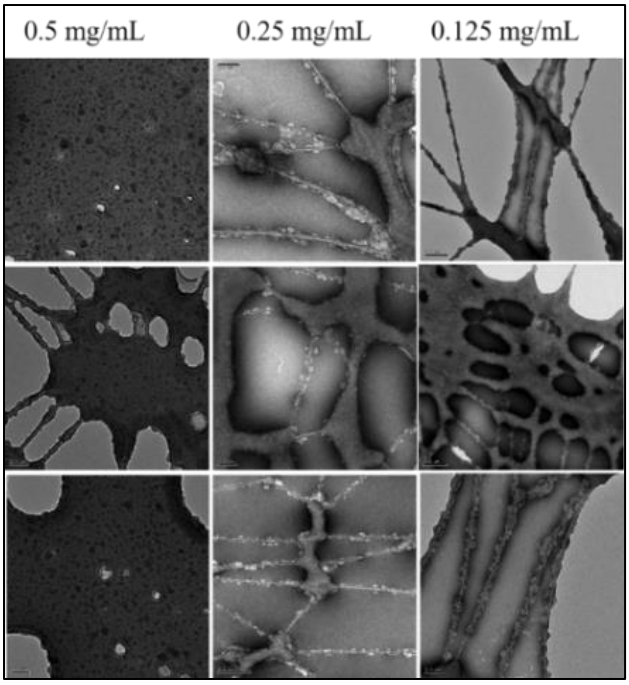

Figure 4.1 TEM images of micelles obtained from 20% PNIPAM-*g*-PC, **P-1** deposited on copper mesh grid stained with 2% aqueous uranyl acetate.

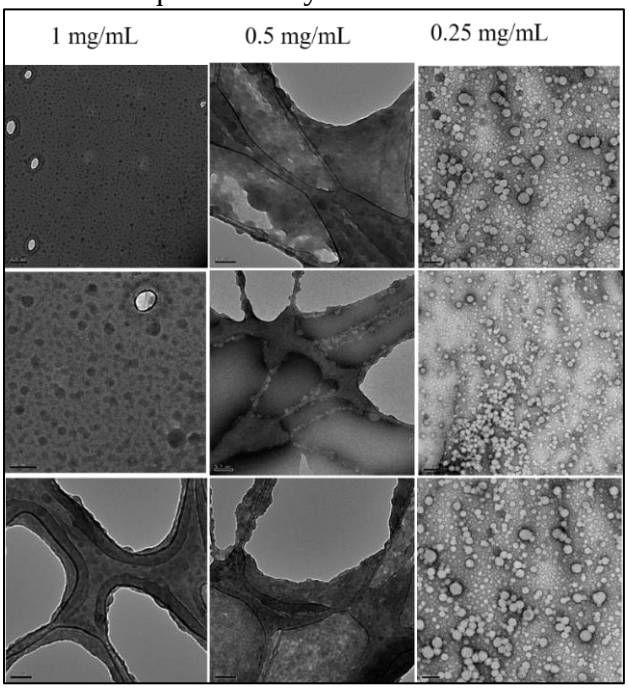

Figure 4.2 TEM images of micelles obtained from 50% PNIPAM-*g*-PC, **P-2** deposited on copper mesh grid stained with 2% aqueous uranyl acetate.

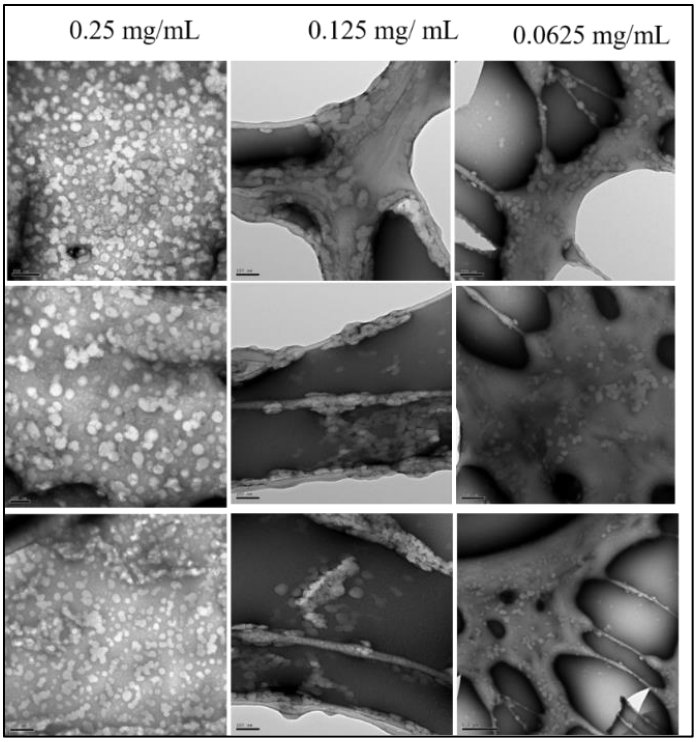

Figure 4.3 TEM images of micelles obtained from 50% PEG-*g*-PC, **P-3** deposited on copper mesh grid stained with 2% aqueous uranyl acetate.

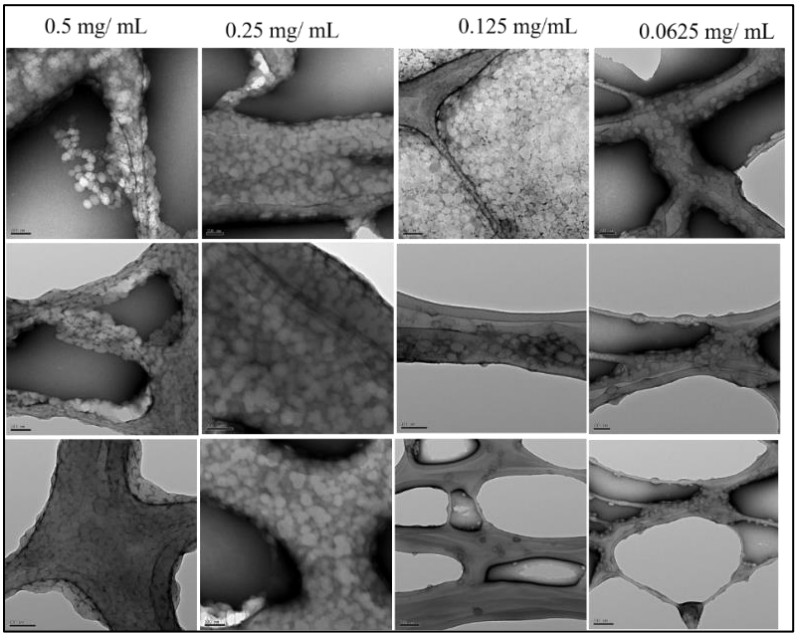

Figure 4.4 TEM images of micelles obtained from 70% PEG-*g*-PC, **P-4** deposited on copper mesh grid stained with 2% aqueous uranyl acetate.

Polycarbodiimide polymers show regioregularity when the two pendant groups possess large steric difference and, the high helix inversion energy is associated with such polymers. The helical inversion barrier depends on the nature of the pendant groups and stiffness of the backbone. For helices with low energy of inversion barrier, they possess more dynamic character whereas static helices possess the high energy of helical inversion.[13] The presence of bulky groups, like aromatics in imine positions, will induce a high helical inversion barrier, thus the static helical character is more pronounced. Our understanding behind the formation of spherical nano-carriers is due to the presence of propargyl and hexyl groups inducing more dynamic helical character. The presence of alkyl chains which are appended on guanidine-like backbone forms helical reversals As a result, this polymer backbone exists as a series of left and right helical reversals which can be transferred randomly throughout the backbone. The high population of helical reversals contributes to the loss of the rigid nature of the backbone, thus it causes the polymer chain to be bent. This also involves to gain low persistence lengths to polymer chains. Upon dispersion of the polymer solution in an aqueous medium, hydrophobic PC confines into the core of the spheres whereas the hydrophilic PNIPAM and PEG segments would form the corona of the sphere in an aqueous medium (**Figures 4.5** and **4.6**).

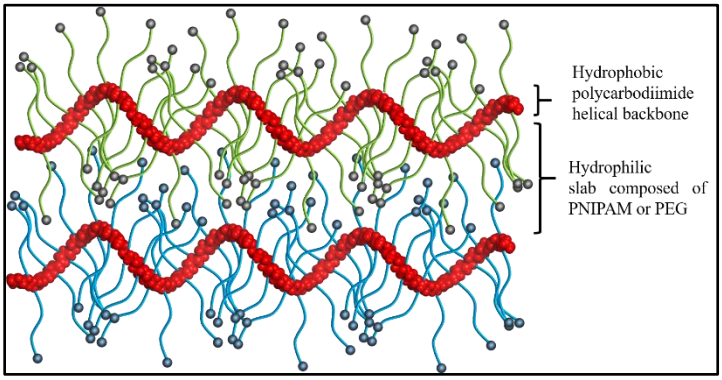

Figure 4.5 Cartoon featuring dimeric bundle of amphiphilic brush co-polymers.

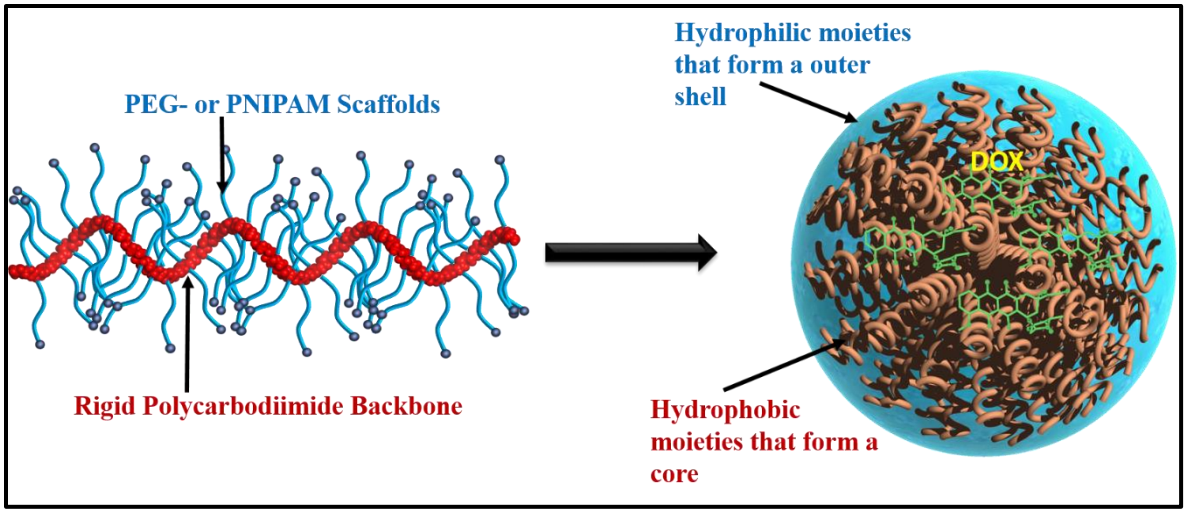

Figure 4.6 Cartoon representing the self-assembly behavior of brush co-polymers into nano-spheres.

4.3.3 Determination of critical micelle concentration (CMC)

We conducted CMC studies by encapsulating pyrene as a fluorescence probe. Pyrene has very characteristics fluorescence spectra depending on the polarity of the medium and it is very sensitive to changes of surrounded microenvironment.[23,24] Upon encapsulation of pyrene into the micellular structure, it should be entrapped into the hydrophobic core and the intensity changes of 334.5 nm and 337.5 nm as indicative peaks for the encapsulation phenomena. When the 337.5 nm peak intensity gets slightly higher than the intensity of 334.5 nm peak, it would be conclusive for pyrene encapsulation. The ratio of these two peaks can be used to confirm the encapsulation of pyrene into the hydrophobic core and this method can be used to determine the CMC values (**Table 4.1**). Comparing the PNIPAM grafted polymers, **P-2** has the higher CMC value as it composed of more hydrophilic corona and micellization is induced at higher concentration values. The same trend was observed in PEGylated polymers, *i.e.*, **P-3** possesses the lowest

CMC value. Generally, as the hydrophobic composition increases, the CMC value is decreased. Overall, these all four brush co-polymers form stable micellar domains in an aqueous medium.

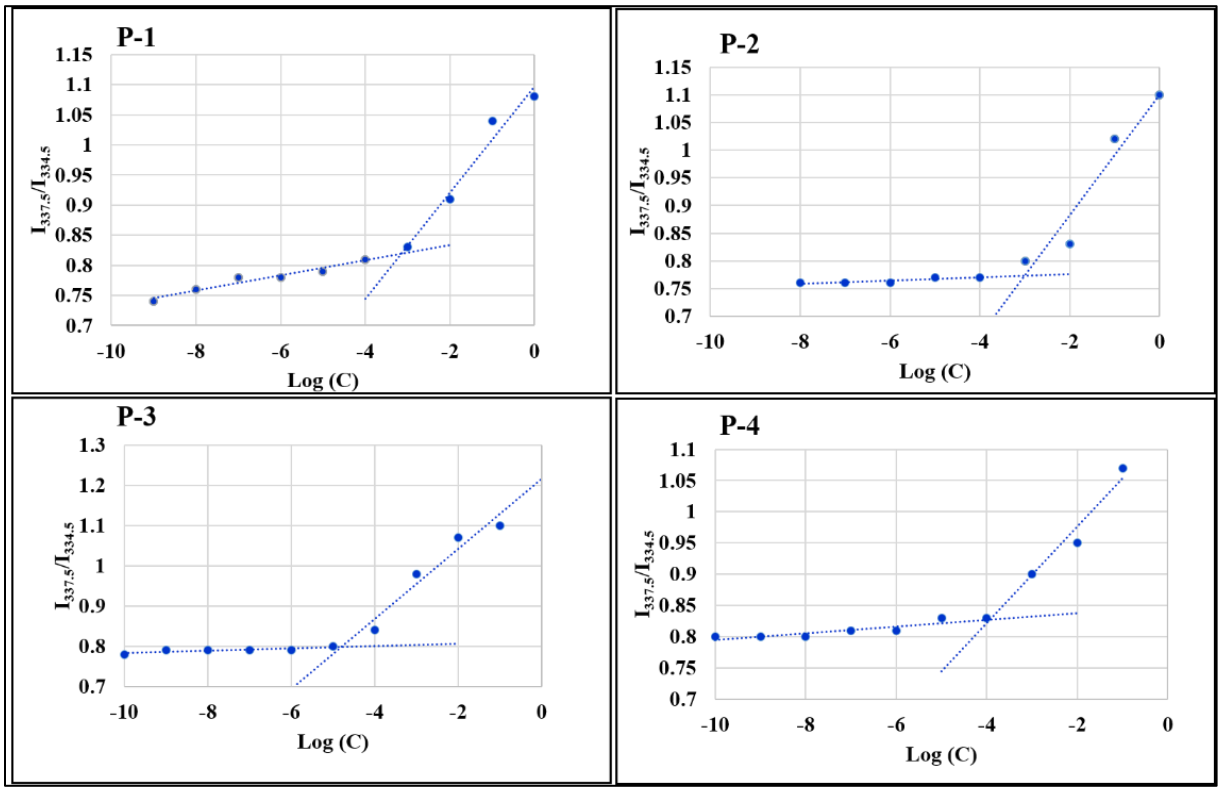

Figure 4.7 Graphs showing CMC values for brush co-polymers.

Table 4.1 Summary of CMC values for brush co-polymers

Polymer	Composition	CMC (mg/mL)
P-1	20% PNIPAM:80% PC	7.94×10^{-4}
P-2	50% PNIPAM:50%PC	1.05×10^{-3}
P-3	50%PEG:50%PC	1.58×10^{-5}
P-4	70%PEG:30%PC	1.11×10^{-4}

4.3.4 Drug encapsulating studies

The implication of this synthesis extends towards the formation of nano-carriers which have potential in drug delivery applications. Very interestingly, this hydrophobic PC segments form the core of micellar structure and the core of the nano-sphere would benefit to encapsulate some hydrophobic drugs.[25] Thus, Doxorubicin has been used as a hydrophobic cargo to determine drug loading capacity (DLC) and encapsulating efficiency (EE). UV-Vis studies were performed to determine DLS and EE by measuring the absorbance at 495 nm. The changes in D_h before and after drug encapsulation was determined by performing DLS measurement and it is clear upon encapsulation of drug that the diameter of the micelles become large (**Figure 4.7**). It also is shown in TEM studies and AFM studies (**Figures 4.8 and 4.9**). For all four types of polymers, upon encapsulation of drug, the diameter range exist within 200 nm, which is effective towards the EPR (Enhanced Permeability and Retention) effect during the release of chemotherapeutic drugs in cancer therapy. The D_h values for PEGylated micelles were above 100 nm and this behavior may be due to the presence of hydrophobic PC scaffolds with low molar mass PEG chains. Both **P-3** and **P-4** showed higher DLC and EE implying that encapsulation of hydrophobic cargo is higher than **P-1** and **P-2** (**Table 4.2**).

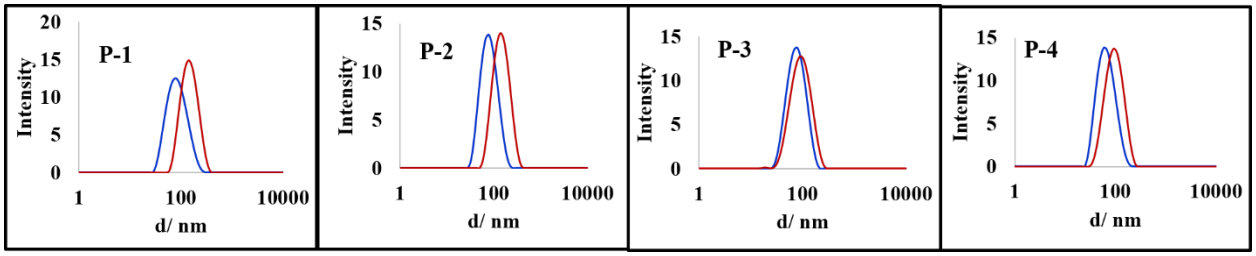

Figure 4.8 DLS profiles showing D_h before (blue line) and after (red line) encapsulation of DOX.

Table 4.2 Summary of hydro dynamic radius (D_h) before and after DOX encapsulation, drug loading capacity (DLC), and EE (encapsulation efficiency)

	D_h Before DOX Loading / nm[a]	D_h After DOX loading / nm[a]	DLC (w%)[b]	EE (w%)[b]
P-1	60.4 (±0.1)	84.1 (±0.1)	1.6	16
P-2	69.5(±0.2)	85.3 (±0.3)	1.76	18
P-3	74.8(±0.3)	133.3 (±0.2)	2.40	24
P-4	75.8(±0.3)	135.4 (±0.1)	2.73	27

[a] Determined by using dynamic light scattering
[b] Determined by using UV-Vis, at λ = 495 nm

TEM imaging also confirms the enlargement of micelle diameter in the range of 100 nm-200 nm. The micellar size that allows for preferential accumulation at tumor tissues around 40-200 nm via the enhanced permeability and retention use for passive targeting.[26,27] The results obtained from this study is in good agreement towards practical applications. The micellar wall has been contracted and this may take place due to vacuum condition during the imaging. For AFM imaging, the polymer samples were drop cast and spherical micelles were observed in the range of 100-150 nm.

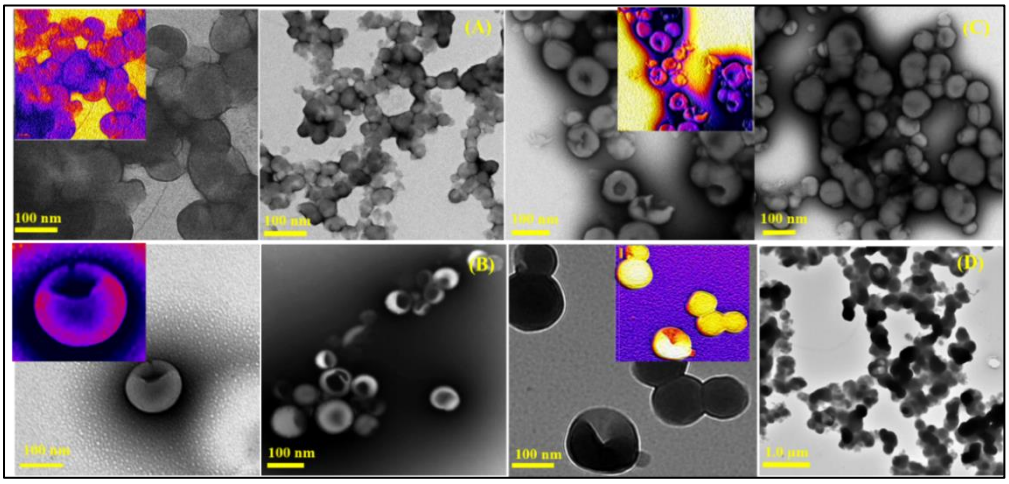

Figure 4.9. TEM images of micellar nano-structures deposited on copper mesh grid stained with 2% aqueous uranyl acetate.

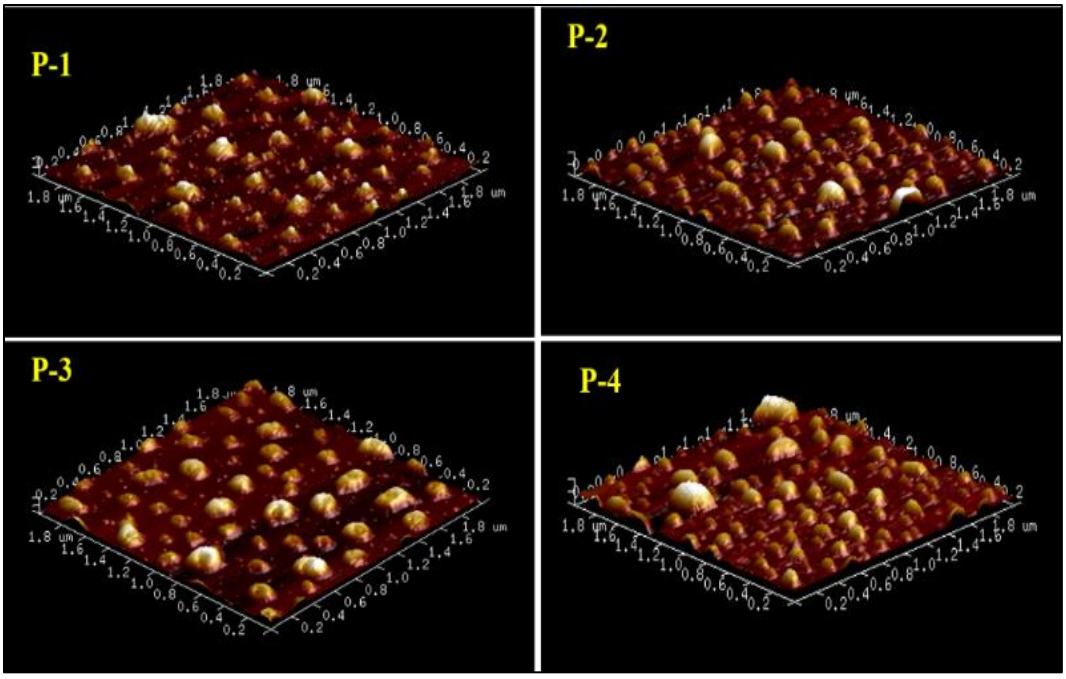

Figure 4.10 AFM images of micellar nano-structures drop cast on silicon wafers, image size = 2 x 2 µm.

4.3.1 Polymer degradation

We have carried out polymer degradation studies in acidic medium. All four polymers are composed of nitrogen rich amidine backbones and this backbone possesses hybrid characteristics of both polyisocyanide and polyisocyanate. The presence of the hybrid nature, polycarbodiimides possess sp^2 nitrogen which is termed as imine nitrogen as well as sp^3-*n* (where *n* is the degree of distortion towards planarity) nitrogen which is referred to as the amine nitrogen. This amine nitrogen can be protonated in acidic conditions and the positively charged core of the micelle can be disintegrated due to repulsion among positively charged polycarbodiimide segments by ensuring the release of encapsulated drug molecules. We hypothesized that protonation of imine nitrogen causes drastic changes in polymer structure making its hydrophilic properties more pronounced.[28,29] The results reveal that the degeneration

of micellar assemblies takes place after suspending in pH = 3 solution for 2-12 hr., thus release of encapsulated cargo occurs as evident by UV-Vis. The detected amount of DOX is low as low drug loading capacity. Therefore, fine tuning of polymer chemical composition and the drug release profiles is still needed for real world applications.

4.4 Conclusion

Polycarbodiimide based graft co-polymers were synthesized with azide functionalized PNIPAM and PEG random-coil polymers. Interestingly, these polymers self-assemble into micellar nano-architecture in an aqueous medium as evident by TEM, DLS, and AFM. Self-assembly behavior of these hybrid rod-coil macromolecules is interesting due to the presence of the more dynamic helical character of helical rod backbone and the presence of a high population of helical reversals. These defects induce the formation of the core of the micelles whereas random coil chains occupy in the corona. The polymer composition with high hydrophobic content shows low CMC values as well as high encapsulation efficiency towards hydrophobic drug, Doxorubicin. Fine tuning of nano-structure of brush co-polymers will be needed to enhance drug encapsulation efficiency and control, sustained release. Considering their CMC and self-assembly behavior to encapsulate hydrophobic cargoes, these types of polymer architecture possess potential as drug delivery vehicles and future work will focus on the fine tuning of macromolecular structure and its functions to achieve real-world applications.

4.5 Materials and method

2000 Da PEG, 15000 Da PNIPAM were purchased from Sigma-Aldrich and Doxorubicin was purchased from Fisher and used without further purification. ^{1}H NMR, ^{13}C NMR, and ^{31}P NMR

were recorded on Bruker Advance III^{TM} 500 MHz NMR spectrometer at room temperature Tapping-mode atomic force microscopy (AFM) was performed using a Nanoscope IV Multimode Veeco instrument, equipped with an E-type vertical engage scanner. All images were acquired at room temperature by using silicon cantilevers with nominal spring constant of 42 N/m and 320 kHz OTESPA tips purchased from Bruker. For all AFM analysis, the samples were drop casted on silicon wafers (Wafer world, diameter, d = 2.5 cm) spun at 1000 rpm for 30 s. All FTIR spectra were collected by using Thermo Scientific Nicolet380 TR-FTIR spectrometer. For dynamic light scattering (DLS) measurement, Malvern Zetasizer particle sizer Nano ZS model equipped with He-Ne laser source at 633 nm, Max 4 Mw was used. Transmission electron microscope (TEM) images were recorded on a Tecnai Spirit electron microscope operating at 200 kV (UT Southwestern Medical School). The carbon coated copper grid was used as a support and negative staining with 2% aqueous uranyl acetate was applied to the specimens. Size exclusion chromatography (SEC) was conducted on a Shimadzu Prominence Modular HPLC/GPC system with a refractive index (RI) detector to determine the molar masses of homo polymers and graft co-polymers.

4.5.1 Synthesis

Synthesis of (*N*-propargyl-*N*'-hexyl) urea

First, 15.9 mL (1.2 eq., 108.9 mmol) of hexyl isocyanate was placed in a round bottom flask which contained 200.0 mL of DCM and it was cooled in an ice bath. Then, 5.010 g (1 eq., 70.8 mmol) was added slowly and was stirred for 3 hours. The product was isolated by evaporating the solvent and was recrystallized from hot ethanol. Finally, the clean product was isolated by filtration and it was dried under vacuum for 2 days.

Yield = 15.20 g (93%, white crystals).

^{1}H NMR (500 MHz, $CDCl_3$, δ ppm): 6.10 (br, s, 1H, N-H), 5.85 (br, s, 1H. N-H), 3.93, 3.92 (d, 2H, CH_2-N-propargyl), 3.15 - 3.11 (m, 2H, N-CH_2), 2.15 (s, 1H, alkyne H) 1.47, 1.45, 1.44, 1.30, 1.29, 1.26 (m, overlapped, 8H, CH_2), 0.86, 0.85, 0.83 (t, 3H, CH_3).

^{13}C NMR (126 MHz, $CDCl_3$, δ ppm): 158.86 (C=O), 81.23 (terminal alkyne C), 70.50 (alkyne), 40.40 (CH_2 attached to alkyne C), 31.61, 30.27, 29.84, 26.66, 22.59 (CH_2 in hexyl chain), 14.01 (CH_3).

Synthesis of (*N*-propargyl-*N*'-hexyl)carbodiimide monomer

Dehydration of urea was carried out with 11. 580 g (1.25 eq., 27.4 mmol) of above isolated urea, 7.7 mL (2.5 eq., 54.9 mmol) of triethyl amine and 4.002 g (1 eq., 21.9 mmol) of PPh_3Br_2 in DCM under nitrogen. At the end of the reaction time, excess of hexane was added and the precipitate formed was filtered out. Then the filtrate was extracted with hexane and the monomer was isolated upon evaporation of solvents. Then the monomer was purified with SiO_2 column by using 1:3= EtOAc: hexane as an eluent.

Yield = 62% (2.341 g, colorless oily product).

^{1}H NMR (500 MHz, $CDCl_3$, δ ppm): 3.86 (s, 2 H, N-CH_2), 3.25, 3.24, 3.23 (t, 2H, N-CH_2) 2.37 - 2.35 (t, 2H, CH_2), 2.01 (s, 1H, terminal alkyne H), 1.61 - 1.22 (m, overlapped, 8H, CH_2), 0.88, 0.87, 0.85 (t, 3H, CH_3).

^{13}C NMR (126 MHz, $CDCl_3$, δ ppm): 158.44 (N=C=N, imine C), 80.94 (terminal alkyne C), 70.82 (alkyne C), 40.56, 31.57, 30.17, 30.01, 26.61, 22.59, 14.03 (alkane CH_2 and CH_3).

Synthesis of poly(*N*-propargyl-*N*'-hexyl) carbodiimide

The monomer:initiator ratio used here is 250:1.

Inside the glove box, 1.002 g (250 eq., 6.1 mmol) of carbodiimide monomer was placed in a small vial and diluted with 0.4 mL of $CHCl_3$. Then 11.1 mg (1 eq., 24.4 µmol) of (*S*)- BINOL-Ti(IV) initiator was added and was allowed to stir overnight. At the end of the reaction, the gelled product was dissolved in $CHCl_3$ and precipitated from MeOH and dried under vacuum.

Yield = 94 % (0.940 g, off-white solid, M_n = 8000 Da).

Synthesis of PNIPAM grafted polycarbodiimides

Copper-catalyzed azide-alkyne cycloaddition (CuAAc) was carried out to synthesize all brush co-polymers. Azide functionalized PNIPAM (M_n = 15000) and PEG (M_n = 2000 Da) with alkyne groups appended polycarbodiimides homopolymer (PC) were used in different proportions as mentioned.

20% PNIPAM-*graft*-PC, **P-1**

120.1 mg of PC (5 eq., 0.7 mmol), 16.0 mg of PNIPAM (1 eq., 0.2 mmol), 3.0 mg of copper(I)iodide (0.1 eq., 14.6 µmol) and 0.1 mL of DBU (4 eq., 0.6 mmol) were dissolved in anhydrous THF. It was placed in a 100 mL round bottom flask under nitrogen. The 'click' reaction was carried out at 40 ^{0}C for 18hr. At the end of the reaction time, the medium was concentrated by evaporation of THF and it was precipitated from cold methanol three times. The polymer was isolated and dried under vacuum.

Yield = 90% (122.1 mg, off white spongy polymer, M_n = 53000 Da).

^{1}H NMR (500 MHz, $CDCl_3$, δ ppm): 8.14 (s, triazole ring H), 5.39 (br, N-H from PNIPAM), 4.15 (br, Imine N-CH_2), 3.98 (br, CH from PNIPAM), 3.35 - 3.18 (br, amine N-CH_2 and

overlapped CH_2-O from RAFT agent), 2.49 (br, CH_2 from RAFT agent), 2.18 - 2.03 (br, remaning terminal alkane H), 1.62, 1.51, 1.27, 1.12 (overlapped, CH_2 from hexyl chains and isopropyl groups from PNIPAM), 0.86 (br, CH_3 from hexyl chains).

^{13}C NMR (126 MHz, $CDCl_3$, δ ppm): 174.82 (amide C=O), 151.30 (N=C, imine), 145.87 (C-N=N), 83.63, 80.55 (alkyne C), 72.05, 68.96 (alkene C=C), 49.12 (N-CH_2), 41.61 - 14.45 (alkane C).

50% PNIPAM-*graft*-PC, **P-2**

200.0 mg of PC (1 eq., 1.2 mmol), 69.2 mg of PNIPAM (0.5 eq., 0.6 mmol), 11.5 mg of copper(I) iodide (0.05 eq., 0.6 μmol) and 0.4 mL of DBU (2 eq., 2.4 mmol) were used.

Yield = 83% (224.0 mg, off white spongy polymer, M_n = 59000 Da).

^{1}H NMR (500 MHz, $CDCl_3$, δ ppm): 8.14 (s, triazole ring H), 5.27 (br, N-H from PNIPAM), 4.15 (br, Imine N-CH_2), 3.99 (br, CH from PNIPAM), 3.36 - 3.18 (br, amine N-CH_2 and overlapped CH_2-O from RAFT agent), 2.52 (br, CH_2 from RAFT agent), 2.19 - 2.04 (br, remaning terminal alkyne H), 1.52 - 0.87 (overlapped, CH_2 from hexyl chains and isopropyl groups from PNIPAM), 0.86 (br, CH_3 from hexyl chains).

^{13}C NMR (126 MHz, $CDCl_3$, δ ppm): 174.71 (amide C=O), 150.27 (N=C, imine), 146.73 (C=N imine), 80.14 - 69.06 (remaining alkyne and C=C in triazol ring), 49.26 (N-CH_2), 42.90, 41.73, 32.44, 31.68, 27.90, 22.73, 14.48 (alkanes).

50% PEG-*graft*-PC, **P-3**

300.0 mg of PC (1 eq., 1.8 mmol), 56.7 mg of PEG (0.5 eq., 0.9 mmol), 17.1 mg of copper(I) iodide (0.05 eq., 0.9 μmol) and 0.5 mL of DBU (2 eq., 7.3 mmol) were used.

Yield = 275.3 mg (77%, slightly brownish powder-like polymer, M_n = 49000 Da).

^{1}H NMR (500 MHz, $CDCl_3$, δ ppm): 8.13 (s, 1H, triazol H), 5.22, 4.12 (br, imine N-CH_2 next to alkyne) 3.61 (br, PEG CH_2-O), 3.47 - 3.41 (br, overlapped, O-CH_3) 2.50 (br, overlapped, remaining H from terminal alkyne), 2.18 - 2.05 (br, alkyne H terminal), 2.02, 1.60, 1.52, 1.26, 0.85 (br, CH_2 and CH_3 in hexyl chains).

^{13}C NMR (126 MHz, $CDCl_3$, δ ppm): 145.87 (imine, C=N), 70.54 (O-CH_2 from PEG), 48.82, 32.07, 31.31, 29.68, 27.61, 26.95, 14.16 (alkane CH_2 and CH_3).

70% PEG-*graft*-PC, **P-4**

300.1 mg of PC (1 eq., 1.8 mmol), 79.5 mg of PEG (0.7 eq., 1.3 mmol), 24.3 mg of copper(I) iodide (0.07 eq., 0.1 mmol) and 0.8 mL of DBU (2.8 eq., 5.1 mmol) were used.

Yield = 234.4 mg (62 %, slightly brownish powder-like polymer, M_n = 51000 Da).

^{1}H NMR (500 MHz, $CDCl_3$, δ ppm): 8.10 (s, 1H, triazol H), 5.21- 4.12(br, imine N-CH_2 next to alkyne), 3.86 - 3.16 41 (br, overlapped, O-CH_3 and N- CH_2 from polycarbodiimide), 2.47 - 2.16 (br, overlapped, remaining H from terminal alkyne), 1.49 - 0.82 (br, CH_2 and CH_3 in hexyl chains).

^{13}C NMR (126 MHz, $CDCl_3$, δ ppm): 145.89 (imine, C=N), 80.22, 72.32, (alkene and alkyne C) 70.75 (O-CH_2 from PEG), 68.99 (O-CH_3 from PEG), 49.05 (amine N-CH_2), 38.37, 36.10, 32.40, 31.34, 27.73, 22.73, 14.37 (alkanes, CH_2 and CH_3).

4.5.2 Characterizations

Preparation of Micelles

Micelles were prepared through nanoprecipitation method. 10 mg/mL polymer stock solution were prepared and 500 µL of polymer solutions were transferred into 5 mL of deionized water under sonication. It was allowed to stand for 1 hr at room temperature and then transferred to

snake skin dialysis tubing (MWCO 3500 Da). Then the sample was dialyzed against 2.0 L of deionized water for 48 hrs. The dialyzed solution was filtered by using 450 µm syringe filters. Then hydrodynamic radius was analyzed using DLS and morphological studies were carried out using AFM and TEM.

Determination of critical micelle concentration (CMC)

Series of concentration solutions were prepared for all four polymers as follows. $1\text{-}10^{-10}$ mg/mL for **P-1**,$1\text{-}10^{-8}$ mg/mL for **P-2**, $10^{-3}\text{-}10^{-8}$ mg/mL for **P-3** and $10^{-2}\text{-}10^{-10}$ mg/mL for **P-4**. Then $1.31 * 10^{-4}$ mg/mL stock solution of pyrene in THF was prepared and each polymer sample was mixed with 50 µL of pyrene. Then polymer/pyrene solution was transferred to 10 mL of deionized water. Then it was stirred slowly for overnight by allowing time to form micelles and evaporation of THF. Then the fluorescence intensity was measured at 390 emission wavelengths and the ration of pyrene excitation was taken at 337.5 nm and 334.5 nm. Then CMC was calculated for all four samples by plotting graphs of $I_{337.5}/I_{334.5}$ *vs* log of polymer concentration.

Preparation of DOX encapsulated micelles

DOX. HCL (1 eq.,) was neutralized with three triethylamine (3 eq.,) in DMSO. Then 0.5 mg/mL of the polymer solution in THF was prepared and the relevant amount of DOX was added to the polymer solution to maintain the DOX concentration as 0.05 mg/mL (Polymer:DOX = 10:1). Then it was allowed to stir for 1 hr and injected into 10 mL of DI water very slowly. Then it was allowed to stand for 6 hr to get stable micelles. Then it was transferred into dialyzed bag (MWCO 3500 Da) and immersed in 2 L of DI water beaker for 48 hr (the release media was removed after 24 hr and the fresh media was added). The amount of DOX released was

measured by using UV-Visible spectroscopy at 495 nm. The calibration plot for DOX was plotted against concentration series of DOX solutions.

Polymer degradation and drug release

DOX. HCL (1 eq.,) was neutralized with three triethylamine (3 eq.,) in DMSO. Then 0.5 mg/mL of the polymer solution in THF was prepared and the relevant amount of DOX was added to the polymer solution to maintain the DOX concentration as 0.05 mg/mL (Polymer:DOX = 10:1). Then it was allowed to stir for 1 hr and injected into 10 mL of DI water very slowly and stand for 6 hr to get stable micelles. After that, it was transferred into dialyzed bag (MWCO 3500 Da) and it was immersed in 2.0 L of DI water beaker for 48 hr (the release media was removed after 24 hr and the fresh media was added). Once the dialysis was completed, the 3 mL of micelle solution was mixed with 15 mL of pH = 3 solution and the absorbance was measured periodically at λ= 495 nm.

4.6 References

(1) Bury, K.; Neugebauer, D. Novel Self-Assembly Graft Copolymers as Carriers for Anti-Inflammatory Drug Delivery. *Int. J. Pharm.* **2014**, *460* (1–2), 150–157 DOI: http://dx.doi.org/10.1016/j.ijpharm.2013.10.051.

(2) Liu, K.; Pan, P.; Bao, Y. Synthesis, Micellization, and Thermally-Induced Macroscopic Micelle Aggregation of Poly(vinyl Chloride)-G-poly(N-Isopropylacrylamide) Amphiphilic Copolymer. *RSC Adv.* **2015**, *5* (115), 94582–94590 DOI: 10.1039/C5RA16726D.

(3) Ren, J. M.; Ishitake, K.; Satoh, K.; Blencowe, A.; Fu, Q.; Wong, E. H. H.; Kamigaito, M.; Qiao, G. G. Stereoregular High-Density Bottlebrush Polymer and Its Organic Nanocrystal Stereocomplex through Triple-Helix Formation. *Macromolecules* **2016**, *49* (3), 788–795 DOI: 10.1021/acs.macromol.5b02295.

(4) Liu, G.; Zhuang, W.; Chen, X.; Yin, A.; Nie, Y.; Wang, Y. Drug Carrier System Self-Assembled from Biomimetic Polyphosphorycholine and Biodegradable Polypeptide Based Diblock Copolymers. *Polymer (Guildf).* **2016**, *100*, 45–55 DOI: http://dx.doi.org/10.1016/j.polymer.2016.08.012.

(5) Liang, X.; Liu, F.; Kozlovskaya, V.; Palchak, Z.; Kharlampieva, E. Thermoresponsive Micelles from Double LCST-Poly(3-Methyl-N-Vinylcaprolactam) Block Copolymers for Cancer Therapy. *ACS Macro Lett.* **2015**, *4* (3), 308–311 DOI: 10.1021/mz500832a.

(6) Wilson, D. A.; Nolte, R. J. M.; van Hest, J. C. M. Autonomous Movement of Platinum-Loaded Stomatocytes. *Nat Chem* **2012**, *4* (4), 268–274.

(7) Lutz, J.-F.; Akdemir, Ö.; Hoth, A. Point by Point Comparison of Two Thermosensitive Polymers Exhibiting a Similar LCST: Is the Age of Poly(NIPAM) Over? *J. Am. Chem. Soc.* **2006**, *128* (40), 13046–13047 DOI: 10.1021/ja065324n.

(8) Deng, L.; Ren, J.; Li, J.; Leng, J.; Qu, Y.; Lin, C.; Shi, D. Magnetothermally Responsive Star-Block Copolymeric Micelles for Controlled Drug Delivery and Enhanced Thermo-Chemotherapy. *Nanoscale* **2015**, *7* (21), 9655–9663 DOI: 10.1039/C5NR00642B.

(9) Zhang, H.; Tong, X.; Zhao, Y. Diverse Thermoresponsive Behaviors of Uncharged UCST Block Copolymer Micelles in Physiological Medium. *Langmuir* **2014**, *30* (38), 11433–11441 DOI: 10.1021/la5026334.

(10) Mackiewicz, N.; Nicolas, J.; Handké, N.; Noiray, M.; Mougin, J.; Daveu, C.; Lakkireddy, H. R.; Bazile, D.; Couvreur, P. Precise Engineering of Multifunctional PEGylated Polyester Nanoparticles for Cancer Cell Targeting and Imaging. *Chem. Mater.* **2014**, *26* (5), 1834–1847 DOI: 10.1021/cm403822w.

(11) Kennemur, J. G.; Kilgore, C. A.; Novak, B. M. Adjusting Conformational Switching Behavior of Helical Polycarbodiimides through Substituent Induced Polarity Effects. *J. Polym. Sci. Part A Polym. Chem.* **2011**, *49* (3), 719–728 DOI: 10.1002/pola.24484.

(12) Merten, C.; Reuther, J. F.; DeSousa, J. D.; Novak, B. M. Identification of the Specific, Shutter-like Conformational Reorientation in a Chiroptical Switching Polycarbodiimide by VCD Spectroscopy. *Phys Chem Chem Phys* **2014**, *16* (23), 11456–11460 DOI: 10.1039/c4cp01226g.

(13) Kim, J.; Novak, B. M.; Waddon, A. J. Lyotropic Liquid Crystalline Properties of Poly(N,N‘-Di-N-Hexylguanidine). *Macromolecules* **2004**, *37* (4), 1660–1662 DOI: 10.1021/ma035135e.

(14) Reuther, J. F.; Siriwardane, D. A.; Campos, R.; Novak, B. M. Solvent Tunable Self-Assembly of Amphiphilic Rod-Coil Block Copolymers with Chiral, Helical Polycarbodiimide Segments: Polymeric Nanostructures with Variable Shapes and Sizes. *Macromolecules* **2015**, *48* (19), 6890–6899 DOI: 10.1021/acs.macromol.5b01564.

(15) Budhathoki-Uprety, J.; Peng, L.; Melander, C.; Novak, B. M. Synthesis of Guanidinium Functionalized Polycarbodiimides and Their Antibacterial Activities. *ACS Macro Lett.* **2012**, *1* (3), 370–374 DOI: 10.1021/mz200116k.

(16) Budhathoki-Uprety, J.; Novak, B. M. Synthesis of Alkyne-Functionalized Helical Polycarbodiimides and Their Ligation to Small Molecules Using "Click" and Sonogashira Reactions. *Macromolecules* **2011**, *44* (15), 5947–5954 DOI: 10.1021/ma200960e.

(17) Demirci, S.; Kinali-Demirci, S.; Caykara, T. Stimuli-Responsive Diblock Copolymer Brushes via Combination of "click Chemistry" and Living Radical Polymerization. *J. Polym. Sci. Part A Polym. Chem.* **2013**, *51* (12), 2677–2685 DOI: 10.1002/pola.26657.

(18) Lin, Y.-C.; Kuo, S.-W. Hierarchical Self-Assembly Structures of POSS-Containing Polypeptide Block Copolymers Synthesized Using a Combination of ATRP, ROP and Click Chemistry. *Polym. Chem.* **2012**, *3* (4), 882–891 DOI: 10.1039/C2PY00574C.

(19) Wang, S.; Cheng, Z.; Zhu, J.; Zhang, Z.; Zhu, X. Synthesis of Amphiphilic and Thermosensitive Graft Copolymers with Fluorescence P(St-Co-(P-CMS))-G-PNIPAAM by Combination of NMP and RAFT Methods. *J. Polym. Sci. Part A Polym. Chem.* **2007**, *45* (22), 5318–5328 DOI: 10.1002/pola.22277.

(20) Wu, D.; Song, X.; Tang, T.; Zhao, H. Macromolecular Brushes Synthesized by "grafting From" Approach Based on "click Chemistry" and RAFT Polymerization. *J. Polym. Sci. Part A Polym. Chem.* **2010**, *48* (2), 443–453 DOI: 10.1002/pola.23804.

(21) Goodwin, A.; Novak, B. M. Synthesis of New Rigid Rod Helical Polymers through the Living Polymerization of Carbodiimides Using Titanium(IV) Complexes. *Macromolecules* **1994**, *27* (19), 5520–5522 DOI: 10.1021/ma00097a037.

(22) Shibayama, K.; Seidel, S. W.; Novak, B. M. Living Polymerization of Carbodiimides Initiated by Copper(I) and Copper(II) Amidinate Complexes. *Macromolecules* **1997**, *30* (11), 3159–3163 DOI: 10.1021/ma961750p.

(23) Schatz, C.; Smith, E. G.; Armes, S. P.; Wanless, E. J. Reversible pH-Triggered Encapsulation and Release of Pyrene by Adsorbed Block Copolymer Micelles. *Langmuir* **2008**, *24* (15), 8325–8331 DOI: 10.1021/la801127r.

(24) Li, J.; Li, X.; Ni, X.; Wang, X.; Li, H.; Leong, K. W. Self-Assembled Supramolecular Hydrogels Formed by Biodegradable PEO–PHB–PEO Triblock Copolymers and α-Cyclodextrin for Controlled Drug Delivery. *Biomaterials* **2006**, *27* (22), 4132–4140 DOI: http://dx.doi.org/10.1016/j.biomaterials.2006.03.025.

(25) Adams, M. L.; Lavasanifar, A.; Kwon, G. S. Amphiphilic Block Copolymers for Drug Delivery. *J. Pharm. Sci.* **2003**, *92* (7), 1343–1355 DOI: 10.1002/jps.10397.

(26) Akimoto, J.; Nakayama, M.; Okano, T. Temperature-Responsive Polymeric Micelles for Optimizing Drug Targeting to Solid Tumors. *J. Control. Release* **2014**, *193*, 2–8 DOI: http://dx.doi.org/10.1016/j.jconrel.2014.06.062.

(27) Lavasanifar, A.; Samuel, J.; Kwon, G. S. Poly(ethylene Oxide)-Block-Poly(l-Amino Acid) Micelles for Drug Delivery. *Adv. Drug Deliv. Rev.* **2002**, *54* (2), 169–190 DOI: http://dx.doi.org/10.1016/S0169-409X(02)00015-7.

(28) Jenekhe, S. A.; Chen, X. L. Self-Assembly of Ordered Microporous Materials from Rod-Coil Block Copolymers. *Science (80-.).* **1999**, *283* (5400), 372 LP-375.

(29) Jenekhe, S. A.; Chen, X. L. Self-Assembled Aggregates of Rod-Coil Block Copolymers and Their Solubilization and Encapsulation of Fullerenes. *Science (80-.)* **1998**, *279* (5358), 1903 LP-1907.

CHAPTER 5

UV AND THERMO CONTROLLABLE AZOBENZENE-DECORATED POLYCARBODIIMIDE SWITCHES

Authors - Siriwardane, D.A.; Kulikov, O.V.; Batchelor, B.; Novak, B.M.

Department of Chemistry and Biochemistry, BE 26

The University of Texas at Dallas

800 West Campbell Road

Richardson, TX 75080-3021

Manuscript is in preparation for publishing in macromolecules journal.

5.1 Abstract

Molecular switches offer wide applicability in various areas through conformational changes which can be controlled over external stimuli. In this regard, azobenzenes are excellent candidates to contribute towards rational design of molecular switches as they may exist in a form of *cis* and *trans* isomer predominantly when UV irradiated at a specific wavelength. It is believed that exposure of polymer sample in solution to UV light may induce transformation of azobenzene scaffold into *cis* isomer that undergoes rearrangement to the respective *trans* form under visible light or heat. This attribute the changes in helical backbone through isomerization phenomena of azobenzene pendant groups as evident by specific optical rotation data (SOR). In the solid state, isomerization that induces reorganization of helical backbone is also confirmed by Fourier Transform Infrared Spectroscopy (FTIR) studies carried out by thermal annealing. Thin film AFM (Atomic Force Microscopy) measurement of the polymer showed surface smoothing through photomigration effect under sequential triggering event. The experimental data revealed that under photochemical stimuli (solution state) and thermal triggering condition (solid state), it causes the conformational changes of azobenzene groups appended to the helical backbone thus induces the changes in liquid crystalline phases as well as polymer topology changes in thin films. The changes in polymer crystallinity as well as thin film morphology also may occur through the changes in helical pitch of the backbone with respect to the isomerization process of azobenzenes. Thus, these conformational changes can be transformed into macroscopic changes in the properties of material. Overall, this type of UV responsive polymer architecture could be successfully used in targeted drug delivery, molecular sensors, the design of reconfigurable emulsions under external stimuli conditions.

5.2 Introduction

Synthesis of artificial helical systems became an emergent area of polymer chemistry due to their versatile applications as chiroptical switches,[1] reconfiguring emulsions,[2] optoelectronics,[3] drug delivery agents,[4] and fluorescence imaging in *vivo*.[5] The design of molecular switches showing bistability in response to the external stimuli such as solvent,[6] pH,[7] ions,[8] and temperature has been growing area of interest. The presence of two specific molecular conformations that can be precisely altered upon one another is an important strategy for the creation of molecular switches. By employing the bistability concept, various polymeric systems have been designed for a specific function. These systems capable of controlling a specific event selectively upon triggering with a light, pH, solvent and temperature, provide advantages over chiral separation,[9] polymeric liquid crystals,[10] and catalysis support.[11] With regard to helical polymers such as polycarbodiimides and polyisocyanates, the helical inversions, *e.g.*, between *P* and *M* helices,[12] helix-to-coil,[13] and coil-helix[14,15] transitions, helical expansion-contractions (helical breathing) would become a promising and practical area of research. We have extensively studied chiroptical switching behavior of polycarbodiimides capable of exhibiting conformational changes with respect to solvent and temperature. For instance, poly(*N*-naphthyl-*N*'-octadecylcarbodiimides) show temperature and solvent induced chiroptical switching behavior and these changes occur due to the reversible shutter-like reorientation of naphthalene scaffolds.[16] This unique reorientation causes polymer backbone to undergo changes in helical pitch as evident by VCD (Vibrational Circular Dichroism) and DFT calculations. Aforementioned results prompted us to investigate deeper how isomerization of azobenzene pendant groups photochemically and thermally influence the polymer helicity. It is noteworthy to

mention that azobenzene motifs have been conjugated with various types of molecules including virus based nano wires,[17] peptides,[18] proteins,[19] nucleic acids, and ion channels[8] for spatial and temporal control of various activities rely on conformational changes upon illumination of the azo chromophores. This concept is very interesting to regulate specific functions reversibly through illumination and removal of the trigger. For instance, Wooley and coworkers reported that control over α-helical conformation changes in peptides through photomodulation.[5] Importantly, they developed an elegant azobenzene based photo switches linked to peptides to regulate the affinity towards DNA binding *via* photoisomerization.

Here we report the synthesis and investigation of the chiroptical switching behavior of azobenzene decorated polycarbodiimide polymer. To design a novel type of photo-responsive, optically sensitive polycarbodiimides, we introduced an azobenzene moiety that can reversibly undergo a photo-induced isomerization between more stable *trans* form and its corresponding *cis* configuration to the helical polycarbodiimide scaffolds. The discovery of azobenzene systems as photoswitches is one of the milestones in photochemistry as it shows isomerization between *trans* and *cis* upon UV irradiation.[20-22] In this work, our specific goal was to understand the chiroptical switching behavior of polycarbodiimide backbone occurring through isomerization of azobenzene pendant scaffolds in poly(*N*-(1,2-diphenyldiazene)-*N*'-hexylcarbodiimide) of both *R*- and *S*-configurations. This investigation will direct us to discovery of macromolecular switches which show bistability between two conformations that can be interconverted one another upon external stimuli event.

5.3 Discussion

5.3.1 Incorporation of azobenzenes on helical polycarbodiimides

Incorporation of different functionalities (*i.e*., modifiable pendant groups) into helical backbone has become a powerful tool in the synthesis of functional polymers. These properties extensively depend on their microstructures thus enhancing the chemical diversity of polymeric architectures would lead for diverse applications. Inspired by stiff rod-like architecture, it assures the exposure of these modifiable groups, thus incorporation of various functionalities is guaranteed to create the novel chiral architectures in the macromolecular world.[23,24] Emphasizing our previous work, we have investigated the chiroptical switching behavior of polycarbodiimides which have been decorated with anthracene and naphthyl arene pendants in regioregular fashion to yield poly(*N*-anthracene-*N*'-octadecyl)carbodiimides (PAOD) and poly(*N*-naphthyl-*N*'-octadecyl)carbodiimides (PNOC) respectively.[16,25,1] The IR spectra of PNOC in various solvents show variations of two distinct imines stretching modes at 1621cm^{-1} and 1640 cm^{-1} and this provides the evidence for switching of helical backbone. As the specific optical rotation increases depending on the solvent employed, we observed variations in the intensity of these two modes and the same variations were detected upon changing the temperature of PNOC solutions in THF. This suggested that chiroptical switching process is caused by changes in populations of two distinct conformations.

In this work, we report the synthesis of polycarbodiimides which are decorated with azobenzene photochromic groups at imine positions. We have selected the azo derivatives which show *cis* and *trans* conformational changes upon irradiation.[26-28] These azobenzene derivatives appeared to be the promising candidates for molecular switches as the conformational changes are

reversible (**Figure 5.1**). To explore the feasibility of chiroptical switching behavior, azobenzene appended helical polycarbodiimides polymer has been synthesized by using chiral monomer of *N*-(1,2-diphenyldiazene)-*N*'-hexylcarbodiimide (**Schemes 5.1** and **5.2**). Through the reversible coordination-insertion polymerization mechanism with chiral (*R*)- and (*S*)-BINOL-Ti(IV) initiators, excess helical sense polymers were synthesized exhibiting SOR values at +290˚ for (*R*)- screw sense and -289˚ for (*S*)- screw sense of **P-1**, correspondingly.

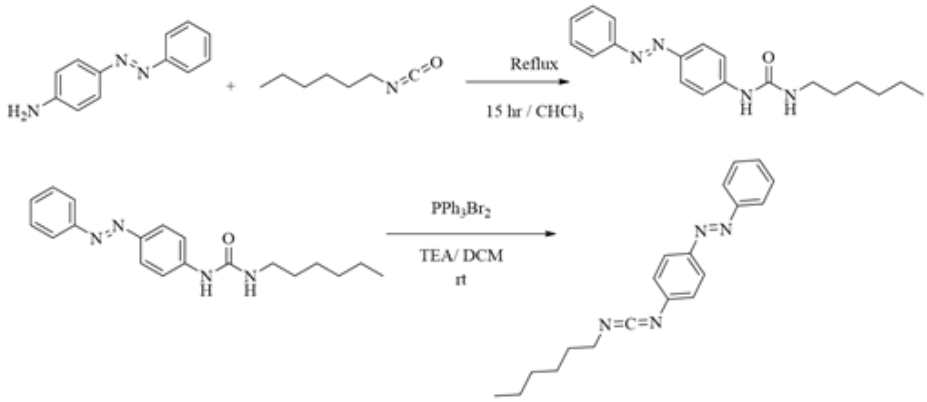

Scheme 5.1 Synthesis of urea and carbodiimide monomer.

We have also applied racemic (*RAC*)-BINOL-Ti(IV) initiator to synthesize azo-decorated polycarbodiimide and screw sense has been induced *via* sergeants-and-soldiers effect. To validate the screw sense, 10 mol % of the chiral stimulant of (*R*)-*N*-methyl-*N*'-phenethylcarbodiimide was utilized. During the polymerization, small chiral stimulant biased the helicity of polymer which was evident from vibrational circular dichroism (VCD) and SOR data. Owing +48˚ SOR for (*R*)-*N*-methyl-*N*'-phenethylcarbodiimide monomer, the final polymer after random co-polymerization possesses -78˚ SOR. It is conclusive that the polymer helicity is

governed by helical backbone.[29] To confirm that we also synthesized 50:50 helix sense selective random block co-polymer by using both **M-1** and **M-2** (**Scheme 5.2**).

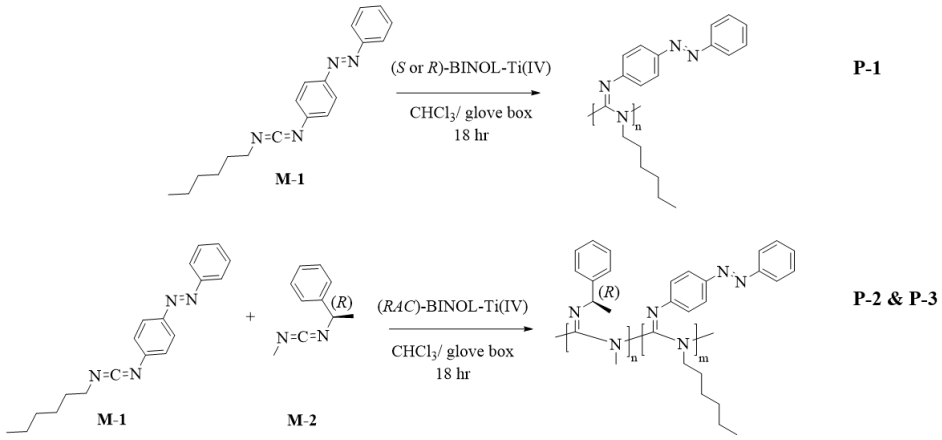

Polymer	n (mol%)	m (mol%)	Synthesis strategy
P-1	0	100	Screw-sense
P-2	90	10	'Sergeants and soldiers' effect
P-3	50	50	Random co-polymerization

Scheme 5.2 Synthesis of azobenzene-decorated polycarbodiimides.

5.3.2 Isomerization of azobenzene under UV illumination

First, we have irradiated the polymer solution with 365 nm UV light. The UV spectrum of azobenzene derivatives represents two characteristics absorption bands that correspond to π-π* and more intense band pertaining to n-π* transitions. We believe that the azobenzene scaffolds appendant to polymer backbone exist predominantly as *trans* isomers at the initial state.[30] Upon irradiation with 365 nm UV, 360 nm peak which was observed at room temperature was shifted to shorter wave length of 348 nm and the intensity has been decreased due to hypsochromic effect (blue shift) (**Figures 5.1-5.3**). The electronic n-π* transition is only allowed in *cis* isomers (forbidden for *trans* isomers) with a characteristic band at 448 nm indicative of the formation of *cis* isomer upon UV irradiation.

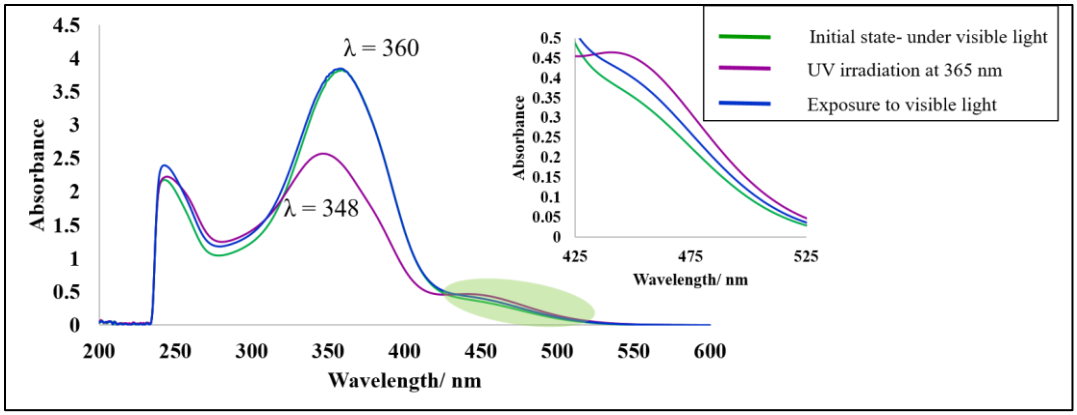

Figure 5.1 UV-Vis spectra for **P-1**: presence of UV trigger and removal of the UV source.

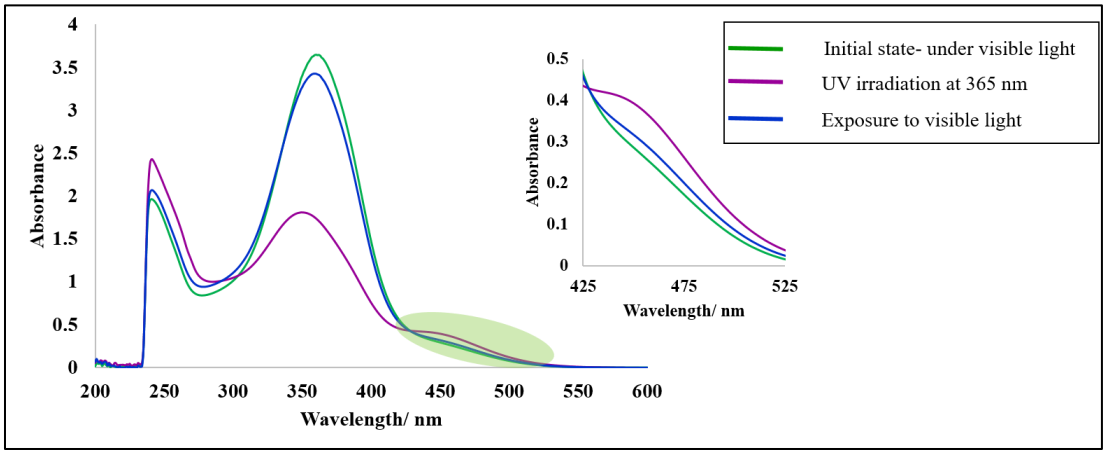

Figure 5.2 UV-Vis spectra for **P-2**: the presence of UV trigger and removal of the UV source.

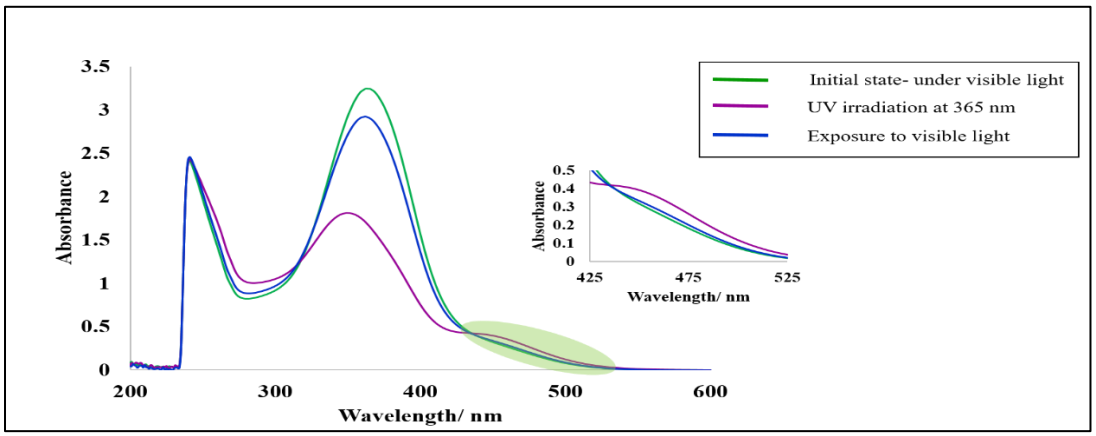

Figure 5.3 UV-Vis spectra for **P-3**: presence of UV trigger and removal of the UV source.

Photoisomerization can be induced upon elevating the isomers to electronically excited state and return to ground state through non-radiative decay. Although *trans-cis* isomerization of azo derivatives has been studied extensively, its exact pathway is still unclear and requires further clarification. In general, there is two proposed mechanisms: (i) bending of NNC bond *via* plane inversion, (ii) rotation by torsion of two benzene rings.[30,31] The energy of the incident radiation selectively determines the mechanism of photoisomerization. For the inversion mechanism, the excitation from ground state (S0) to first excited state (S1) is involved, whereas the major contributor to rotation mechanism is the excitation from second excited state (S2) (**Figure 5.4**).[31]

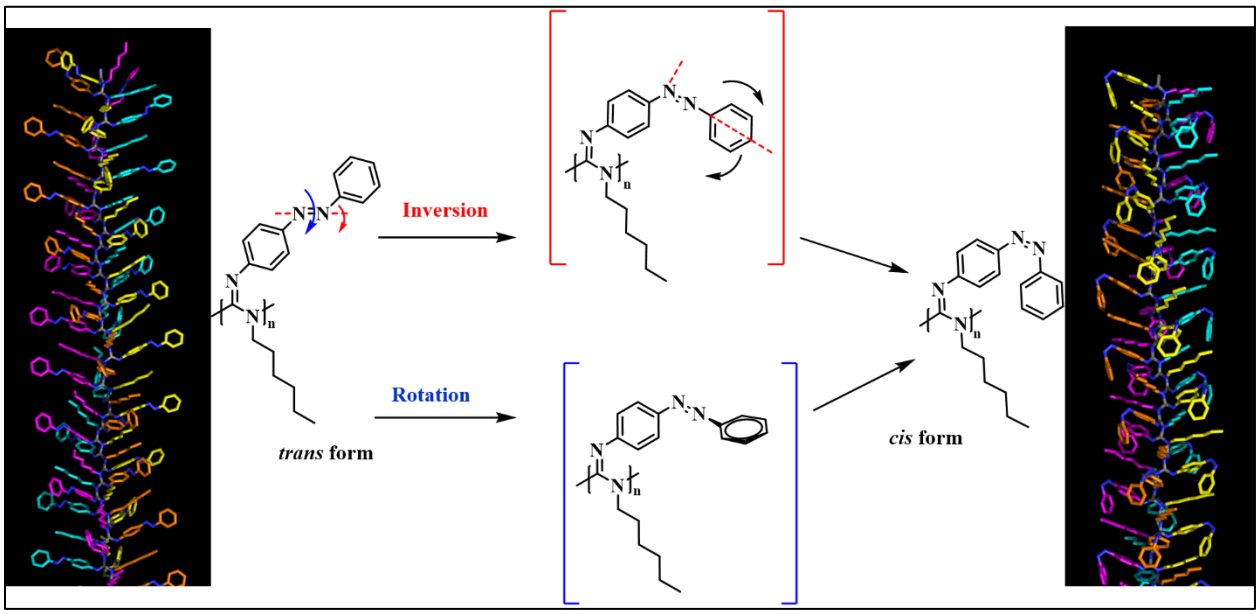

Figure 5.4 Proposed *trans-cis* isomerization mechanism for azobenzene-decorated polycarbodiimides.

To clarify the effect of azobenzene pending groups isomerization effect on polycarbodiimide backbone chirality, we have investigated the behavior of **P-1, P-2,** and **P-3** when exposed to UV-365 nm irradiation and then exposing the visible light.

5.3.3 Effect of isomerization on helical backbone

We have irradiated the polymer sample with 365 nm UV light and SOR was recorded at 5 min intervals for 1 hour. Interestingly, the SOR is almost linearly dependent on time and upon heating at 40 ˚C for 2 hr period, it returns to initial SOR value that is, in turn, UV-Vis data (**Figures 5.5** and **5.6**). Moreover, SOR is decreasing further to revert the starting point. In fact, the racemization process in polycarbodiimides is also possible upon heating, but for temperature as low as 40 ˚C, their change of SOR by 200˚ seems unlikely within 2 hr period. Thus, it is conclusive that the isomerization from *trans* to *cis* occurs under UV irradiation and these two configurations interact with polarized light in a different way. Thus, SOR data is changed. The very interesting phenomena associated with azopolymers is photo-induced mass movement. By applying this concept to these polymer systems, the change of azo-pendants configurations induces the spring-like contraction and expansion movement.[33] We believe that such UV triggered re-configurations generate photoisomerization force which can induce changes in the helical backbone. Stupp lab ascribed the change of the helical pitch of nanofibers exposed to UV light to isomerization process.[34] Through the isomerization process, *cis* configuration possesses less planarity than *trans* isomer, thus it increases sterically induced torque which leads to a low chiral pitch. Similarly, azobenzene decorated polycarbodiimide showed configurational changes under UV illumination thus, undergoing expansion-contraction motion of helical backbone (**Figure 5.7**). This bias the change of the helical pitch which is inferred from SOR data. The rate of change of SOR under UV irradiation was found to be three times higher than that of thermally annealed samples. These may be due to an interplay of energies associated with UV light compared to heating. However, the effect of isomerization phenomena of azobenzene pendant

groups appeared to be insufficient to change the helicity of the backbone (helical inversion) under UV illumination. Based on temperature annealing, solution UV- Vis studies, the isomerization does not occur, but absorbance at 360 nm has been increased with a temperature that is conclusive of π-π* transitions in *trans* isomers.

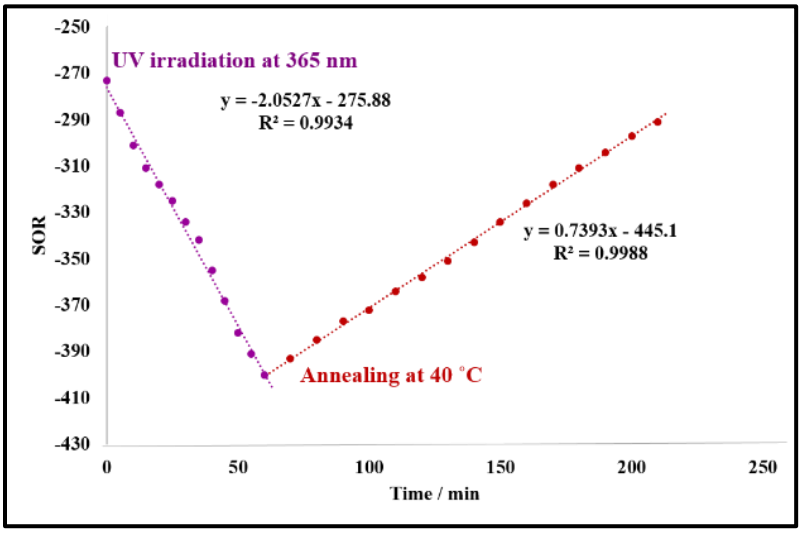

Figure 5.5 Change of SOR for (*S*)-**P-1** upon illumination under UV light and after removal of the trigger.

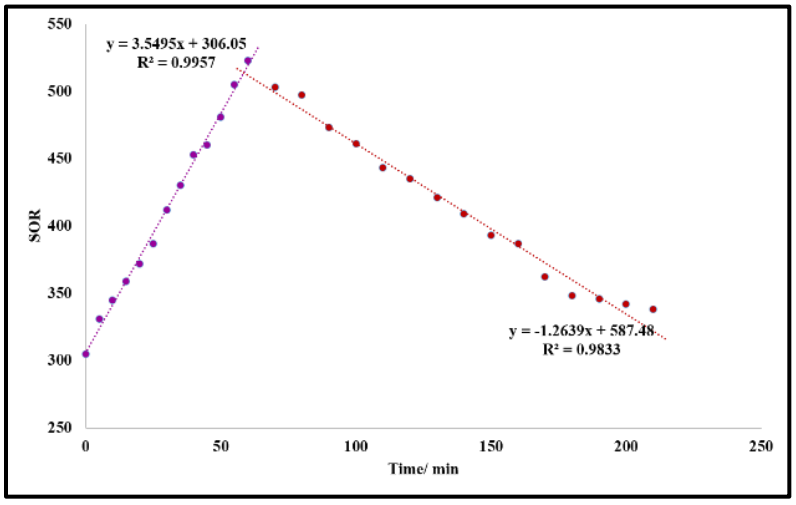

Figure 5.6 Change of SOR for (*R*)-**P-1** upon illumination under UV light and after removal of trigger.

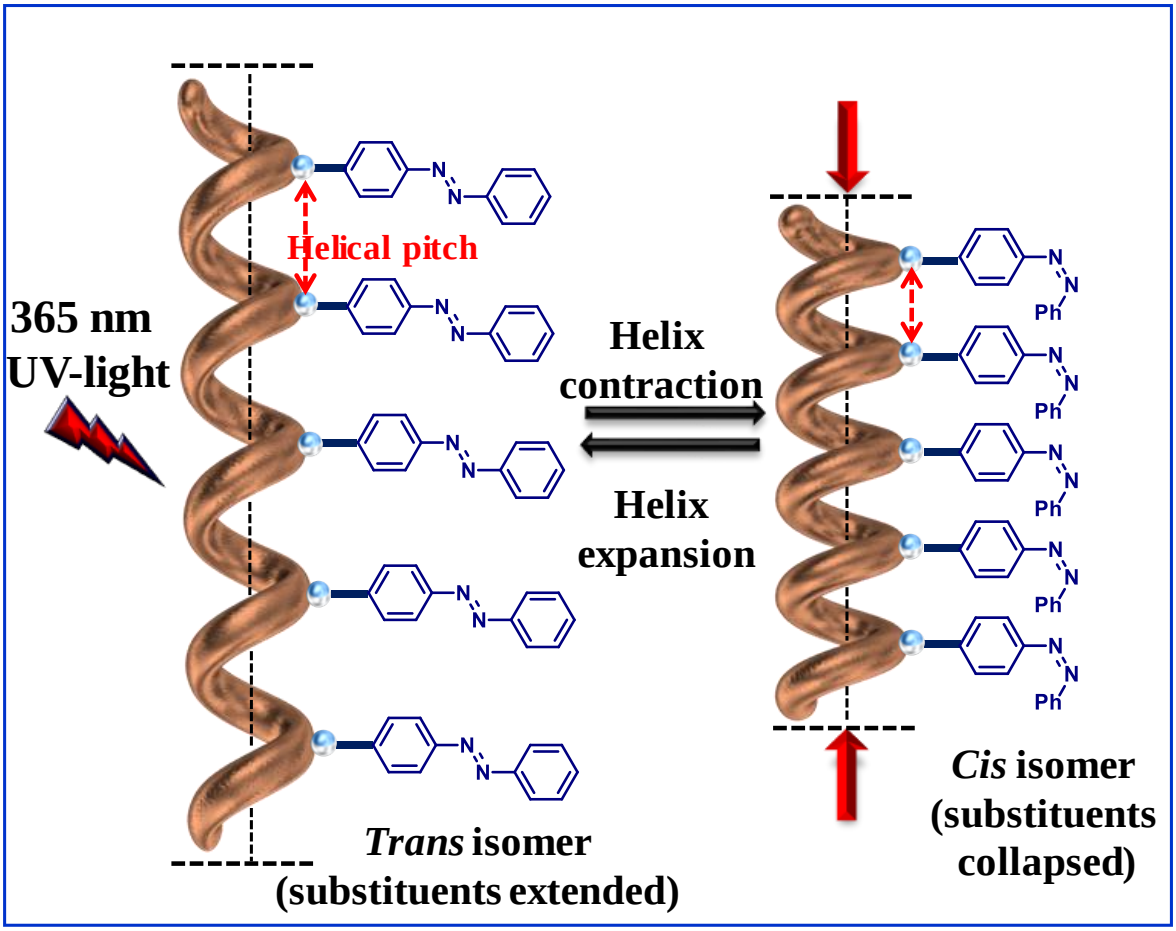

Figure 5.7 Cartoon featuring the change of helical pitch of the polymer with respect to isomerization process.

In the solid state, DSC studies were performed from -20 to160 ˚C temperature range showing no evidence for thermotropic behavior (**Figure 5.8**). Further, we have investigated changes at different temperatures in FTIR spectra upon thermal annealing and poly(*N*-phenyl-*N*'-hexylcarbodiimide was used as a control. The simultaneous changes in azo region (N=N and C-N stretches) and carbodiimide stretch (C=N) were observed with thermal annealing and we believed that changes in helical backbone takes place with annealing process.

5.3.4 Effect of thermal annealing

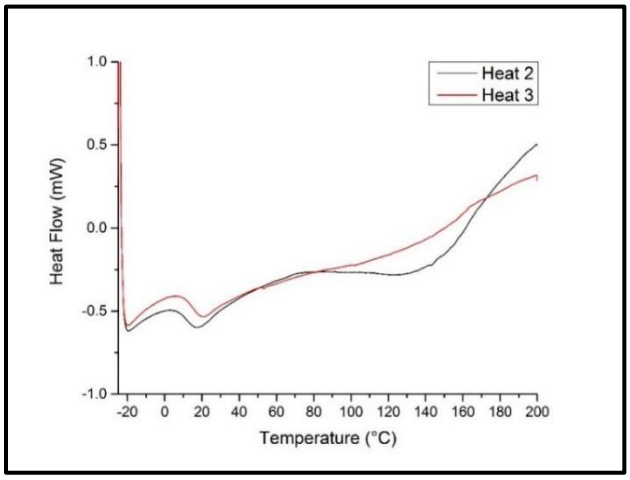

Figure 5.8 DSC thermogram for (***S*)-P-1**.

5.3.5 FTIR studies under thermal annealing

For this study, the polymer was melted by heating up to 160 ˚C, the FTIR spectra were recorded while cooling and second cycle of heating. Under thermal annealing condition, main changes in FTIR spectrum are associated with 1100-1250 cm^{-1} (C-N stretch), around 1400 cm^{-1}(N=N stretches), and 1620-1680 cm^{-1} which correspond to the imine (C=N stretches) (**Figures 5.9 - 5.12**). The peak at 1115 cm^{-1} was diminished and new peaks appeared at 1150 cm^{-1} and 1120 cm^{-1}. Also, the peak at 1250 cm^{-1} disappeared while appearing is the new peak at 1233 cm^{-1}. These changes are encountered for stretches in Aromatic C-N bond during the isomerization. This 1233 cm^{-1} peak may be attributed the C-N of *cis* isomer. FTIR spectra showed that the change of 1398 cm^{-1} peak into 1420 cm^{-1}. This peak may be corresponding to N=N (azo bond) bond and higher stretching frequency due to dipole moment generated in *cis* isomer. Interestingly, along with these changes, in imine region, the new peak appeared at 1678 cm^{-1} and 1638 cm^{-1}. In initial polymer 1626 cm^{-1} peak was observed and under the thermal condition as the temperature

increase the intensity of 1678 cm^{-1} is decreased while the intensity of 1636 cm^{-1} is increased. These changes may attribute transmute in the chiral pitch of the helical backbone. The same experiment was performed on poly(*N*-phenyl-*N*'-hexyl)carbodiimide and the FTIR spectra did not show any significant changes in imine region (**Figure 5.13**). Therefore, we believe that the reconfiguration of azo bond (N=N) appended on the helical backbone induces changes upon thermal annealing

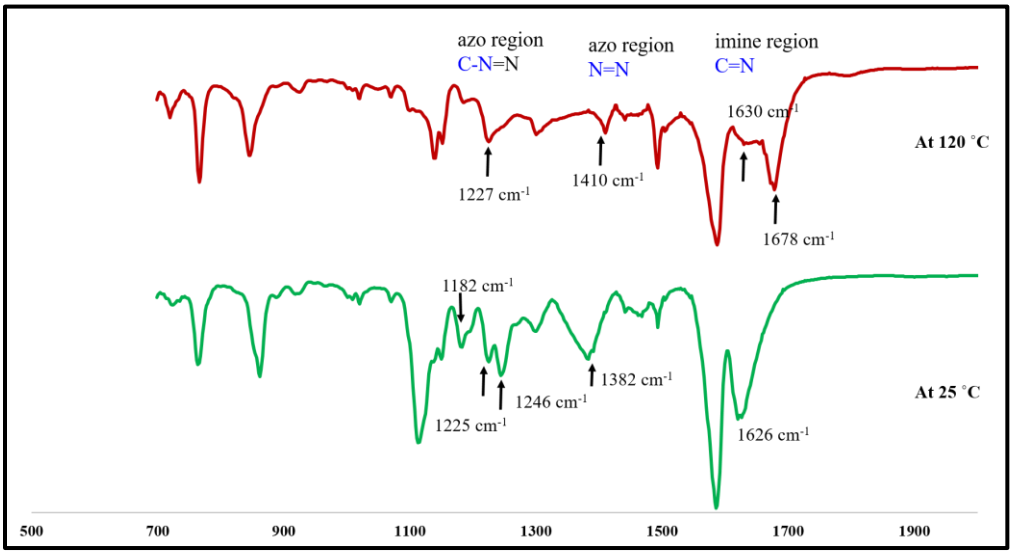

Figure 5.9 FTIR spectra for **(*S*)-P-1** at 25 ˚C and at 120 ˚ C under thermal annealing.

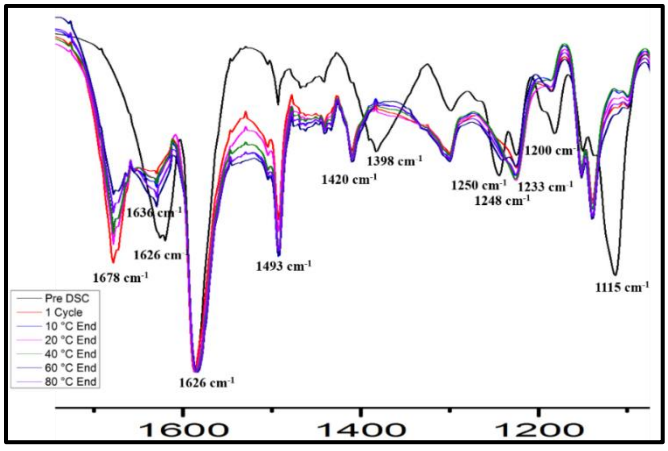

Figure 5.10 Overlay of FTIR spectra for **(*S*)-P-1** at different temperatures.

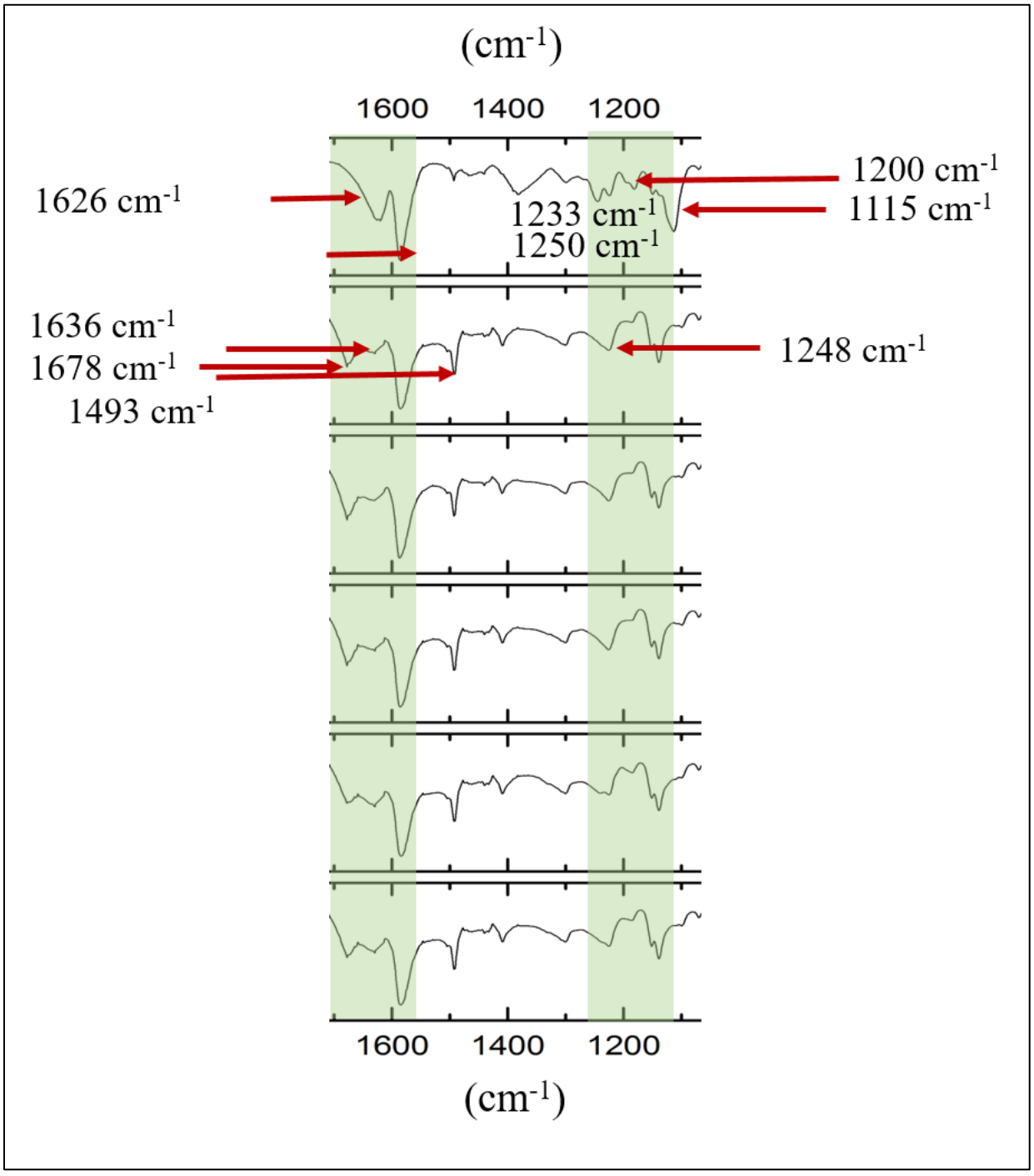

Figure 5.11 FTIR spectra displaying changes of peaks upon thermal annealing for **(*S*)-P--1**.

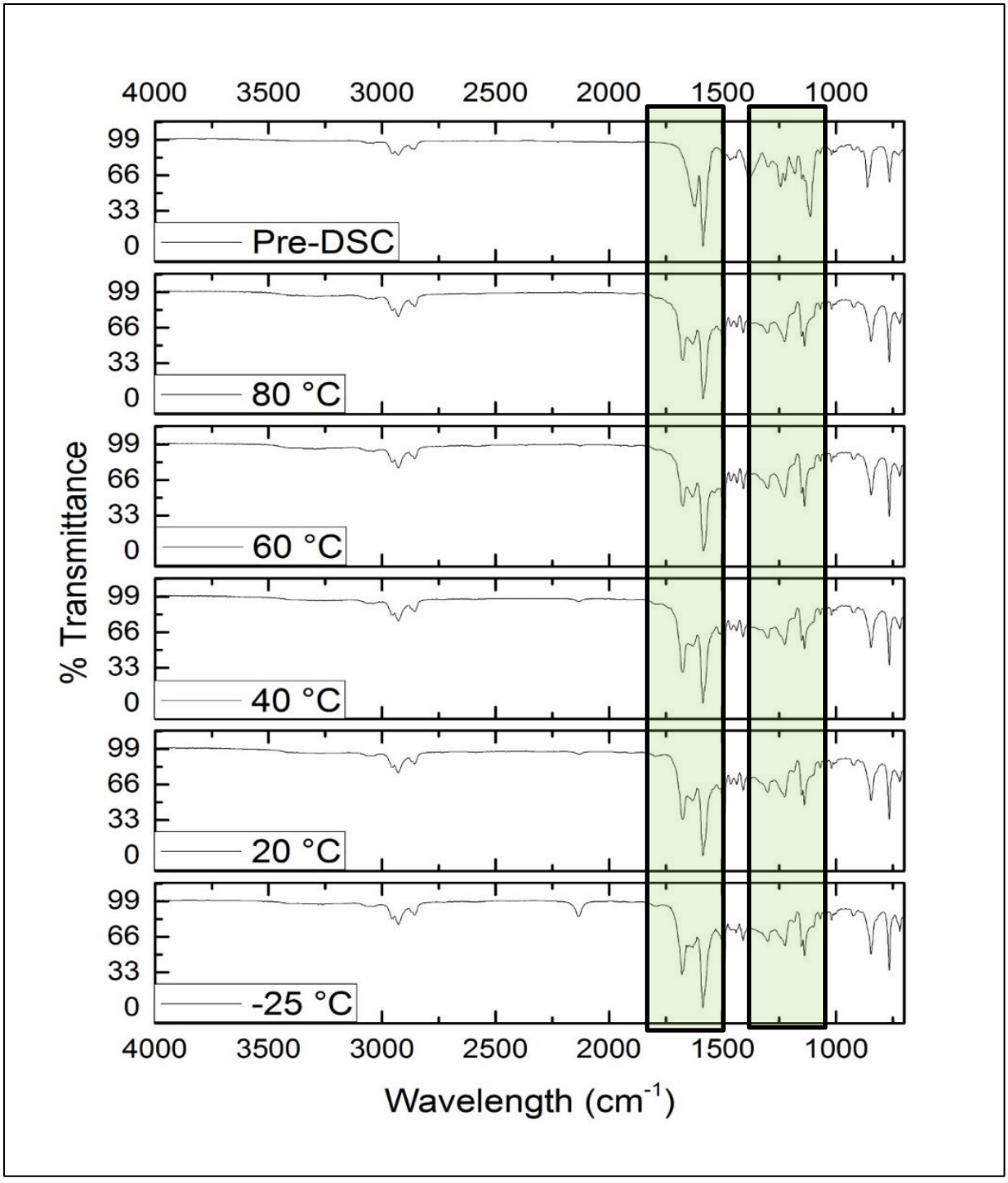

Figure 5.12 FTIR spectra displaying changes of peaks upon cooling for **(*S*)-P-1**: the highlighted areas indicate the changes in N=N, C-N bond stretches (around 1200 cm^{-1}) and imine stretch C=N (Around 1680-1700 cm^{-1}).

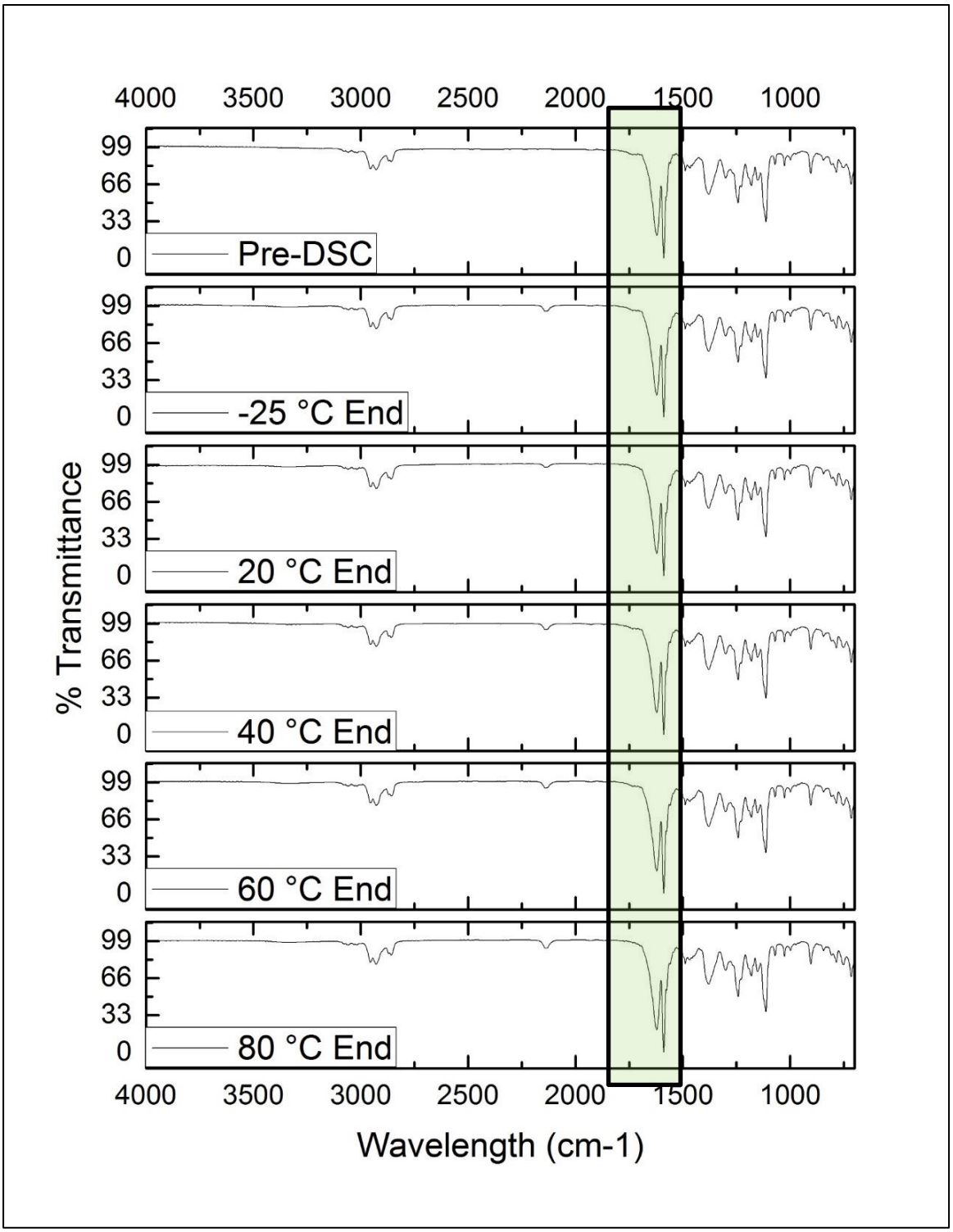

Figure 5.13 FTIR spectra displaying changes of peaks upon thermal annealing poly(*N*-phenyl-*N*'-octadecyl)carbodiimide.

We have evaluated the temperature dependence study of *p*-XRD experiment and data revealed that minor changes in *d*-spacing values. Mainly, we have noted that 6.52 Å has been shifted into 6.12 Å under thermal annealing. Also, the crystallinity of material has been increased and this can account for rearrangement of macromolecules due to melting (**Figures 5.14** and **5.15**).

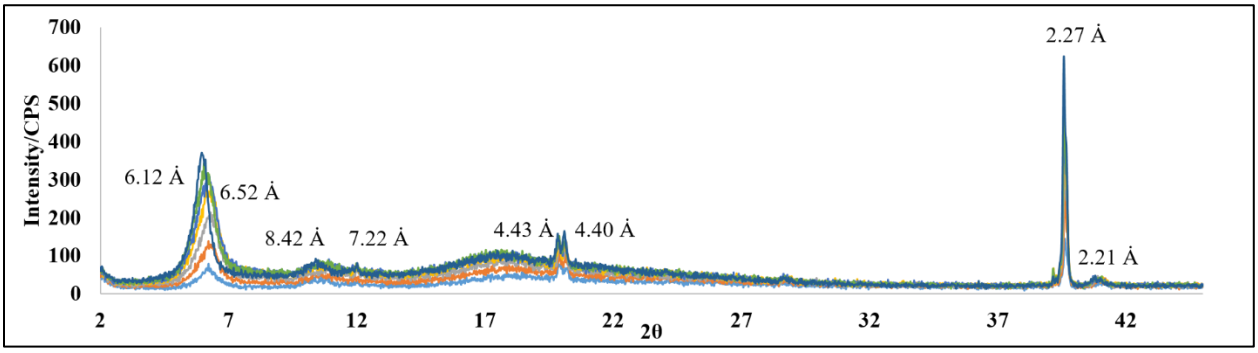

Figure 5.14 *p*-XRD profiles for **(*S*)-P-1** at a different temperature.

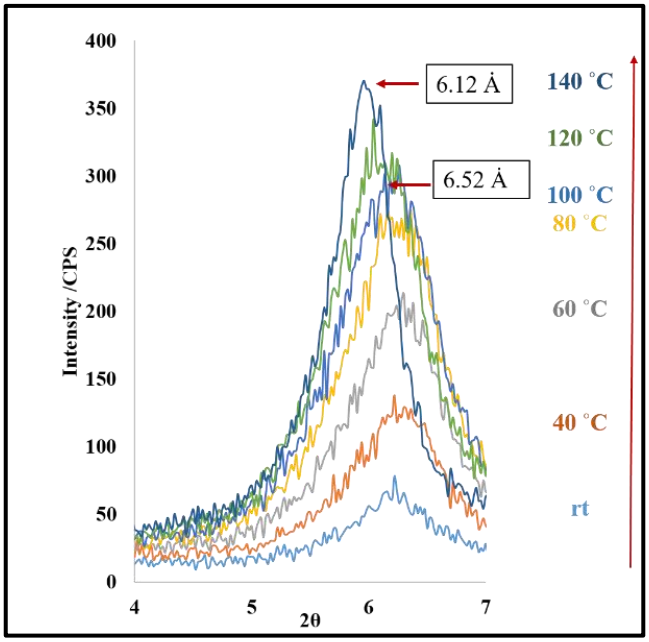

Figure 5.15 *p*-XRD spectrum for **P-1** under thermal annealing.

5.3.6 Polymer thin film topology studies by using TM-AFM

We have investigated polymer topology studies by using TM-AFM. In these thin films, we believed that photo-induced surface deformation occurs under UV triggering event. These photoinduced movements of azopolymers have been explained by various theories and models including diffusion model based on random walk motion,[35] thermo-diffusion model,[36] and fluid mechanics model are to name a few. Interestingly, reconfigurable azo-pendants behave as a molecular machine and polymer material mass migration is driven by the isomerization process of azobenzenes.[33] When the trigger, *i.e.*, UV light, is present, the spring-like or contraction-expansion motion of azo-pendants generate photoisomerization force and it leads to translational motion of polymer chains on the surface in any direction that was explained in the work of Ninzi who postulated worm-like motion concept.[35] These mass movement takes place due to sterically induced torque in *cis* configuration. We have investigated topology of polymer thin film both in $C_2H_2Cl_4$ and $CHCl_3$ solvents. We believed that these changes of polymer roughness occur due to the photomigration effect as shown in **Figures 5.16** and **5.17**. The surface smoothing effect has been taking place for both **P-1** and **P-2** and more isotropic shape of the *cis* configuration probably associated with this phenomena.[37] In **P-3** when casting from $C_2H_2Cl_4$, surface smoothing was not significant due to random co-polymer. When $CHCl_3$ was used, irregularly shaped aggregations were found for **P-3** under UV illumination and there are no significant changes in surface properties (**Figure 5.18**). This aggregation may arise due to presence of the second type of the monomer (**M-3**) in polymer structure and it may cause solubility issues. As a result, the polymer topologies arise from azobenzene pendants is not significant in **P-3**.

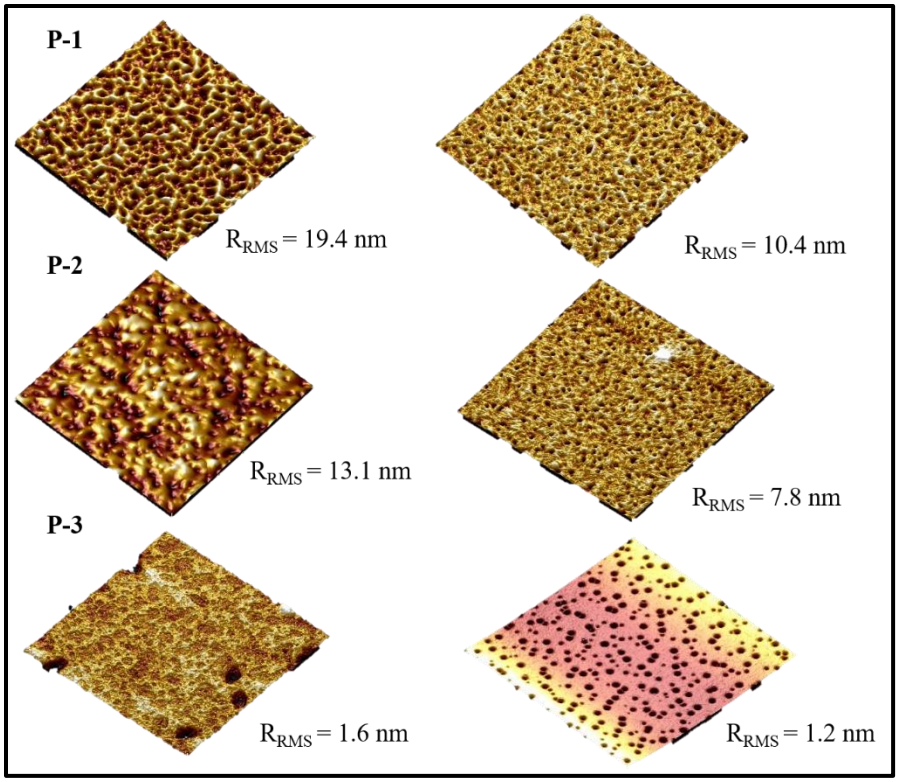

Figure 5.16 AFM images of azopolymers drop-cast from $C_2H_2Cl_4$ on silicon wafers, C = 2.0 mg/mL, 10 x10 µm size (surface roughness R_{RMS} is calculated as the root mean square of a surface).

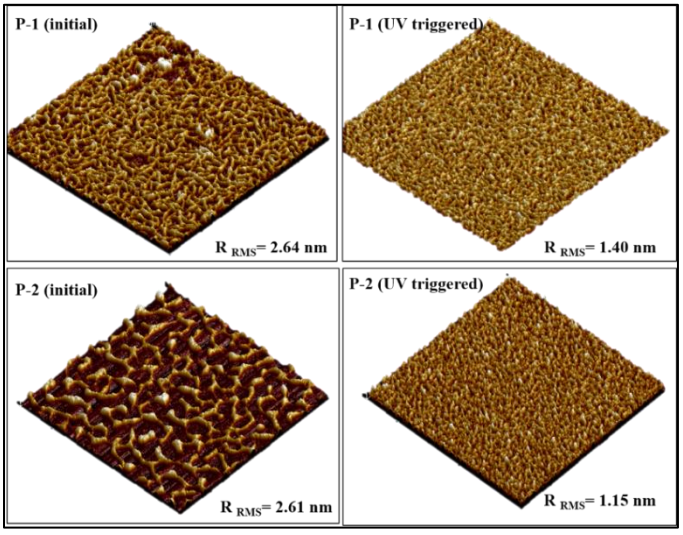

Figure 5.17 AFM images of azopolymers spin cast from $CHCl_3$ on silicon wafers, C = 0.25 mg/mL, 5x5 µm size.

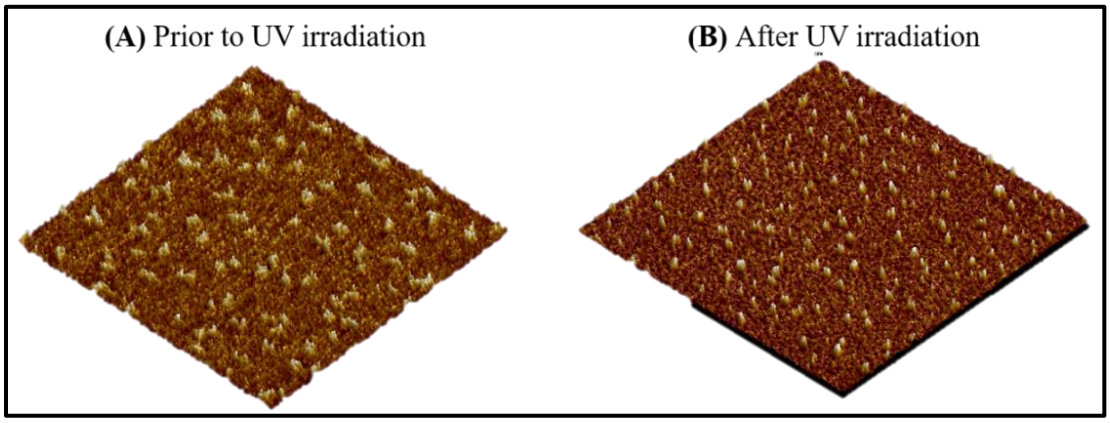

Figure 5.18 AFM images of azopolymer (***S***) **P-3** spin cast from $CHCl_3$ on silicon wafers, C = 0.25 mg/mL, 5x5 µm size.

5.3.7 Lyotropic liquid crystalline behavior

We were curious to observe liquid crystalline property of these three polymers. It is well documented that liquid crystalline behavior of azobenzene conjugated molecules.[38,39] These azobenzene derivatives undergo liquid crystalline phase transitions under triggering conditions.[10,40] *Trans* to *cis* isomerization of azobenzene compounds under UV illumination changes its configuration into bent shape and this non-mesogenic nature interrupts the liquid crystalline order.[10] Also, liquid crystalline materials can be doped with photoresponsive compounds and liquid crystalline phase transitions occur because of changes in helical pitch. This contributes to altering its chirality through the manipulation of cholesteric pitch.[41] By keeping mind these previously reported liquid crystalline behavior of azobenzene decorated materials., we have investigated liquid crystalline behavior (*S*) family of 12.3% (w/w) of **P-1**, **P-2**, and **P-3** in chloroform. We have observed that prior to UV illumination, all three polymers showed nematic liquid crystalline domains whereas the ordered liquid crystalline phase was disrupted upon triggering event (**Figure 5.18**). These changes occur due to formation of non-

mesogenic, bent shaped *cis* isomer under UV illumination.[10,22] The isomerization process of azobenzenes also can induce the changes in helical pitch and the change of the liquid crystalline phase is also possible due to change in helical backbone configuration.

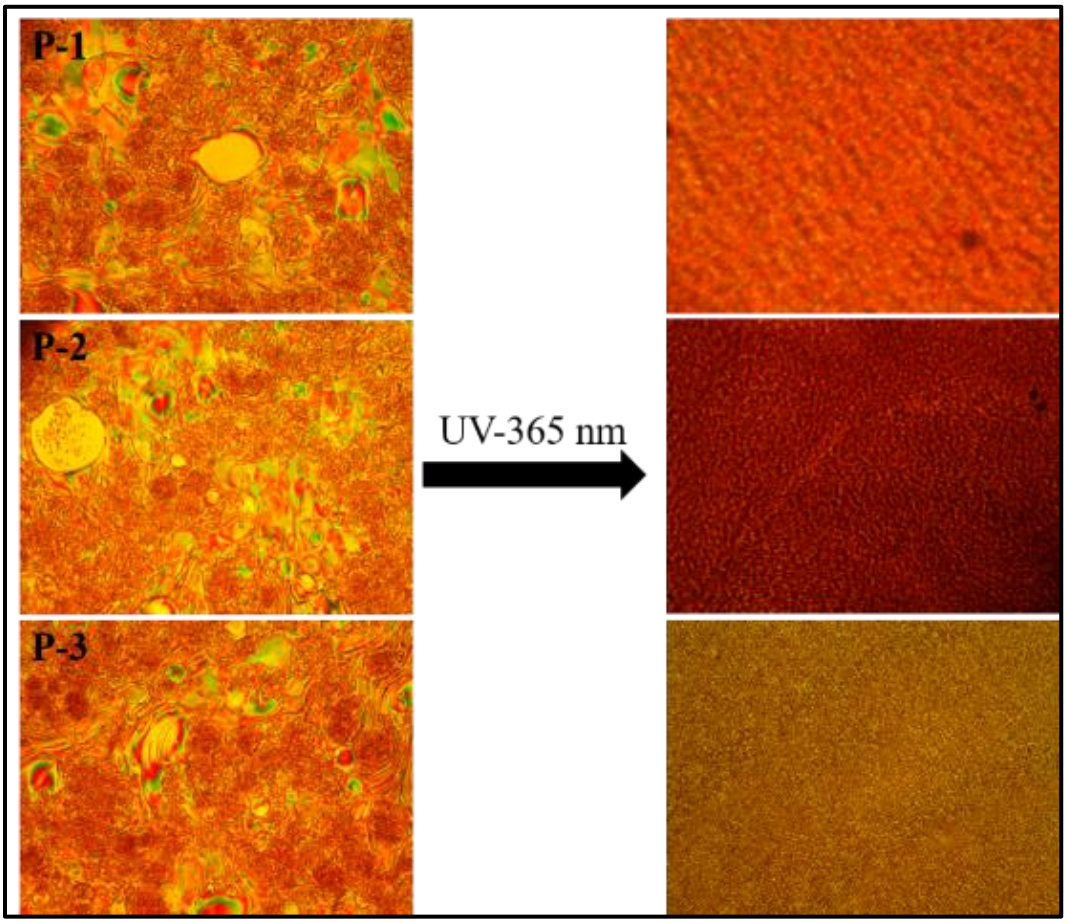

Figure 5.19 Polarized optical microscope images of azobenzene decorated polymers featuring change of liquid crystalline phases prior to and after UV illumination.

Further, we have mounted the polymer films on silicon wafer along with tetrachloroethane solvent and irradiate with UV light for 3 hours. The SEM imaging of such films showed that the surface smoothing has been taking place. The initial polymer adopts in to rough, fiber-like morphology (**Figure 5.20**).

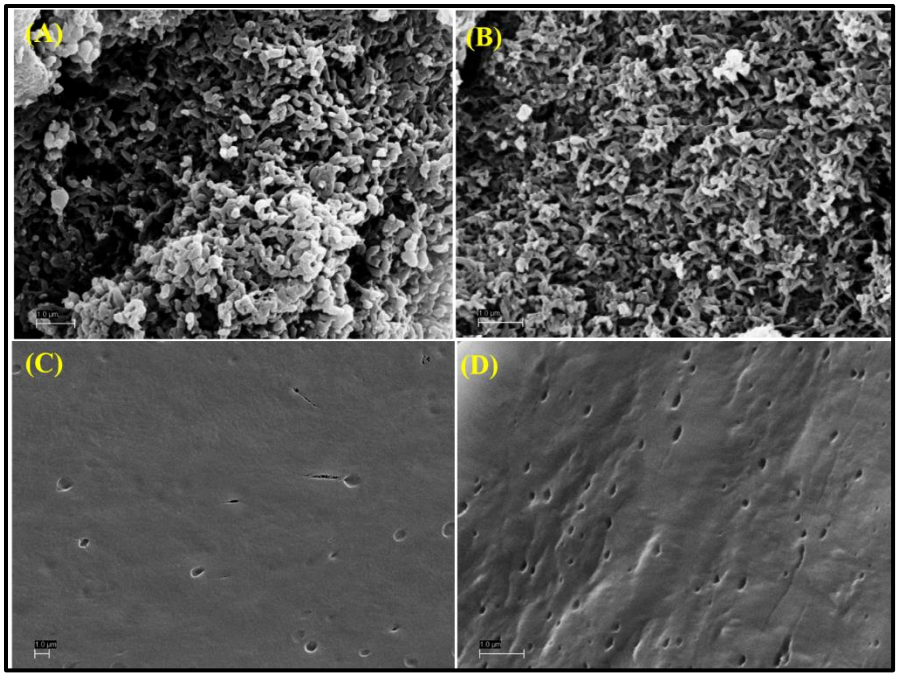

Figure 5.20 SEM images for (*S*)P-1 film mounted on silicon wafers; (A) and (B) before UV irradiation, (C) and (D) after UV irradiation).

5.4 Conclusions:

Azobenzene decorated polycarbodiimides polymers have been synthesized *via* screw sense polymerization with chiral BINOL initiators and chiral stimulant. The isomerization of azobenzene chromophore appended on the helical backbone is taking place under illumination with UV-365 nm light in solution. In the solid state, FTIR experiment revealed that changes in helical backbone occurred as a result of isomerization process upon thermal annealing at 120 C˚. Phenomenologically, we demonstrated for the first time that photoisomerization and closely related photomigration process of azobenzene-decorated polycarbodiimide scaffolds may change the thin film surface roughness and liquid crystallinity of polymeric material as evident by a combination of AFM, SEM, and POM techniques. This type of reconfigurable polymeric molecular switches can advance many areas of applied research, which may result in the

emergence of unique polymeric materials including chiral sensors, drug delivery systems, photovoltaics, and optical tweezers. Our future work focuses on the simulation studies to investigate the change of helical pitch.

5.5 Materials and methods

5.5.1 Instrumentation

^{1}H NMR, and ^{13}C NMR were recorded by using Bruker Advance III^{TM} 500 MHz NMR spectrometer at room temperature. Specific optical rotation (SOR) data were recorded on JASCO P-1010 polarimeter at λ= 585 nm and at sample concentration, 2.0 mg/mL by using 100 mm path length cell. Solution state vibrational circular dichroism spectra were obtained on Bio Tool Chiral-2X VCD spectrometer by dissolving samples in deuterated toluene (C = 25 mg/mL and l = 50 µm). Raguku Ultima III X-Ray diffractometer was used to record all *p*-XRD profiles on powder samples. Tapping mode atomic force microscopy (TM-AFM) was done by using Nanoscope IV Multimode Veeco instrument on silicon wafers (diameter, d = 2.5 cm, Wafer World). All imaging was performed at room temperature with silicon cantilever with a nominal constant of 42 N/m and 320 kHz OTESPA tip. Scanning electron microscopy imaging was done by using Zeiss Supra 40 instrument at UTD nano characterization facility. The samples were mounted on a silicon wafer and coated with conductive Pd/Au film. The potential applied to the inspection sample was 10 kV. Size exclusion chromatography (SEC) on a Viscotek VE 3580 system equipped with ViscoGel columns (GMHHR-M), connected to a refractive index detectors was used to determine the molar mass of all polymers.

5.5.2 Synthesis

Synthesis of *N*-(1,2-diphenyldiazene)-*N*'-hexylurea

First, 5.000 g (1 eq., 39.3 mmol) of hexylisocyanate was placed along with 150 mL of $CHCl_3$ in 250 mL round bottom flask and it was cooled down in an ice bath. Then, 7.751 g (1 eq., 39.3 mmol) of 4-aminoazobenzene was added dropwise while stirring and it was refluxed at 60 ˚C overnight. At the end of the reaction time, the solvent was evaporated and product was obtained as a red solid. It was recrystallized from hot ethanol and dried under vacuum overnight.

Yield = 10.320 g (81%, red needle-like short crystals).

^{1}H NMR (500 MHz, $CDCl_3$, δ ppm): 7.91-7.43 (overlapped multiplets, 9H, Ar-H), 6.57 (br, 1H, Ar-N-H), 4.80 (br, 1H, C-N-H), 3.30, 3.29, 3.27, 3.26 (q, 2H, N-CH_2), 1.57-1.25 (overlapped multiplet, 8H, alkane H), 0.90, 0.89, 0.87 (t, 3H, terminal CH_3).

^{13}C NMR (126 MHz, $CDCl_3$, δ ppm): 155.04 (C=O, amide carbonyl), 152.87 (C-N=N), 148.53 (C-N=N), 141.73 (C-NH), 130.73, 129.19, 124.39, 122.81, 119.81(Ar C=C), 40.76 (NH-CH_2), 31.65, 30.17, 26.72, 22.72 (hexyl chain CH_2), 14.17 (terminal CH_3).

Synthesis of *N*-(1,2-diphenyldiazene)-*N*'-hexylcarbodiimide monomer

13.031 g (1.25 eq., 30.8 mmol) of PPh_3 Br_2 was placed in cold DCM. Then 8.6 mL (2.5 eq., 61.6 mmol) of triethylamine was added dropwise under nitrogen. Then the mixture was allowed to stir for 10 min and 8.101 g (1 eq., 24.6 mmol) of urea was added slowly while stirring. After stirring for 1 hr at room temperature, the ice bath was removed and excess of hexanes was added. Precipitated solid was filtered and discarded. The monomer was extracted into hexanes and purified by SiO_2 column by using DCM as an eluent.

Yield = 6.32 g (86%, clear red oil).

^{1}H NMR (500 MHz, $CDCl_3$, δ ppm): 7.91 - 7.19 (overlapped multiplets, 9H, Ar-H), 3.48, 3.47, 3.46, (t, 2H, N-CH_2), 1.74 - 1.31(m, overlapped, 8 H, alkanes), 0.92, 0.90, 0.89 (t, 3H, CH_3).

^{13}C NMR (126 MHz, $CDCl_3$, δ ppm): 152.70 (C-N=N), 149.50 (N=C=N, carbodiimide), 144.11, 134.31, 130.77 (C-N), 129.08, 124.22, 124.02, 122.74, 120.16 (Ar C=C), 46.87 (N-CH_2), 31.27, 26.47, 22.55, 14.01 (C-H, alkanes).

Synthesis of poly(*N*-(1,2-diphenyldiazene)-*N*'-hexylcarbodiimide), **P-1**

To synthesize (*R*)- and (*S*)- polymers, (*R*)- BINOL-Ti(IV) and (*S*)-BINOL-Ti(IV) initiators were used, respectively. The monomer to initiator ratio was 250:1.

Inside the glovebox, 1.502 g (250 eq., 4.9 mmol) of monomer was placed in an oven dried sample vial along with 1.0 mL of $CHCl_3$. Then, 8.8 mg (1 eq., 19.6 μmol) (*S*)- and (*R*)- initiators were added separately and it was allowed to stir overnight. At the end of the reaction time, material from the vial was dissolved in $CHCl_3$ and precipitated from MeOH three times and then dried under vacuum for 2 days.

For (***S***)-**P-1**Yield = 1.101 g (73%), M_n = 21000 Da.

^{1}H NMR (500 MHz, $CDCl_3$, δ ppm): 7.71- 6.54 (br, Ar H), 3.59 - 2.63 (br, N-CH_2), 1.58 - 0.41 (br, alkanes).

^{13}C NMR (126 MHz, $CDCl_3$, δ ppm): 152.87 (C-N=N), 150.24 (C=N, imine), 148.45, 147.71, 130.25, 129.06 (C-N), 128.76, 123.93, 123.76, 122.53, 119.87 (Ar C=C), 47.40 (N-CH_2), 31.45, 29.64, 28.21, 26.15, 22.35, 13.62 (C-H, alkanes).

For (***R***)-**P-1**Yield = 1.321 g (88%), M_n = 22500 Da.

Synthesis of poly(*N*-(1,2-diphenyldiazene)-*N*'-hexylcarbodiimide)-*random*-poly(*N*-phenethyl-*N*'-methylcarbodiimide), **P-2**

Inside the glove box, 0.500 g (250 eq., 16.3 mmol) of *N*-(1,2-diphenyldiazene)-*N*'-hexylcarbodiimide and 26.1 mg (25 eq., 1.6 mmol) of *N*-phenethyl-*N*'-methylcarbodiimide monomers were placed along with 1.0 mL of $CHCl_3$. Then, 2.9 mg (1 eq., 6.5 µmol) of (*RAC*)-BINOL Ti-(IV) initiator was added and it was allowed to stir for 18 hr. At the end of the reaction time, the gelled polymer was dissolved in $CHCl_3$ and precipitated from MeOH three times. The product was dried under vacuum for 2 days.

Yield = 0.44 g (84%), M_n = 20300 Da.

^{1}H NMR (500 MHz, $CDCl_3$, δ ppm): 7.89, 7.76, 7.42, 7.26, 7.01, 6.86 (br, overlapped, Ar-H), 5.94, 5.39, 5.06 (br, methyn H from PPEMC), 3.69, 3.66 (br, amine N-CH_2), 3.27, 3.24 (br, N-CH_3), 2.67 (br, amine N-CH_2), 1.65, 1.30, 0.88, 0.74, 0.55, 0.47 (alkanes, CH_2 and CH_3).

^{13}C NMR (126 MHz, $CDCl_3$, δ ppm): 152.95 (C-N=N), 150.54, (imine, C=N) 148.41(imine, C=N), 130.77 - 119.58 (Ar C=C), 47.54 (methyn C, C-H), 32.15, 28.68, 27.04, 22.97, 14.17 (alkanes, CH_2 and CH_3).

Synthesis of poly(*N*-(1,2-diphenyldiazene)-*N*'-hexylcarbodiimide)-*random*-poly(*N*-phenethyl-*N*'-methyl)carbodiimide, **P-3**

Same procedure was carried out for **P-3** with 0.503 g (1 eq., 1.6 mmol) of *N*-(1,2-diphenyldiazene)-*N*'-hexylcarbodiimide, 0.261 g (1eq., 1.6 mmol) of *N*-phenethyl-*N'*-methylcarbodiimide and 23.1 mg of (*RAC*)-BINOL-Ti(IV) initiator.

Yield = 0.65 g (85%), M_n = 20150 Da.

^{1}H NMR (500 MHz, $CDCl_3$, δ ppm): 7.91, 7.90, 7.51, 7.47, 7.36 (br, overlapped, Ar- H), 4.98, 4.59 (br, methyn H, C-H), 3.25, 2.74 (br, overlapped, N-CH_3 and N-CH_2), 1.81, 1.64, 1.30, 0.90, 0.12 (br, overlapped, CH_2 and CH_3, alkanes).

^{13}C NMR (126 MHz, $CDCl_3$, δ ppm): 152.84 (C-N=N), 147.77 (imine C=N), 129.52, 128.78, 127.99, 126.21, 122.89, 122.50 (Ar C=C), 34.72 (amine N-CH_3), 31.46, 26.69, 22.24, 14.18 (alkanes, CH_2 and CH_3).

5.5.3 UV-Vis experiment

4.1 mg of (***S***)- **P-1**, **P-2**, and **P-3** were dissolved in 50.0 mL of $CHCl_3$. The UV-Vis spectra were recorded after 10 min of irradiation with UV-365 nm source.

5.5.4 SOR experiment

2.0 mg/mL solutions of both (***S***)- and (***R***)-**P-1** were prepared and SOR was measured at λ = 589 nm upon UV irradiation for 1 hour. Then, the samples were annealed at 40 ˚C and SOR was recorded until it showed the constant value.

5.5.5 TM-AFM imaging

4.0 mg/mL solutions were prepared for **P-1**, **P-2**, and **P-3** polymers in $C_2H_2Cl_4$ (1,1,2,2-tetrachloroethane) and two sets of samples were drop cast on silicon wafer separately. Then one set of samples was exposed to UV-365 nm radiation for 18 hr. Thin film morphology was studied by TM-AFM.

5.5.6 Solid state FTIR studies

For FTIR studies 10.0 mg of (***S***)-**P-1** was used**.** Differential scanning calorimetry (DSC) was performed on the Mettler Toledo DSC-1 using temperature range from -20 - 160 ˚C at a rate of 10 °C per minute and also, at -20 °C to 200 °C at a rate of 10 °C per minute, interrupting the run at multiple temperatures (*i.e*., -25 °C, 10 °C, 20 °C, 40 °C, 60 °C, and 80 °C). The samples were then immediately tested on the Shimadzu IRAffinity-1 Fourier Transform Infrared (FTIR) spectrometer using the Pike MIRacle attenuated total reflectance (ATR) attachment. Poly(*N*-phenyl-*N*'-hexylcarbodiimide) was used as control polymer.

5.6 References

(1) Kennemur, J. G.; Kilgore, C. A.; Novak, B. M. Adjusting Conformational Switching Behavior of Helical Polycarbodiimides through Substituent Induced Polarity Effects. *J. Polym. Sci. Part A Polym. Chem.* **2011**, *49* (3), 719–728 DOI: 10.1002/pola.24484.

(2) Zarzar, L. D.; Sresht, V.; Sletten, E. M.; Kalow, J. A.; Blankschtein, D.; Swager, T. M. Dynamically Reconfigurable Complex Emulsions via Tunable Interfacial Tensions. *Nature* **2015**, *518* (7540), 520–524 DOI: 10.1038/nature14168.

(3) Dinçalp, H.; Yavuz, S.; Haklı, Ö.; Zafer, C.; Özsoy, C.; Durucasu, İ.; İçli, S. Optical and Photovoltaic Properties of Salicylaldimine-Based Azo Ligands. *J. Photochem. Photobiol. A Chem.* **2010**, *210* (1), 8–16 DOI: http://dx.doi.org/10.1016/j.jphotochem.2009.12.012.

(4) Mooter, G. Van den; Maris, B.; Samyn, C.; Augustijns, P.; Kinget, R. Use of Azo Polymers for Colon-Specific Drug Delivery. *J. Pharm. Sci.* **1997**, *86* (12), 1321–1327 DOI: 10.1021/js9702630.

(5) Beharry, A. A.; Wong, L.; Tropepe, V.; Woolley, G. A. Fluorescence Imaging of Azobenzene Photoswitching in Vivo. *Angew. Chemie - Int. Ed.* **2011**, *50* (6), 1325–1327 DOI: 10.1002/anie.201006506.

(6) Venkataramani, S. Magnetic Bistability of Molecules. *Science (80-.).* **2011**, *445* (January), 445–449 DOI: 10.1126/science.1201180.

(7) Wei, F.; Ye, S. Molecular-Level Insights into N − N π - Bond Rotation in the pH- Induced Interfacial Isomerization of 5 - Octadecyloxy-2- (2- Pyridylazo) Phenol Monolayer Investigated by Sum Frequency Generation Vibrational Spectroscopy. **2012**.

(8) Rananaware, A.; Samanta, M.; Bhosale, R. S.; Kobaisi, M. Al; Roy, B.; Bheemireddy, V.; Bhosale, S. V.; Bandyopadhyay, S.; Bhosale, S. V. Photomodulation of Fluoride Ion Binding through Anion-π Interactions Using a Photoswitchable Azobenzene System. *Sci. Rep.* **2016**, *6* (October 2015), 22928 DOI: 10.1038/srep22928.

(9) Vojtylová, T.; Niezgoda, I.; Galewski, Z.; Hamplová, V.; Sýkora, D. A New Approach to the Chiral Separation of Novel Diazenes. *J. Sep. Sci.* **2015**, *38* (24), 4211–4215 DOI: 10.1002/jssc.201500816.

(10) Kundu, S.; Kang, S.-W. Photo-Stimulated Phase and Anchoring Transitions of Chiral Azo-Dye Doped Nematic Liquid Crystals. *Opt. Express* **2013**, *21* (25), 31324–31329 DOI: 10.1364/OE.21.031324.

(11) Bergbreiter, D. E.; Osburn, P. L.; Li, C. Soluble Polymer-Supported Catalysts Containing Azo Dyes. *Org. Lett.* **2002**, *4* (5), 737–740 DOI: 10.1021/ol017198s.

(12) Maxein, G.; Zentel, R. Photochemical Inversion of the Helical Twist Sense in Chiral Polyisocyanates. *Macromol.* **1995**, *28*, 8438–8440 DOI: 10.1021/ma00128a068.

(13) Sahl, M.; Muth, S.; Branscheid, R.; Fischer, K.; Schmidt, M. Helix–Coil Transition in Cylindrical Brush Polymers with Poly-L-Lysine Side Chains. *Macromolecules* **2012**, *45* (12), 5167–5175 DOI: 10.1021/ma300377v.

(14) Ciardelli, F.; Fabbri, D.; Pieroni, O.; Fissi, A. Photomodulation of Polypeptide Conformation by Sunlight in Spiropyran-Containing poly(L-Glutamic Acid). *J. Am. Chem. Soc.* **1989**, *111* (9), 3470–3472 DOI: 10.1021/ja00191a076.

(15) Yu, Z.; Hecht, S. Remote Control over Folding by Light. *Chem. Commun.* **2016**, *52* (40), 6639–6653 DOI: 10.1039/C6CC01423B.

(16) Merten, C.; Reuther, J. F.; DeSousa, J. D.; Novak, B. M. Identification of the Specific, Shutter-like Conformational Reorientation in a Chiroptical Switching Polycarbodiimide by VCD Spectroscopy. *Phys Chem Chem Phys* **2014**, *16* (23), 11456–11460 DOI: 10.1039/c4cp01226g.

(17) Murugesan, M.; Abbineni, G.; Nimmo, S. L.; Cao, B.; Mao, C. Virus-Based Photo-Responsive Nanowires Formed By Linking Site-Directed Mutagenesis and Chemical Reaction. *Sci. Rep.* **2013**, *3*, 1820.

(18) Renner, C.; Moroder, L. Azobenzene as Conformational Switch in Model Peptides. *ChemBioChem* **2006**, *7* (6), 868–878 DOI: 10.1002/cbic.200500531.

(19) Mart, R. J.; Allemann, R. K. Azobenzene Photocontrol of Peptides and Proteins. *Chem. Commun.* **2016**, *52* (83), 12262–12277 DOI: 10.1039/C6CC04004G.

(20) Kumar, G. S.; Neckers, D. C. Photochemistry of Azobenzene-Containing Polymers. *Chem. Rev.* **1989**, *89* (8), 1915–1925 DOI: 10.1021/cr00098a012.

(21) Xia, X.; Yu, H.; Wang, L.; ul-Abdin, Z. Recent Progress in Ferrocene- and Azobenzene-Based Photoelectric Responsive Materials. *RSC Adv.* **2016**, *6* (107), 105296–105316 DOI: 10.1039/C6RA16201K.

(22) Wei, Y.; Tang, Q.; Gong, C.; Lam, M. H.-W. Review of the Recent Progress in Photoresponsive Molecularly Imprinted Polymers Containing Azobenzene Chromophores. *Anal. Chim. Acta* **2015**, *900*, 10–20 DOI: http://dx.doi.org/10.1016/j.aca.2015.10.022.

(23) Budhathoki-Uprety, J.; Novak, B. M. Synthesis of Alkyne-Functionalized Helical Polycarbodiimides and Their Ligation to Small Molecules Using "Click" and Sonogashira Reactions. *Macromolecules* **2011**, *44* (15), 5947–5954 DOI: 10.1021/ma200960e.

(24) Budhathoki-Uprety, J.; Peng, L.; Melander, C.; Novak, B. M. Synthesis of Guanidinium Functionalized Polycarbodiimides and Their Antibacterial Activities. *ACS Macro Lett.* **2012**, *1* (3), 370–374 DOI: 10.1021/mz200116k.

(25) Reuther, J. F.; Novak, B. M. Evidence of Entropy-Driven Bistability through 15N NMR Analysis of a Temperature- and Solvent-Induced, Chiroptical Switching Polycarbodiimide. *J. Am. Chem. Soc.* **2013**, *135* (51), 19292–19303 DOI: 10.1021/ja4098803.

(26) Ikeda, T. Photomodulation of Liquid Crystal Orientations for Photonic Applications. *J. Mater. Chem.* **2003**, *13* (9), 2037–2057 DOI: 10.1039/b306216n.

(27) Duan, J.; Wang, M.; Bian, H.; Zhou, Y.; Ma, J.; Liu, C.; Chen, D. Azobenzene Mesogen-Passivated Gold Nanoparticles: Controlled Preparation, Self-Organized Superstructures, Thermal Behavior and Photoisomerization. *Mater. Chem. Phys.* **2014**, *148* (3), 1013–1021 DOI: 10.1016/j.matchemphys.2014.09.012.

(28) Viswanathan, N. K.; Kim, D. Y.; Bian, S.; Williams, J.; Liu, W.; Li, L.; Samuelson, L.; Kumar, J.; Tripathy, S. K. Surface Relief Structures on Azo Polymer Films. *J. Mater. Chem.* **1999**, *9* (9), 1941–1955 DOI: 10.1039/a902424g.

(29) Siriwardane, D. A.; Kulikov, O.; Reuther, J. F.; Novak, B. M. Rigid, Helical Arm Stars through Living Nickel Polymerization of Carbodiimides. *Macromolecules* **2017** DOI: 10.1021/acs.macromol.6b02456.

(30) Ube, T.; Ikeda, T. Photomobile Polymer Materials with Crosslinked Liquid-Crystalline Structures: Molecular Design, Fabrication, and Functions. *Angew. Chemie Int. Ed.* **2014**, *53* (39), 10290–10299 DOI: 10.1002/anie.201400513.

(31) Merino, E.; Ribagorda, M. Control over Molecular Motion Using the Cis-Trans Photoisomerization of the Azo Group. *Beilstein J. Org. Chem.* **2012**, *8*, 1071–1090 DOI: 10.3762/bjoc.8.119.

(32) Garcia-amoro, J.; Martı, M.; Finkelmann, H.; Velasco, D. Kinetico-Mechanistic Study of the Thermal Cis-to-Trans Isomerization of 4 , 4 ′ -Dialkoxyazoderivatives in Nematic Liquid Crystals. *Society* **2010**, 1287–1293 DOI: 10.1021/jp909557h.

(33) Sekkat, Z. Optical Tweezing by Photomigration. *Appl. Opt.* **2016**, *55* (2), 259–268 DOI: 10.1364/AO.55.000259.

(34) Li, L.; Jiang, H.; Messmore, B. W.; Bull, S. R.; Stupp, S. I. A Torsional Strain Mechanism To Tune Pitch in Supramolecular Helices. *Angew. Chemie Int. Ed.* **2007**, *46* (31), 5873–5876 DOI: 10.1002/anie.200701328.

(35) Nunzi, P. L. and C. F. and J.-M. Anisotropy of the Photo-Induced Translation Diffusion of Azobenzene Dyes in Polymer Matrices. *Pure Appl. Opt. J. Eur. Opt. Soc. Part A* **1998**, *7* (1), 71.

(36) Voit, A.; Krekhov, A.; Enge, W.; Kramer, L.; Köhler, W. Thermal Patterning of a Critical Polymer Blend. *Phys. Rev. Lett.* **2005**, *94* (21), 214501.

(37) Cristofolini, L.; Fontana, M. P.; Berzina, T.; Konovalov, O. Molecular Relaxation and Microscopic Structure of Multilayers and Superlattices of a Photosensitive Liquid-Crystalline Polymer. *Phys. Rev. E* **2002**, *66* (4), 41801.

(38) Ichimura, K. Photoalignment of Liquid-Crystal Systems. *Chem. Rev.* **2000**, *100* (5), 1847–1874 DOI: 10.1021/cr980079e.

(39) Rahman, M. L.; Hegde, G.; Azazpour, M.; Yusoff, M. M.; Kumar, S. Synthesis and Characterization of Liquid Crystalline Azobenzene Chromophores with Fluorobenzene Terminal. *J. Fluor. Chem.* **2013**, *156*, 230–235 DOI: http://dx.doi.org/10.1016/j.jfluchem.2013.10.004.

(40) Wang, Y.; Li, Q. Light-Driven Chiral Molecular Switches or Motors in Liquid Crystals. *Adv. Mater.* **2012**, *24* (15), 1926–1945 DOI: 10.1002/adma.201200241.

(41) Aßhoff, S. J.; Iamsaard, S.; Bosco, A.; Cornelissen, J. J. L. M.; Feringa, B. L.; Katsonis, N. Time-Programmed Helix Inversion in Phototunable Liquid Crystals. *Chem. Commun.* **2013**, *49* (39), 4256–4258 DOI: 10.1039/C2CC37161H.

CHAPTER 6

MISCELLANEOUS STUDIES

6.1 Introduction

The versatility of polycarbodiimide architectures expands continuously through amplifying chiral structural control and achieving greater chemical functionality.[1] These modifications emerge as a powerful tool to access diverse nano-structures for various applications including controlled drug delivery vehicles,[2] stimuli responsive materials[3] and self-assemblies.[4] In this regard, the development of new initiators bearing specific functionalities and post-polymerization modifications develop well-defined polymeric nano-structures including block co-polymers, graft co-polymers and multi-arm star polymers. This chapter summarizes the proposed methodologies to synthesize different polymer architectures.

6.2 Development of -OH functionalized Ni(II) initiator and synthesis of OH (hydroxyl) functionalized polycarbodiimides

In the presence of triphenylphosphine and specific aryl bromides, bis(1,5-cyclooctadiene) nickel (0), i.e., $Ni(COD)_2$, undergoes oxidative addition into the aryl bromide bond by forming a square-planar Ni(II) complex.[5] By using functionalized aryl bromides, the specific functional groups can be incorporated into the η_1-aryl ligand which acts as the necessary initiator ligand for the initiation of carbodiimide polymerizations. Helix-sense selective polymerization can be induced by utilizing chiral monomers with achiral initiators. For polycarbodiimide synthesis, chiral *N*-phenethyl-*N*'-methylcarbodiimide (PMC) monomers are prime candidates to achieve helix-sense selective polymerization due to the resulting polymers (PPMC; poly(*N*-phenethyl-*N'*-

methylcarbodiimide) possessing many interesting properties such as cholesteric liquid crystallinity, rigid-rod backbone structure, and enantiomerically pure helical secondary structure. To synthesize -OH functionalized polycarbodiimide homopolymer, a TMS protected -OH functionalized aryl ligand can be utilized. The Ni(II) center would provide polymerization initiating site for carbodiimide monomers and thus, the protected -OH group would be the end-functional group for the polycarbodiimide homopolymer. Upon deprotection of this terminal TMS, the -OH group would initiate the ring opening metathesis polymerization (ROMP) of lactides in the presence of catalytic amount of Zn^{+2} and the di-block co-polymer can be synthesized (**Scheme 6.3**).[6,7]

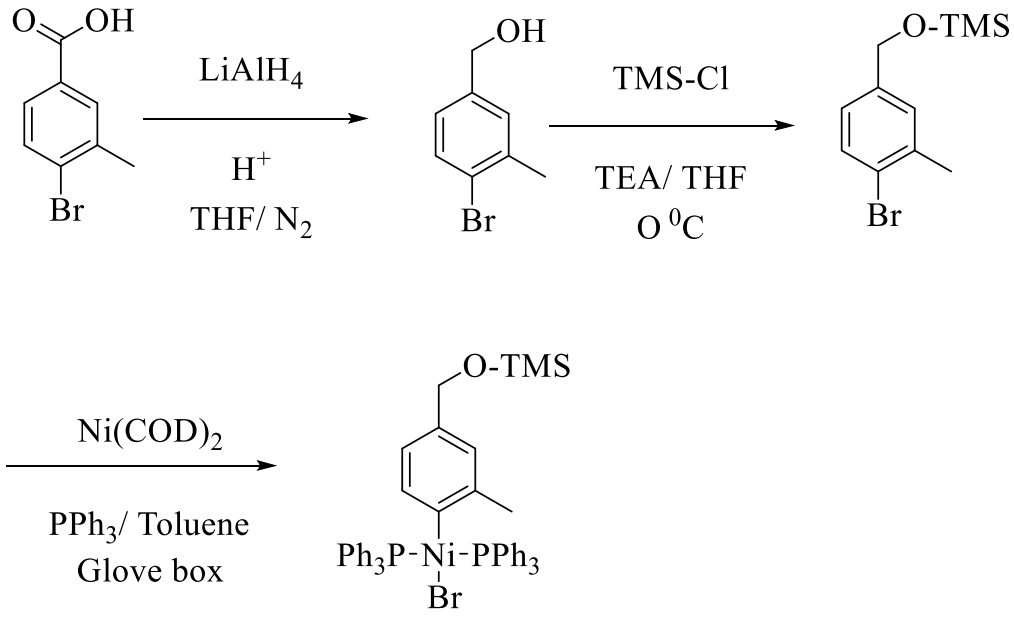

Scheme 6.1 Proposed reaction scheme for the synthesis of OH-functionalized Ni(II) initiator.

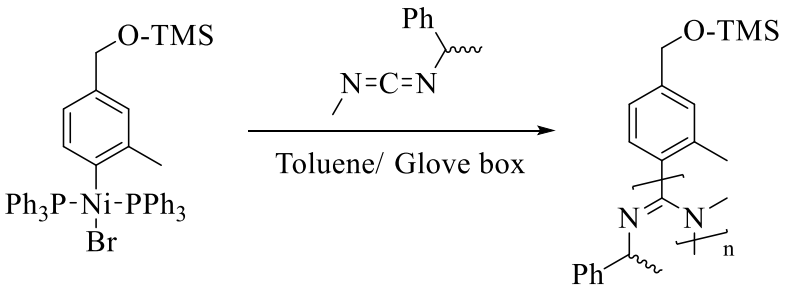

Scheme 6.2 Polymerization of PPMC monomer.

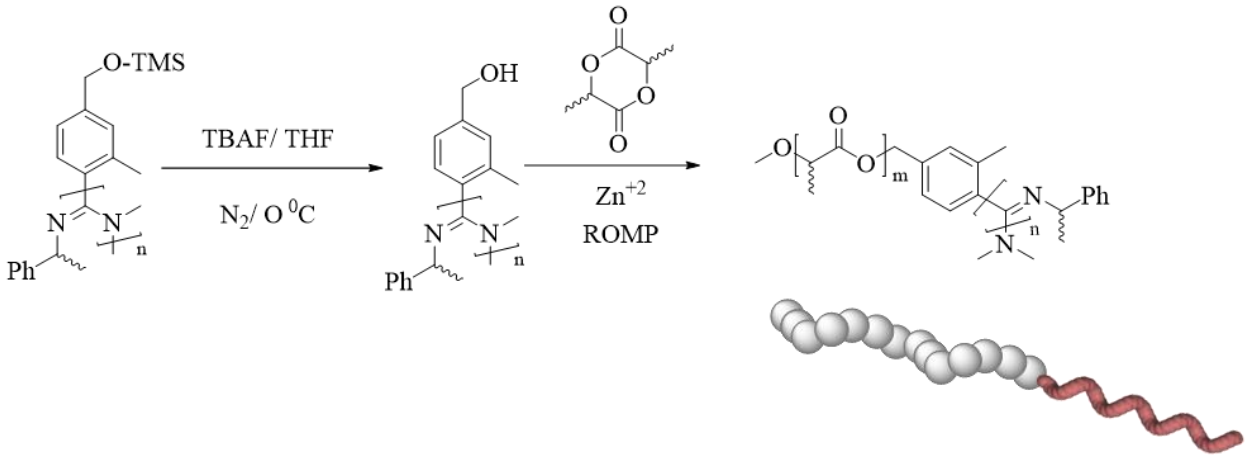

Scheme 6.3 Synthesis of diblock co-polymer.

6.3 Synthesis of graft co-polymers by using 'graft-from' strategy

Novel initiator system has been designed by using 5-Norbornene-2-methanol and 4-bromo-3-methylbenzoic acid through Steglich esterification reaction.[8] This ester derivative can be utilized to synthesize the Ni(II) initiator, which is a viable catalyst for carbodiimide polymerizations (**Scheme 6.4**). The oxidative addition of this aryl compound into $Ni(COD)_2$ would yield square planar complex and the Ni(II) center acts as an initiating site for polymerization. Each polymer chain bears norbornene terminal and in the presence of catalytic amount of Ru based initiators (Grubb's initiators), ring opening metathesis polymerization (ROMP) of norbornene can be conducted (**Scheme 6.6**).[9-11] This would yield the graft co-polymer and this polymer architecture

imparts intriguing properties including liquid crystallinity and self-assembly behavior not shown by linear polymer architectures.

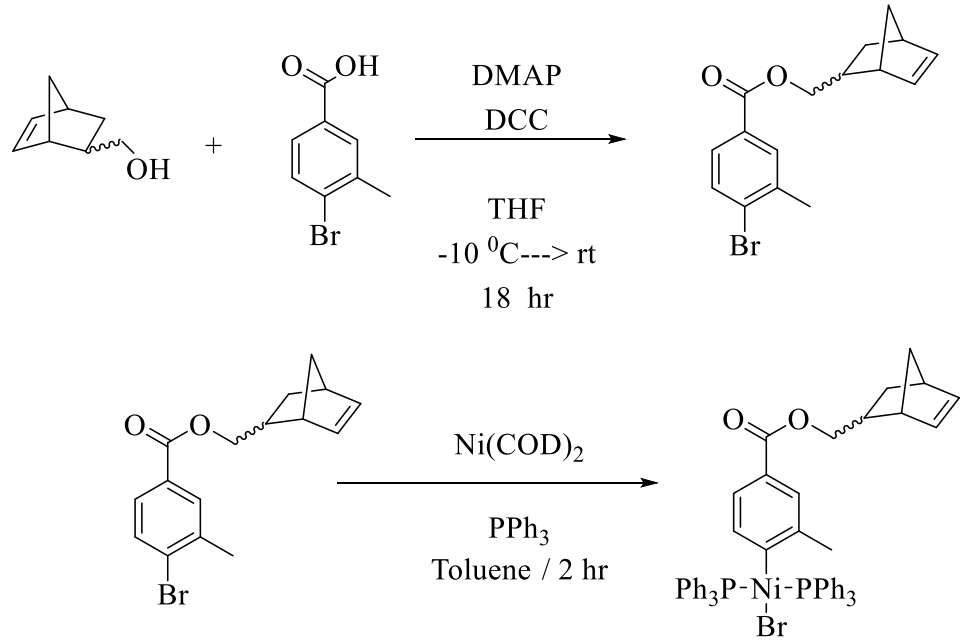

Scheme 6.4 Proposed synthesis route for Norbornene-based Ni(II) initiator.

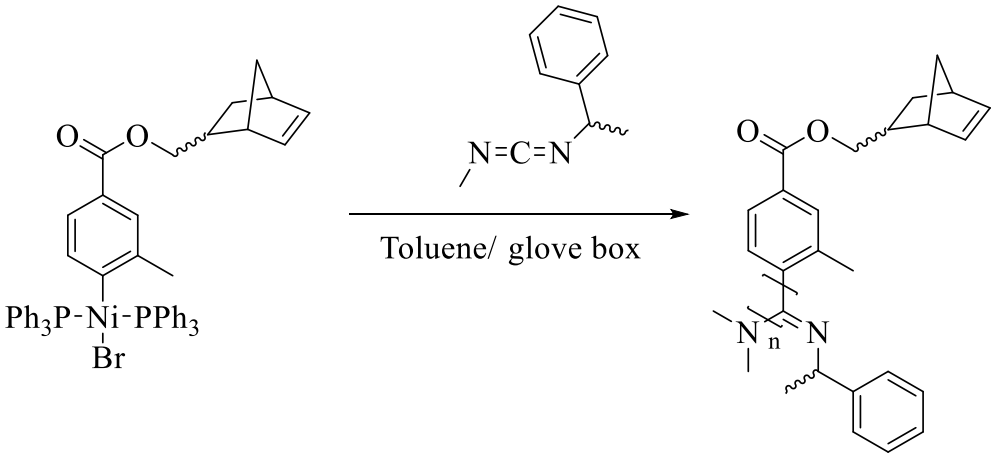

Scheme 6.5 Proposed synthesis route for the polymerization of carbodiimides.

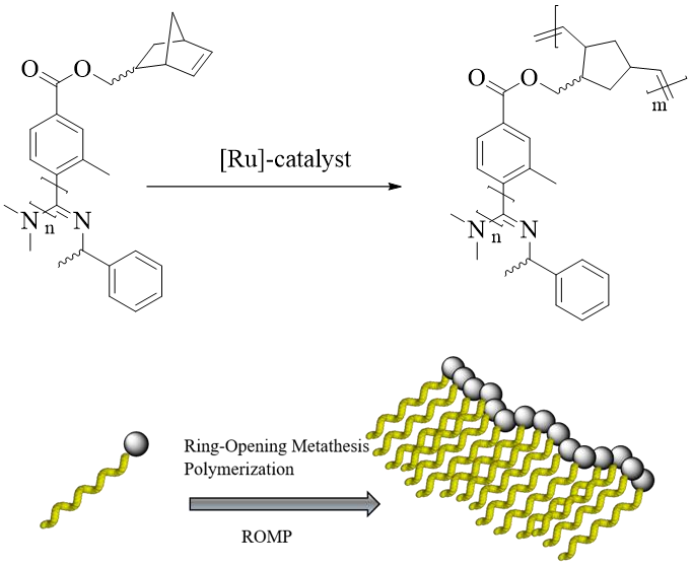

Scheme 6.6 Proposed synthesis route for graft co-polymer.

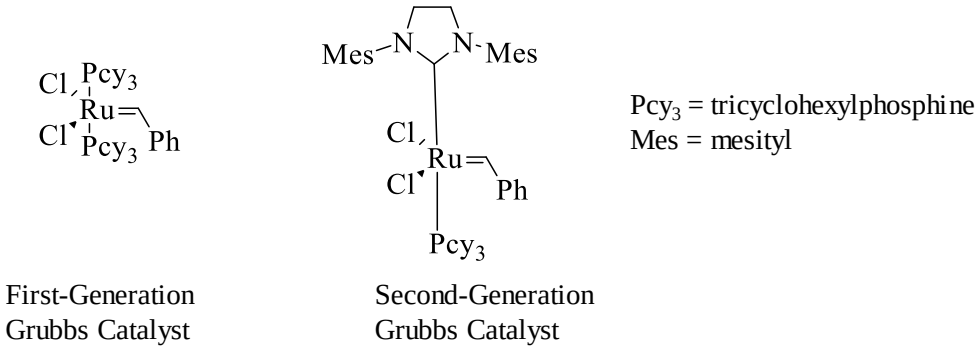

Figure 6.1 Grubb's catalysts for ROMP of Norbornene.

6.4 Synthesis of multi-arm star polymer

Multi-arm star polymers composed of several polymeric arms emanate from a common core. The synthesis strategies utilized here are either core-first[12-14] method or arm-first method.[15,16] In the core-first method, a multi-functional core can be synthesized and the polymeric arms can grow

radially from that core. The synthesis strategy utilized in the arm-first method involves the synthesis of the end-functional polymer chain and these multi-arms are attached to a common core.[17] Versatile and efficient synthetic strategies are utilized in this polymer architecture for controlled arm length and molecular weight.

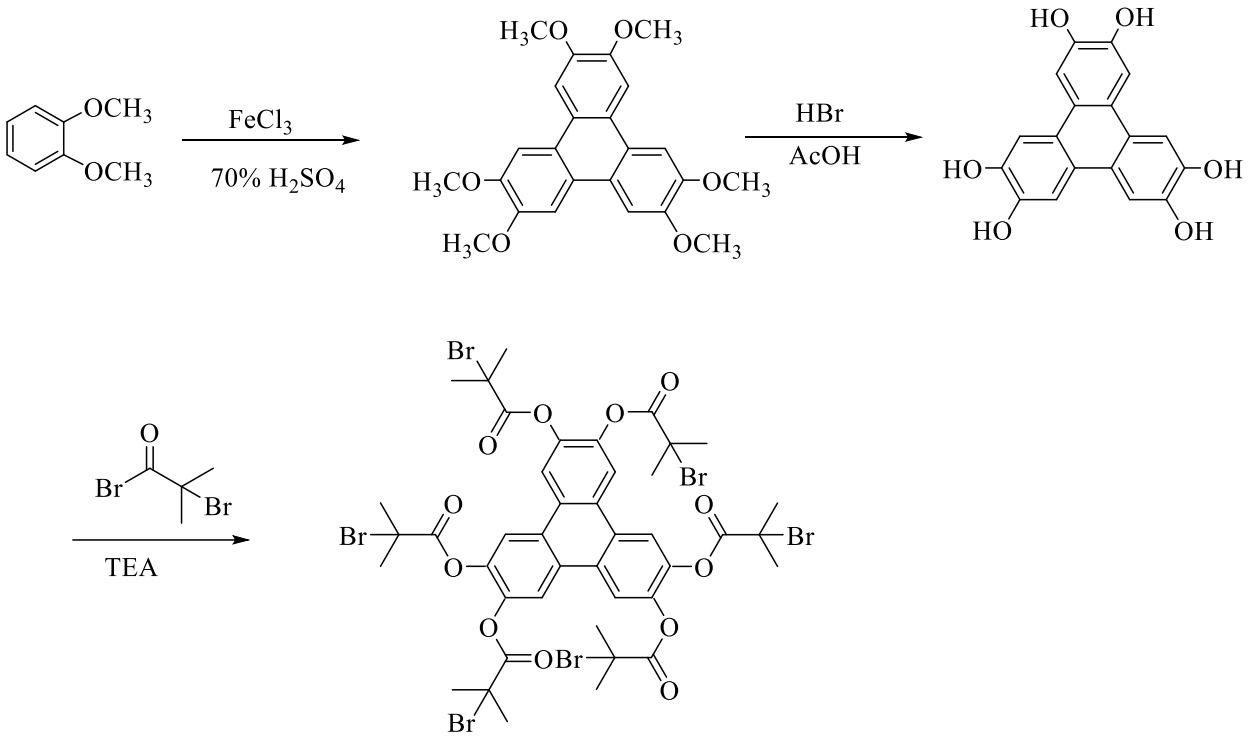

Scheme 6.7 Synthesis of initiator which composed of multiple initiating sites for ATRP.

This initiator composed of six tertiary initiating sites is used for atom transfer radical polymerization of vinyl monomers including styrene, *N*-isopropylarylamide (NIPAM) monomers (**Scheme 6.8**). This initiator is utilized to create a star-polymer architecture which bears six random-coil polymer arms extending from the core and each polymer chain contains a -Br functionalized living chain end. This -Br group can be substituted by an $-N_3$ group through

nucleophilic substitution reaction in the presence of NaN_3. As a result, this star contains provision for click reaction with alkyne functionalized various polymers (**Scheme 6.9**).

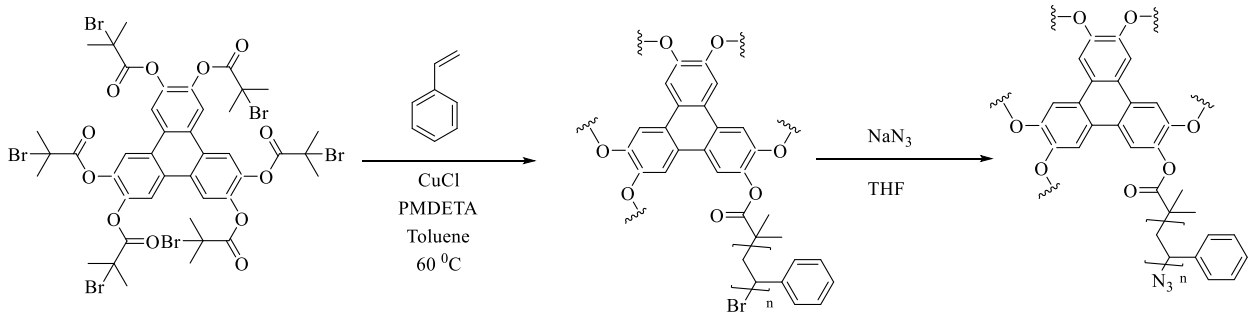

Scheme 6.8 Proposed synthesis of six-arm star polymer.

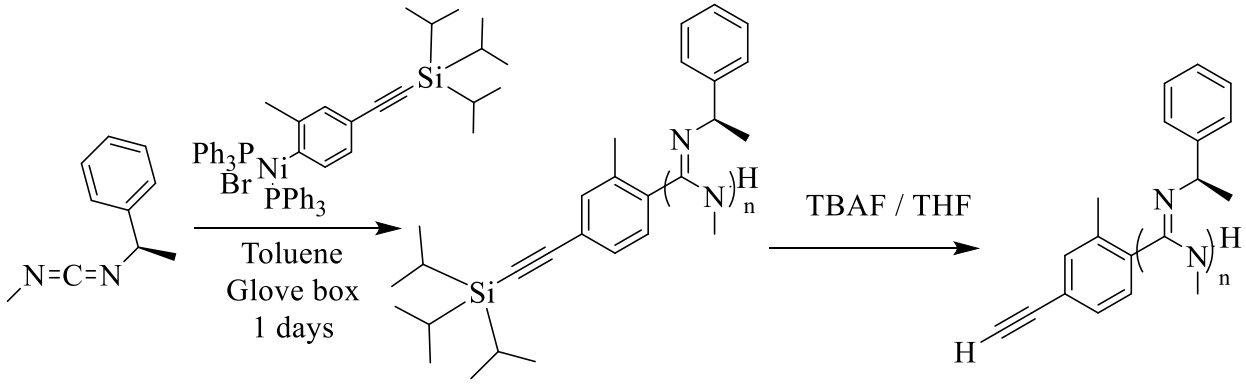

Scheme 6.9 Synthesis of alkyne end-functionalized PPEM.

Alkyne functionalized PPEM polymer can be clicked onto azide functionalized arms to yield di-block, multi-arm star polymer (**Scheme 6.10**). By employing this synthetic strategy, multi-arm star polymers can be synthesized which bears arms composed of rigid rod-random coil block co-polymers. Their self-aggregation studies would be more interesting when compared with individual polymer chains.

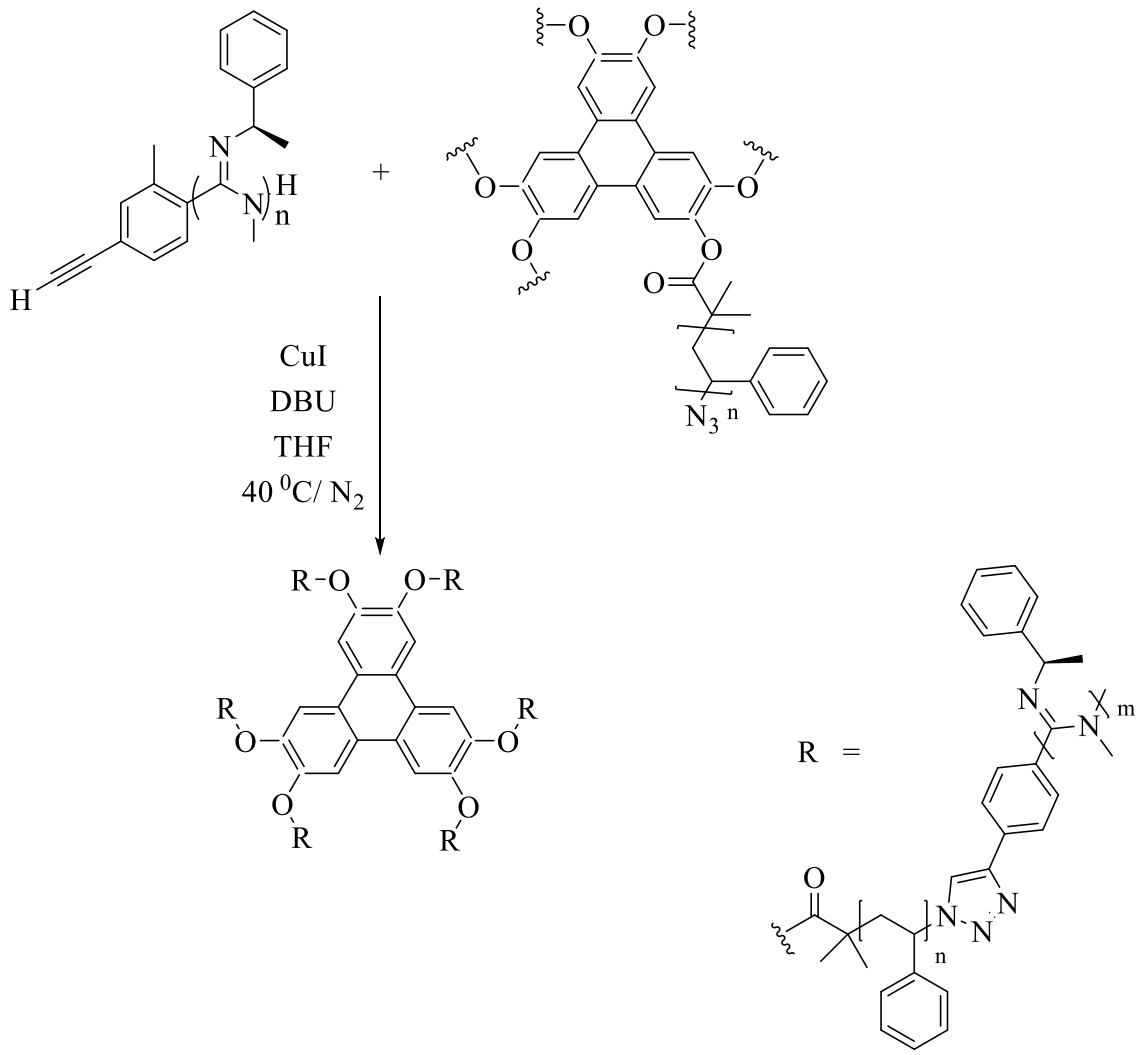

Scheme 6.10 Proposed synthesis of the di-block-six-arm star polymer.

6.5 Conclusion

Various end-functionalized polymer chains can be synthesized by carefully selecting the aryl ligand on Ni(II) center. Previous studies revealed that the polymerization of carbodiimide monomers with Ni(II) initiators shows controlled, living fashion without chain termination reactions. This synthesis strategy greatly enhances the creation of various macromolecular architectures built on polycarbodiimides. These architectures may possess different amphiphilic

nature which leads to the formation of different types of aggregations namely micelles, vesicles and polymersomes which can be utilized in different applications such as drug delivery, molecular machines, and carriers for catalysts.

6.6 References

(1) Romulus, J.; Henssler, J. T.; Weck, M. Postpolymerization Modification of Block Copolymers. *Macromolecules* **2014**, *47* (16), 5437–5449 DOI: 10.1021/ma5009918.

(2) Adams, M. L.; Lavasanifar, A.; Kwon, G. S. Amphiphilic Block Copolymers for Drug Delivery. *J. Pharm. Sci.* **2017**, *92* (7), 1343–1355 DOI: 10.1002/jps.10397.

(3) Gil, E. S.; Hudson, S. M. Stimuli-Responsive Polymers and Their Bioconjugates. *Prog. Polym. Sci.* **2004**, *29* (12), 1173–1222 DOI: http://dx.doi.org/10.1016/j.progpolymsci.2004.08.003.

(4) Reuther, J. F.; Siriwardane, D. A.; Campos, R.; Novak, B. M. Solvent Tunable Self-Assembly of Amphiphilic Rod-Coil Block Copolymers with Chiral, Helical Polycarbodiimide Segments: Polymeric Nanostructures with Variable Shapes and Sizes. *Macromolecules* **2015**, *48* (19), 6890–6899 DOI: 10.1021/acs.macromol.5b01564.

(5) Reuther, J. F.; Bhatt, M. P.; Tian, G.; Batchelor, B. L.; Campos, R.; Novak, B. M. Controlled Living Polymerization of Carbodiimides Using Versatile, Air-Stable Nickel(II) Initiators: Facile Incorporation of Helical, Rod-like Materials. *Macromolecules* **2014**, *47* (14), 4587–4595 DOI: 10.1021/ma5009429.

(6) Isono, T.; Kondo, Y.; Ozawa, S.; Chen, Y.; Sakai, R.; Sato, S.; Tajima, K.; Kakuchi, T.; Satoh, T. Stereoblock-like Brush Copolymers Consisting of Poly(l-Lactide) and Poly(d-Lactide) Side Chains along Poly(norbornene) Backbone: Synthesis, Stereocomplex Formation, and Structure–Property Relationship. *Macromolecules* **2014**, *47* (20), 7118–7128 DOI: 10.1021/ma501647m.

(7) Xu, T.; Tang, Z.; Zhu, J. Synthesis of Polylactide-Graft-Glycidyl Methacrylate Graft Copolymer and Its Application as a Coupling Agent in Polylactide/bamboo Flour Biocomposites. *J. Appl. Polym. Sci.* **2012**, *125* (S2), E622–E627 DOI: 10.1002/app.36808.

(8) Neises, B.; Steglich, W. Simple Method for the Esterification of Carboxylic Acids. *Angew. Chemie Int. Ed. English* **1978**, *17* (7), 522–524 DOI: 10.1002/anie.197805221.

(9) Sutthasupa, S.; Shiotsuki, M.; Sanda, F. Recent Advances in Ring-Opening Metathesis Polymerization, and Application to Synthesis of Functional Materials. *Polym J* **2010**, *42* (12), 905–915.

(10) Bielawski, C. W.; Grubbs, R. H. Living Ring-Opening Metathesis Polymerization. *Prog. Polym. Sci.* **2007**, *32* (1), 1–29 DOI: http://dx.doi.org/10.1016/j.progpolymsci.2006.08.006.

(11) Chaves, H. K.; Ferraz, C. P.; Carvalho Jr, V. P.; Lima-Neto, B. S. Tuning the Activity of Alternative Ru-Based Initiators for Ring-Opening Metathesis Polymerization of Norbornene and Norbornadiene by the Substituent in 4-CH2R-Piperidine. *J. Mol. Catal. A Chem.* **2014**, *385*, 46–53 DOI: http://dx.doi.org/10.1016/j.molcata.2014.01.012.

(12) Xia, X.; Ye, Z.; Morgan, S.; Lu, J. "Core-First" Synthesis of Multiarm Star Polyethylenes with a Hyperbranched Core and Linear Arms via Ethylene Multifunctional "Living" Polymerization with Hyperbranched Polyethylenes Encapsulating Multinuclear Covalently Tethered Pd-Diimine Catalysts. *Macromolecules* **2010**, *43* (11), 4889–4901 DOI: 10.1021/ma1005843.

(13) Gaynor, S. G.; Edelman, S.; Matyjaszewski, K. Synthesis of Branched and Hyperbranched Polystyrenes. *Macromolecules* **1996**, *29* (3), 1079–1081 DOI: 10.1021/ma9513877.

(14) Matyjaszewski, K.; Gaynor, S. G.; Kulfan, A.; Podwika, M. Preparation of Hyperbranched Polyacrylates by Atom Transfer Radical Polymerization. 1. Acrylic AB* Monomers in "Living" Radical Polymerizations. *Macromolecules* **1997**, *30* (17), 5192–5194 DOI: 10.1021/ma970359g.

(15) Gao, H.; Matyjaszewski, K. Structural Control in ATRP Synthesis of Star Polymers Using the Arm-First Method. *Macromolecules* **2006**, *39* (9), 3154–3160 DOI: 10.1021/ma060223v.

(16) Baek, K.-Y.; Kamigaito, M.; Sawamoto, M. Core-Functionalized Star Polymers by Transition Metal-Catalyzed Living Radical Polymerization. 1. Synthesis and Characterization of Star Polymers with PMMA Arms and Amide Cores. *Macromolecules* **2001**, *34* (22), 7629–7635 DOI: 10.1021/ma010973z.

(17) Han, D.; Tong, X.; Zhao, Y. Synthesis and Characterization of Six-Arm Star Polystyrene-Block-Poly (3-Hexylthiophene) Copolymer by Combination of Atom Transfer Radical Polymerization and Click Reaction. *J. Polym. Sci. Part A Polym. Chem.* **2012**, *50* (20), 4198–4205 DOI: 10.1002/pola.26221.

APPENDIX A

NMR SPECTRA OF SOME UREAS, MONOMERS AND POLYMERS FOR CHAPTER 2

^{1}HNMR of 2,4,6-tri(4-bromo-3-methyl)-1,3,5-triazine (**Compound -1**)

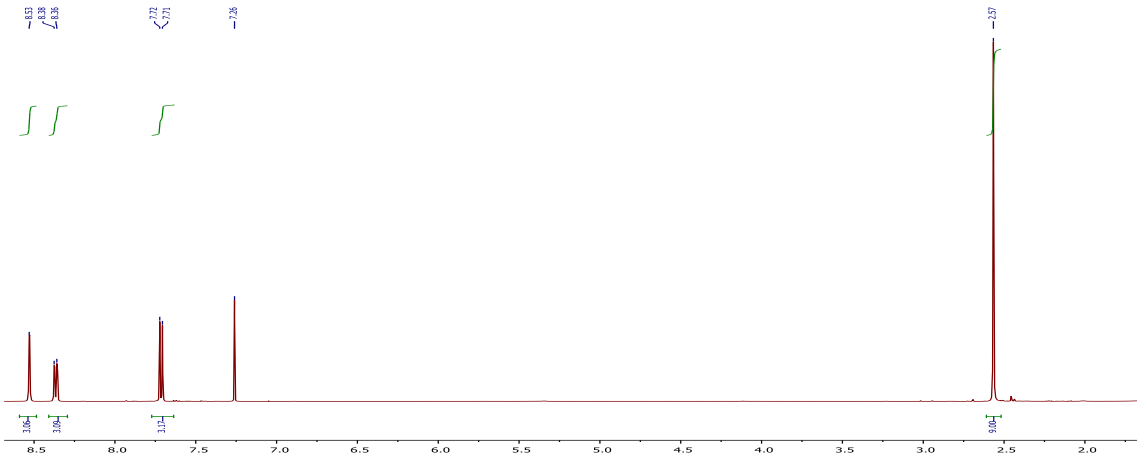

^{13}C NMR of 2,4,6-tri(4-bromo-3-methyl)-1,3,5-triazine (**Compound -1**)

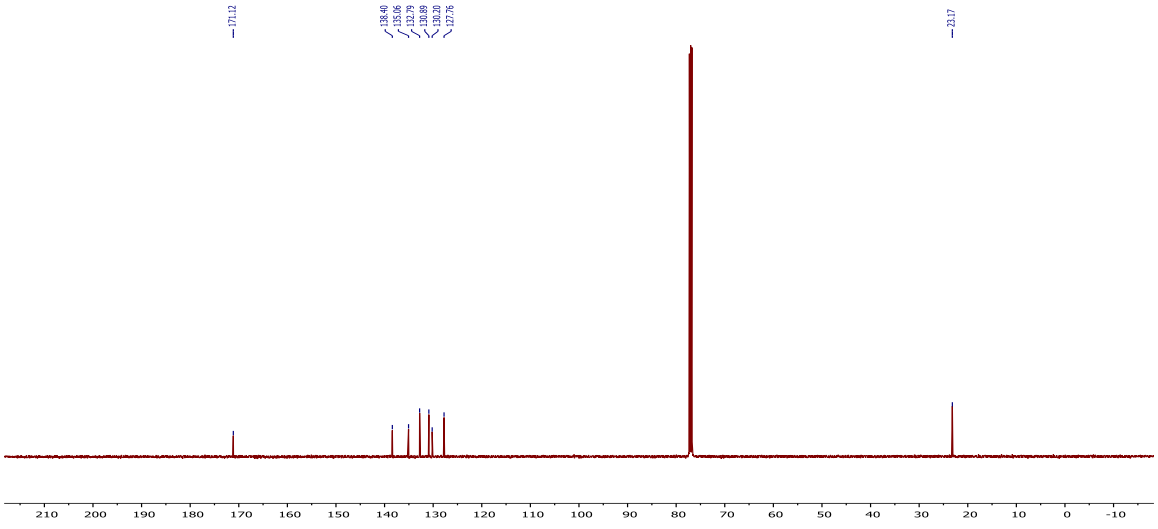

^{1}H NMR of **Cat-8**

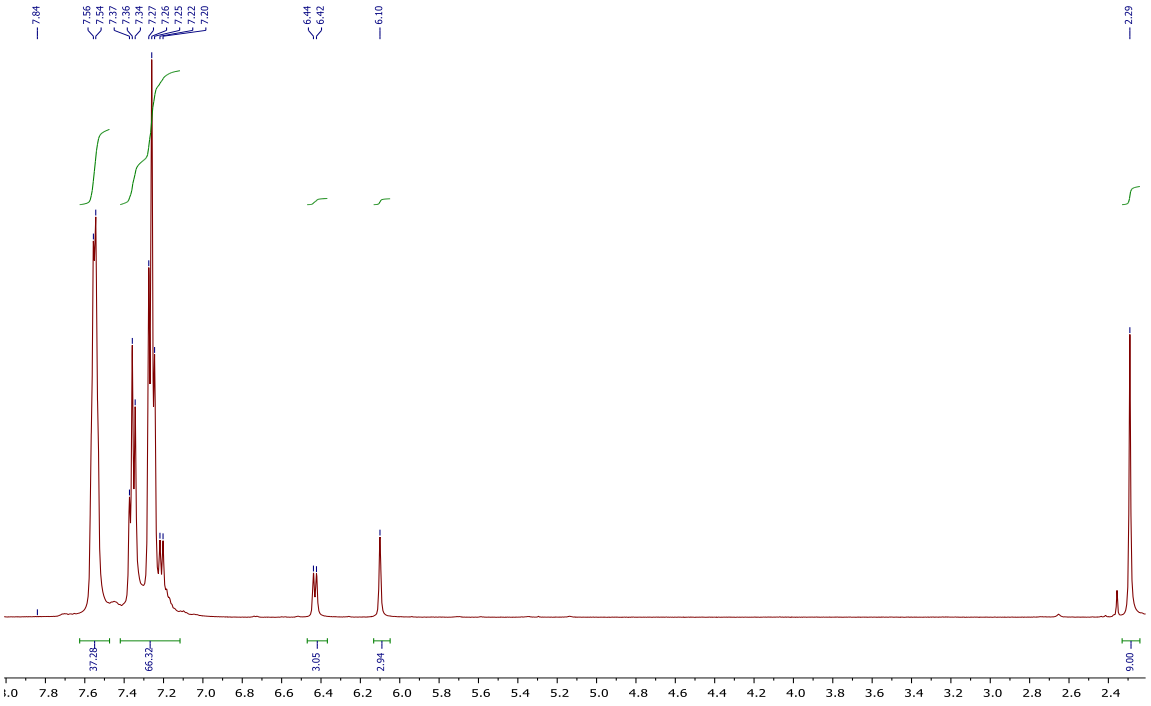

^{31}P NMR of PPH_3 (a) and *tris*-Ni(ii) initiator (**Cat-8**) (b)

(A) PPh_3

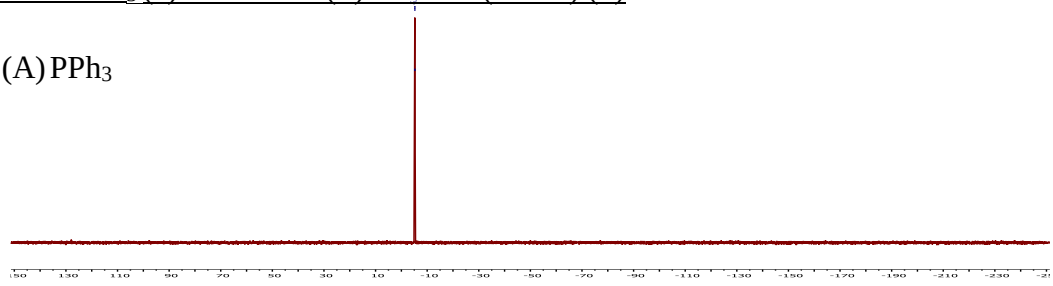

(B)

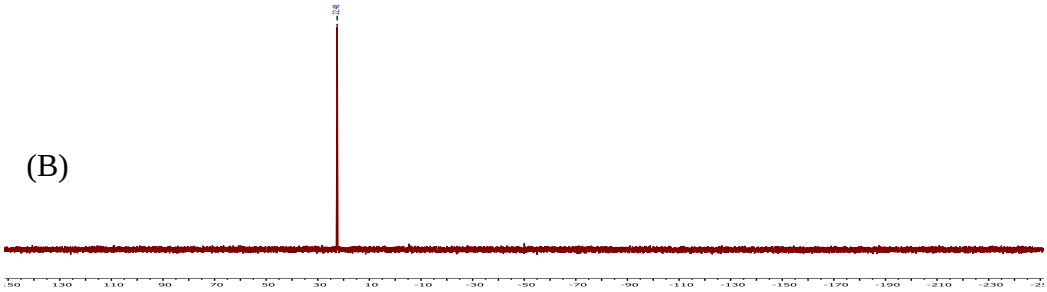

^{1}H NMR of (**Cat-6**)

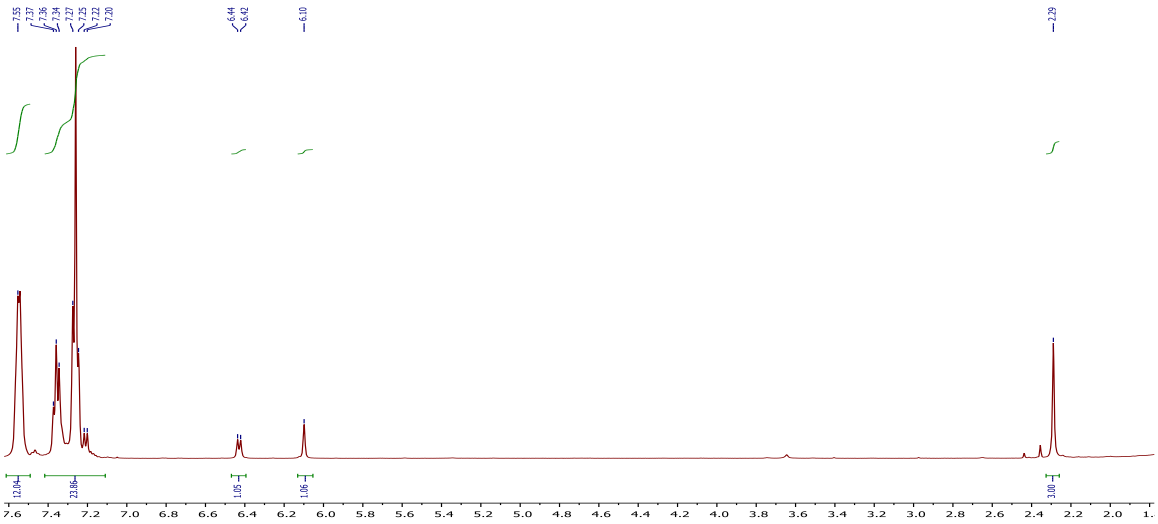

^{13}C NMR of **Cat-6**

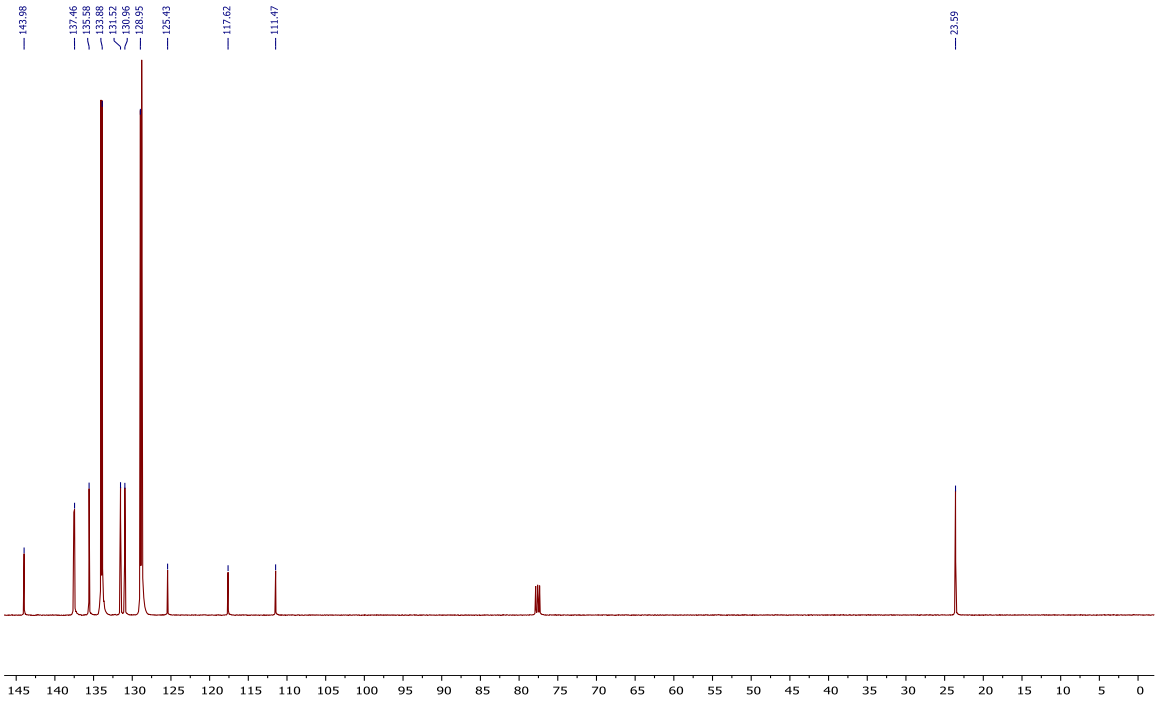

^{31}P NMR of **Cat-6**

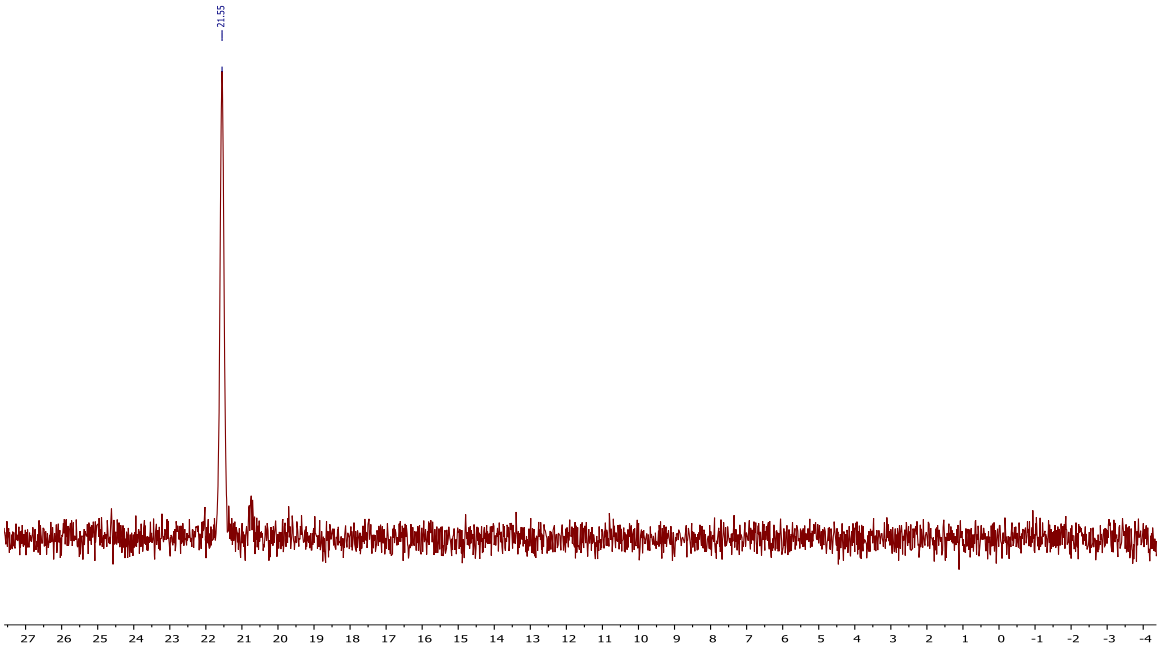

^{1}H NMR of *N*-1-phenylethyl-*N*'-methylurea, (**Compound - 2**)

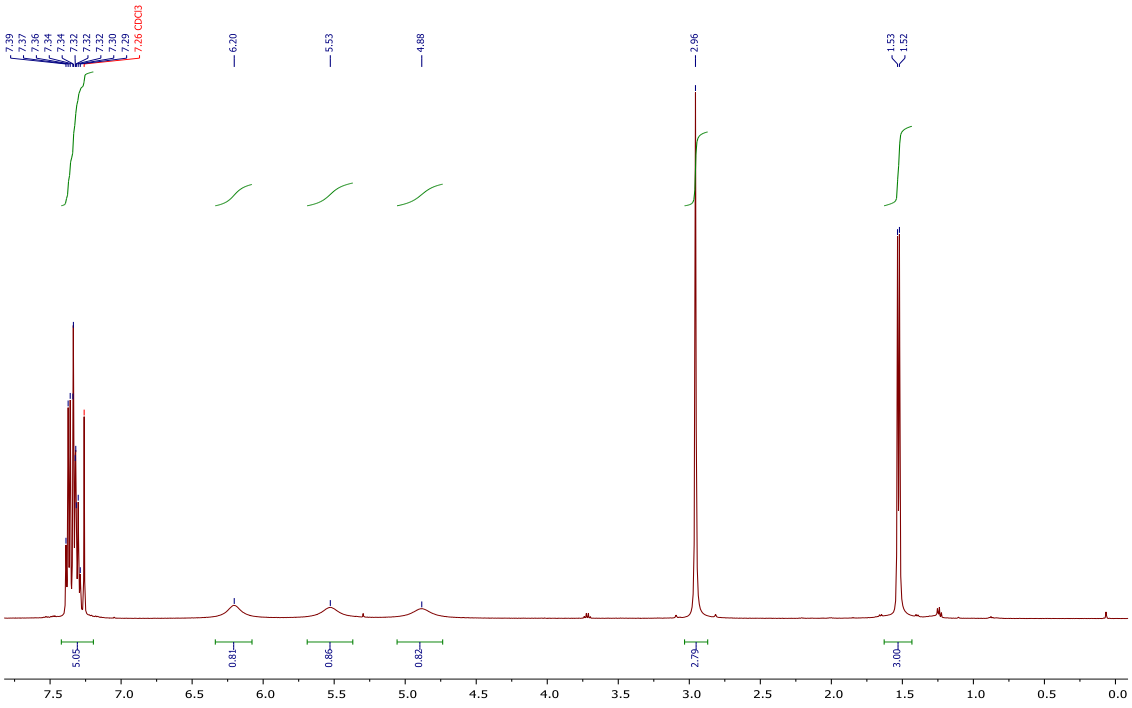

^{13}C NMR of *N*-1-phenylethyl-*N*'-methylurea, (**Compound -2**)

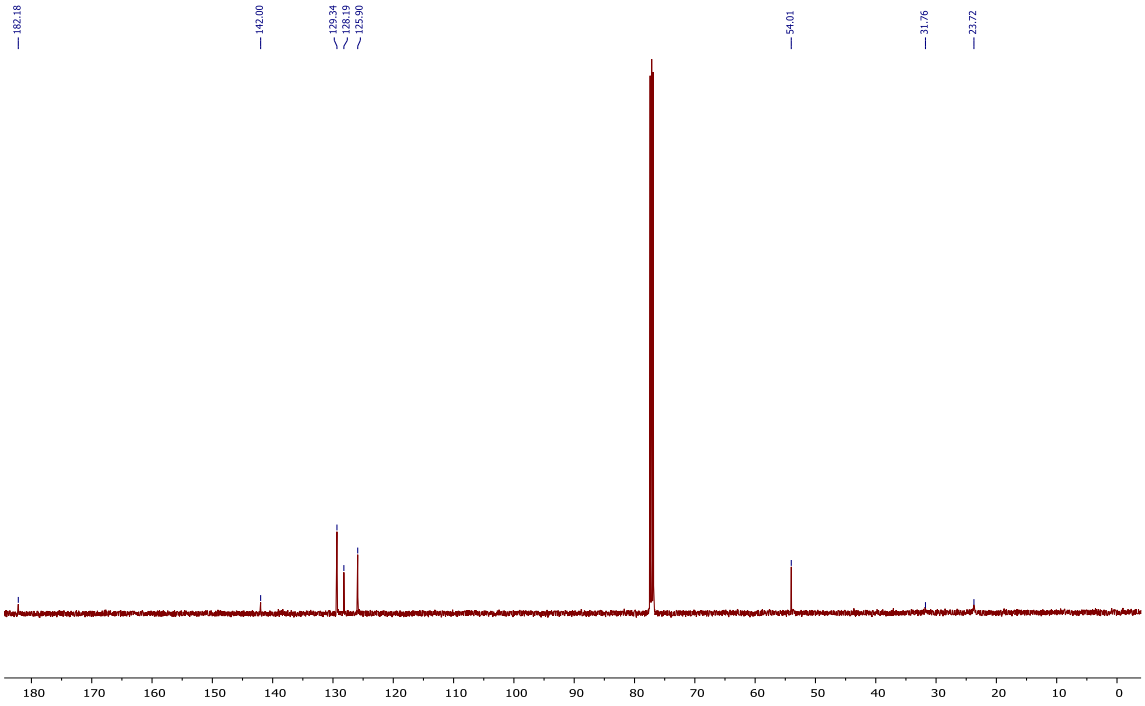

^{1}H NMR of *N*-phenylethyl-*N*'-metylcarbodiimide monomer, (**Compound-3**)

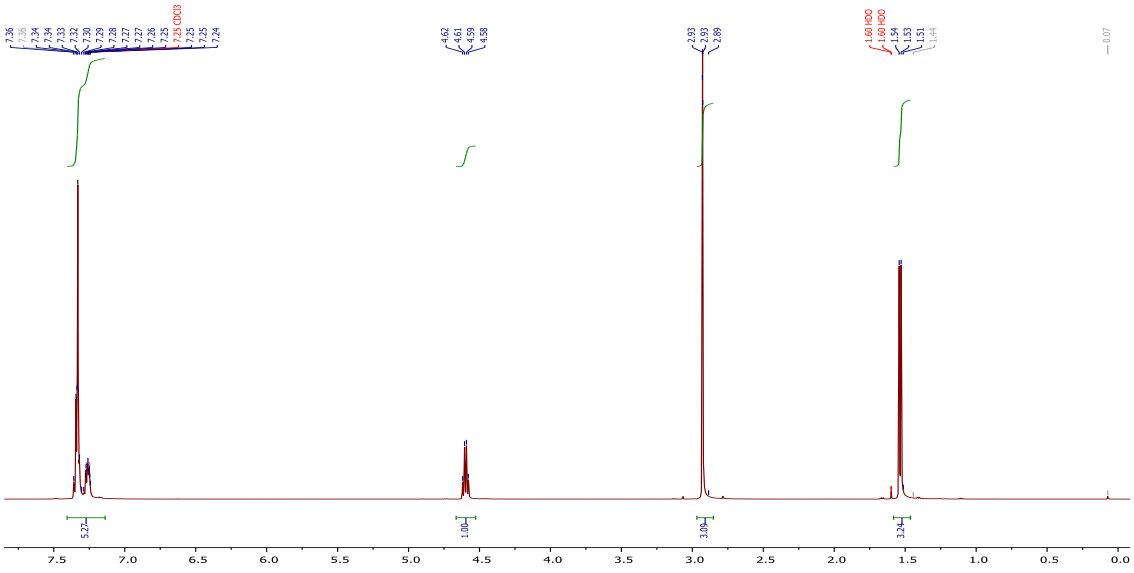

^{13}C NMR of *N*-phenylethyl-*N*'-metylcarbodiimide monomer, (**Compound-3**)

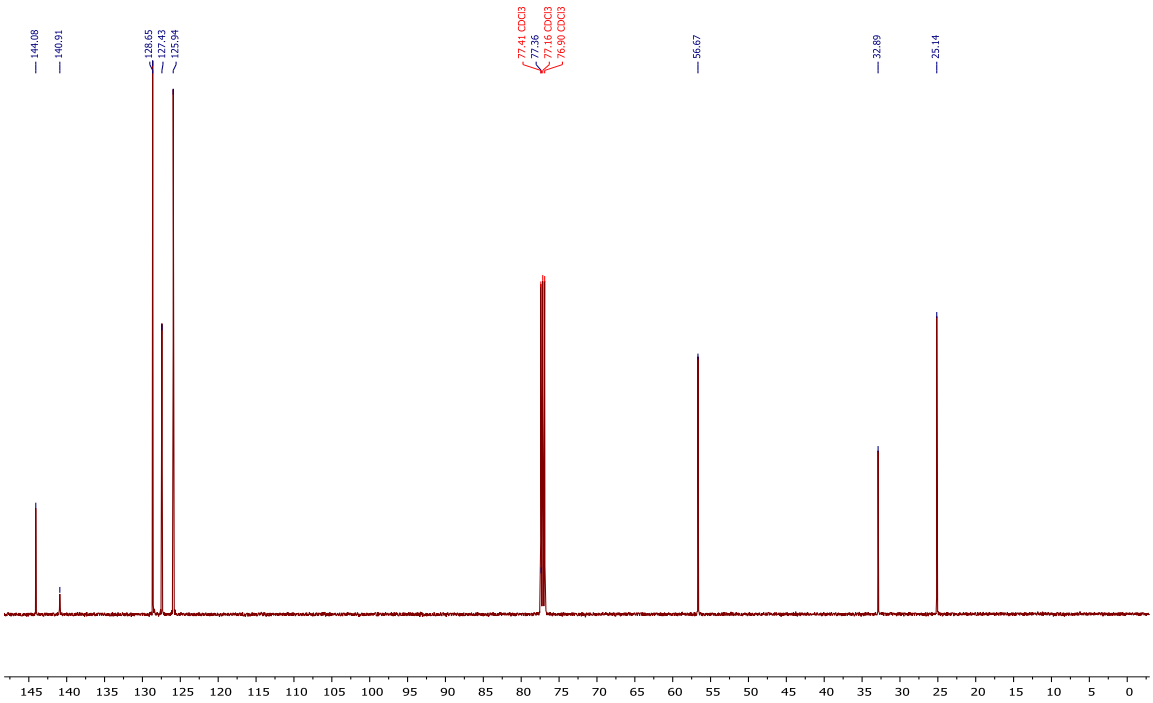

^{1}HNMR of 3-arm star polymer, (**Poly-11**)

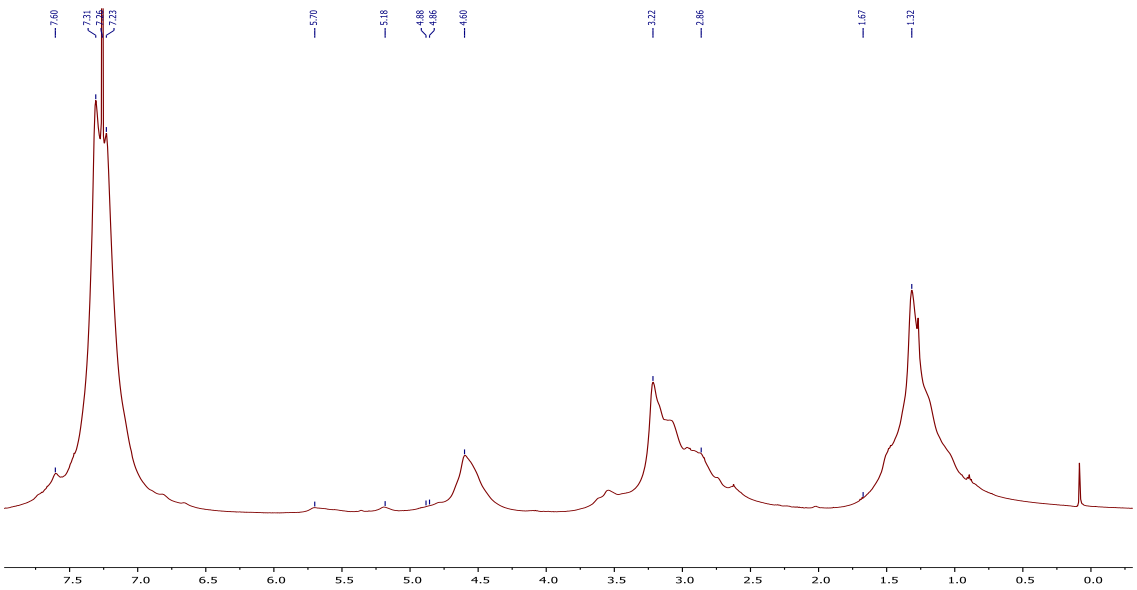

^{13}C NMR of 3-arm star polymer (**Poly-11**)

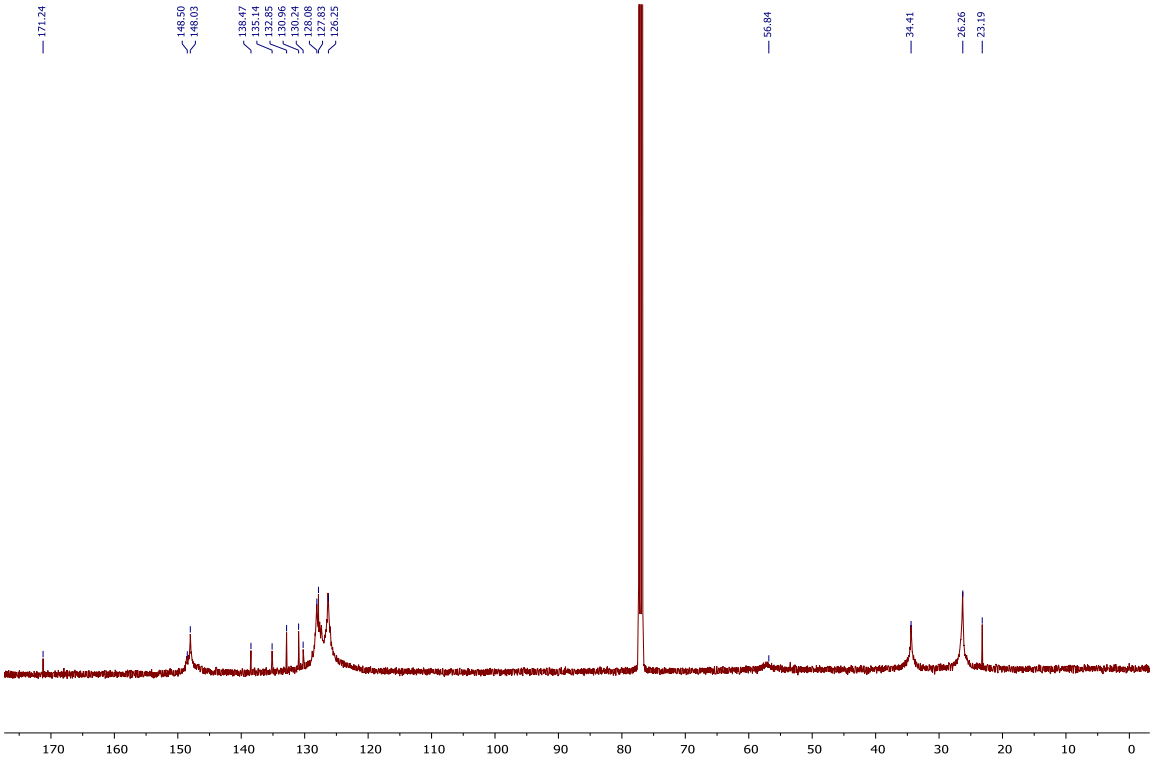

APPENDIX B

NMR SPECTRA OF SOME UREAS, MONOMERS AND POLYMERS FOR CHAPTER 3

^{1}H NMR of *N*-methyl-*N*'-(5-methyl-2-isopropylphenyl)thiourea

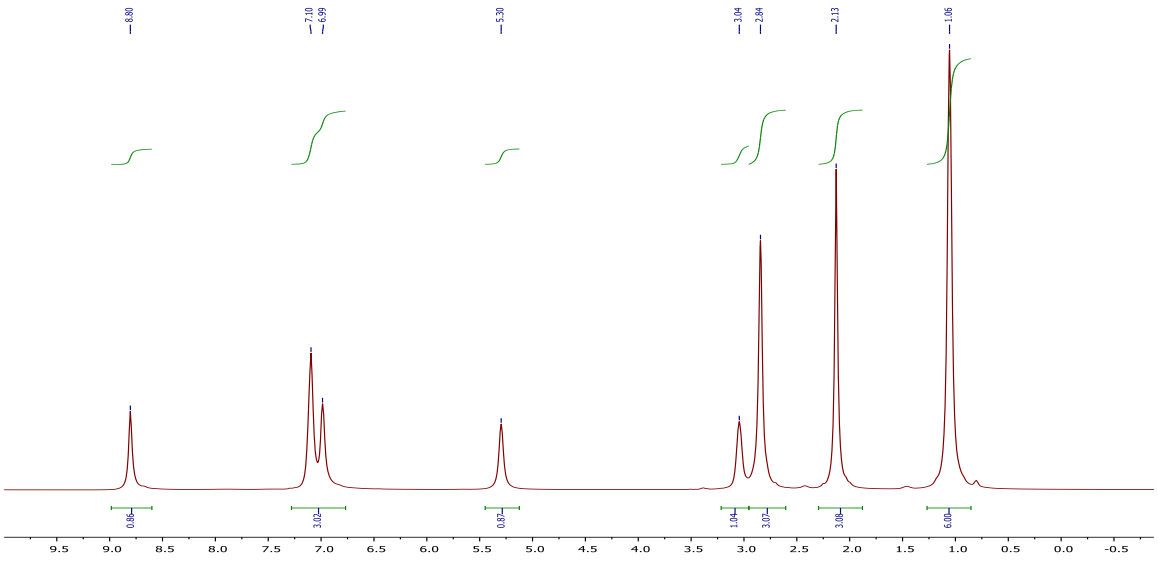

^{13}C NMR of *N*-methyl-*N*'-(5-methyl-2-isopropylphenyl)thiourea

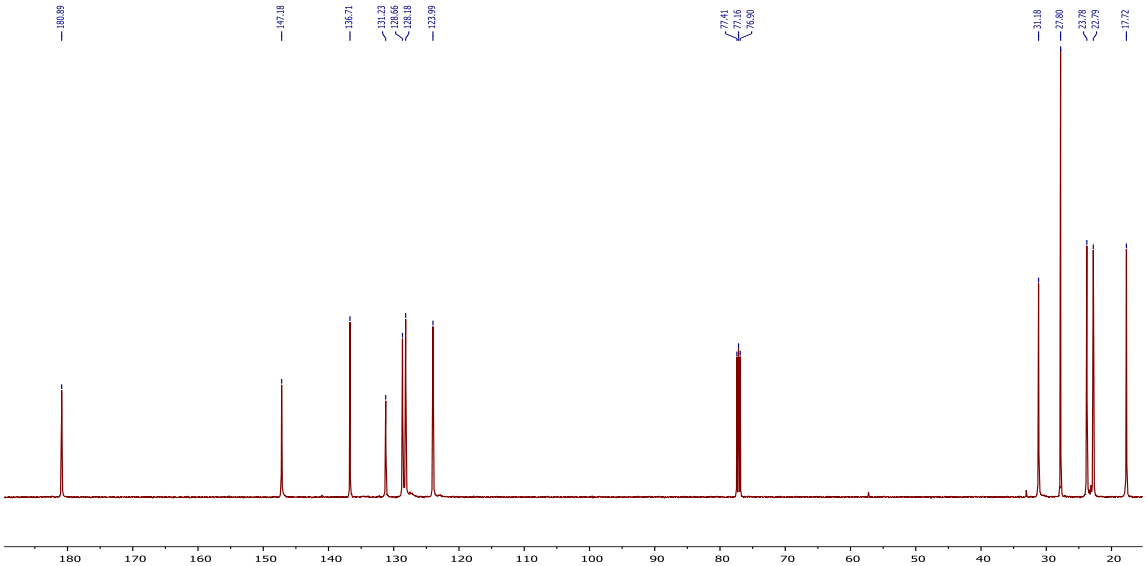

^{1}H NMR of *N*-methyl-*N*'-(2-isopropylphenyl)thiourea

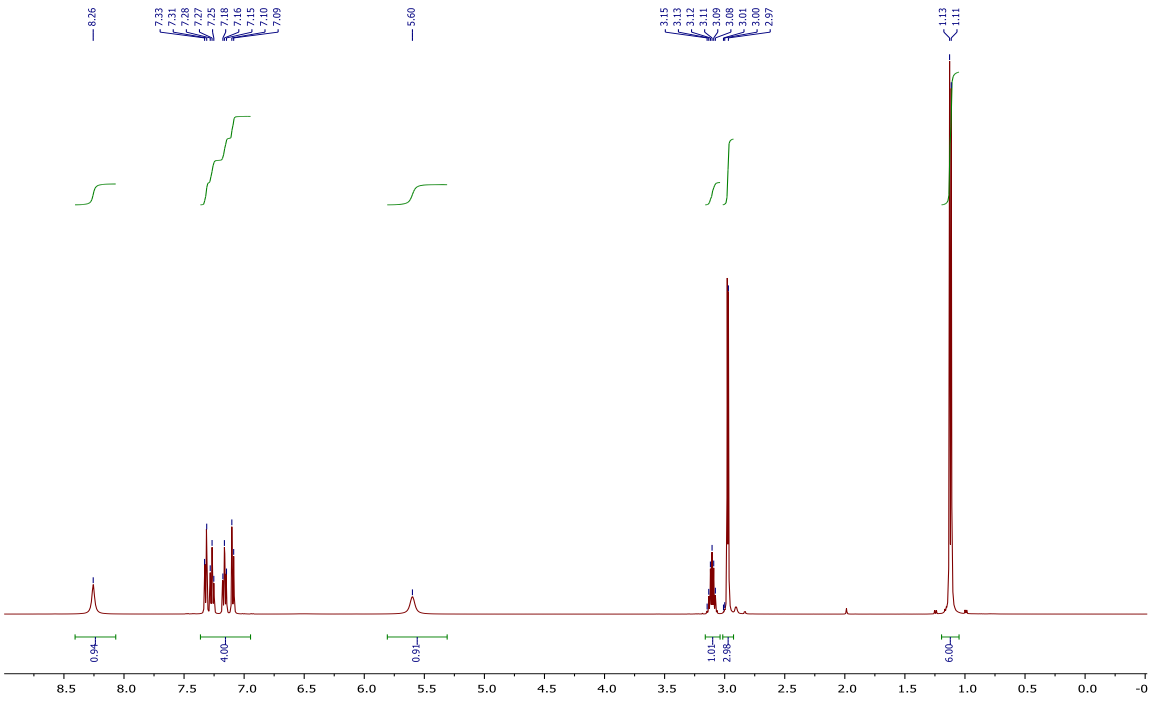

^{13}C NMR of *N*-methyl-*N*'-(2-isopropylphenyl)thiourea

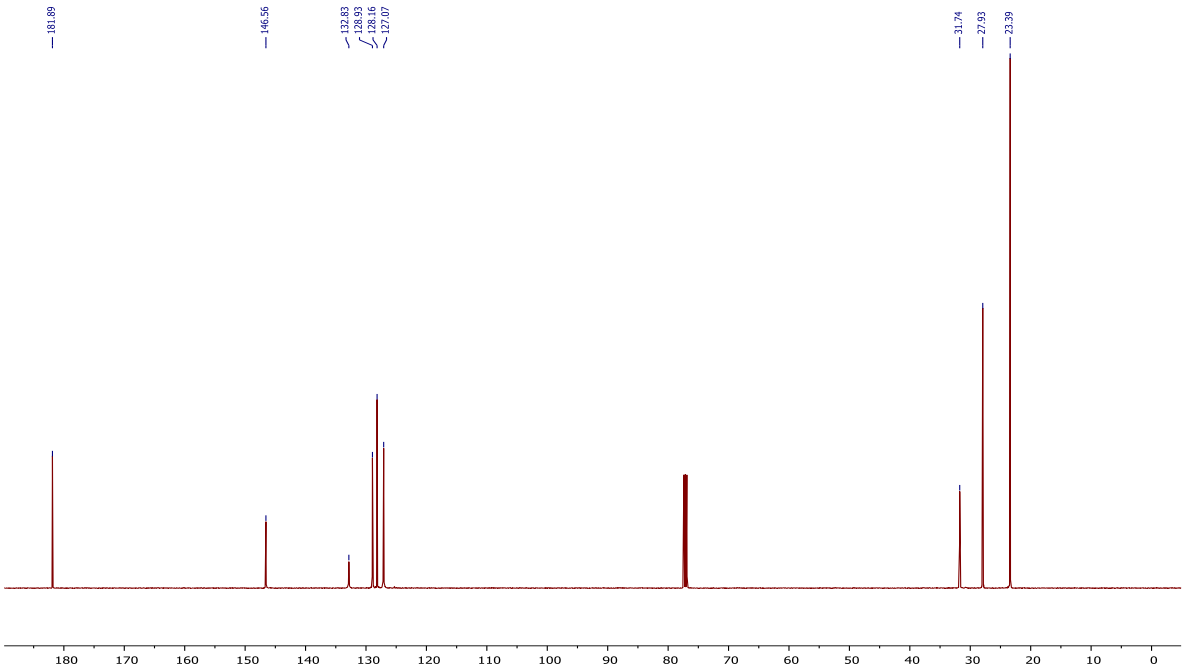

^{1}H NMR of *N*-methyl-*N*'-(3-isopropylphenyl)thiourea

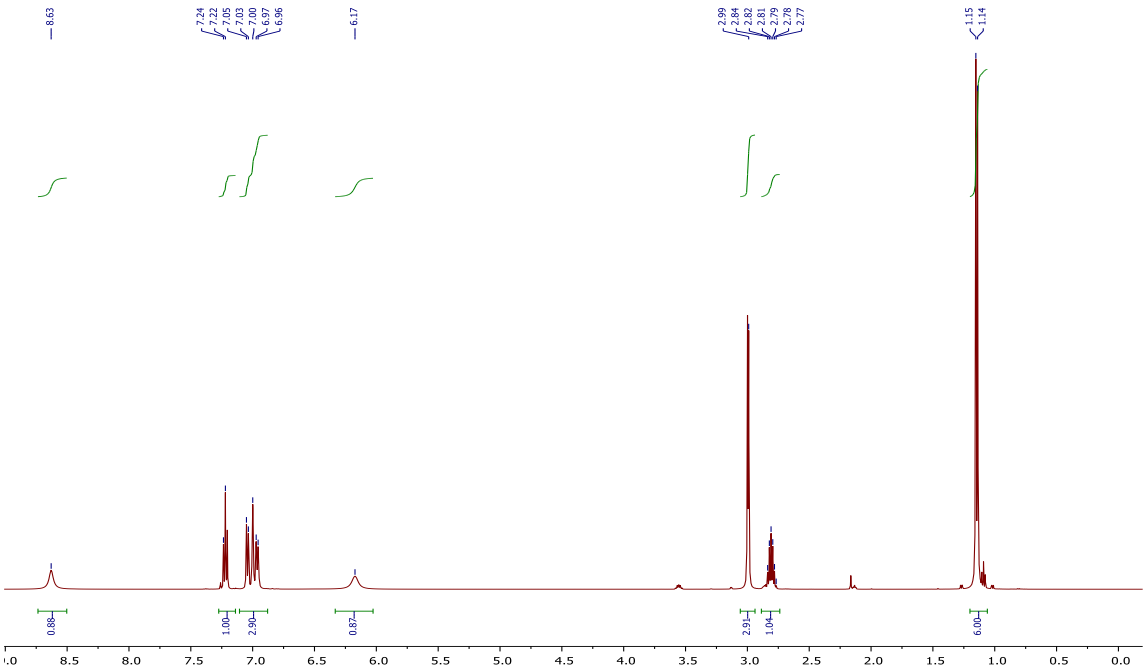

^{13}C NMR of *N*-methyl-*N*'-(3-isopropylphenyl)thiourea

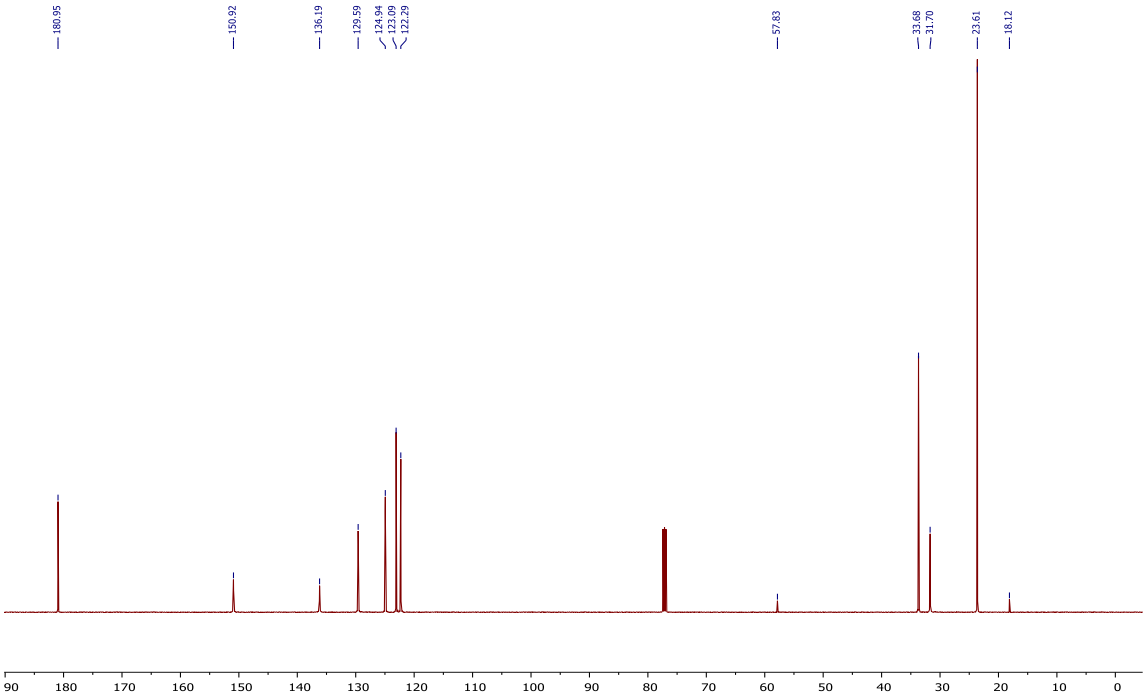

^{1}H NMR of *N*-methyl-*N*'-(4-isopropylphenyl)thiourea

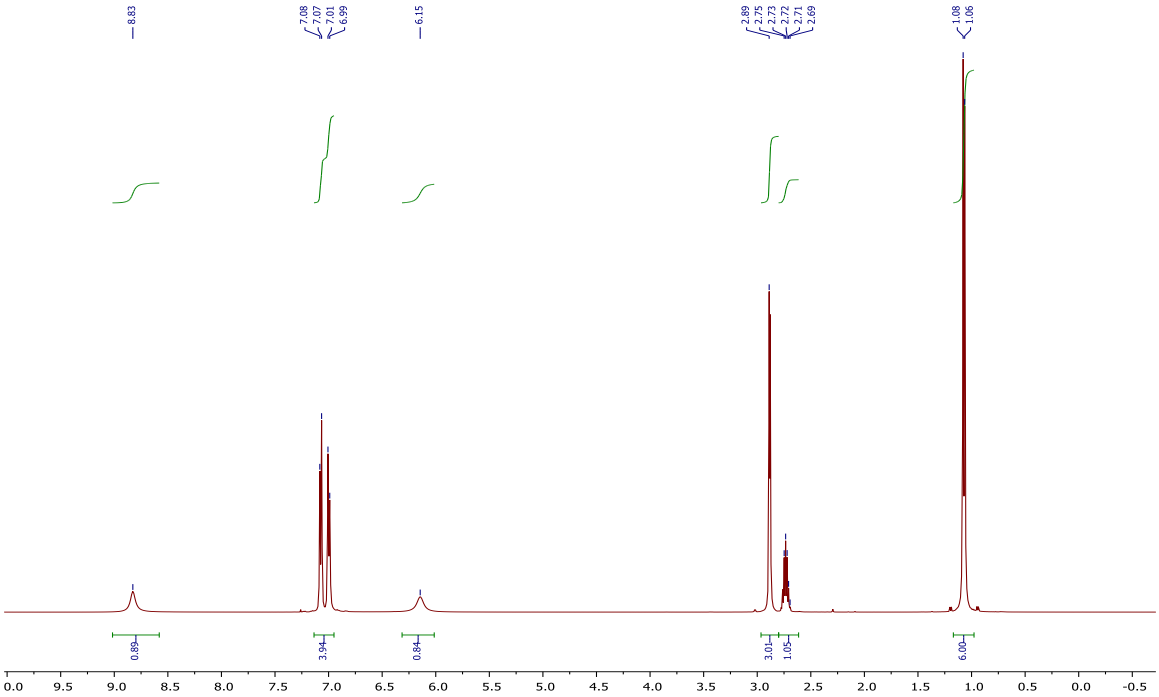

^{13}C NMR of *N*-methyl-*N*'-(4-isopropylphenyl)thiourea

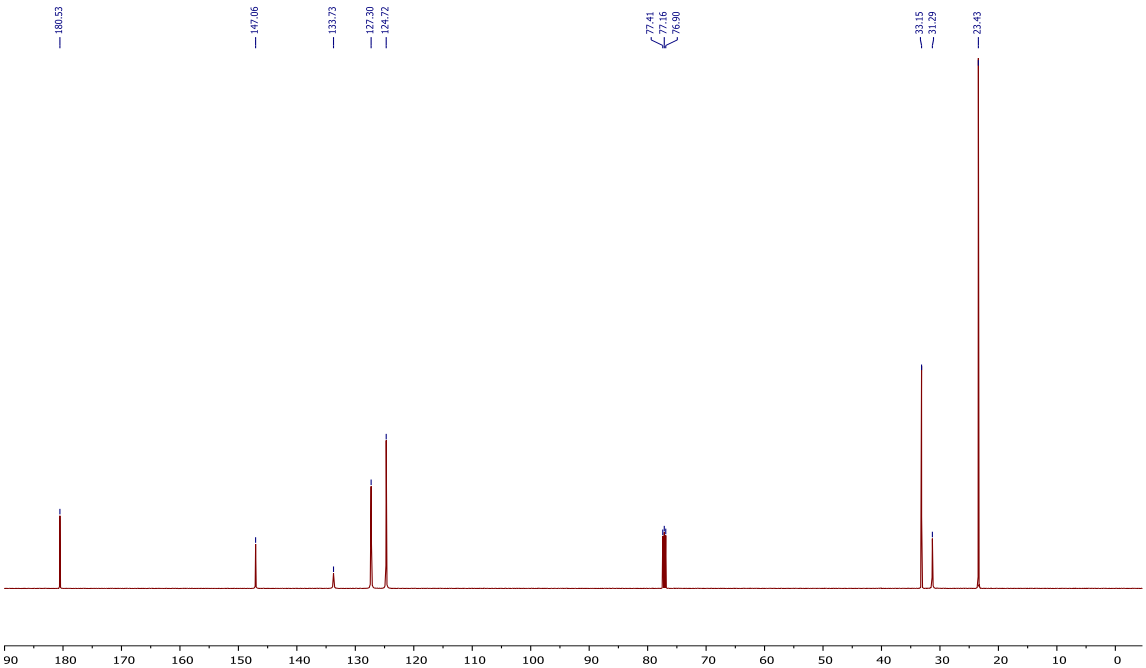

^{1}H NMR of *N*-methyl-*N*'-(5-methyl-2-isopropylphenyl)carbodiimide

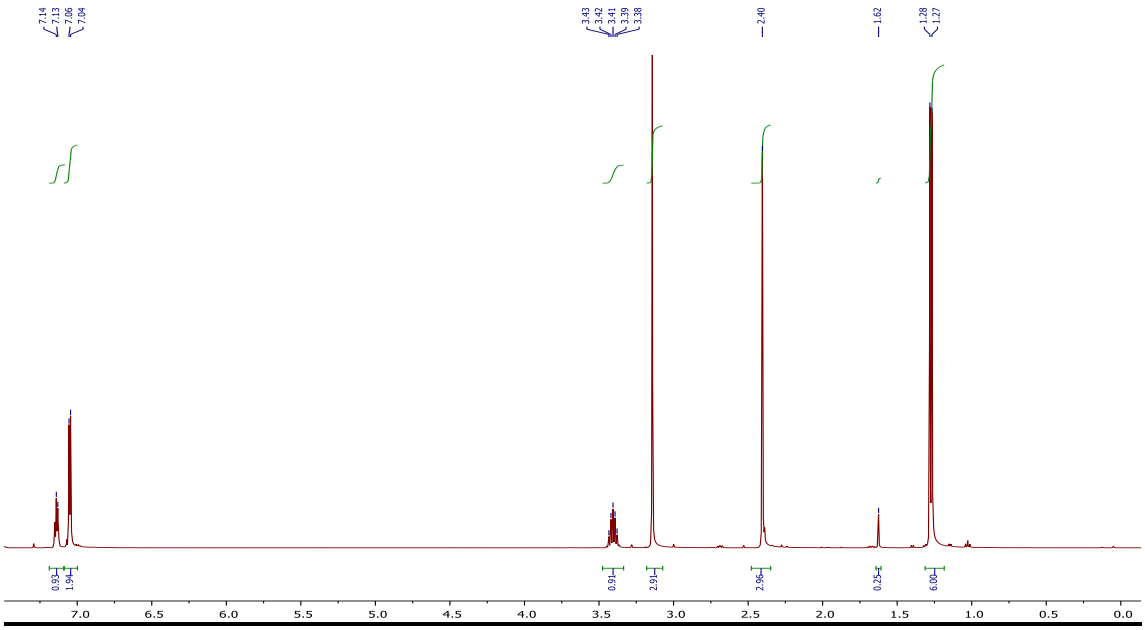

^{13}C NMR of *N*-methyl-*N*'-(5-methyl-2-isopropylphenyl)carbodiimide

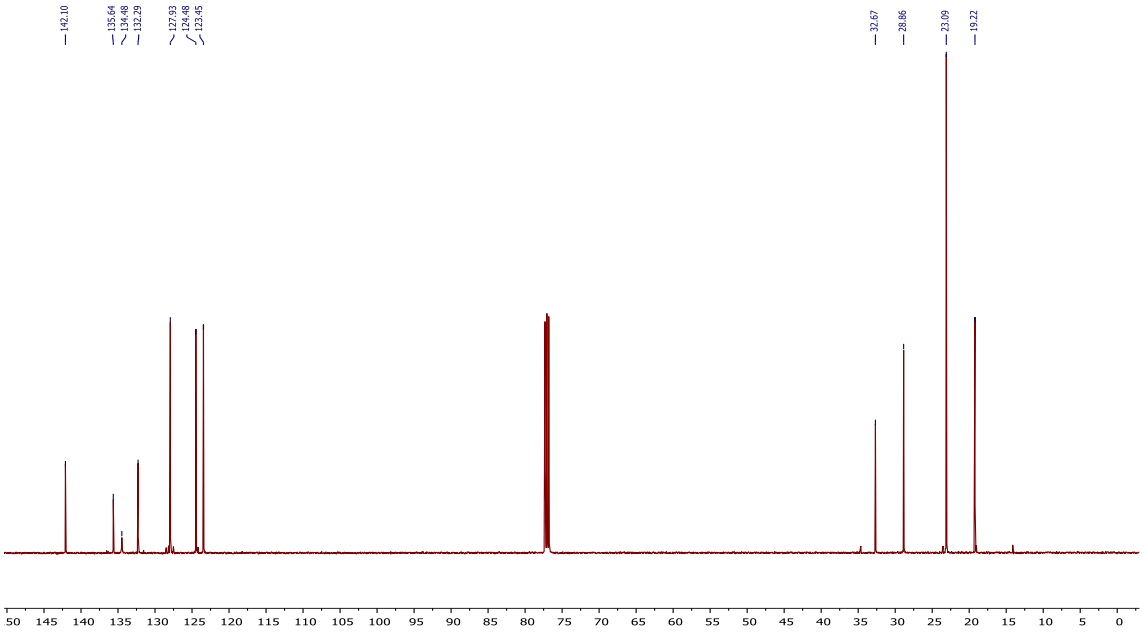

^{1}H NMR of *N*-phenyl-*N*'-octadecylcarbodiimide

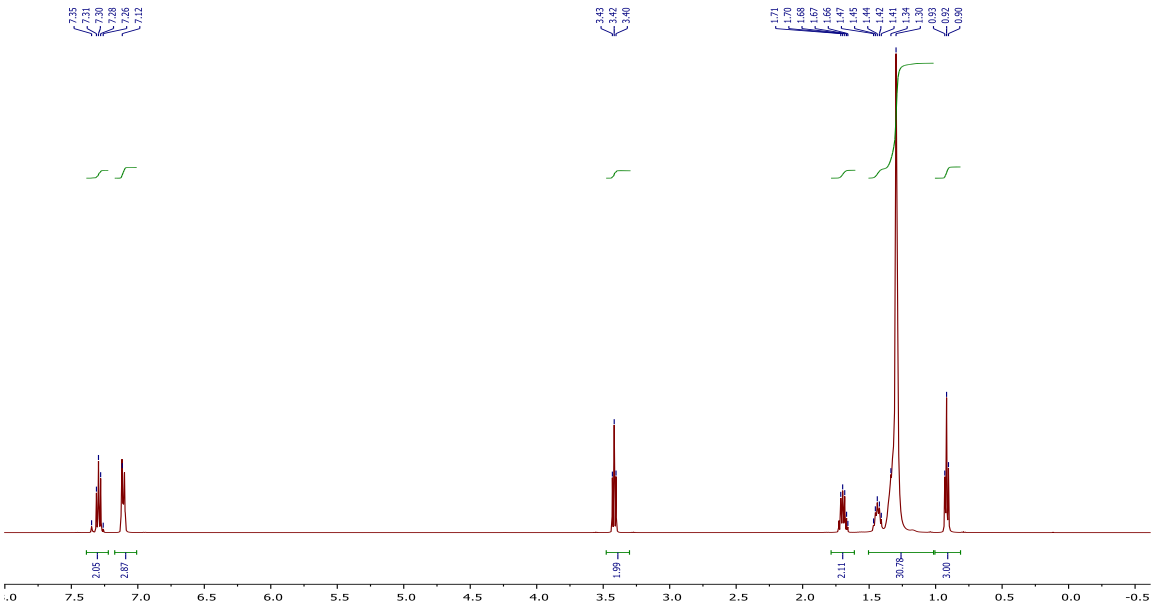

^{13}C NMR of *N*-phenyl-*N*'-octadecylcarbodiimide

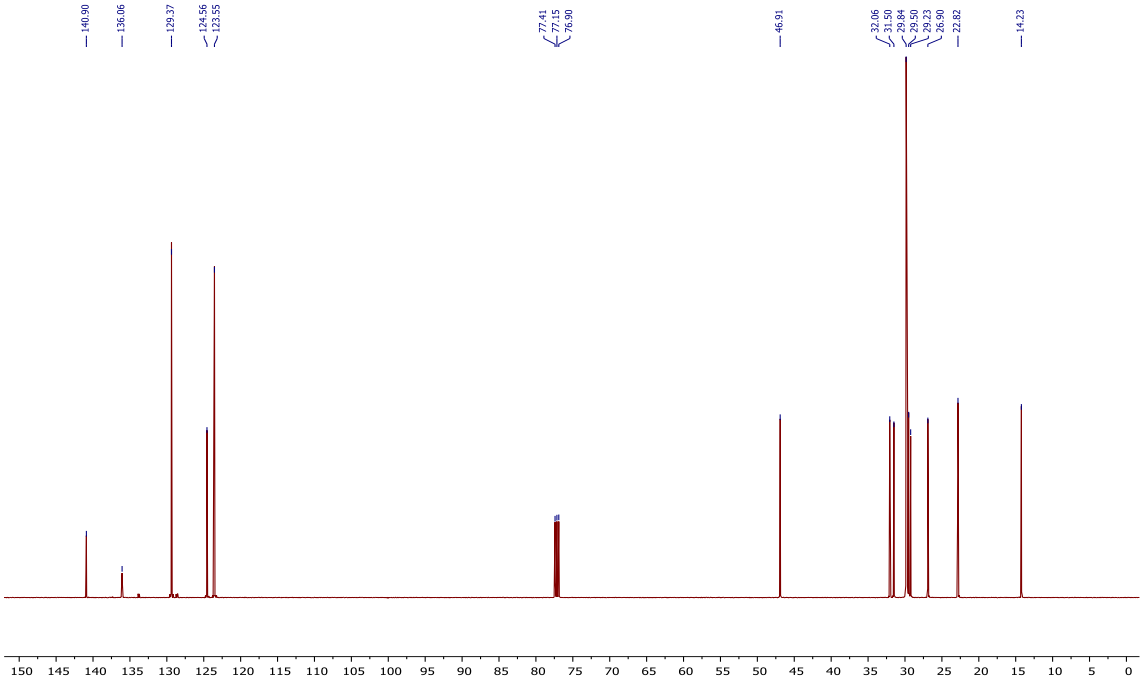

^{1}H NMR of *N*-methyl-*N*'-(2-isopropylphenyl)carbodiimide

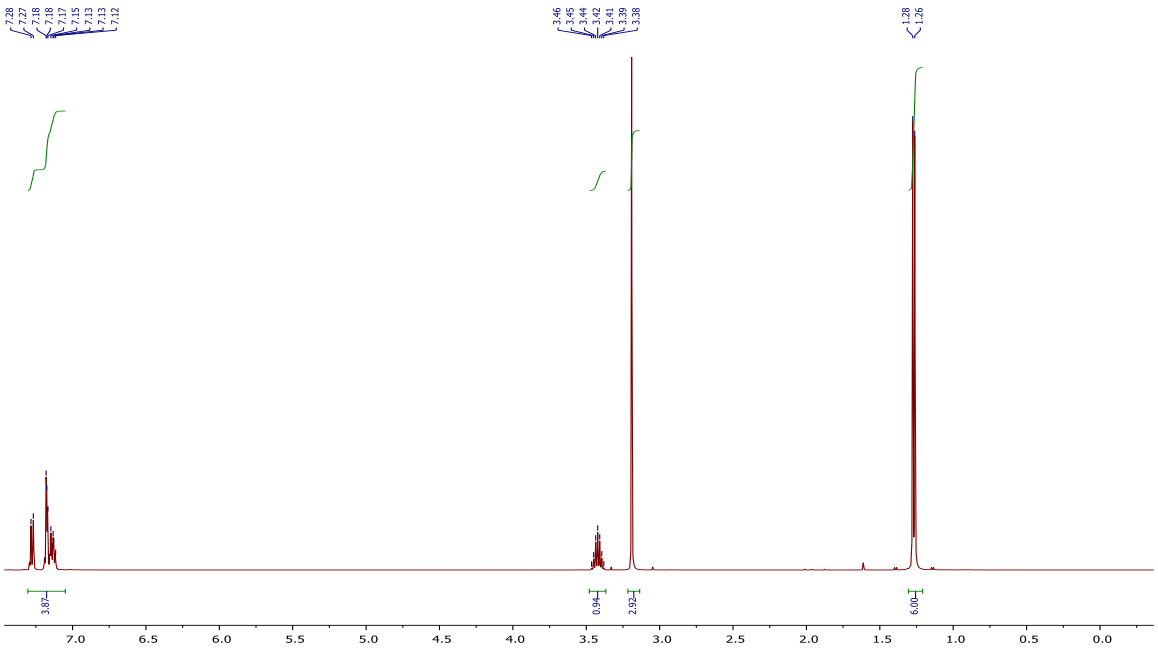

^{13}C NMR of *N*-methyl-*N*'-(2-isopropylphenyl)carbodiimide

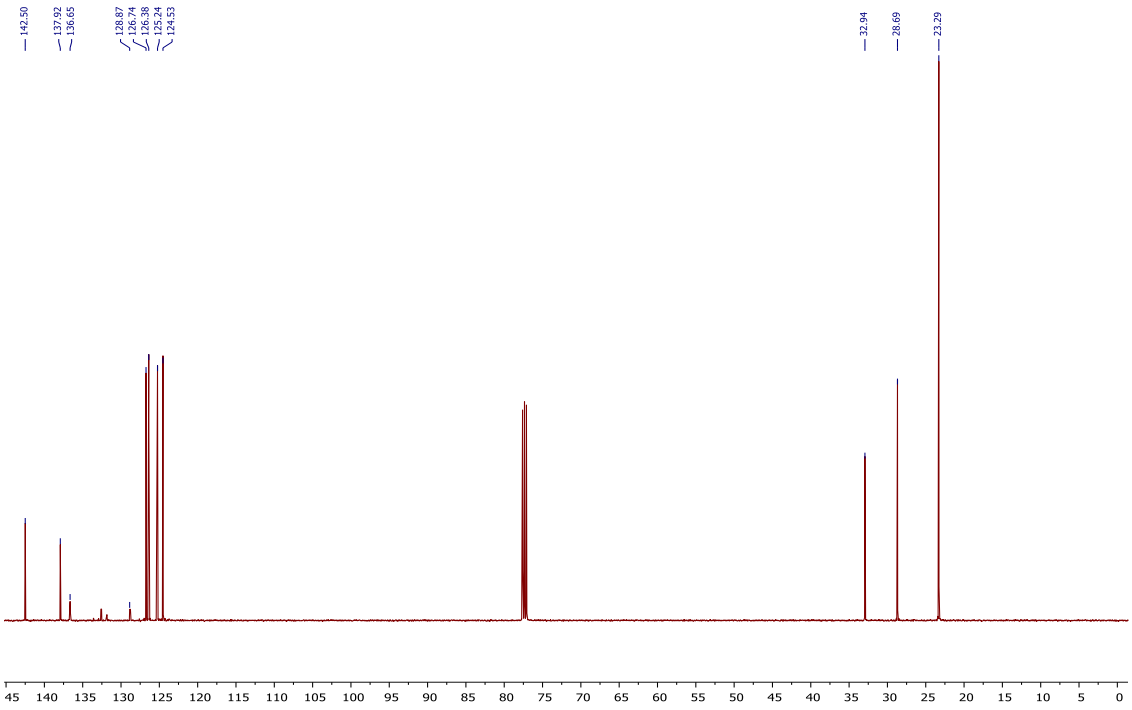

^{1}H NMR of *N*-methyl-*N*'-(3-isopropylphenyl)carbodiimide

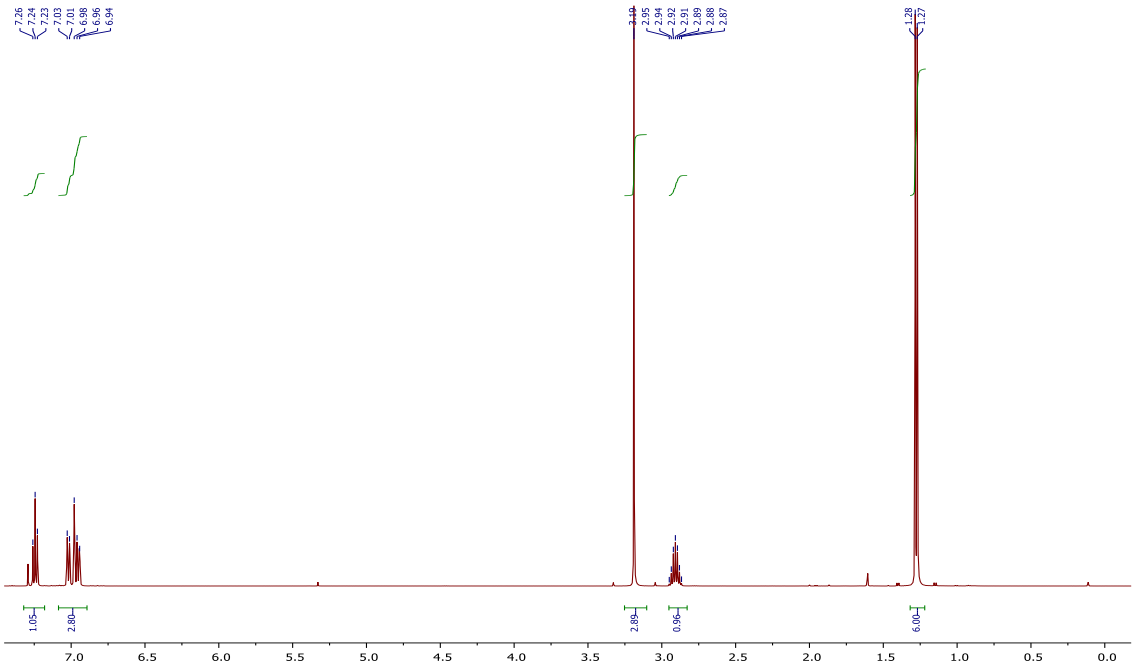

^{13}C NMR of *N*-methyl-*N*'-(3-isopropylphenyl)carbodiimide

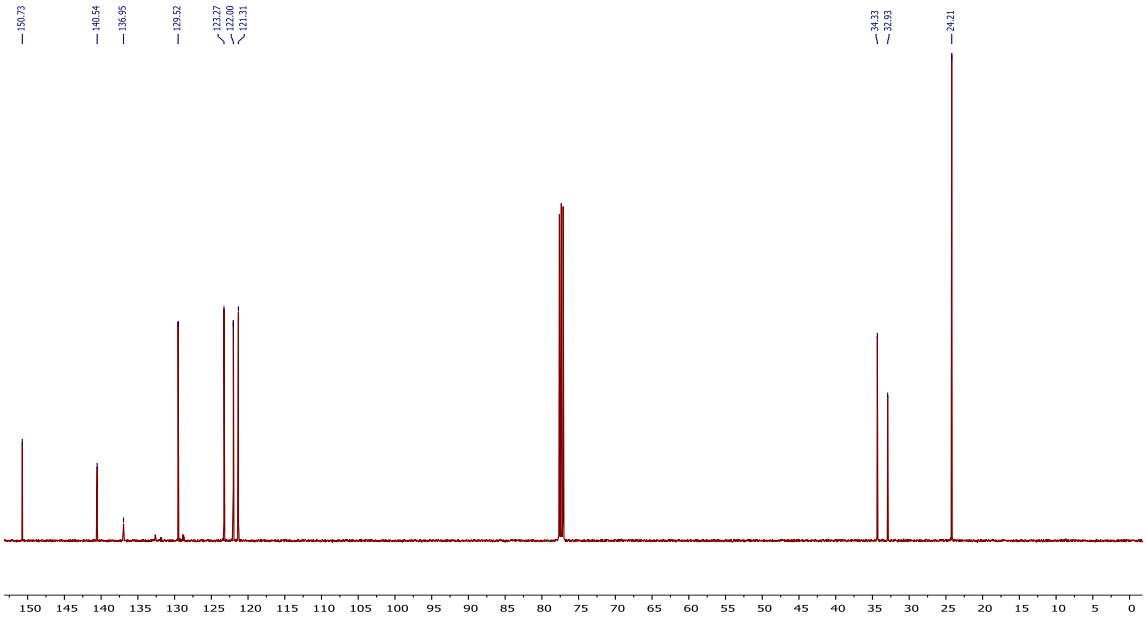

^{1}H NMR of *N*-methyl-*N*'-(4-isopropylphenyl)carbodiimide

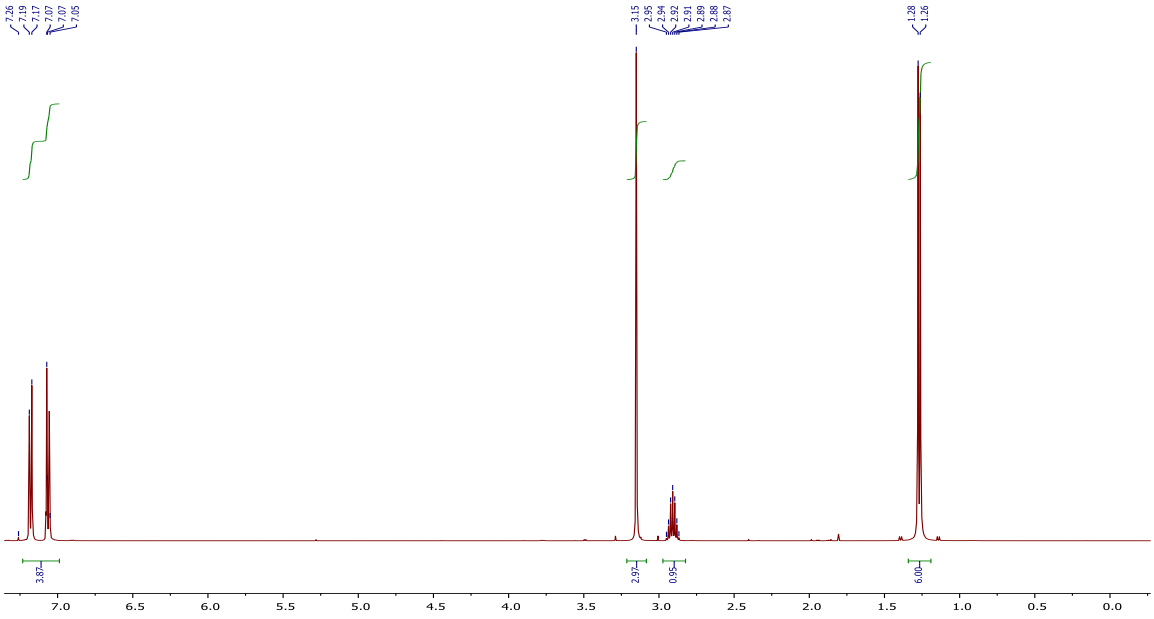

^{13}C NMR of *N*-methyl-*N*'-(4-isopropylphenyl)carbodiimide

^{1}HNMR of (***R***)-**P-1**

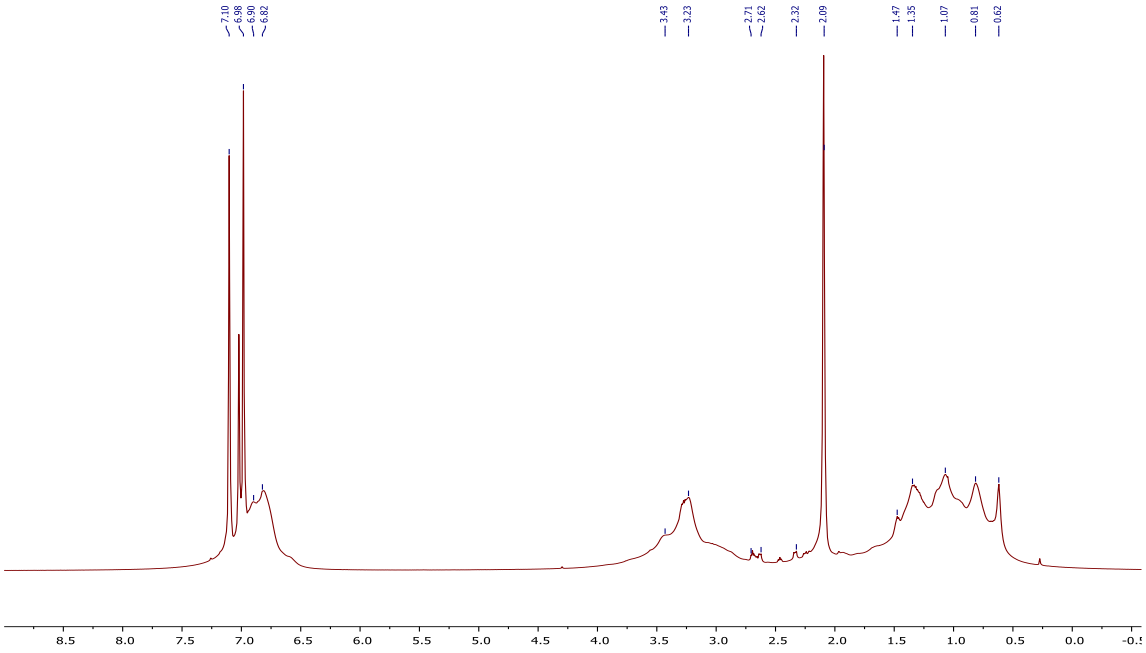

^{13}C NMR of (***R***)-**P-1**

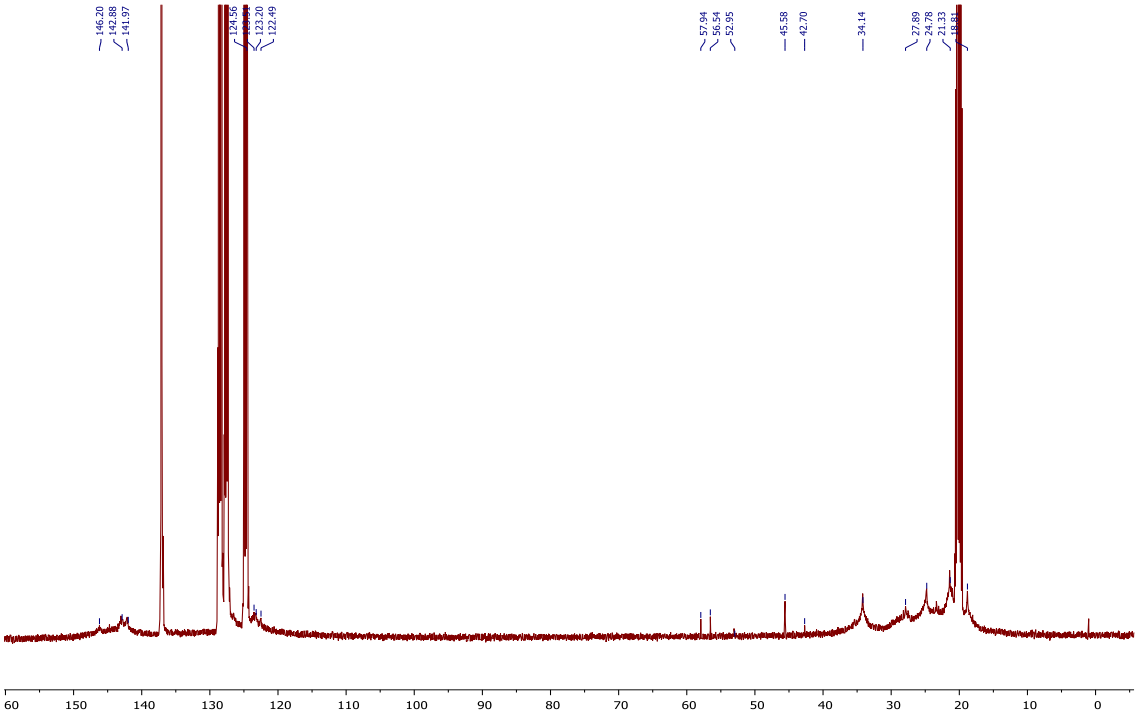

^{1}H NMR of (***S***)-**P-1**

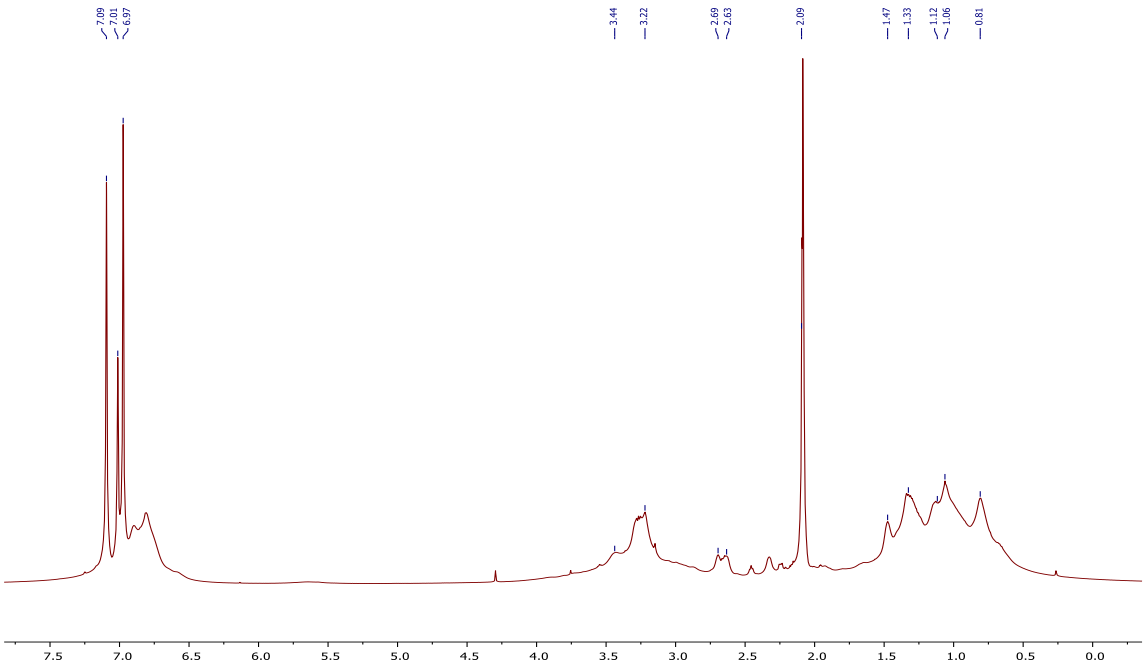

^{13}C NMR (solid state) of (*S*) P-1

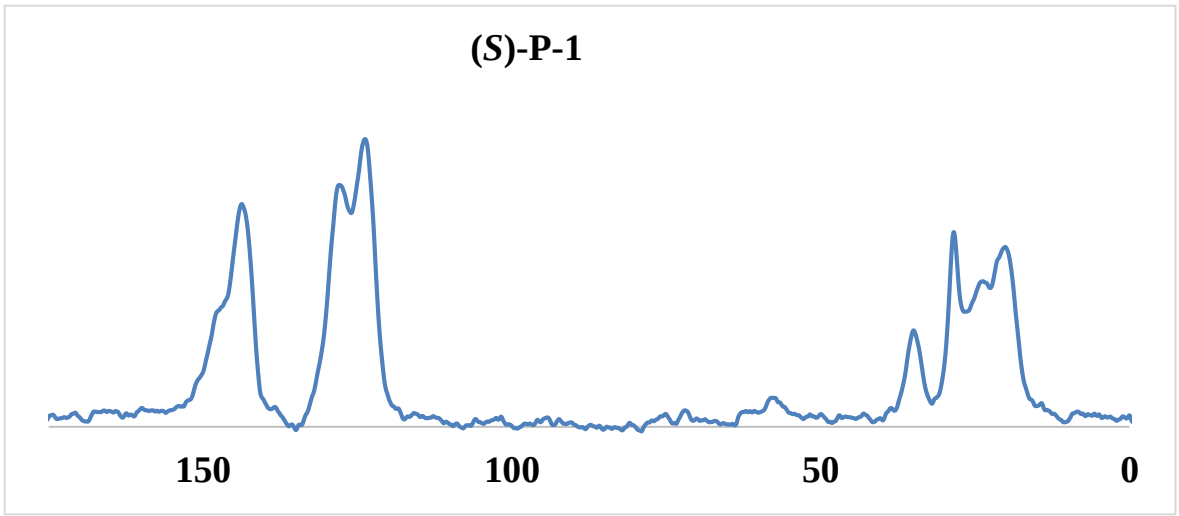

^{1}H NMR of (***RAC***)-**P-1**

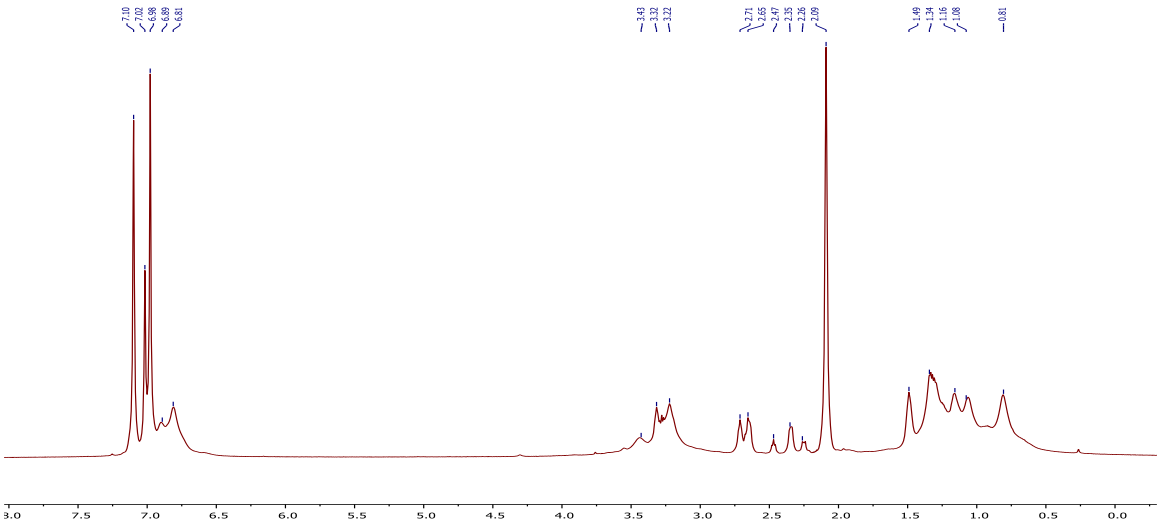

^{13}C NMR (solid state) of (***RAC***)-**P-1**

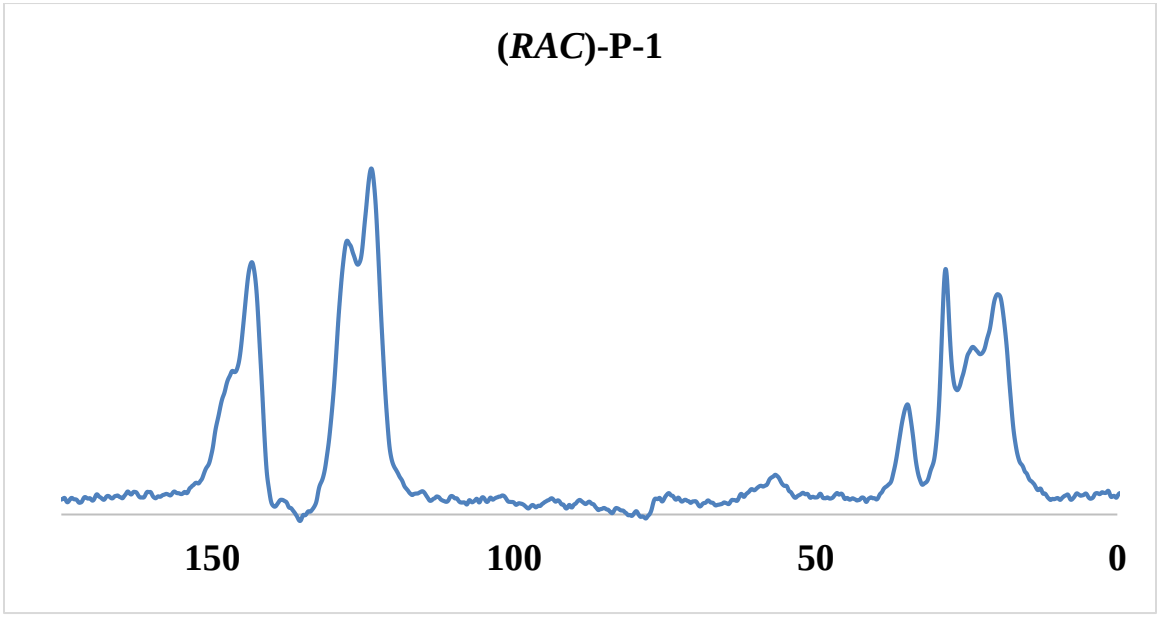

^{1}H NMR of (***S***)-**P-1,2**

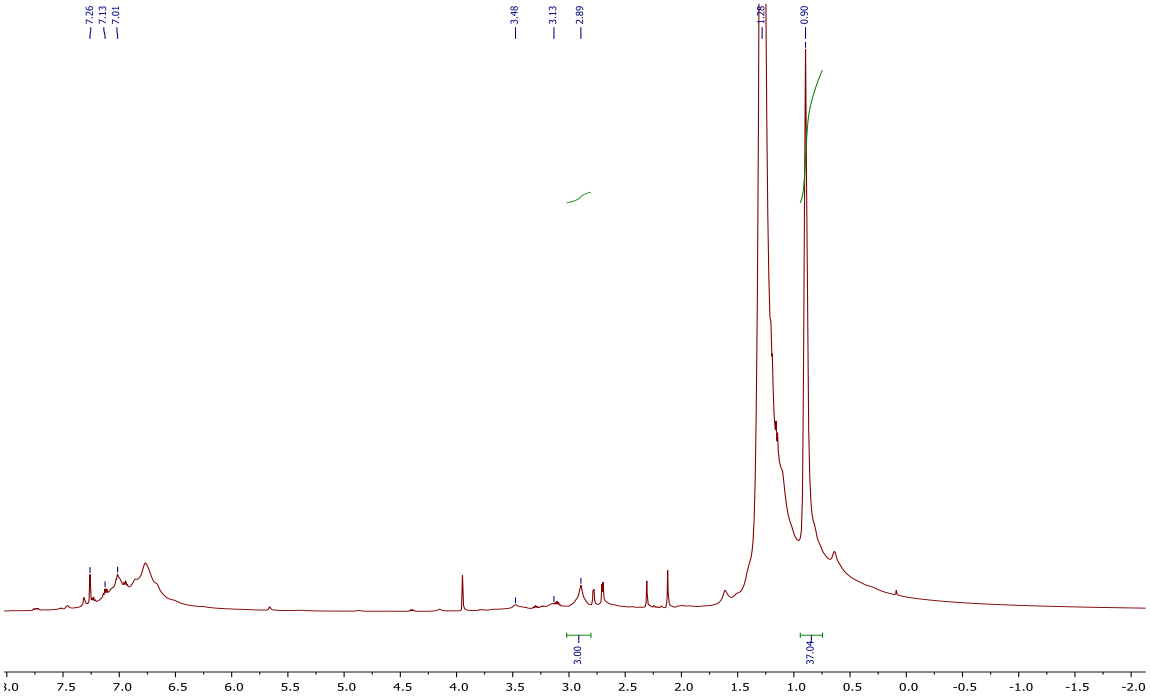

^{13}C NMR of (***S***)-**P-1,2**

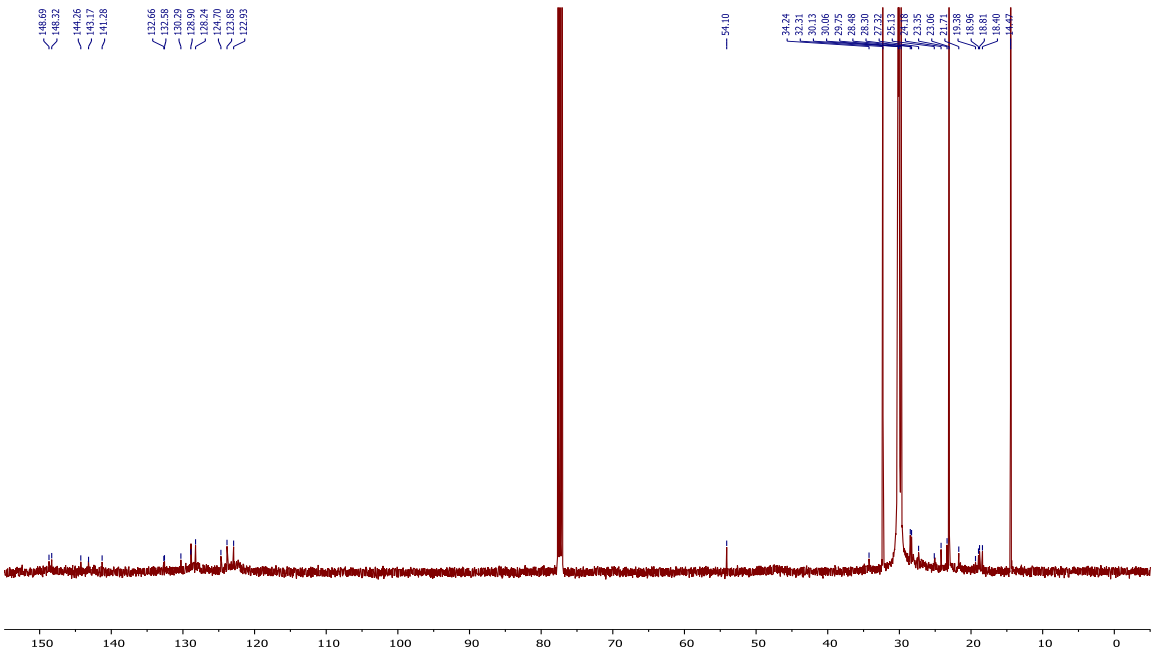

^{1}H NMR of poly(*N*-methyl-*N*'-(4-isopropylphenyl)carbodiimide), **(*S*)-P-5**

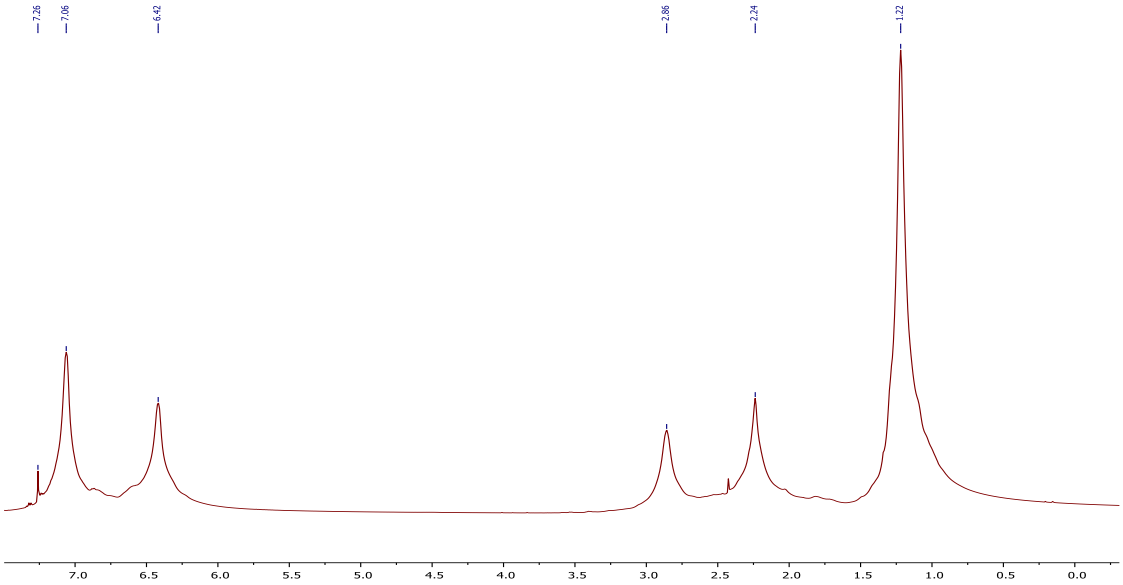

^{13}C NMR of poly(*N*-methyl-*N*'-(4-isopropylphenyl)carbodiimide), (***S***)-**P-5**

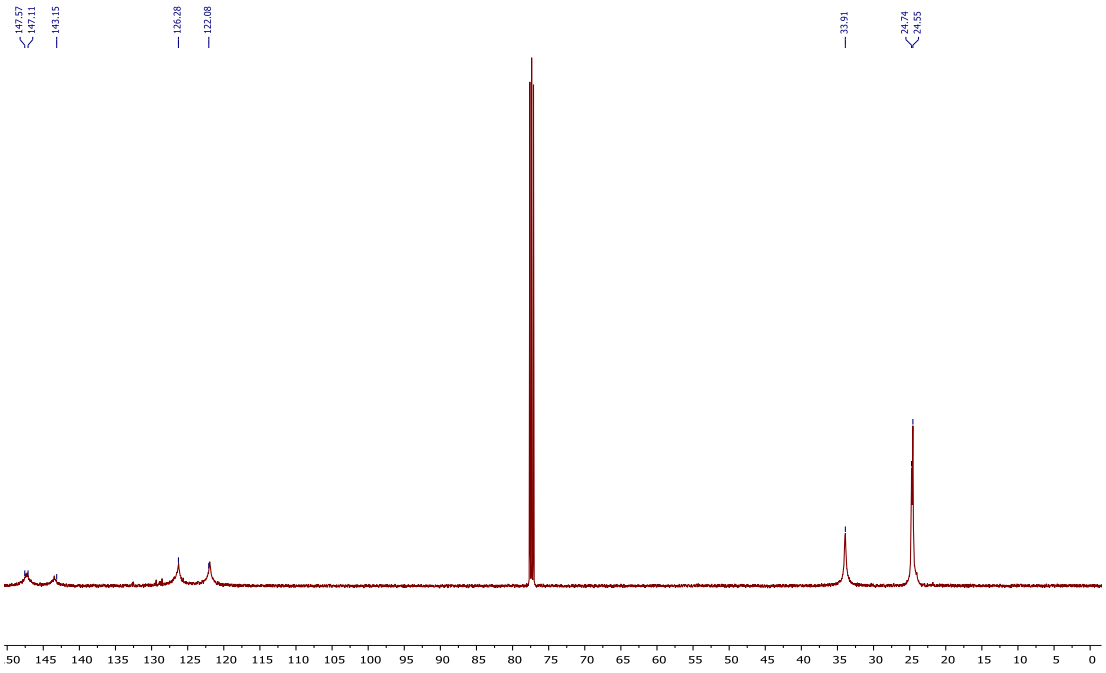

APPENDIX C

NMR SPECTRA OF SOME UREAS, MONOMERS AND POLYMERS FOR CHAPTER 4

^{1}H NMR of *N*-propargyl-*N*'-hexylurea

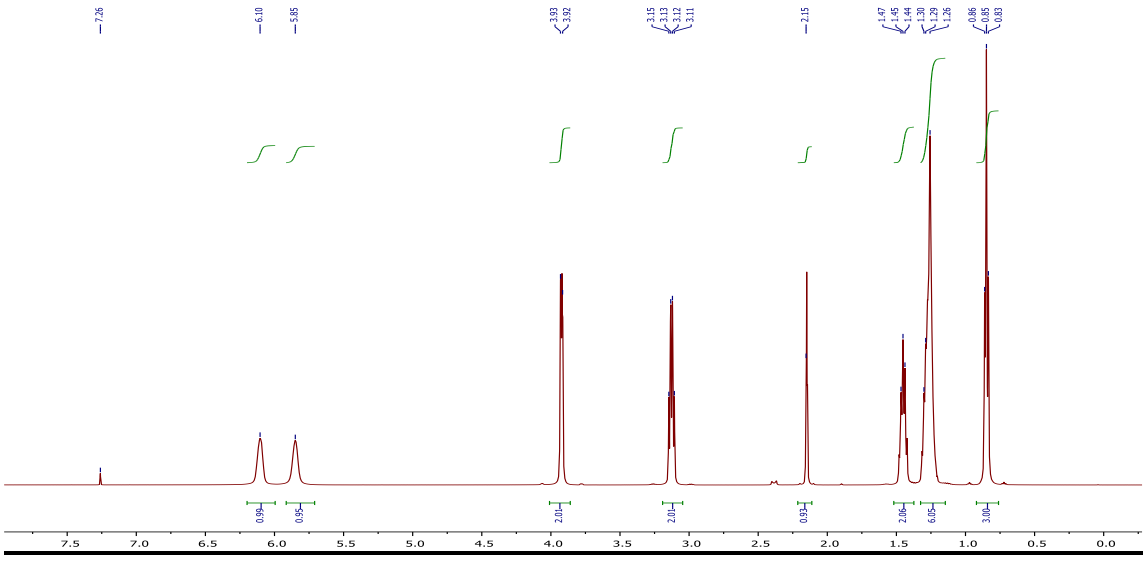

^{13}C NMR of *N*-propargyl-*N*'-hexylurea

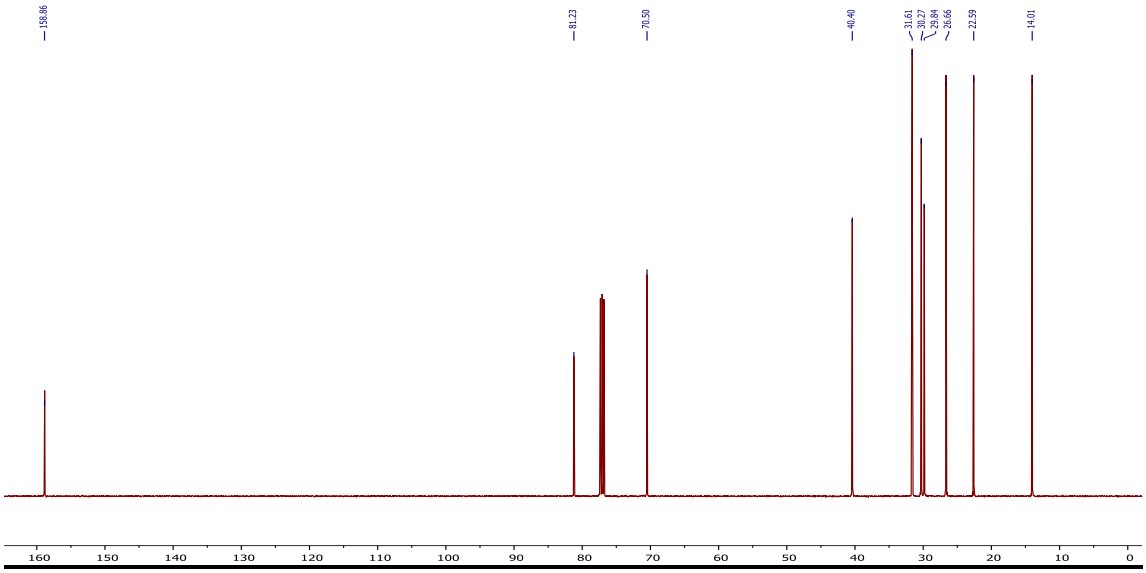

^{1}H NMR of (*N*-propargyl-*N*'-hexyl)carbodiimide monomer

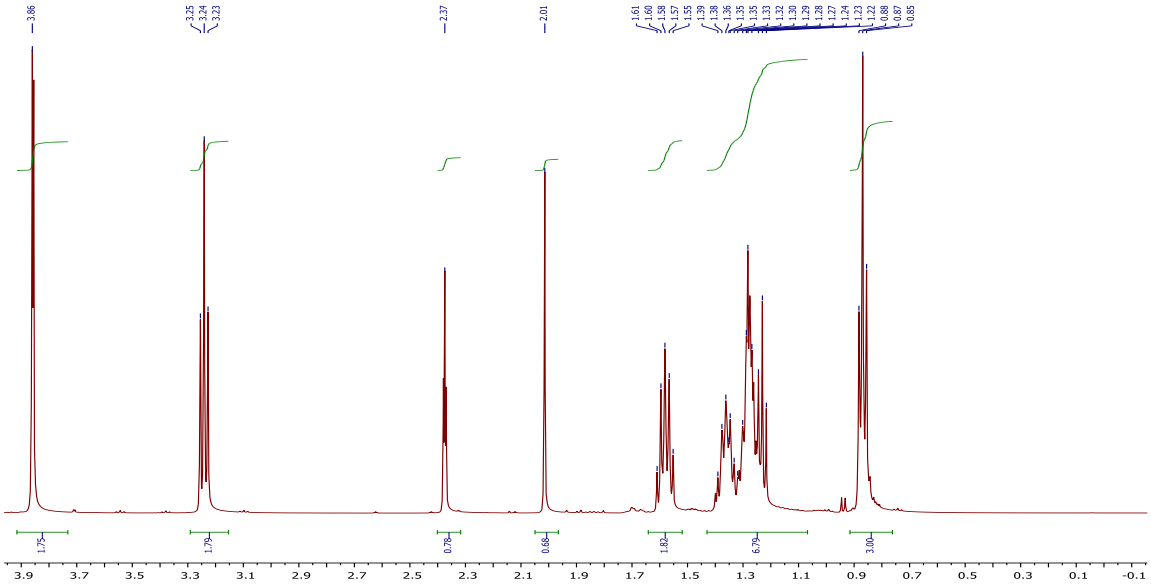

^{13}C NMR of (*N*-propargyl-*N*'-hexyl)carbodiimide monomer

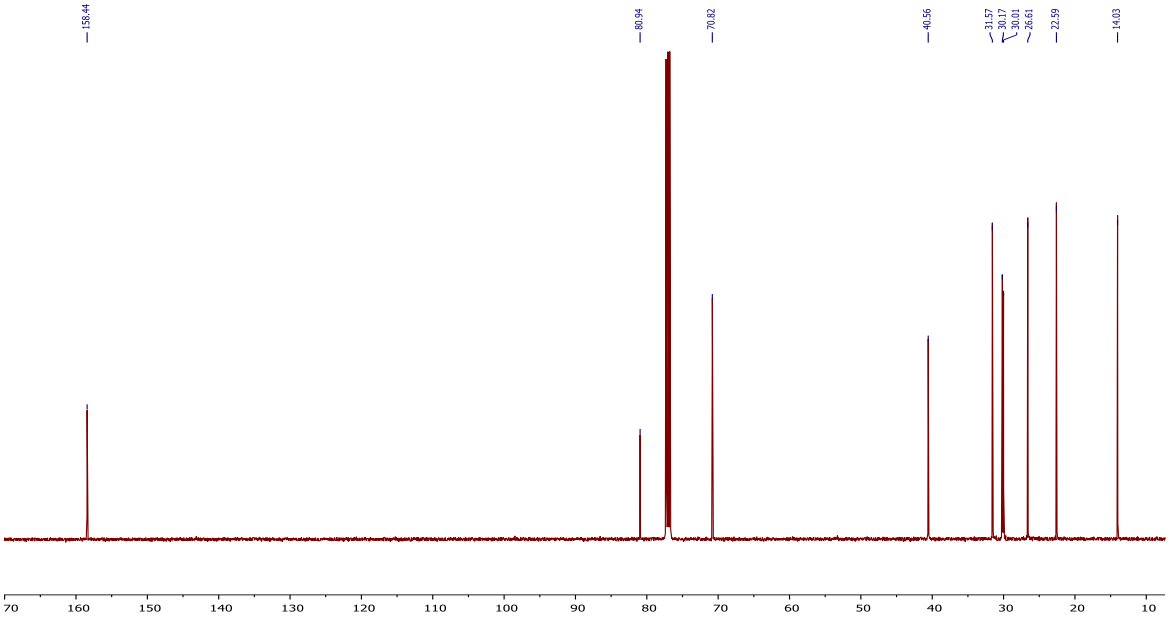

^{1}H NMR of poly(*N*-propargyl-*N*'-hexylcarbodiimide)

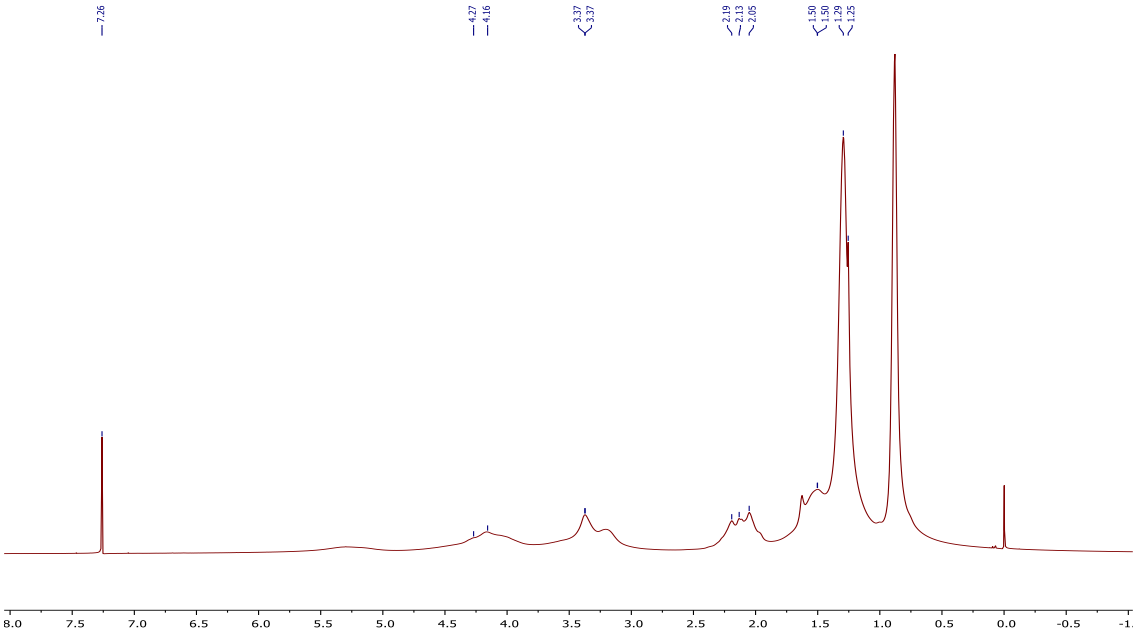

^{1}H NMR of 20% PNIPAM-*graft*-PC, **P-1**

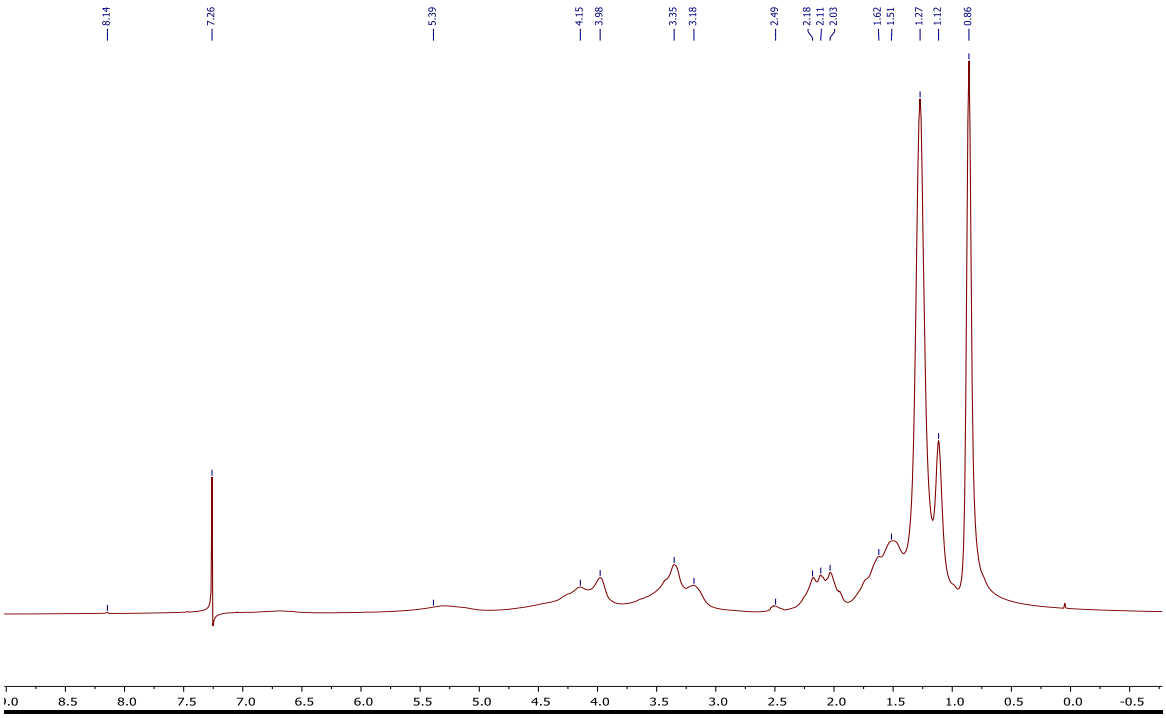

^{13}C NMR of 20% PNIPAM-*graft*-PC, **P-1**

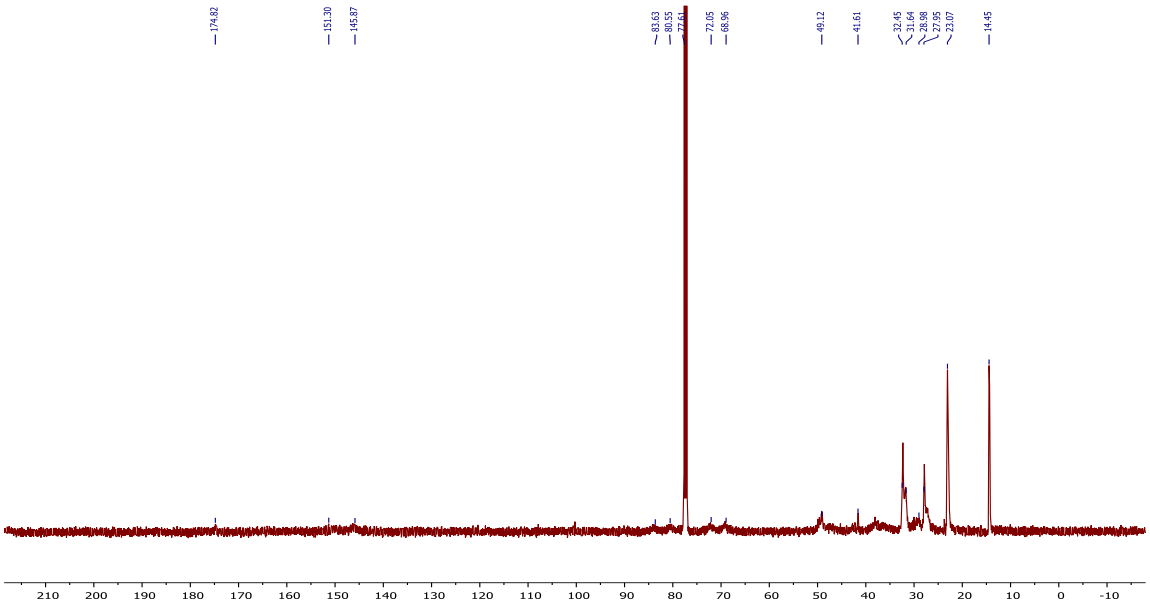

^{1}H NMR of 50% PNIPAM-*graft*-PC, **P-2**

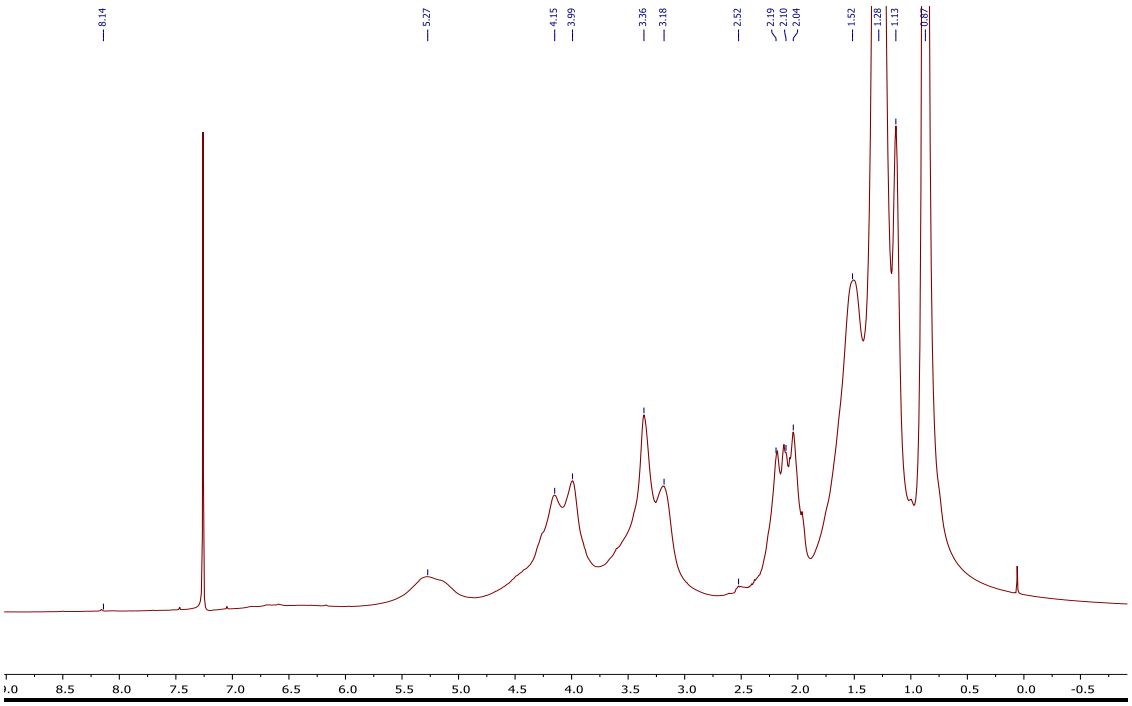

^{13}C NMR of 50% PNIPAM-*graft*-PC, **P-2**

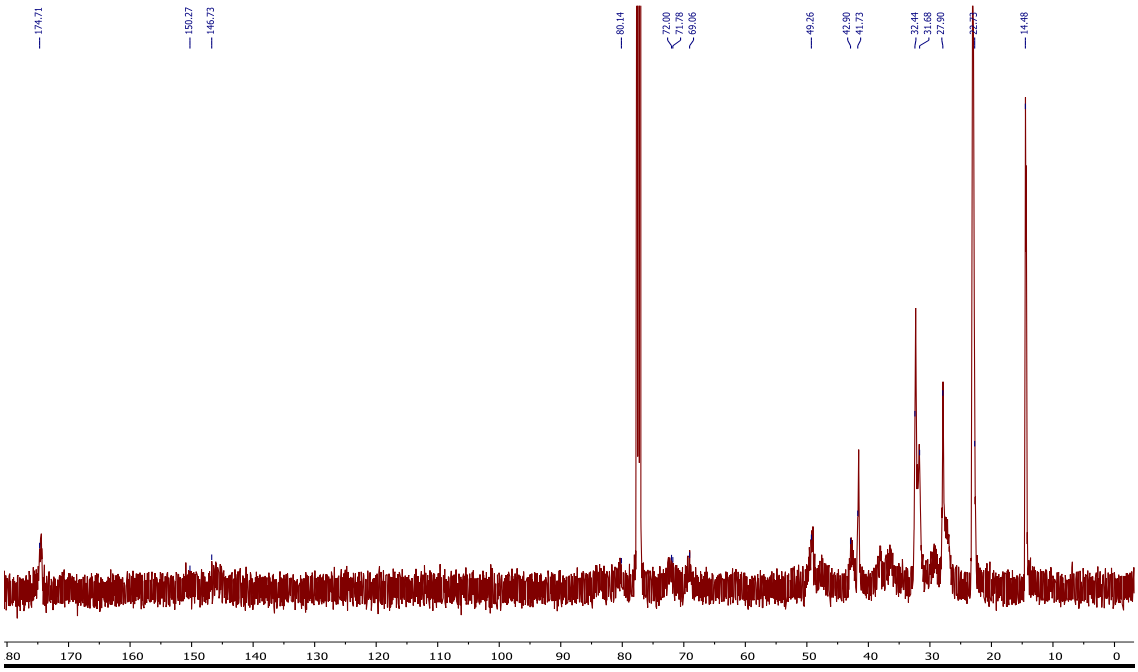

^{1}H NMR of 50% PEG-*graft*-PC, **P-3**

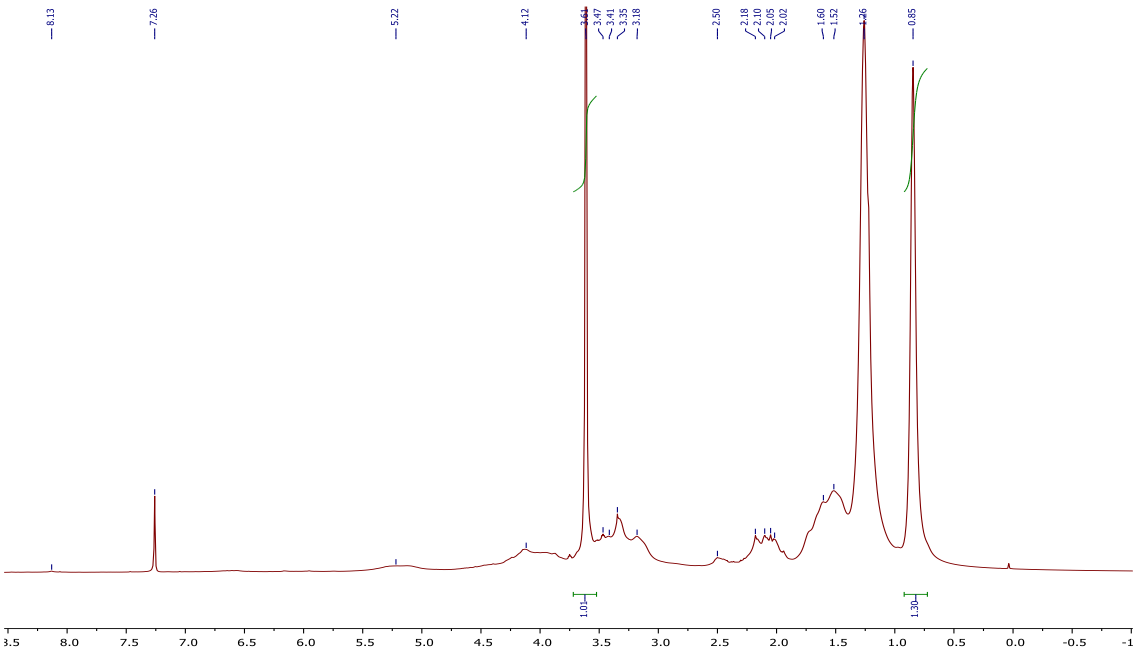

^{13}C NMR of 50% PEG-*graft*-PC, **P-3**

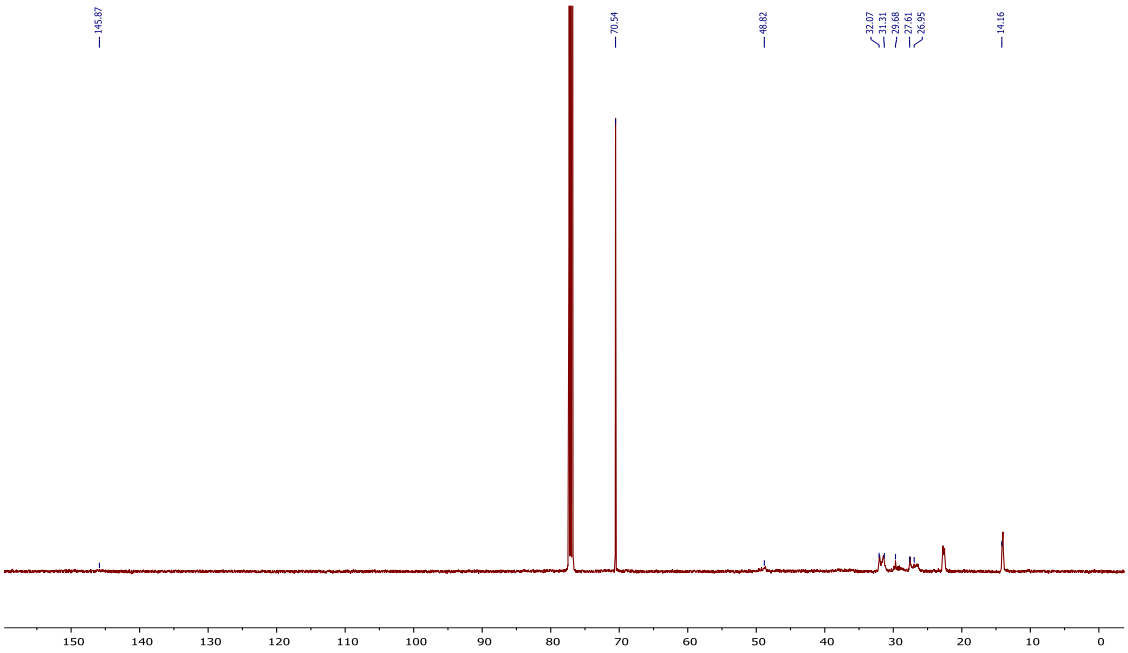

^{1}H NMR of 70% PEG-*graft*-PC, **P-4**

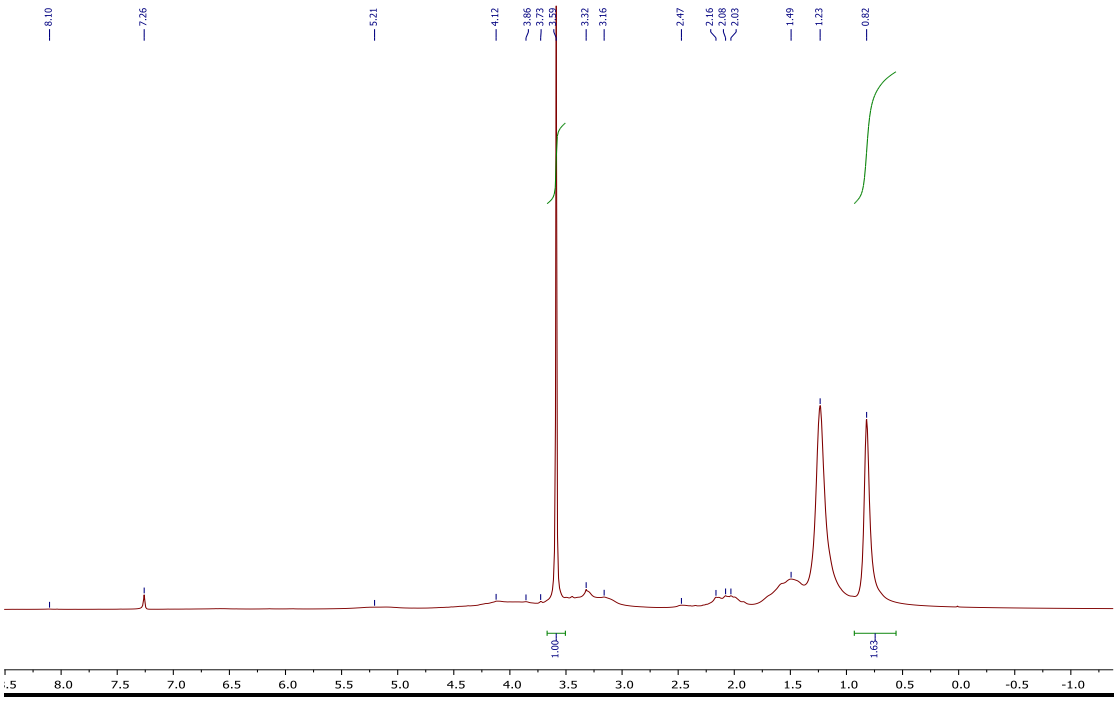

^{13}C NMR of 70% PEG-*graft*-PC, **P-4**

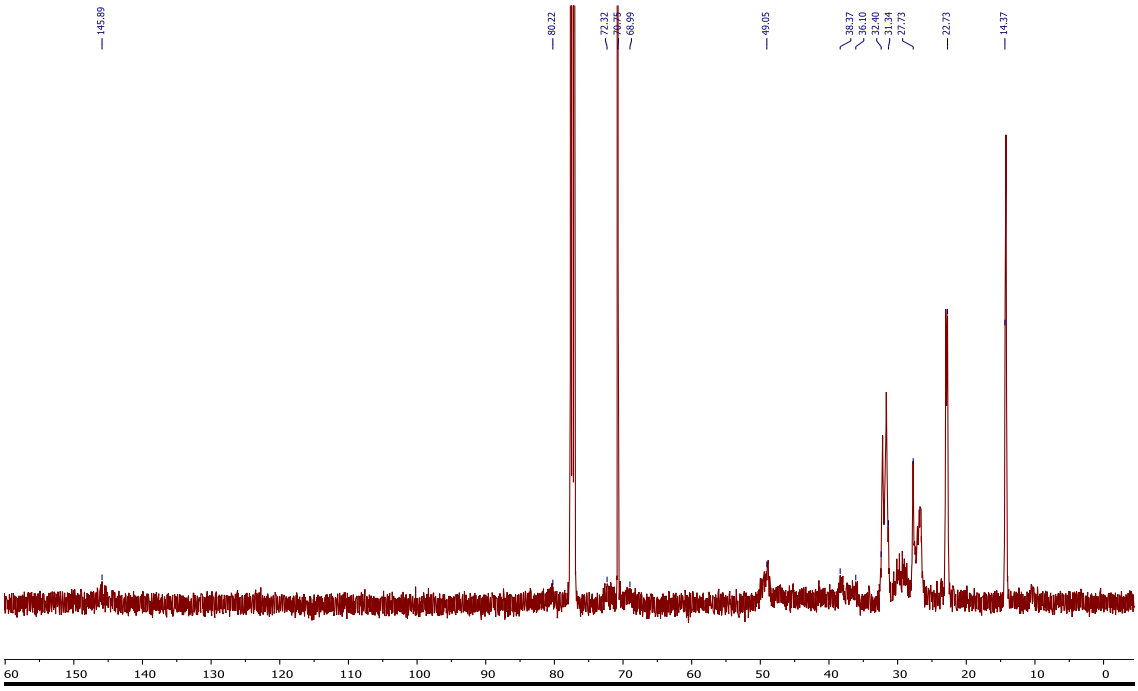

APPENDIX D

NMR SPECTRA OF SOME UREAS, MONOMERS AND POLYMERS FOR CHAPTER 5

^{1}H NMR of *N*-(1,2-diphenyldiazene)-*N*'-hexylurea

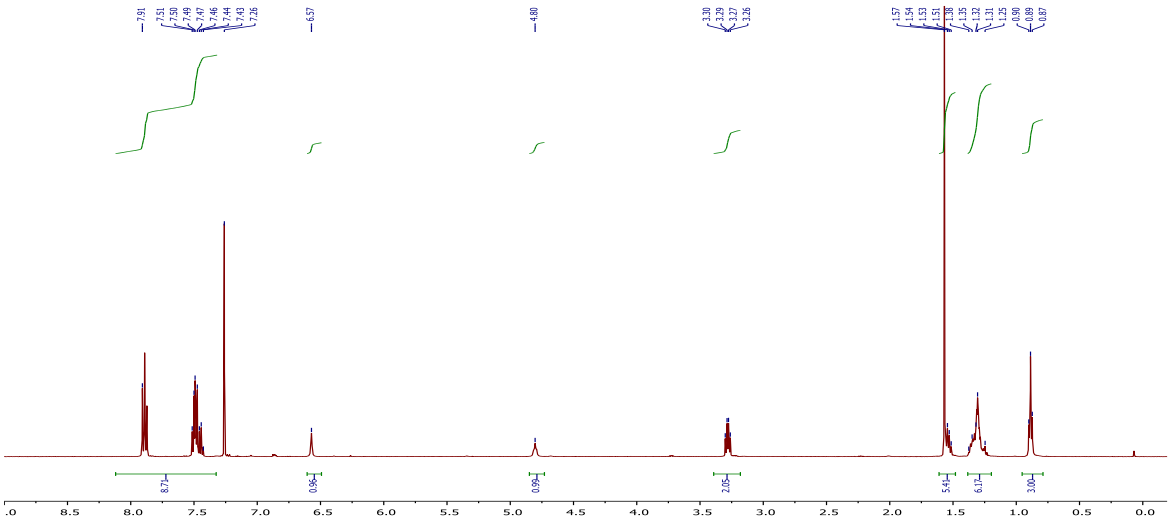

^{13} C NMR of *N*-(1,2-diphenyldiazene)-*N*'-hexylurea

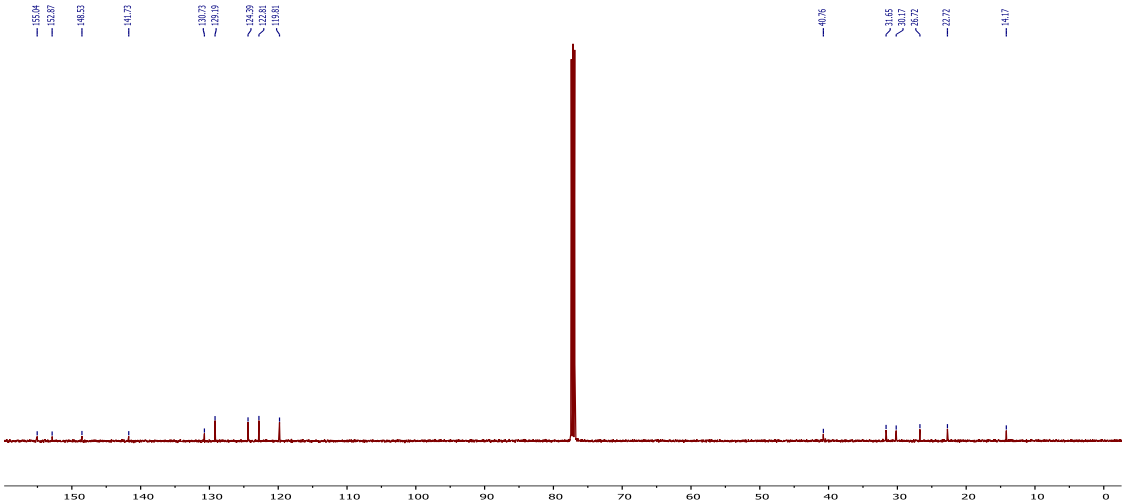

^{1}H NMR of *N*-(1,2-diphenyldiazene)-*N*'-hexylcarbodiimide monomer

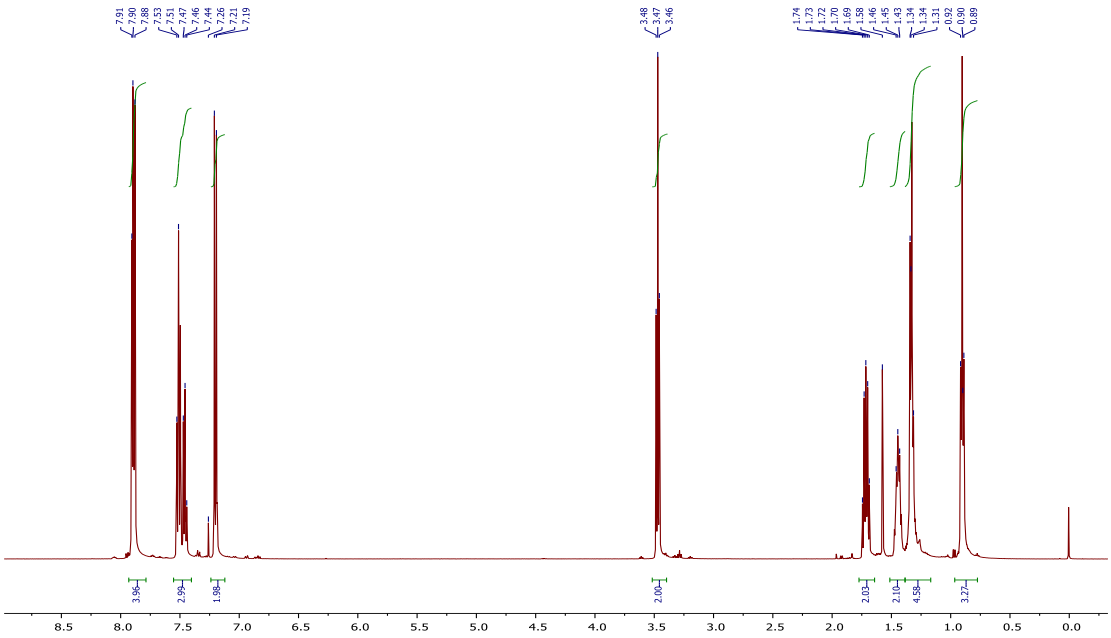

^{13}C NMR of *N*-(1,2-diphenyldiazene)-*N*'-hexylcarbodiimide monomer

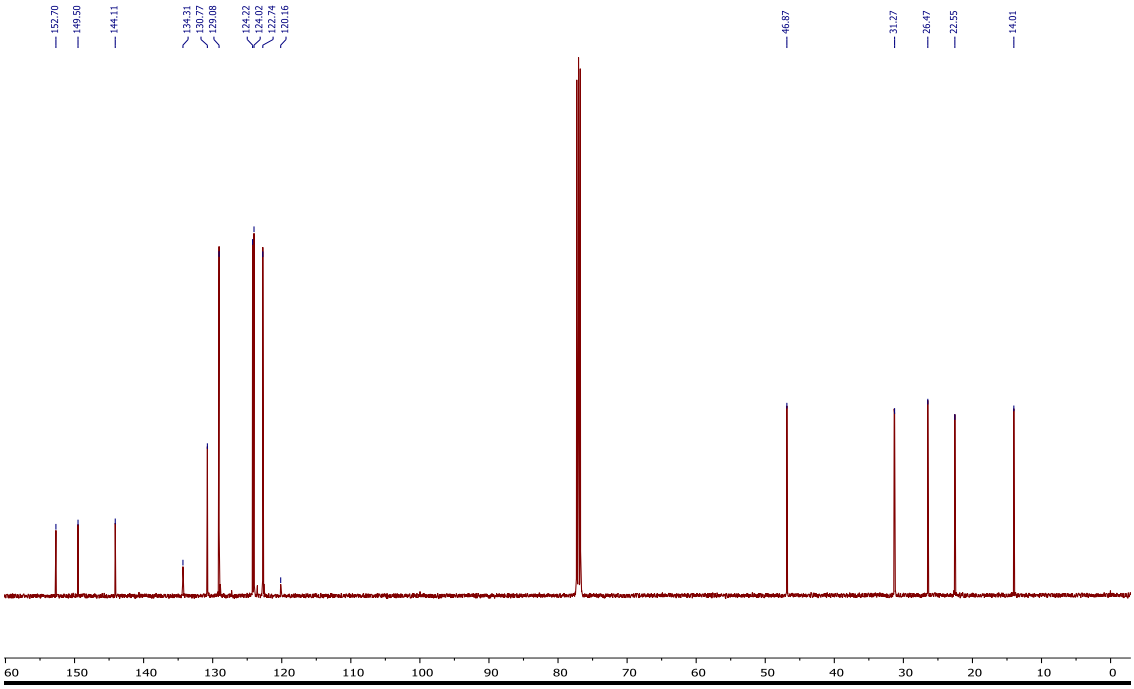

^{1}H NMR of poly(*N*-(1,2-diphenyldiazene)-*N*'-hexylcarbodiimide), **P-1**

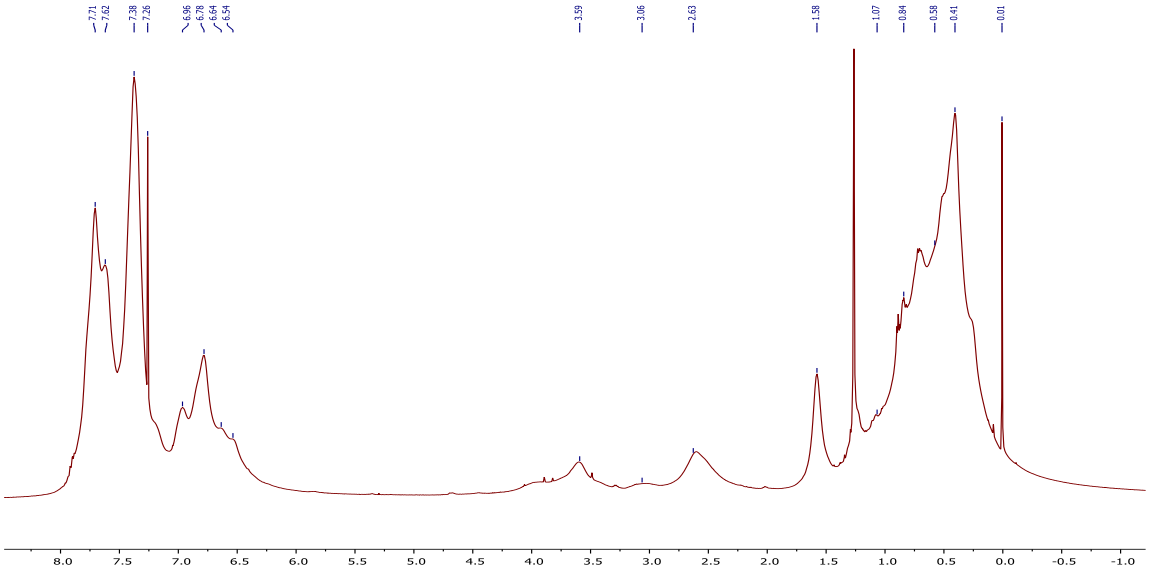

^{13}C NMR of poly(*N*-(1,2-diphenyldiazene)-*N*'-hexylcarbodiimide), **P-1**

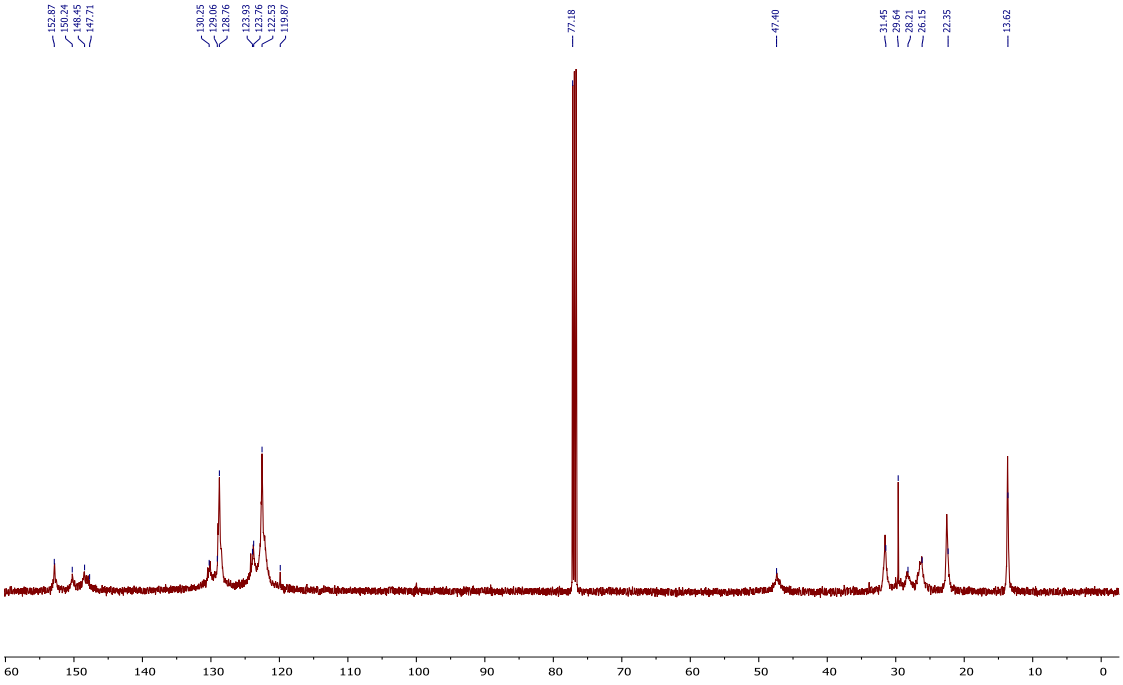

^{1}H NMR of poly(*N*-(1,2-diphenyldiazene)-*N*'-hexylcarbodiimide)-*random*-poly(*N*-phenethyl-*N*'-methyl)carbodiimide, **P-2**

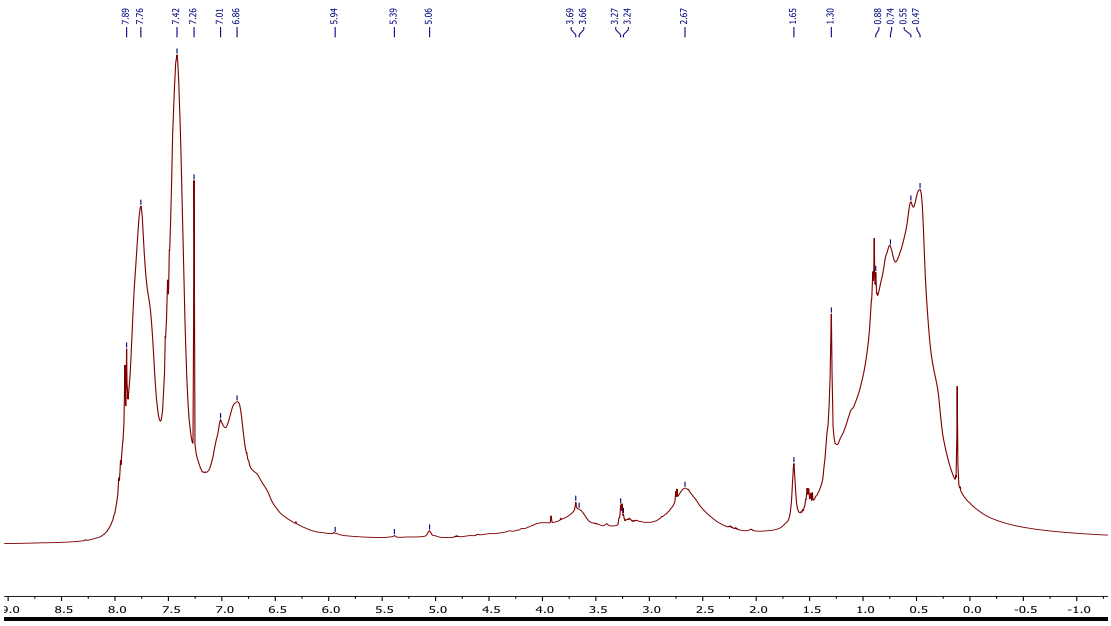

^{13}C NMR of poly(*N*-(1,2-diphenyldiazene)-*N*'-hexylcarbodiimide)-*random*-poly(*N*-phenethyl-*N*'-methyl)carbodiimide, **P-2**

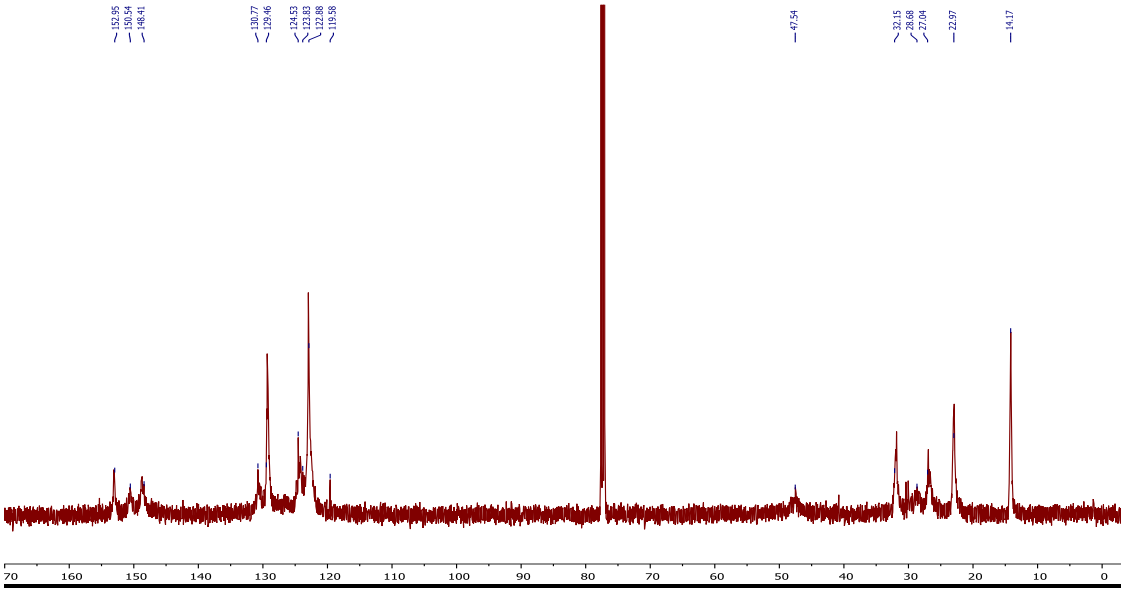

^{1}H NMR poly(*N*-(1,2-diphenyldiazene)-*N*'-hexylcarbodiimide)-*random*-poly(*N*-phenethyl-*N*'-methyl)carbodiimide, **P-3**

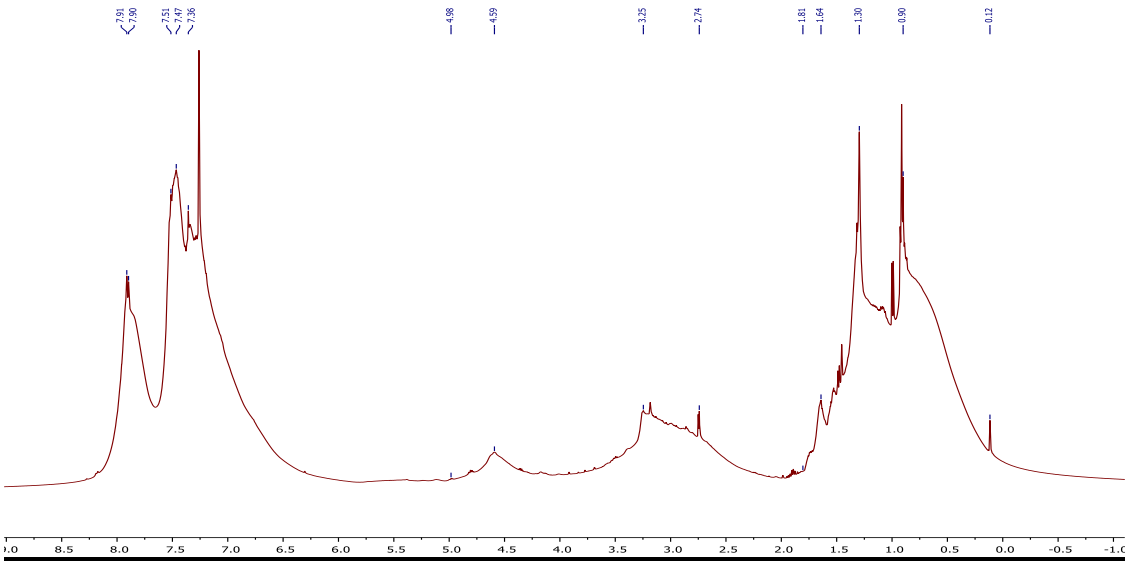

^{13}C NMR poly(*N*-(1,2-diphenyldiazene)-*N*'-hexylcarbodiimide)-*random*-poly(*N*-phenethyl-*N*'-methyl)carbodiimide, **P-3**

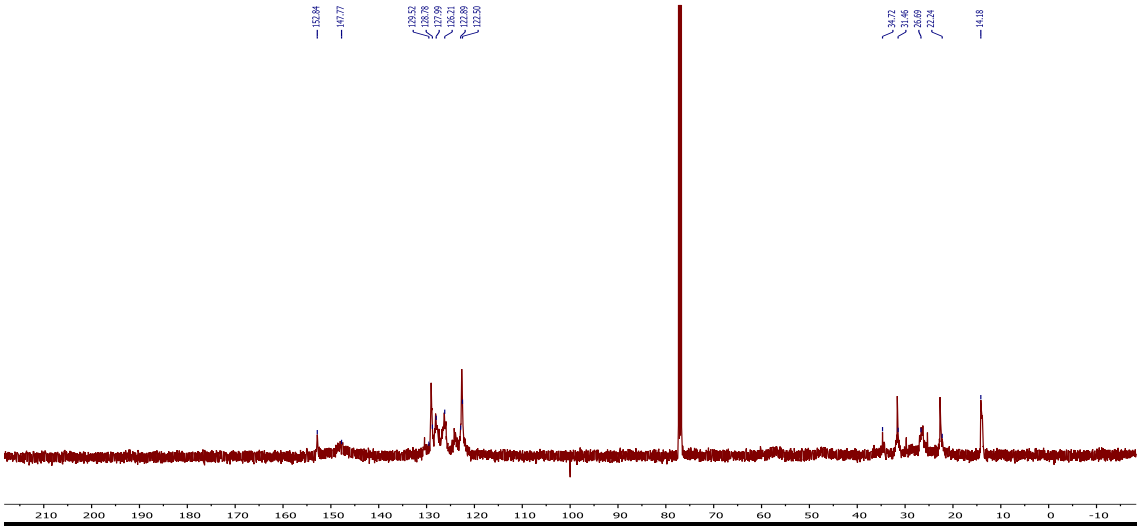

BIOGRAPHICAL SKETCH

Dumindika Aththanayake Siriwardane was born in Kandy, Sri Lanka and she completed her high school education at Mahamaya Girls' college, Kandy. She received her BSc(sp.) in chemistry from the University of Peradeniya in 2007. After that, she joined the National Institute of Fundamental Studies (NIFS) as a research assistant and conducted research on natural product isolation from endophytic fungi and screened their bioactivities. In 2012, she entered The University of Texas at Dallas for her Ph.D. and her research studies are focused on different polymer architectures built on chiral polycarbodiimides and their potential applications.

CURRICULUM VITAE

Dumindika A. Siriwardane
Department of Chemistry and Biochemistry,
The University of Texas at Dallas,
Richardson, TX 75080-3021
dxs124830@utdallas.edu

SUMMARY OF QUALIFICATIONS

- Possess multi-disciplinary research experiences, skilled in multi-step monomer and polymer synthesis, natural product isolation, and screening for bioactivities
- Experience in different polymerization techniques and invention of polymer self-assembly behavior and chiroptical switching behavior
- Proficient in small molecule and polymer characterization techniques including NMR, IR, Fluorescence, DLS, *p*-XRD, AFM, TEM, SEM, VCD, and CD
- Skilled learning new concept quickly, working well under pressure, and communicating ideas clearly and effectively

EDUCATION

- Ph.D. in Chemistry - Ph.D. expected in May - 2017
  Prof. Bruce M. Novak, the University of Texas at Dallas, Richardson, TX
- B.Sc. in chemistry - Second Class Upper Honor, 2007
  University of Peradeniya, Sri Lanka

PROFESSIONAL EXPERIENCES

- Teaching and Research Experiences
- Assistant lecture Rajarata University
- Teaching Assistance University of Peradeniya
- Research Assistant National Institute of Fundamental Studies, Kandy

RESEARCH INTEREST

- Polymer Chemistry
- Natural Product Isolation and Bioactivities
- Combinatorial Chemistry in Drug Discoveries

PUBLICATIONS

1. **Siriwardane, D. A**.; Kulikov, O.V.; Reuther, J. F.; Novak, B.M, Rigid, Helical Arm Stars through Living Nickel Polymerization of Carbodiimides. *Macromolecules* **2017** DOI: 10.1021/acs.macromol.6b02456.
2. Kulikov, O. V.; **Siriwardane, D. A.,** McCandless, G. T.; Mahmood, S. F.; Novak, B. M., Self-assembling Morphologies Obtained from Helical Polycarbodiimide Copolymers and Their Triazole Derivatives. *J. Vis. Exp.*, e55124, doi:10.3791/55124 (2016).
3. Mammoottil, N. R.; Reuther, J. F.; **Siriwardane, D. A**.; Kulikov, O. V; Novak, B. M. Developments in Synthesis, Characterization, and Self-Assembly of Polycarbodiimide Systems. *J. Polym. Sci. Part A Polym. Chem.* **2017**, n/a-n/a DOI: 10.1002/pola.28583.
4. Kulikov, O. V.; **Siriwardane, D. A.**; Reuther, J. F.; McCandless, G. T.; Sun, H.-J.; Li, Y.; Mahmood, S. F.; Sheiko, S. S.; Percec, V.; Novak, B. M., Characterization of Fibrous Aggregated Morphologies and Other Complex Architectures Self-Assembled from Helical Alkyne and Triazole Polycarbodiimides (*R*)- and (*S*)-Families in the Bulk and Thin Film. *Macromolecules* **2015,** *48* (12), 4088-4103.
5. Reuther, J. F.; **Siriwardane, D. A.**; Campos, R.; Novak, B. M., Solvent Tunable Self-Assembly of Amphiphilic Rod–Coil Block Copolymers with Chiral, Helical Polycarbodiimide Segments: Polymeric Nanostructures with Variable Shapes and Sizes. *Macromolecules* **2015,** *48* (19), 6890-6899.
6. Reuther, J. F.; **Siriwardane, D. A.**; Kulikov, O. V.; Batchelor, B. L.; Campos, R.; Novak, B. M., Facile Synthesis of Rod–Coil Block Copolymers with Chiral,

Helical Polycarbodiimide Segments via Postpolymerization CuAAC "Click" Coupling of Functional End Groups. *Macromolecules* **2015,** *48* (10), 3207-3216.

7. Kulikov, O. V.; **Siriwardane, D. A.**; McCandless, G. T.; Barnes, C.; Sevryugina, Y. V.; DeSousa, J. D.; Wu, J.; Sommer, R.; Novak, B. M., Self-Assembly of n-Alkyl- and Aryl-Side Chain Ureas and Their Derivatives as Evidenced by SEM and X-ray Analysis. *European Journal of Organic Chemistry* **2015,** *2015* (34), 7511-7518.
8. Kulikov, O. V.; McCandless, G. T.; **Siriwardane, D. A.**; Sevryugina, Y. V.; Novak, B. M., Peculiarities of the crystal packing of n-alkyl side chain ureas—precursors in the synthesis of helical polycarbodiimides. *Tetrahedron Letters* **2015,** *56* (46), 6309-6313.
9. **Siriwardane, A M D A**; Kumar, S, N.; Jayasinghe, L.; Fujimoto, Y, Chemical investigation of metabolites produced by an endophytic Aspergillus sp. isolated from Limonia acidissima. *Natural Product Research* (29), 1-4.
10. Alakolanga, A. G. A. W.; **Siriwardane, A. M. D. A**.; Kumar, N. S.; Jayasinghe, L.; Jaiswal, R.; Kuhnert, N., LC-MSn identification and characterization of the phenolic compounds from the fruits of Flacourtia indica (Burm. F.) Merr. and Flacourtia inermis Roxb. *Food Research International* **2014** (62), 388-396.
11. **Siriwardane, D. A**.; Kulikov, O.V.; Novak, B.M, Helix Sense Selective Polymerization of Achiral Carbodiimide Monomers Bearing Isopropyl Scaffolds and Effect of Regioregularity on Stereocomplexation, (Manuscript is in preparation).
12. **Siriwardane, D. A**.; Kulikov, O.V.; Novak, B.M, PNIPAM and PEG grafted Hairy Polycarbodiimides as Nano-Carriers for Hydrophobic Drugs, (Manuscript is in preparation).
13. **Siriwardane, D. A**.; Kulikov, O.V.; Novak, B.M, UV and Thermo Controllable Azobenzene-Decorated Polycarbodiimide Switches, (Manuscript is in preparation).

CONFERENCE PRESENTATIONS

1. 'Synthesis of PEG and PNIPAM Grafted Polycarbodiimide Brush Co-polymers and Their Self-Assembly into Nano Carriers' – Oral Presentation, **Dumindika A. Siriwardane,** Bruce M. Novak. SWRM, Galveston, TX. November 2016.
2. 'Molecular Screws of Polycarbodiimides and Their Helix Sense Selective Polymerization' - Oral Presentation, **Dumindika A. Siriwardane,** Oleg Kulikov, Bruce M. Novak. 251st ACS National Meeting in San Diego, CA. February, 2016.
3. 'Preparation of Helical Star Polymers Using Tris-Nickel Initiators' – Oral Presentation, **Dumindika A. Siriwardane,** James F. Reuther, Bruce M. Novak. 249th ACS National Meeting in Denver, CO. March 2015.

TECHNICAL SKILLS

- Multi-step organic, inorganic and polymer synthesis.
- Anaerobic Chemistry (Use and maintenance of Schlenk lines and Inert air glove box)
- Polymer characterization (GPC, DSC, TGA, MALDI-TOF, *p*-XRD)
- Polymer and small molecule spectroscopic characterization (**GC-MS, IR, UV-Vis, NMR including ^{1}H, ^{13}C, ^{15}N, and ^{31}P**)
- Chiral Characterization (**VCD, CD, Polarimetry**)
- Microscopy Techniques (Fluorescence spectroscopy, UV-Vis, Polarizing optical microscope, TM-AFM, SEM, TEM)
- Microbiology - Handling laminar flow hood
- Combinatorial chemistry for drug discovery
- Mentoring graduate student, undergraduates, and high school students

AWARDS & HONORS

- National Research Council, Sri Lanka - Merit award for Publication in 2014
- Selected for UTD Small Travel Grant.

- Selected for chairing Poly session in 251st ACS National Meeting in San Diago, CA.
- One Publication has been selected as **a cover image** in **Macromolecular journal**

  Characterization of Fibrous Aggregated Morphologies and Other Complex Architectures Self-Assembled from Helical Alkyne and Triazole Polycarbodiimides (*R*) - and (*S*) - Families in the Bulk and Thin Film. *Macromolecules* **2015,** *48* (12), 4088-4103. http://pubs.acs.org/toc/mamobx/48/12

LANGUAGES

- English
- Sinhala

PROFESSIONAL MEMBERSHIPS

- Member - American Chemical Society
- Member - Division of Polymer Chemistry
- Member - Society of Asian Scientists and Engineers